ROBOTICS SERIES

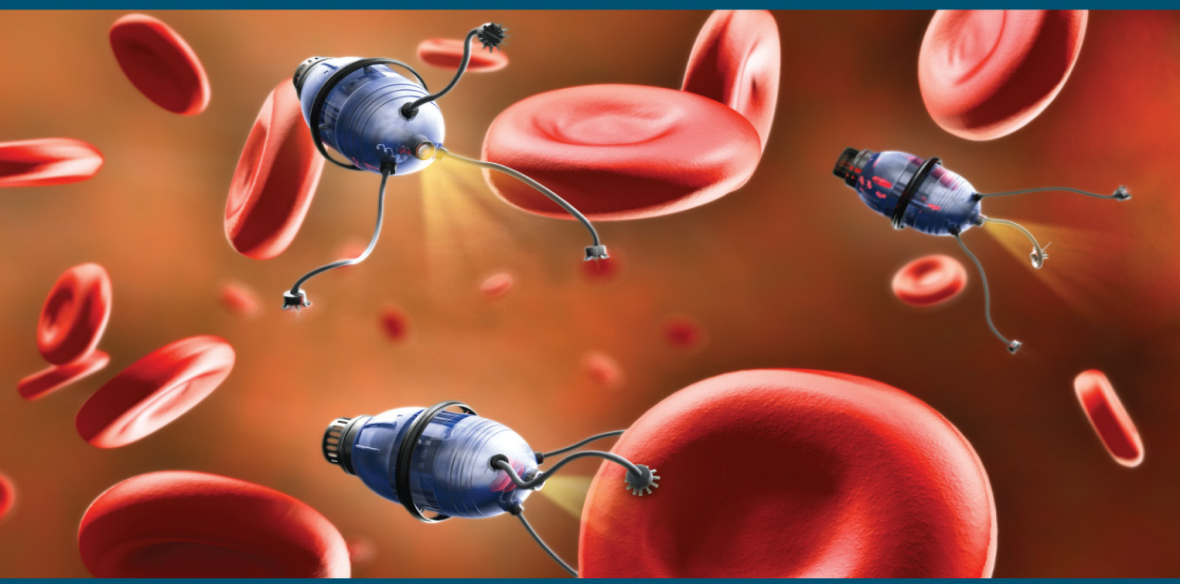

Intracorporeal Robotics

From Milliscale to Nanoscale

Michaël Gauthier
Nicolas Andreff and Etienne Dombre

ISTE WILEY

Intracorporeal Robotics

Intracorporeal Robotics

From Milliscale to Nanoscale

Michaël Gauthier
Nicolas Andreff
Etienne Dombre

ISTE WILEY

First published 2014 in Great Britain and the United States by ISTE Ltd and John Wiley & Sons, Inc.

Apart from any fair dealing for the purposes of research or private study, or criticism or review, as permitted under the Copyright, Designs and Patents Act 1988, this publication may only be reproduced, stored or transmitted, in any form or by any means, with the prior permission in writing of the publishers, or in the case of reprographic reproduction in accordance with the terms and licenses issued by the CLA. Enquiries concerning reproduction outside these terms should be sent to the publishers at the undermentioned address:

ISTE Ltd
27-37 St George's Road
London SW19 4EU
UK

www.iste.co.uk

John Wiley & Sons, Inc.
111 River Street
Hoboken, NJ 07030
USA

www.wiley.com

© ISTE Ltd 2014
The rights of Michaël Gauthier, Nicolas Andreff and Etienne Dombre to be identified as the author of this work have been asserted by them in accordance with the Copyright, Designs and Patents Act 1988.

Library of Congress Control Number: 2013957115

British Library Cataloguing-in-Publication Data
A CIP record for this book is available from the British Library
ISBN 978-1-84821-371-5

Printed and bound in Great Britain by CPI Group (UK) Ltd., Croydon, Surrey CR0 4YY

Table of Contents

Introduction ix

Chapter 1. Intracorporeal Millirobotics 1

1.1. Introduction 1
1.2. Principles. 2
1.2.1. Partially intracorporeal devices with active distal mobilities 2
1.2.2. Intracorporeal manipulators 5
1.2.3. Intracorporeal mobile devices 16
1.3. Scientific issues 20
1.3.1. Modeling 20
1.3.2. Design 24
1.3.3. Actuation and transmission. 26
1.3.4. Sensing 30
1.3.5. Control. 34
1.4. Examples of devices 37
1.4.1. The robotic platform of the Araknes project 39
1.4.2. A snake-like robot made of concentric super-elastic tubes 44
1.4.3. MICRON: a handheld robotized instrument for ophthalmic surgery 48
1.5. Conclusion 52

Chapter 2. Intracorporeal Microrobotics 55

2.1. Introduction 55
2.2. Novel paradigms for intracorporeal robotics 56

2.2.1. Classification of intracorporeal robots 56
2.2.2. Physical principles in use at microscale 57
2.3. Methods 66
2.3.1. Models 66
2.3.2. Design 71
2.3.3. Actuation 75
2.3.4. Sensing 80
2.3.5. Control 86
2.4. Devices 97
2.4.1. Magnetically guided catheters 97
2.4.2. Distal tip mobility for endoluminal microphonosurgery 98
2.4.3. Autonomous active capsules 102
2.4.4. Magnetically guided capsules 104
2.5. Conclusion 107

Chapter 3. *In vitro* Non-Contact Mesorobotics 109

3.1. Introduction 109
3.2. Principles 111
3.2.1. Introduction 111
3.2.2. Laser trapping 114
3.2.3. Electrostatic principles 118
3.3. Scientific challenges 122
3.3.1. Modeling 122
3.3.2. Design 129
3.3.3. Perception 131
3.3.4. Control 131
3.4. Experimental devices 132
3.4.1. Laser trapping 132
3.4.2. DEP systems 139
3.5. Conclusion 147

Chapter 4. Toward Biomedical Nanorobotics 149

4.1. Applicative challenges 149
4.1.1. In vitro applications 149
4.1.2. Nanoassembly for biomedical applications 150
4.1.3. In vivo applications 150

4.2. Scientific challenges 150
4.2.1. New paradigm removing frontiers between sciences. 150
4.2.2. Energy sources 151
4.2.3. How far away is this future? 152

Bibliography 153

Index 183

Introduction

For almost 30 years, research in medical robotics has led to many prototypes that have been validated technically, and some clinically. There are many specialties in this regard. Orthopedics, neurosurgery, endoscopic microsurgery (mainly gynecology, urology, fetal surgery, etc.), cardiac, thoracic and vascular surgery, ear, nose and throat (ENT) surgery, etc., are a few among others.

It is clear that robotics may facilitate surgical approaches such as minimally invasive surgery (MIS), natural orifice transluminal endoscopic surgery (NOTES), single port access (SPA) surgery and interventional radiology, and it is very promising in microsurgery. We list in Table I.1 some benefits for the patient and the surgeon of robots in the operating room (OR). To summarize, surgical robotics may contribute to less invasive and more accurate surgical gestures. It may also be useful in transcending human limitations.

Considering the benefits, it is surprising that only a few prototypes have managed to find their way into OR or medical offices. Several reasons are generally raised of which a few of the most important are given below:

− The cost issue: the cost effectiveness of robotic systems has not yet been proved. Several factors worked against it: the cost of the OR is increased; a technical team is required; the surgical team has to be trained; the setup and 'skin-to-skin' times are longer than conventional procedure. The compatibility with the cluttered environment of the OR should also be improved: the robots are still too bulky; quite often, the weight, dimension

and footprint of the robot are out of proportion with respect to the force it has to exert and the workspace it has to cover during an operation.

− The clinical added value: as noted in the report of the IARP Workshop on Medical Robotics[1], the medical added value has to be improved: *Medical robotics suffers from a "chicken and egg" phenomenon in the sense that systems need to be developed before they can be tested clinically, but only through the latter will their true effectiveness and utility be proven […]*.

− Safety issues: a medical robot is a complex system that consists of (1) an articulated and motorized mechanical structure, (2) a human–machine interface, (3) electronic components and (4) a software controller. These components are used to perform operations in a constrained and not fully structured environment, inside and/or outside of the patient's body, in cooperation with the surgeon, and in the presence of the medical staff. Thus, it is easy to understand that a system failure or dysfunction can be extremely critical [SAN 13b].

This analysis pushes for the development of a new generation of robotic systems along three major challenges [DOM 12b]:

– Cost: they will be less bulky and less expensive than the current systems.

– Ergonomics: they will be of *plug and play*-type like most tools and equipment in the OR in order to minimize the installation time. They will also be easy to use in order not to require special technical skills of the staff. Moreover, the sensors will be sterilizable, otherwise disposable, and highly integrated into the architecture of these systems.

– Safety and medical added value: they will be increasingly less invasive and will not significantly extend the duration of the intervention. Moreover, the doctor/robot interfaces will be specifically designed to facilitate the implementation while ensuring that the level of operational safety is as high as possible.

1 http://www.nsf.gov/eng/roboticsorg/IARPMedicalRoboticsWorkshop Report.htm.

Fields of application	Potential benefits to the surgeon	Potential benefits to the patient
– Orthopedic surgery	– ↗ Precision – Possibility of carrying out complex cutting, drilling, milling – Integration of multimodal preoperative and intraoperative information (vision, force) – ↗ safety (virtual fixture)	– Less revision surgery – Expected longer lifetime of prostheses
– Minimally invasive endoscopic surgery	– 3rd hand – Greater comfort – Elimination of the fulcrum effect – Additional internal mobilities – Compensation of physiological movements	– Toward an increasingly less invasive surgery and without visible scars
– Neurosurgery – Interventional radiology – Radiotherapy	– ↗ Precision – ↗ Safety (avoidance of vital structures) – Compensation of physiological movements – ↘ Exposure to radiations – Precise spatial tracking of the dosimetric planning	– ↘ Invasiveness – Early treatment of increasingly smaller tumors – ↘ Exposure to radiations of healthy tissues
– Microsurgery	– Downscaling of the forces and displacements – Surgeon's tremor filtering	– Development of innovative procedures beyond the accuracy limits of the surgeon

Table I.1. *Medical robots: benefits for the surgeons and patients*

The above specifications (cost, ergonomics and safety) imply that the future surgical robots should be smaller and dedicated to a limited number of

functionalities with a certain level of autonomy appropriate for the complexity of the task they are supposed to achieve. In any case, the surgeon must maintain control of the gesture no matter what, at any time of the operative or exploratory procedure. From this observation, we understand that for many surgical applications, it makes sense to integrate the mobilities and the sensors inside the body rather than outside. In other words, rather than manipulating a multimillennial rigid instrument (like scissors or clamps) with an extracorporeal robot, the idea is to develop intracorporeal robots, offering at least the same performance of movement quality, safety and interaction with the doctor.

Surgical robotics raises several ethical issues that should be addressed very early in the design process. Some of them are covered by regulations already applicable in the pharmaceutical and medical equipment industry. For intracorporeal robotics, specific issues arising from miniaturization should also be addressed, but they have not yet received the attention they require. The IEEE Robotics and Automation Society[2] has launched a Technical Committee on Roboethics[3] to provide a "framework for taking care of ethical implications of robotics research". A biannual workshop dedicated to the subject has been organized in conjunction with the IEEE International Conference on Robotics and Automation (ICRA) from 2005 to 2011. A Workshop on Legal, Economic and Socio-Ethical Implications for the Next Generation of Robots[4] was held at ICRA 2013. It was organized by the partners of the FP7 project RoboLaw[5]. One can also refer to the pioneering initiative of G. Veruggio[6] in the framework of the European Robotics Research Network (EURON) and the work of R.C. Arkin[7] at Georgia Tech as other entry points to the subject.

Crossing the border of the skin opens up new clinical horizons but requires overcoming several technical barriers. These barriers depend on the size of the biological objects to be manipulated: organs, tissues, cells and internal components of cells. The latter are at nanoscale while the cell size is mostly below 100 μm and usually around 5 to 10 μm. The physical principles that describe the behavior of the objects are different according to their size: the dynamics of large micro-objects (e.g. 100 μm) is limited by inertia while

2 http://www.ieee-ras.org/.
3 http://www.ieee-ras.org/robot-ethics.
4 http://www.robolaw.eu/ws_icra2013.htm.
5 http://www.robolaw.eu/index.htm.
6 http://www.veruggio.it/.
7 http://www.cc.gatech.edu/aimosaic/faculty/arkin/.

the dynamics of smaller objects (e.g. 1 μm) is limited by viscosity. It is then convenient to divide the world into the following groups:

– The macroworld is dominated by volume effects (inertia and weight).

– In the microworld, volume effects (dielectrophoresis and magnetophoresis), surface effects (van der Waals' force) and linear effects (viscous force) are balanced.

– The nanoworld is dominated by surface effects and linear effects.

In this book, we will consider four scales of object sizes, which are justified by the class of problems encountered and the solutions implemented to manipulate objects and reach targets within the body (note that the size of the object has no evident relation to the size of the device that manipulates it):

– At milliscale (Chapter 1), the dimensions of the objects range from a few millimeters to a few centimeters, and the forces required to manipulate tissues range from a few millinewtons to several newtons. Most of the robotic systems at this scale use the manipulation principles of the macroworld.

– At microscale (Chapter 2), comprising objects below 1 mm up to 10 μm, the forces are in the order of tens of nanonewtons up to a few millinewtons. Original manipulation principles under magnetic field or by swimming in a liquid media have been validated.

– At mesoscale (Chapter 3), between 100 nm and 10 μm, the forces range from piconewtons to tens of nanonewtons. We have introduced this term to designate a scale where the contact with any tool could destroy the object, which requires implementing non-contact manipulation principles.

– At nanoscale (Chapter 4), between 1 nm and 100 nm, the manipulation of objects is still a challenge that will require a paradigm change. As will be discussed, progress will depend on multidisciplinary research bringing together biology, chemistry, robotics and, more widely, engineering sciences.

The book reviews the physical principles as well as the scientific and methodological challenges that have to be tackled to design and control intracorporeal robotic systems at each of the above-mentioned scales. The most prominent devices and prototypes of the state of the art are described in the first three chapters to illustrate the benefit that can be expected for

surgeons and patients. In Chapter 4, we will discuss perspectives on nanorobotics.

To conclude this Introduction, let us recall that a robot is defined as *"an actuated mechanism programmable in two or more axes with a degree of autonomy, moving within its environment, to perform intended tasks"* (ISO 8373:2012 document). Devices that use robotic or mechatronic technologies or components found in robots but unable to carry out autonomous motion should be referred to differently (e.g. robotic system, robotic manipulator and robotic positioner). For the sake of simplicity, the term "robot" will be used more widely for any programmed, teleoperated or comanipulated device.

Chapter 1

Intracorporeal Millirobotics

1.1. Introduction

Intracorporeal millirobots are at the boundary of conventional surgical robots that are installed in the operating room (OR) along the table or on the patient. They still work in the macroworld, where volumic forces and torques (such as weight) dominate. Under this designation, we mean devices with either partially or fully intracorporeal actuated degrees of freedom (DoFs). Their dimensions in the body can reach at the maximum a few tens of millimeters. The dimensions of the surgical site range from a few millimeters to a few centimeters; however, when it is mobile, the millirobot may cover a workspace of several cubic centimeters. The forces exerted on tissues by the robot range from a few millinewtons to several newtons, up to tens of newtons for retraction of organs or gripping a needle.

At this scale, many prototypes have been developed, even though very few of them have entered the OR. In many cases, they look like conventional robots for which rigid body kinematic models and vision-based or force-based control algorithms may be used. More or less, they could be seen as miniaturized versions of existing solutions.

However, to comply with the environment constraints (biological tissues, safety, etc.) and the task constraints (access to deep anatomical spaces, preservation of vital structures, high dexterity, etc.), many efforts have been made to design original kinematics with advanced sensing capabilities for manipulation and locomotion purposes. A promising approach is now to

integrate robotics in instruments rather than to think of the robot as a simple instrument holder.

In section 1.2, we will present a variety of millimetric devices providing intracorporeal manipulation and/or mobility capabilities. In section 1.3, we will address scientific issues that are specific to robotics at milliscale. These issues cover the main fields of robotic research in modeling, design, actuation, sensing and control. In section 1.4, we will present in more detail three robotic systems that are representative of the state of the art at the milliscale: a dual-arm master–slave system, a snake-like robot made up of concentric tubes and a handheld robotized instrument.

1.2. Principles

We present in this section the principles of three classes of devices:

− partially intracorporeal devices with active distal mobilities;

− intracorporeal manipulators;

− intracorporeal mobile devices.

Their purpose is functional exploration (in the case of capsules) as well as intervention (to remove a polyp, place a stent, deliver a drug in a localized manner, etc., but also cut, retract, dissect and cauterize as in conventional surgery). Emphasis has been put on several representative devices of each class to review functional qualities and limits of potential robotic solutions. A more comprehensive review of many prototypes worldwide can be found in [DOM 12b].

1.2.1. *Partially intracorporeal devices with active distal mobilities*

Under this denomination, we mean conventional instruments that have been modified to improve dexterity and/or precision of the surgeon or the radiologist. We include, for instance, any device providing two additional actuated DoFs between the entry port in the body and the tool (retractor, forceps, needle driver, but also tip of an endoscope), not accounting for the closing/opening of the jaws of the tool if any. The partially intracorporeal device is generally attached to an external device that can be a robot providing supplementary DoFs. It is driven externally by the surgeon, either directly in a comanipulation mode (section 1.3.5.3) or from a master workstation in a teleoperation mode (section 1.3.5.2) (Figure 1.1).

With such a definition, we consider entering into this class the actuated instruments for endoscopic surgery and the catheters. Typically, the diameter of these instruments is restricted to 8–10 mm in abdominal surgery, 5–6 mm in cardiac surgery, even 2.5–3 mm for intrauterine fetal surgery [HAR 05, ZHA 09a], 0.5–2 mm for an active catheter.

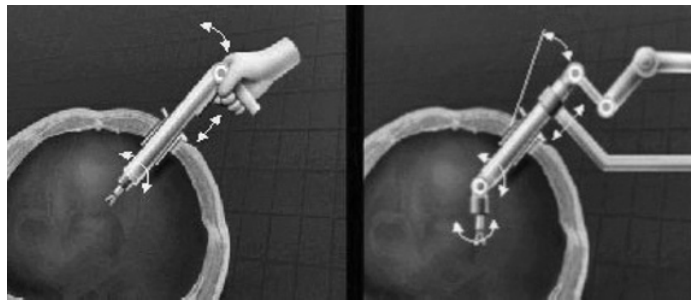

a) b)

Figure 1.1. *Partially intracorporeal DoFs: a) comanipulated instrument; b) teleoperated instrument [SAL 04]*

1.2.1.1. *Actuated instruments for endoscopic surgery*

As opposed to open surgery, endoscopic surgery has revolutionized surgical practice since the early 1970s. Often referred to as minimally invasive surgery (MIS), it reduces postsurgery wounds, the risk of infection, the recovery time and the cost of treatment. But it suffers from a certain number of shortcomings: loss of internal mobility due to kinematic constraints induced by the trocar, hand–eye coordination due to the inversion of directions of motion of the hands and the tool tip, loss of force and tactile feedback, restricted workspace and surgeon's fatigue. These limitations have motivated the development and introduction of robots in the OR. Since the mid-1990s, with the robotic systems ZEUS (Computer Motion[1]) and Da Vinci (Intuitive Surgical[2]), master–slave architecture has been adopted for MIS: the instruments are carried by two or three slave manipulators teleoperated by the surgeon from a remote master console. Along the same lines, it is worth mentioning the platforms Raven II from University of Washington [HAN 13] and MiroSurge from DLR [HAG 10] that are dedicated to research in robotic surgery.

1 Merged with Intuitive Surgical since 2003.

2 http://www.intuitivesurgical.com/.

In these systems, the active part of each instrument may have up to two actuated DoFs (not including actuation of the gripper) mounted at the distal end of a rigid hollow tube through which the driving cables pass (Figure 1.2, left). Such additional DoFs may also be mounted at the distal part of a lightweight handheld system (Figure 1.2, right) that gives the surgeon the ability to comanipulate the instrument without using a master arm [ZAH 10]. In both cases, the additional pan and tilt rotations compensate for the loss of mobility induced by the constraint of passage through the trocar.

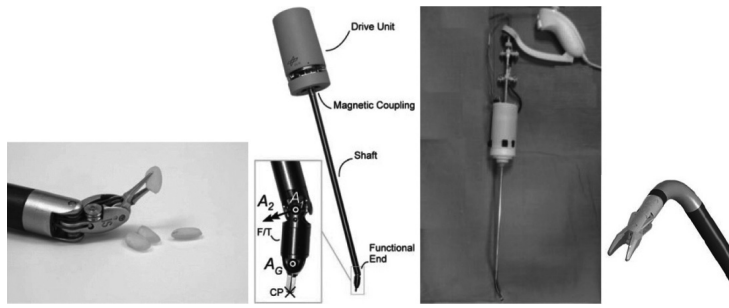

Figure 1.2. *From left to right: close-up of the Da Vinci Endowrist tip manipulating rice grains; DLR MICA instrument of the MIRO platform for endoscopic surgery and close-up of the two-DoF wrist mounted with a force/torque (FT) sensor [HAG 10]; the EndoControl*[3] *handheld laparoscopic instrument JAiMY [ZAH 10]; close-up of the two-DoF bending and rotary wrist of JAiMY*

1.2.1.2. *Actuated catheters*

A catheter is a thin (a few millimeter in diameter), long (of the order of a meter) and hollow tube that allows the passage of functional catheters of smaller diameter. These may hold various miniature sensors (pressure, ultrasound probe, optical fiber, etc.) or instruments, e.g. for the local administration of a drug, the insertion of a prosthesis (stent, angioplasty balloon, etc.), the endovascular coiling of aneurysms, the puncture/biopsy for diagnostic purposes or tumor destruction (radiofrequency abalation, laser therapy, etc.) [CHA 00]. The catheter is inserted into an artery, usually in the groin. It is steered, under radiographic control, by the doctor who rotates it around its longitudinal axis and pushes it to its destination. This is made difficult because of the narrowness of the vessel, the frictions on the wall and the many bifurcations. The difficulty for the surgeon is thus to transmit force and motion to the end effector with little or no relevant kinesthetic feedback,

3 http://www.endocontrol-medical.com/.

and with a restricted and sparse visual feedback to limit the radiation doses, while avoiding perforation of the artery.

An active catheter is shown in Figure 1.3 [SZE 11]. It is endowed with guidance abilities to facilitate its introduction in bifurcations that exhibit restrictive directions (including very acute closed angles). There are some similarities between an active catheter and a teleoperated robotized colonoscope, however, the diameter is nearly one order of magnitude lower, typically 1–2 mm (the diameter can be reduced to 0.5–1 mm in the case of a guidance catheter). The other difference, and the major difficulty, is that the catheter must move in an artery where the pressure and the blood flow are important. Many prototypes of active catheters have been developed over the last 10 years where many actuation concepts have been explored as will be presented in section 1.3.3.

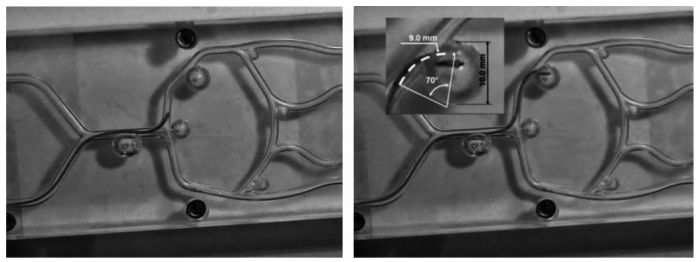

Figure 1.3. *Navigation of an active catheter in a phantom of an aneurysm in the Willis Polygon (Ø = 1.1 mm, radius of curvature = 9 mm) [SZE 11]*

To protect the surgeon against radiation, master–slave systems, which allow the doctor to remotely control the catheter, are now available, such as the Sensei X Robotic System, and more recently the Magellan Robotic System, both marketed by Hansen Medical[4], or the Amigo RSC from Catheter Robotics[5]. These systems offer a steering unit that pushes and allows bidirectional rotations of the catheter tip.

1.2.2. *Intracorporeal manipulators*

We give the name intracorporeal manipulators to any device providing full (or at least more than 2) mobility to the tool with actuated DoFs located

4 http://www.hansenmedical.com/.

5 www.catheterrobotics.com/rcs-main.htm.

between the entry port in the body and the tool. These devices may be minimanipulators (scaled version of conventional robot arms) or flexible instruments designed to perform new techniques of surgery without visible scaring. We also include in this class modular approaches aiming at assembling and disassembling (or possibly deploying and retracting) robots and platforms within the body.

1.2.2.1. *Minimanipulators*

Typically, minimanipulators have a centimetric size, generating submillimetric to centimetric displacements and can exert forces of the order from 1 N (e.g. to insert a needle into a coronary artery) to several tens of newtons to retract tissue. Different options may be adopted in the design:

− discrete architectures with embedded actuators;

− discrete architectures with remote actuators (outside the patient);

− continuum architectures (or snake-like or elephant trunk like architectures) with remote actuators.

Discrete architectures have a limited number of rigid links and discrete joints. A first example of such robot with embedded actuators, designed for *natural orifice transluminal endoscopic surgery* (NOTES) (section 1.2.2.2), is shown in Figure 1.4 [LEH 08, TIW 10]: it consists of two prismatic arms each connected to a central body by a revolute joint, together providing four planar DoFs. Each arm is fitted with either a grasper forceps or a cautery end effector. The central body contains a stereo camera pair and magnets that interact with external magnets to attach the robot to the interior abdominal wall. It is inserted through the esophagus and into the peritoneal cavity using an overtube in a configuration where the arms are disconnected from the central body.

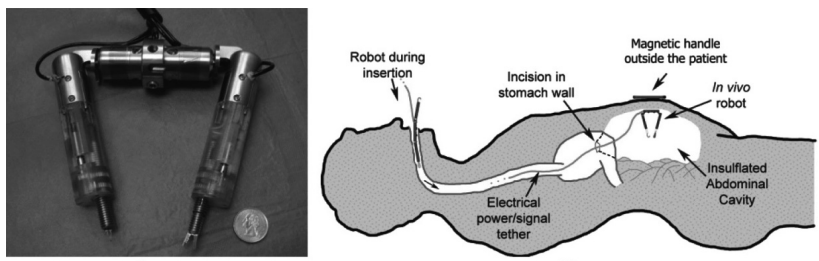

Figure 1.4. *a) In vivo two-arm dexterous robot from Vanderbilt University; b) NOTES procedure [LEH 08, TIW 10]*

Another example is the modular robot DRIMIS [SAL 04] (Figure 1.5(a)), which is the result of an optimization procedure using multiobjective evolutionary algorithms, coupled with a realistic simulation of the intended surgical task (anastomosis during coronary artery bypass grafting). Several one-DoF and two-DoF modules (Ø 10 mm, 25–40 mm long) were designed with different axis organization. Typically, a six-DoF arm is 120 mm long.

The arms of the dual-arm robot SPRINT have a similar kinematics. The platform was developed in the frame of the EU FP7 Araknes project[6] [PIC 10, SAN 11] (Figure 1.5(b)). Each arm has six DoFs plus the gripper. Four additional DoFs are provided by the external positioning device. In its current version, the size is 18 mm in diameter and 120 mm in length. It can exert forces up to 5 N. The robot is intended to be attached to the umbilical access port in *single-port access* (SPA) surgery (see section 1.2.2.2). A detailed description of the system is presented in section 1.4.1.

Figure 1.5. *Architectures with rigid links and discrete joints: a) DRIMIS (ISIR) [SAL 04]; b) SPRINT (Araknes project) [PIC 10, SAN 11]*

When miniature actuators are embedded in the structure, one of the difficulties is the routing of the electrical cables, another is the small power-to-weight ratio of the actuators available at this size, dramatically restricting the forces that can be exerted by the robot on tissues. The latter no longer holds with remote actuators. However, remote actuation implies using mechanical wires to drive the joint, which is a more tricky issue than routing electrical cables. An example of such an architecture designed by Ikuta *et al.* [IKU 03] is depicted in Figure 1.6: the Hyper Finger (Mark-3) is a seven-DoF (including the forceps griping action) wire-driven active forceps for laparoscopic surgery (Ø 10 mm). A special decoupled two-DoF "ring-joint"

6 http://www.araknes.org/home.html.

mechanism was developed, where each DoF can be driven independently. It is teleoperated with an analogous seven-DoF master finger.

An interesting alternative to the discrete aforementioned minimanipulators is the continuum robots. They have a smaller outer diameter with comparable performance specifications [XU 12]. They more or less extend the design used for bending the tip of active catheters. The actuators are placed outside the patient, pulling cables or "tendons" of different technologies to control distributed stiffness and curvature, as will be discussed in section 1.3.3. Zhang *et al.* [ZHA 11] have designed a six-DoF wire-driven robotic manipulator for fetal surgery, namely to place a detachable silicone balloon in the fetal trachea for treatment of congenital diaphragmatic hernias. The robot is constituted of three units, each having two DoFs. The size is 2.4 mm in diameter. The contact force of the robot is controlled to be less than 0.3 N.

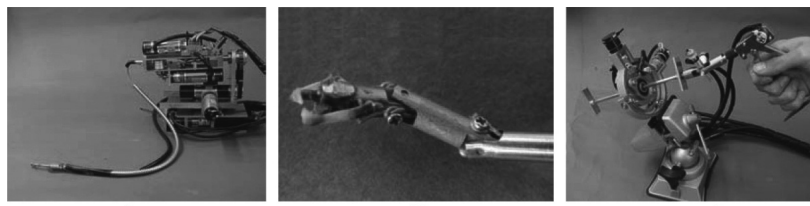

Figure 1.6. *Hyper Finger [IKU 03]: a) seven-DoF slave manipulator at the end of a guide tube; b) close-up of the seven-DoF manipulator; c) master manipulator*

To navigate in a constrained operating workspace, circumventing vital organs and risky areas, a higher number of DoFs is required. HARP (highly articulated robotic probe) is a continuum and hyper-redundant robot proposed by [DEG 06, OTA 08] for pericardial interventions. It is made up of two snake-like concentric tubes (Figure 1.7) that can maintain the three-dimensional (3D) shape of the path they follow: each snake can be rigid or limp, and HARP progresses forward by alternating the rigidity/limpness of both snakes. Each snake consists of 50 rigid cylindrical links articulated by spherical joints (±15° in both directions) and strung together by cables (four for HARP). It is 12 mm in diameter, 300 mm in length and can achieve a 75 mm radius of curvature (reduced to 35 mm in a later version). The flexibility of each tube varies according to the tension of the cables. This

technological approach is now integrated into the robot-assisted platform of Medrobotics[7].

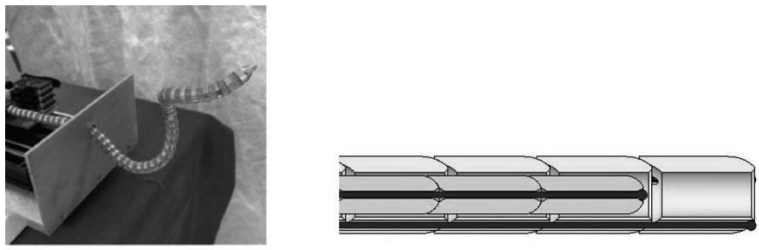

Figure 1.7. *Continuum architecture: a) HARP [OTA 08]; b) side cross-sectional view of the two concentric snakes [DEG 06]*

An interesting concept, proposed by Dupont [SEA 06] and Webster [WEB 06a], consists of several pre-bent concentric hollow tubes made up of a super-elastic material such as Nitinol (Nickel Titanium alloy also referred to as NiTi). The resulting snake-like robot (Figure 1.8) may deform continuously by independently translating and/or rotating each tube with respect to the tube in which it is inserted. It has several advantages: it is lightweight; it can be customized in diameter and length to meet the requirements of the operation at hand; it has a very good dexterity and can be deployed while avoiding vital structures; knowing its stiffness makes it possible to evaluate the interaction forces with tissues. We will discuss more in detail design and modeling issues associated with such a robot in section 1.4.2.

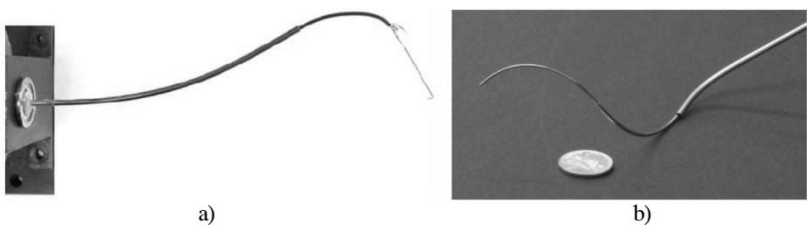

Figure 1.8. *a) Prototype of a miniature concentric tube robot of Boston University grasping a needle [SEA 06];b) prototype of JHU [WEB 06a]*

7 http://www.cardiorobotics.com/.

1.2.2.2. *NOTES and SPA devices*

Two new paradigms of surgery are currently being developed within the field of MIS: the transluminal surgery, also known as NOTES [JAG 05, PAR 05], and the surgery through single trocar or single incision [PIS 99, DAL 02], also known as SPA surgery. The common point of these techniques is the absence of new visible scarring as the entry port for the instruments is the mouth, the nose, the anus, the vagina or the urethra for NOTES, or the umbilicus (that can be seen as a cicatrized natural orifice) for SPA. NOTES and SPA are intended to further reduce postoperative complications compared to traditional laparoscopic MIS. This is not yet in common clinical practice, even if hundreds of operations have been performed in preclinic tests on humans worldwide (cholecystectomies, appendectomies, tubal ligations, hysterectomies, gastric sutures, colic sutures, etc.) [MAR 07a, SWA 07].

For NOTES, the technique relies on the use of cable-driven flexible endoscopes with flexible instruments passing through service channels, with which the surgeon can reach and operate the targeted internal organ. Dedicated prototypes have been developed, with additional DoFs to provide enough mobility to the instruments as the examples in Figure 1.9 depict. However, the manipulation is difficult and non-intuitive for a surgeon alone due to the high number of DoFs and the flexibility. One solution is to require the assistance of a second surgeon, another is to robotize the flexible endoscope such that it can be operated by one surgeon from a master robot. As underlined in [TIW 10], robotics may provide better visualization, precision and maneuverability in large cavities, fine motor control of endoscope distal tip and enhanced surgical dexterity.

Figure 1.9. *Manual flexible endoscopes for NOTES: a) tip of the R-Scope from Olympus Optical; b) Cobra from USGI Medical: the flexible sheath is rigidly lockable at any time in a desired configuration; c) close-up of the tip of Cobra*

An example of a robotized endoscope for gastrointestinal (GI) procedures is shown in Figure 1.10(a). It shows the 3D model of a two-arm manipulator attached to a flexible endoscope [LOW 06], each arm having five DoFs, not accounting for the opening/closing of the end effector. Tendon-sheath actuation is used. The arms are teleoperated from a master system. The size of the whole manipulator is approximately 25 mm in diameter. Compared with conventional colonoscopes with working channels through which a tool can be inserted, for instance, to cut a polyp, such manipulator may serve to perform more dexterous actions such as suturing.

Another concept was implemented in the prototype of the Anubis project [BAR 12] as shown in Figure 1.10(b). It consists of a flexible endoscope (from Karl Storz Endoskope GmbH) and two flexible hollow arms. Each of these three parts is made up of a long flexible passive shaft and an articulated distal tip. The hollow arms are fixed on the circumference of the main endoscope at the end part of its bending tip. This is done due to a special end cap that deflects the arms from the main direction of the endoscope to provide triangulation between the arms and the endoscope. The distal tip of each arm provides two DoFs to which the translation and rotation of the instrument inside the arm should be added.

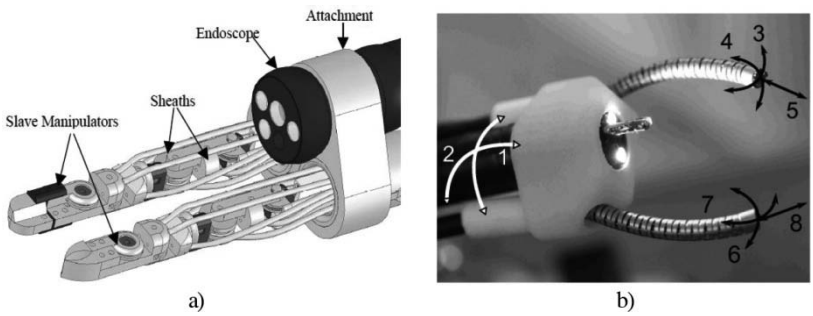

Figure 1.10. *Robotized endoscope for NOTES: a) a two-arm manipulator attached to a flexible endoscope from Nanyang University, Singapore [LOW 06]; b) head of the prototype of Anubis project [BAR 12]*

Several technical and scientific issues are still open and research works are underway in many places to extend this endoluminal approach to more demanding therapeutic procedures. To list a few, progress is required in the design to transmit enough forces for performing the desired task, to improve triangulation for better visualization, etc., while continuing miniaturization. Progress is also required in control to better stabilize the surgical tools once

on the operating site, to compensate for flexibilities, backlashes, dead-bands, etc., in order to improve precision and dynamics.

Concerning SPA, the challenge is in the design of the trocar and instruments going through it, such that they are deployed inside the abdominal cavity in an optimal working configuration. In other words, they should not collide with each other while offering sufficient triangulation to provide enough dexterity and field of view. A few products for manual procedures are now on the shelves such as, for instance, the ASC Triport and Quad-port[8] or the X-Cone from Karl Storz[9] (see, for instance, [NET 09] for a survey of the techniques and devices or more recently the slides of R. Brandina[10]). Intuitive Surgical has also developed a 5-lumen port[11] for SPA surgery with dedicated curved instruments to go with it (incision of Ø 20–25 mm).

Several ongoing projects aim at robotizing the instruments in order to provide teleoperation functionalities to the surgeon. For instance, the insertable robotic effectors platform (IREP) [BAJ 12] (Figure 1.11(a)) is composed of two seven-DoF continuum arms (not accounting for the grippers' action), each equipped with a one-DoF rotary wrist, two two-DoF continuum segments and a two-DoF planar translational module. It is completed with a three-DoF stereo vision module. It requires only a 15 mm diameter incision.

The ViaCath (Figure 1.11(b)) made use of many components developed originally for the Laprotek, the former robotic system for laparoscopy of EndoVia Medical. It has also seven DoFs, consisting of a rotary wrist and two continuum segments as well, but here a segment has two-DoF bending motion and a third DoF varying length by compression. Moreover, the segments do not have the same length (10 mm and 25 mm, respectively) to optimize the range of motion and force capabilities (0.5 N of lateral force). Figure 1.11(c) shows two ViaCaths and an endoscope surrounded in a Ø 19 mm overtube [ABB 07].

8 http://www.advancedsurgical.ie/.

9 https://www.karlstorz.com/cps/rde/xchg/SID-418D6111-3FA54782/karlstorz-en/hs.xsl/8880.htm.

10 http://fr.slideshare.net/urovideo/single-port-technologies.

11 http://www.intuitivesurgical.com/products/davinci_surgical_system/da-vinci-single-site/.

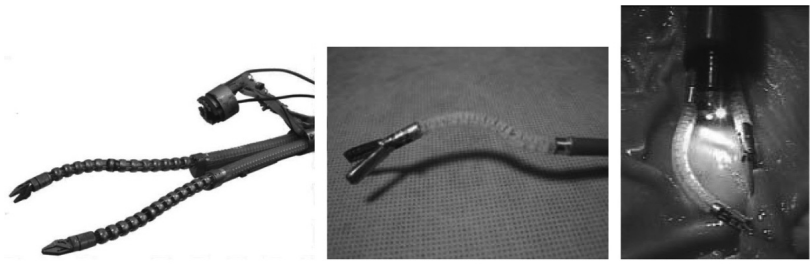

Figure 1.11. *Robotized instruments for SPA: a) IREP from Vanderbilt and Columbia Universities [BAJ 12]; b) the ViaCath instrument c) in a dual-arm configuration [ABB 07]*

Another seven-DoF arm, again with a rotary wrist but with three two-DoF continuum segments, can be found in [XU 09]. Xu and Zheng [XU 12] have shown that a structure consisting of two segments with a varying length, such as the ViaCath, generates the best distal dexterity when compared to a structure with a translational module, such as the IREP, or a structure with three segments. In their work, the distal dexterity is defined as the solid angle swept by the axis of the arm's gripper at selected points in the robot workspace. For them, such a structure would not only generate a larger workspace but would also allow surgeons to better orient tools as desired.

1.2.2.3. *Modular robots and platforms*

To minimize further the invasiveness of operations, it is necessary to make use of more complex instruments, which are necessarily more bulky, or to realize gestures that simultaneously involve several instruments. It can be envisioned to introduce them as spare parts of the trocar and then to proceed to an intracorporeal assembly. At the end of the procedure, the system is disassembled and taken out: in [OHS 08], an assemblable three-fingered five-DoF hand (Ø 5–6 mm, length 61–67 mm depending on the finger) was designed to handle (push, lift, dislocate, etc.) the organs in the abdominal cavity (Figures 1.12(a) and (b)).

Another solution is to introduce deployable instruments, for instance, in [OLE 05] a camera mounted on a pan-tilt turret (Ø 15 mm) equipped with stabilization legs folded during the passage through the trocar. It is simply deposited in the abdominal cavity, providing the surgeon with a global view of the operative field that advantageously supplements the standard endoscopic vision. More complicated is the skillful detachable-fingered hand

described in [TAK 07] to retract organs during laparoscopic surgery (Figure 1.12(c)). It aims at replacing one of the surgeon's hands during hands-assisted laparoscopic surgery (HALS), a technique indicated in complex procedures when the conventional laparoscopic instruments cannot do the work. The three fingers are inserted through a trocar and mounted on a rod inside the abdominal cavity. Therefore, the size of the trocar constrains the diameters of the fingers and of the rod (respectively Ø 8 mm and Ø 12 mm for the version where the fingers are independently driven). The fingers must be easily assembled and disassembled without exerting excessive force in the abdominal cavity.

a) b) c)

Figure 1.12. *Modular robots: a and b) three-fingered five-DoF assemblable hand [OHS 08]; c) detachable-fingered hand to retract organs during HALS [TAK 07]*

A yet more complicated concept is the modular robot designed for the exploration of the GI tract discussed in [HAR 09]. The modules are swallowable and assembled in the stomach cavity (Figure 1.13(a)). The resulting robot is self-reconfigurable to meet the size constraints that it comes across and the tasks it has to perform. A two-DoF structural module was prototyped (Figure 1.13(b)), containing a battery, two brushless motors and a dedicated control board embedding wireless functionalities. The module size (Ø 15.4 mm, length 36.5 mm) should still be miniaturized. Two permanent magnets are attached at each end of the module for self-aligning and docking purposes. A biopsy module has also been developed with compatible components to fit the structural modules. Derived from this concept, the primary goal of the Araknes project was to introduce into the stomach, via the esophagus, centimeter-sized robots (Figure 1.13(c)), each with a very specific function, and to organize them into a network so that they cooperate to achieve common tasks in bariatric surgery (gastroesophageal reflux, stomach stapling, etc.).

Figure 1.13. *Modular platforms: a) artist view of the assembly in the stomach from elementary modules of a reconfigurable platform and b) CAD drawing of a structural module [HAR 09]; ARAKNES project: c) artist' view of the deployment in the stomach of a network of minirobots*

Nagy *et al.* [NAG 07, NAG 08] went further toward miniaturization, also using small permanent magnets as the driving mechanism of self-assembling modules. A magnetic self-aligning hermaphroditic (MASH) connector has been designed: a small magnetic dipole (typically $3 \times 3 \times 1$ mm^3) is glued on each mating face of a module and oriented perpendicular to the connection axis as shown in Figure 1.14(a). It allows a robust and deterministic connection between modules facilitating the implementation of an intramodule communication bus. The MASH connector, associated with a long-range interaction model predicting higher attractive forces, has proven its efficiency, successfully achieving self-assembly of free-floating objects. An example of a snake-type robot is shown in Figure 1.14(b). The modules have a cylindrical shape (Ø 9 mm) with length 7 mm or 14 mm. Small cylindrical magnets (Ø 4 mm, length 10 mm) may be placed between the modules providing a one-DoF rotary joint, thus allowing the robot to adapt itself to the GI tract. The modules may be docked in commercially available pharmaceutical capsules, used as carriers for ingestion.

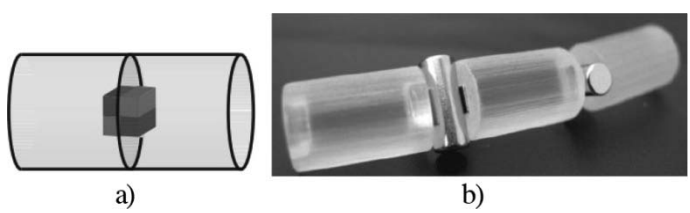

Figure 1.14. *a) Two modules connected by MASH connectors; b) self-assembled two-DoF snake-type modular robot [NAG 07, NAG 08]. Note the two cylindrical magnets between the modules acting as rotary joints*

The underlying scientific and technological challenges to design modular robotic systems are manifold: design of the instruments, sensors, miniaturization and integration of modules, wireless communication between the modules and with the master system, energy autonomy, control and monitoring, teleoperation interface, etc. From the clinical point of view, such systems will require the surgeons to review their operating procedures accordingly.

1.2.3. *Intracorporeal mobile devices*

The development of microtechnologies enables designing smaller and smaller low-cost components and integrating them onto multifunction robotized platforms. In this context, the combination of mobility and manipulation is very attractive. This synergy has proven its potential over the last two decades in field robotics. It is thought to be an efficient solution to access and treat targets that are not reachable with conventional surgical approaches.

As of today, attention has mainly focused on actuated colonoscopes and wireless capsules for endoscopy. Capsule endoscopes, passively traversing the GI tract, are now commercially available, as presented in this section. Current research aims at providing them with active locomotion capabilities. Less effort has been made on mobile devices for navigating on the surface of organs, but two examples of such devices will also be presented in this section.

1.2.3.1. *Actuated colonoscopes*

Colonoscopy, and beyond, the exploration of the GI tract, is a procedure that can effectively benefit in the short-term from advances in robotics. It allows the surgeon, among others things, to detect and remove polyps in the colon before they degenerate in cancerous lesions. It consists of introducing through the rectum a colonoscope of 10–15 mm in diameter, made up of a light source, an optical system and service channels (air, water, instruments). The gastroenterologist's challenge is to push the colonoscope up to the junction of the small intestine (typically 1.5 m from the rectum to the cecum) while controlling the orientation of the head of the instrument using rollers in order to go through colic angles. The colonoscope has a substantial intrinsic stiffness (due to the sheath containing optical fibers and cables for deflecting the head), which allows the doctor to convey the push, but induces a

risk of perforation of the wall (one case out of 2000 cases according to Wikipedia). This exam is usually done under general anesthesia in France, under simple sedation in most European countries, without sedation in some Scandinavian countries[12], in which case the action is uncomfortable, even painful for the patient.

To facilitate the guidance movement of the colonoscope and improve the quality of the clinical examination (5–20% of cancerous lesions will not be detected), several solutions are possible such as to guide the colonoscope through a flexible tube introduced previously and which is stiffened once it is positioned[13]. Other solutions are to add active distal mobilities to guide the head of the colonoscope, to integrate sensors to keep it in axial position and thus reduce the pain felt by the patient, to replace the push produced by the doctor through a self-propulsion, etc.

Originally, work in this area aimed at endowing active mobility to the head of conventional endoscopes [NG 00]. The concept has now evolved into a very lightweight architecture with a reduced diameter flexible sheath to bring the fluids, and connect an endoscopic vision system and instruments as shown in the schematic diagram of Figure 1.15(a) (below). Three examples of implementation are shown in Figure 1.15: the EMIL robot [MEN 01] which is able to move independently in the colon by taking the approach of the inchworm (Ø 12 mm, 115 < length < 195 mm). It consists of two anchoring modules (combining suction and mechanical clamping) and a pneumatic bellow acting as an extensor module. It progresses through successive sequences of extension-retraction: anchoring of the rear module, extension, anchoring the head module, retraction. The functional colonoscope of KIST [KIM 03a] is based on the same principle but improves the integration of functions such as vision, a microcamera, a steering device, a biopsy tool and a water injection channel (Ø 24 mm, 137 < length < 269 mm). A more recent prototype, the Air-emit robot [YAN 12], also inspired by inchworm (Ø 27 mm, 270 mm in length) consists of four artificial rubber muscles in series that are sequentially inflated, thus expanding in the radial direction to anchor against the intestine wall though friction. For these three examples, experiments on pigs have highlighted the limits of the locomotion principle and the friction problems caused by the flexible sheath that completely stops the progression of the device before it reaches the cecum.

12 http://www.fmcgastro.org/default.aspx?page=332.
13 http://www.usgimedical.com/endoscopic.html.

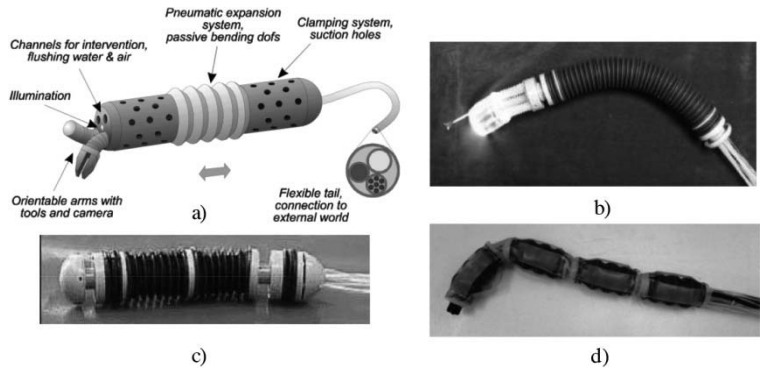

Figure 1.15. *a) Principle of robotized colonoscopy [PEI 01] and different implementations: b) KIST colonoscope [KIM 03a]; c) EMIL [MEN 01]; d) Air-emit [YAN 12]*

1.2.3.2. *Capsule endoscopes*

These capsules are swallowable and progress naturally through peristalsis with the intestinal transit. They have several hours of power autonomy. They are equipped with a light source and one or two minicameras providing images with field of view up to 170° and resolution up to 320 × 320 pixels at 4 Hz. They communicate with the outside world by radio frequency through a transmitter. At least three capsules are currently marketed (Figure 1.16): the ENDOCAPSULE 10 System from Olympus[14] (Japan), MiRO[15] from IntroMedic (South Korea) and PillCam[16] from Given Imaging (Israel). The Sayaka Capsule Endoscopy System from RF System Lab[17] (Japan) is still in development, but we can expect two major improvements such as an inner capsule rotating in a double structure capsule to capture panoramic field of views of the GI, and the absence of a battery, the power being transmitted by a coil through induction. To process the considerable mass of data recorded during an exam (up to 100,000 images), companies provide proprietary software allowing a quick and complete review of the images and providing an aid to the diagnostic.

14 http://www.olympusamerica.com/msg_section/endocapsule/.

15 http://www.intromedic.com/.

16 http://www.givenimaging.com/.

17 http://www.rfsystemlab.com/en/sayaka/index.html.

Figure 1.16. *Examples of capsules (dimensions, number of frames/s (fps), autonomy). From left to right: ENDOCAPSULE 10 System (Ø 11 mm, 26 mm long, 2 fps, 8–12 h); MIRO Cam (Ø 10.8 mm, 24.5 mm long, 3 fps,11 h), Pillcam (Ø 11 mm, 26 mm long, 2 fps, 8–12h), Sayaka (Ø 9 mm, 23 mm long, 30 fps, battery-free)*

The localization of the capsule is still an open issue for these commercial products. A capsule with accurate localization based on magnetic induction was issued by Motilis[18] (an EPFL spin-off company). Yet, the coils in the capsule take all the available space and the capsule can only track its own motion. Nevertheless, it could be very useful for diagnosing abnormal motility (i.e. digestive transit quality), which represents 75% of the troubles in the gut. More recently, Salerno *et al*. [SAL 12] proposed a method for localizing an endoscopic capsule based on an embedded triaxial magnetic sensor that achieves a centimetric accuracy.

Finally, these commercial videocapsules are still passive and need to be turned into real robots, as will be explained later in Chapter 2. The Philips IntelliCap is a good example of an active capsule [SCH 13] that, instead of a camera, embeds pH and temperature sensors to trigger local drug delivery.

1.2.3.3. *Other concepts of mobile robot*

The challenge for these mobile robots is to reach targets on the surface of an organ (e.g. the heart) or within a cavity (e.g. the abdomen) while ensuring adequate adhesion without damaging the tissues. Such robots can then naturally follow the physiological movements of organs that do not have to be stabilized. Both examples presented hereafter are tethered to convey power and motor control, to receive data from biological sensors and camera, and to perform surgical tasks through a service channel.

The *HeartLander* [PAT 05] is an original mobile device developed at Carnegie Mellon University (CMU) for beating-heart intrapericardial intervention. It intends to crawl with an inchworm-like locomotion pattern due to suction pads. Figure 1.17 shows (a) the first prototype and (b) a subsequent version. The front body is attached to three superelastic NiTi

18 http://www.mobilis.com.

wires [OTA 06]: extend, retract and turning phases are accomplished through coordination between the motors controlling the wires and the solenoid valves that regulate the vacuum pressure in each of the suction pads. The total size of both body sections together in the retracted state is 17.7 (length) × 8.2 (width) × 6.5 (height) mm^3. The device has a 1 mm diameter needle channel and a 2 mm diameter general working port.

The *Biopsy robot* from University of Nebraska [REN 06] is driven by differential rotation of two independent wheels designed with helical tread to limit slipperiness (Figure 1.17(c)). The robot is 20 mm in diameter and 100 mm long. A small camera is housed inside the robot between the wheels. The appendage visible in the middle of the cylinder is intended to prevent counter-rotation while allowing the robot to reverse direction. Biopsy forceps are also visible at the end of the appendage. A wireless version of this robot, with an improved design of the inner housing and the wheels, and with improved payload capabilities (an innovative actuated biopsy grasper and physiological sensors) is described in [PLA 08].

Figure 1.17. *Concepts of mobile manipulators for surgery: a) HeartLander first version [PAT 05] and b) subsequent version [OTA 06]; c) the Biopsy robot [REN 06]*

1.3. Scientific issues

In this section, we address scientific issues that are specific to robotics at milliscale. These issues cover the main fields of robotic research in modeling, design, actuation, sensing and control.

1.3.1. *Modeling*

Modeling for intracorporeal millirobotics may be considered at three levels: robot kinematics, interaction with soft tissues and instrument deformation (as needle during insertion). Kinematic models are necessary for

controling the robot while deformation and interaction models may improve the performance and the robustness of a force control scheme.

1.3.1.1. *Modeling of the robot kinematics*

When it is needed for control purposes, usual robotic modeling tools may be used for many devices presented in section 1.2, as their only difference with conventional robots is their size. However, modeling may be an issue for robots with a continuum architecture, such as, for instance, concentric tube robots (see section 1.4.2). It is also an issue for other complex architectures making use of compliant mechanisms such as flexure joints. As reported by Rubbert [RUB 12], these monolithic designs are very promising for surgical applications for several reasons: no backlash and assembly errors, no need of lubricant, no wear debris due to friction, rather simple microfabrication using rapid prototyping techniques, low cost thus disposable or at least sterilizable. However, they require modeling stiffness of the robot links and joints.

1.3.1.2. *Modeling of the environment*

Modeling the environment is necessary to better control the interaction between the instrument and living tissues by improving the stability and robustness of force control schemes. Here, again a trade-off has to be found between real-time constraints, the difficulty of estimating the parameters of the models and precision. On the basis of these criteria, Moreira *et al.* [MOR 12a] only retained the four linear models shown in Figure 1.18 that are composed of a single spring for the elastic model, and serial and/or parallel arrangements of springs and dampers for the viscoelastic models. The corresponding interaction forces are given in Table 1.1.

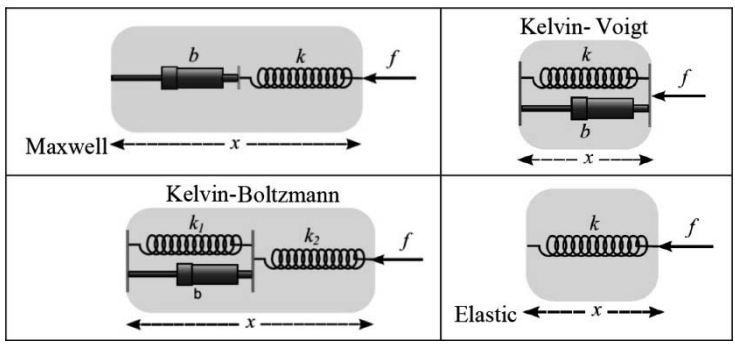

Figure 1.18. *Classical viscoelastic models for real-time uses and purely elastic model*

Model	Equation
Elastic	$f(t) = k\,x(t)$
Kelvin-Voigt	$f(t) = k\,x(t) + b\dfrac{dx(t)}{dt}$
Kelvin-Boltzmann	$f(t) = \beta\,x(t) + \alpha\dfrac{dx(t)}{dt} - \gamma\dfrac{df(t)}{dt}$
Maxwell	$f(t) = k\,x(t) + \alpha\dfrac{df(t)}{dt}$

Table 1.1. *Soft tissues model: f(t), interaction force; x(t), position deformation; k, spring stiffness constant; b, damping factor:* $\alpha = b/k$ *for Maxwell model;* $\alpha = bk_2/(k_1+k_2)$; $\beta = k_1k_2/(k_1+k_2)$; $\gamma = b/(k_1+k_2)$ *for Kelvin–Boltzmann model [MOR 12a]*

Purely elastic models cannot accurately describe interaction between an instrument and soft tissues whose viscous behavior has a strong influence, especially when fast movements are involved. Recall that stress relaxation describes how a material relieves stress under constant strain, and that creep describes how a material strains under constant stress. It comes from the derivative terms of the equations that the Maxwell model is good at predicting stress relaxation but fairly poor at predicting creep. Conversely, the Kelvin–Voigt model is good at predicting creep but fairly poor at predicting stress relaxation. Moreira *et al.* [MOR 12a] have run *in vitro* relaxation tests on a piece of beef. From position input and force output measurements, they estimated the parameters of each models. They showed that the Kelvin–Boltzmann model had the most accurate dynamic and static behavior among the four models and gave the lowest error and lowest root mean square error (Figure 1.19). This can be explained by the presence of both the force and position derivatives in the model.

1.3.1.3. *Modeling of the instrument*

Modeling the robot and the environment may not be sufficient if the instrument held by the robot has non-negligible elastic behavior. This is the case with steerable needles used during percutaneous procedures such as biopsy, drainage of fluids or brachytherapy. Compared with a conventional rigid needle, they can be actively controlled to avoid critical areas by combining insertion and axial rotation (spinning) to change the curvature of the path. Ultimately, a straight path may be achieved by continuously and rapidly rotating the needle as it is inserted. When inserted into soft tissue, Webster III *et al.* [WEB 06b] have shown that a steerable needle follows a

curved path that is prescribed by the geometry of its beveled tip (as opposed to a symmetric tip), its relative stiffness with respect to the tissue, and the insertion and rotation velocities at the needle base. They proposed to approximate its kinematic model with that of a non-holonomic unicycle vehicle (as the needle shaft follows the trajectory of the tip, a bicyle model is not required) Figure 1.20(a).

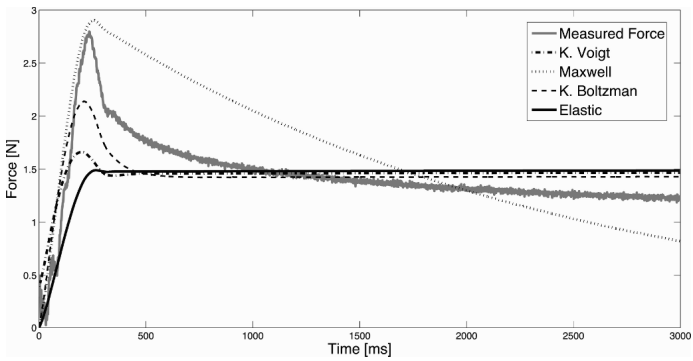

Figure 1.19. *Example of relaxation tests performed on an in vitro specimen [MOR 12a]*

Since this pioneering paper, many works have been done on planning and control of such needles. Minhas *et al.* [MIN 07] introduced the idea of "duty cycled" rotations of the needle to perform insertion with arcs of adjustable curvature. The duty cycle is defined as the ratio of time of rotation to the duty cycle period (time of rotation + insertion). The authors showed that incorporating duty-cycled spinning during needle insertion provides proportional control of the curvature of the needle trajectory through tissue. In a recent work, Bernardes *et al.* [BER 12] proposed to combine closed-loop ultrasonic feedback with an intraoperative, thus online, motion replanning strategy to compensate for system uncertainties and disturbances, and to cope with dynamic changes of obstacles (critical areas) and target positions due, for instance, to physiological motions. Figures 1.20 (b) and (c) give simulation results that confirm the relevance of the method. The work was validated *in vitro* with a six-DoF robot, five DoFs being devoted to the insertion control and one DoF to the duty-cycle control.

Several models have also been developed to estimate the deformation of tissues caused by the insertion of a needle for optimal path planning purposes (see, for instance, [DIM 03, GLO 04, VAN 11]).

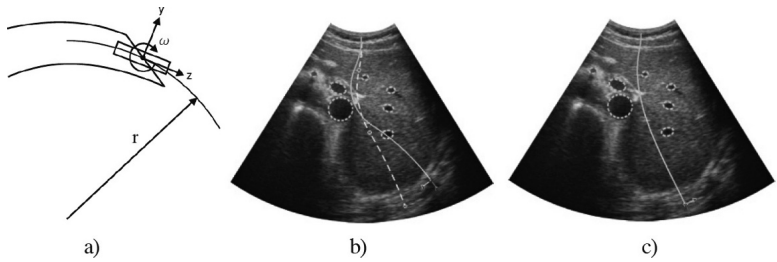

Figure 1.20. *a) Beveled tip needle during steering showing the wheel of the unicycle [WEB 06b]; b) simulated trajectories of the needle tip under disturbances and c) with adaptive replanning for noise compensation: planned path (dashed) and simulated needle trajectory (solid) [BER 12]*

1.3.2. *Design*

The design methodology at a millimetric scale may be the same as described for extracorporeal robots in [DOM 12a]:

− first, is the characterization of gestures and interactions (surgeon/robot, robot/patient, robot/environment) in order to specify the system in terms of the number of DoFs, workspace, speed, effort, precision, etc. Basically, this step requires making use of a force sensor and an optical or magnetic tracking system to collect data for further force and motion analysis;

− then, follows the choice of a kinematic structure and its actuation satisfying the specifications resulting from the characterization step and other constraints such as sterilizability, Computer Tomography (CT) and/or Magnetic Resonance Imaging (MRI) compatibility and safety;

− finally, the synthesis of a controller and the definition of the human machine interface (HMI).

The main difficulties related to the design are:

– the restrictive specifications in terms of power to be transmitted, dimensions and ranges of motion of the instruments;

– miniaturization and integration, including the passage of wires and fluid pipes;

– sterilizability of the device;

– safety, etc.

The diversity of devices presented in section 1.2 shows that conventional kinematics (serial or parallel robots) used in the macroworld cannot cover all the needs within the range of dimensions and forces at millimetric scale. Many other design choices have been explored such as multiarm devices, modular robots, continuum mechanisms, hyper-redundant kinematics, mobile robots, etc. For some applications, such as for GI screening, for instance, bioinspiration is a promising approach to design.[19]

As discussed in [MOG 07], the capsule endoscopes (section 1.2.3.2) suffer from several limitations: among others, they move passively by exploiting peristalsis and they are not able to crawl and inspect a region of interest or to anchor intentionally for a prolonged diagnosis. To give more autonomy to these capsules, several prototypes have been designed, providing them with active locomotion functions mimicking inchworm, beetle, fly, cockroach, fish, etc. Figure 1.21 illustrates some biomimetic locomotion principles (walking, swimming, paddling, etc.) involving legs, cilia, and fins and tails. The inchworm locomotion is certainly the mode that has inspired the majority of solutions. However, as noticed by Menciassi *et al*. [MEN 04], legged locomotion, which is more technically demanding in terms of mechanical hardware and control strategy, has several advantages: faster, no contact or friction with the pathological areas (that could cause ulcers for instance), better adaptation to the luminal diameter, better maneuverability, possible use of legs as a tool, etc. Another benefit is that, due to the leverage effect provided by the legs, the stroke is no longer limited by the length of the body. Finally, legs can be equipped with pads to improve adherence.

Much work has also been done to improve the clamping capabilities of the capsules, especially to avoid mechanical grippers or suction devices that may harm the intestine wall, such as, for instance, the gecko-inspired adhesives developed at the NanoRobotics Lab of CMU[20]. These solutions are alternatives to magnetic guidance that may require a cumbersome external magnetic field generator, as will be presented in Chapter 2.

19 As it is for many other non-surgical tasks. For a review, see the issue-focused section on bio-inspired mechatronics, *IEEE/ASME Transactions on Mechatronics*, vol. 18, no. 2, April 2013.

20 http://nanolab.me.cmu.edu/.

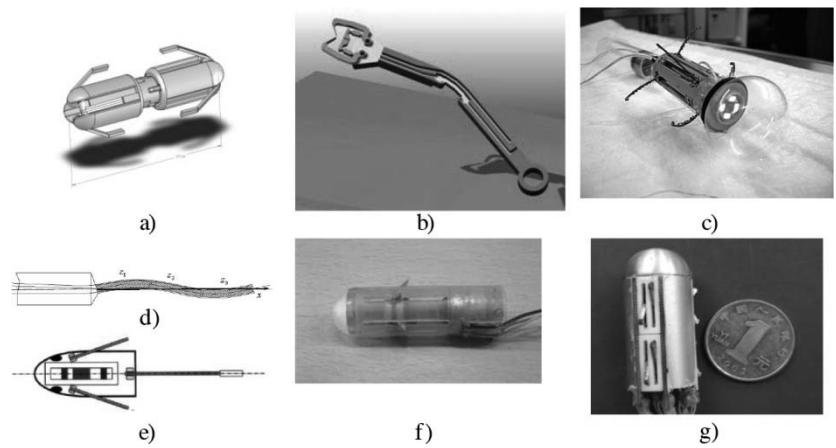

Figure 1.21. *Some examples of biomimetic devices for GI tract inspection: a) inchworm-based locomotion mechanism with legs carrying an adhesive footpad with 4 μm molded PDMS fibers inspired by beetles [CHE 05, KAR 06]; b) bioinspired leg with a compliant knee, including a mechanical grasping system at the tip [MEN 04]; c) legged robotic capsule EMILOC [MOG 07]; d) swimming microrobot with an elastic tail [KÓS 05]; e) swimming robot with fins driven by ICPF actuators (see section 1.3.3) [GUO 02]; f) paddling-based locomotion mechanism [PAR 06]; g) ciliated cell-based locomotion mechanism [LI 06]*

1.3.3. *Actuation and transmission*

The main constraints of the actuators for intracorporeal robotic devices are their biocompatibility and safety, their high output force/torque and, for autonomy, their low power consumption. Many principles of actuation have been explored so far to drive a robot at millimetric scale: conventional principles (electric, hydraulic or pneumatic) such as in the macroworld, and less conventional principles (such as ultrasonic and piezoelectric actuators that are MRI and CT compatible), but also more advanced principles based on active materials. The latter refer to material capable of converting an input energy (electrical, thermal, chemical, etc.) into mechanical work, making it possible to embed the actuation function into the material. The most widely used for intracorporeal robotics are shape memory alloys (SMAs) and electroactive polymers (EAPs). With SMAs, the active principle is a transduction of thermal energy into mechanical energy, while with EAPs it is a transduction of electrical energy into mechanical energy. The most used SMA is NiTi, made up of nickel and titanium, which has an interesting property of biocompatibility. Among the EAPs, two categories are used for

the large strain they can produce: the electric polymers that contract under the action of an electric field or Coulomb force, and the ionic polymers such as ionic conducting polymer film (ICPF) that contract under the displacement of ions. EAPs are a promising material for the development of artificial muscles. Additional information on SMA and EAP can be found, for instance, in [PON 05, BAR 04] and in section 2.3.1.1. The advantages and limitations of these principles of actuation in the context of intracorporeal robotics are summarized in Table 1.2.

In Table 1.3, we give some examples of devices (most of them have been presented in section 1.2) to illustrate the various actuation principles. For a more comprehensive review, the reader may refer to [DOM 12b].

Actuation	Advantages	Limitations
Electric actuators	– Easy to control	– Power-to-mass ratio
Piezoelectric actuators	– Low power consumption – High force output – Short response time – Power-to-mass ratio – MRI and CT compatible	– Low strain (0.1–0.2%)→ small stroke – High supply voltage → safety issues
SMA	– Actuation embedded into the mechanical structure – Large strain (up to 8%) – Low cost – Biocompatible (NiTi)	– Slow response time – Heath removal – Relatively low stiffness – Medium output force – High power consumption
EAP	– Low power consumption – Large strain (more than 10%) – Better dynamics than SMA – Low cost – Biocompatible	– Relatively low stiffness – Low output force – Integration issues

Table 1.2. *Comparative advantages and limitations of actuation principles*

Actuation	Examples
Electric actuators embedded in the mechanical structure	DRIMIS [SAL 04], Biopsy robot [REN 06, PLA 08], legged capsule [QUI 07], modular platform [HAR 09], Vanderbilt's dexterous NOTES arms [LEH 08, TIW 10], Araknes [PIC 10, SAN 11], modular platform [HAR 09]
Electric actuators remotely mounted	Hyper finger Mark-3 [IKU 03], HARP [DEG 06, OTA 08], EndoControl JAiMY [ZAH 10], most of the NOTES and SPA devices, Da Vinci EndoWrist, Artisan Extend Control Catheter (Hansen Medical), Amigo RSC (Catheter Robotics)
Piezoelectric	Multi-DoF ultrasonic motor for active endoscope [TAK 01], impact-based piezo actuator [KIM 05], swimming microrobot [KÓS 05], piezoelectric-driven laparoscopic instrument [ROS 09], MICRON handheld instrument for eye surgery [RIV 03], concentric tube continuum robot [SU 12]
Pneumatic	Heartlander [PAT 05] Semi-autonomous colonoscopes: EndoCrawler [NG 00], EMIL [MEN 01], KIST colonoscope [KIM 03a], Air-emit [YAN 12]
Hydraulic	Catheter for microneuroendoscopy of spinal cord (EU FP7 MINOSC project) [ASC 03], microhydraulic active catheters [HAG 05, IKU 06]
Magnetic	*Internal magnetic field:* active capsule endoscope [WAN 06] *External magnetic field:* swimming microrobot [GUO 05], (re)-configuration of swallowable modular robot [NAG 07, NAG 08]
SMA	Earthworm [LEE 04], ciliated capsule [LI 06], legged capsule [KAR 06], catheter [SZE 11], intracranial robot MINIR [HO 12]
EAP	Fish-like underwater microrobot [GUO 02], ciliary motion based walking robot [KIM 03b]

Table 1.3. *A few examples of actuation for intracorporeal millirobots and entry points of related literature*

The actuation principle affects the design of the robot, in particular when electric actuators are remotely mounted. For robots with a limited number of rigid links and discrete joints, the transmission of power may be made, as shown in Figure 1.22:

– by cables (textile or steel) or metal strips: the advantages (compactness, reflectivity of forces in the absence of frictions, etc.) have their counterparts (small radius of the pulleys reducing the reliability of the cables, tricky assembly, etc.);

– or by rigid linkage mechanisms such as pushes and rods: the gain in stiffness is at the expense of the compactness and simplicity of the robot.

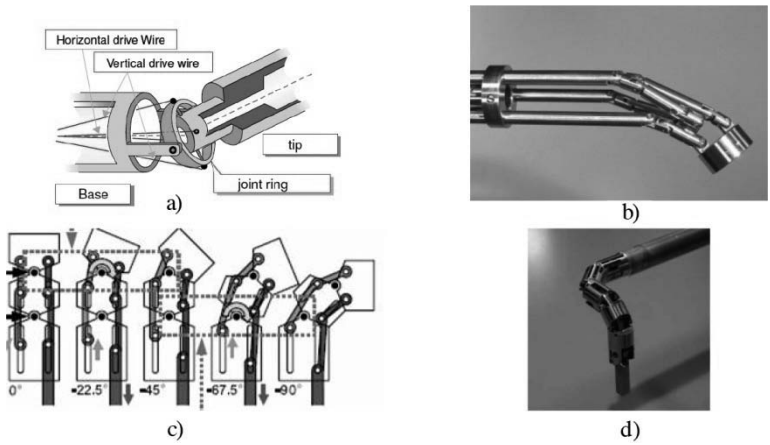

Figure 1.22. *Examples of transmission of power by cables: conceptual design of the "ring joint" of "hyper finger" (see Figure 1.6) driven by decoupled wire-drive mechanism [IKU 03] a); transmission of power by rigid linkage mechanisms: four-DoF parallel kinematic instrument tip for laparoscopy [ROS 09] b); conceptual design c) of a two-DoF bending mechanism of a forceps [YAM 03] d)*

For continuum robots, the design is more complicated and several technological possibilities have been explored. A number of prototypes have been designed based on NiTi super-elastic wires or springs/coils that allow achieving significant angular deflection with a more or less small radius of curvature. A few examples are shown in Figure 1.23, illustrating the design of joint by stacking spheres linked by tendons and the design of flexible joints.

Figure 1.23. *Examples of distributed and flexible joints for continuum robots: above, from left to right: assembly of ball joints and vertebrae to design a forceps holder [VAN 05]; conceptual design and prototype of the "distal dexterity unit" composed of a multibackbone snake-like robot equipped with a parallel tip for throat surgery [SIM 05]. Below from left to right: two-DoF bending manipulator using NiTi spring-link mechanism [ARA 10]; close-up of a machined NiTi spring used in the two-DoF forceps holder (below, right) [PEI 03]*

1.3.4. *Sensing*

At this scale, the same principles are used for vision as in extracorporeal robotics (rigid or flexible full high-definition (HD) endoscopes, which is the current resolution standard for endoscopy, with the slow emergence of on-the-shelf 3D solutions, for instance, from Karl Storz). Force sensing is still an issue, as it is in extracorporeal robotics, and has yet not been widely introduced in the OR. This can be explained by the following stringent specifications:

– From the design point of view, the force sensor has to be small, easy to mount (including the integration of electric wires), biocompatible, sterilizable or disposable (thus low cost) and reliable, all of which raise several difficulties. Typically, the forces may range from a few millinewtons (to detect and manipulate tissues) up to 50 N or more to grip a needle, with a sensitivity of a few tenths of a newton.

– From the operation point of view, the use of a force sensor requires rather complex and time-consuming calibration procedures all over again. The force data have to be properly processed to filter high measurement noise, to compensate for drifts, etc. They also have to be integrated in the control architecture of the robot, which is not possible with most of the on-the-shelf robot controllers.

However, let us recall the importance of force sensing in surgical robotics:

– to measure interaction forces between instrument and tissues for modeling and design specification purposes;

– to feedback interaction forces in a control loop in order to drive the instrument in a comanipulation mode, or to servo the contact force to a desired set point value or to compensate for physiological motions;

– to provide haptic feedback to the surgeon: as pointed out by Menciassi *et al*. [MEN 03] a critical factor in MIS is the severe reduction of sensory capabilities of the surgeon, as finger palpation to characterize tissue hardness or to estimate pulsating flow in vessels;

– to increase safety by stopping the robot whenever excessive forces between the instrument and the tissues are exerted.

During an MIS operation, if the force sensor were mounted at the proximal part of the instrument, it would also measure the forces generated by the friction of the latter due to the passage of the trocar, which can be much greater than the instrument–tissue interaction forces. Thus, different families of solutions have been explored, as summarized in Figure 1.24. The first family consists of integrating miniature sensors at the distal end of the instrument. For example, van Meer *et al.* [VAN 04] designed a sensor based on capacitive detection that was mounted in 5 mm forcep jaws with the possibility to measure forces in two directions (Figure 1.24(a)). The lower example of Figure 1.24(a) [PEI 04] makes use of optical fibers to estimate the deformations of tissues through reflective measurements (Ø 5 mm, range of 2.5 N in axial direction, 1.7 N in radial direction). The second family exploits technologies already developed in the macroworld that are based on mechanical deformation of a beam. A miniature Force/Torque (FT) sensor is placed just before the distal joint (or between the distal joint and the instrument tip) as indicated in Figure 1.24(b). At DLR, Seibold *et al*. [SEI 05] have developed such a six-DoF sensor based on a Stewart platform. Due to its dimension (Ø 10 mm), the ball joints were replaced by flexure

joints. For the set of design parameters selected, the load range is Fx,y,z = 30 N, Mx,y = 300 N·mm, Mz = 150 N·mm. The sensor is sterilizable and is now mounted on the DLR MICA instrument (see Figure 1.2) [HAG 10].

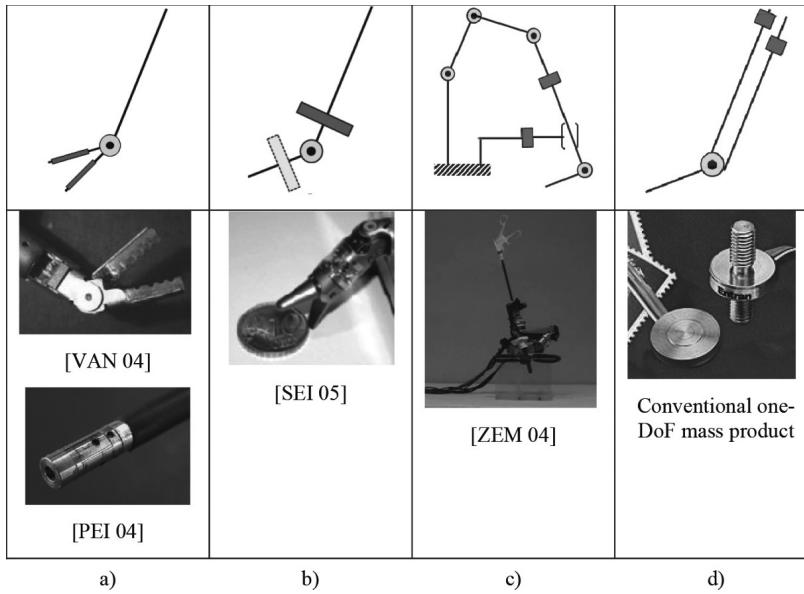

Figure 1.24. *Families of force sensing methods: a) MEMS sensors; b) multiaxis sensor; c) external measurement of interaction forces (MC²E); d) direct measurement of force in the cables when the instrument is cable driven*

The basic idea of the third family shown in Figure 1.24(c) is to make use of two conventional six-axis FT sensors (e.g. from JR3 Inc[21] or ATI Industrial Automation[22]), one mounted at the proximal part of the instrument and the other mounted on the trocar: the advantage of this approach is the reduction of costs and sterilizability constraints. An original implementation of this idea is due to Zemiti *et al.* [ZEM 04] where the instrument is placed inside a passive guidance tube (Figure 1.25(a)). The latter is attached to the upper part of the FT sensor. The lower part of the sensor is placed on a

21 http://www.jr3.com/.

22 http://www.ati-ia.com/.

conventional trocar. If the orientation of the instrument as well as its penetration are controlled by a robot holding the trocar, it is possible to estimate the tool–tissue interaction forces. Writing the generalized forces on the different moving parts, it can be shown that the interaction forces may be easily inferred from the force sensor data if the gravitational forces are known and if the forces due to dynamics are known or negligible. A dedicated device, called MC^2E (a French acronym for compact manipulation for endoscopic surgery) has been designed and validated this approach. It is lightweight and can be mounted directly on the patient. It is a four-DoF actuated mechanism providing an invariant center at the fulcrum point, a frictionless rotation and a translation, respectively, about and along the instrument axis.

The last family of solutions, standing when the distal joints of the instruments are cable driven, consists of directly measuring the cable forces with uniaxial sensors (Figure 1.24(d)). However, the drawbacks (not all the axes are measured, singularities, etc.) are not compensated for by the low cost and rather simple implementation of the sensors in the instrument.

Recently, some other physical principles have received attention. For instance, with a polymer-based touch microsensor glued around the tip of a catheter, it has been shown by Feng *et al*. [FEN 06] that it is possible to feedback to the surgeon small contact forces during intravascular neurosurgery. We already mentioned the work of Peirs *et al.* [PEI 04] estimating the interaction forces from visual information. Such an approach is implemented with the Sensei X system to drive catheter in intravascular procedures. It may require efficient instrument–tissue interaction models and high-performance computational resources to satisfy the real-time constraints of an operation. DiMaio *et al.* have used a 2D linear elastostatic material model, based on finite elements, to derive contact force information during needle insertion, which was processed for graphical and haptic real-time simulation [DIM 03] (Figure 1.25(b)). Basically, this vision-based haptic feedback mimics what the surgeon does in endoscopic surgery. Another approach, based on Moiré fringe, can be used to visually display interaction forces [TAK 10]. The advantage is that it makes use of a cheap and passive mechanism that can be distally mounted on the instrument without requiring embedded electronics and wiring. For a state of the art and an analysis of the problem of force measurement, the reader may refer to [XU 08].

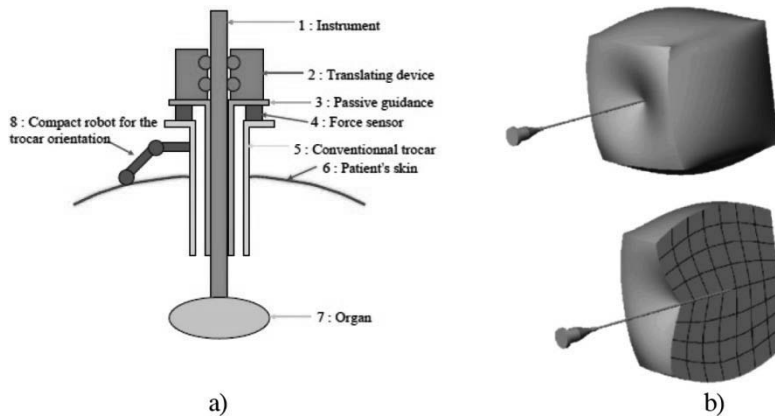

Figure 1.25. *a) Principle of the modified trocar with integrated force sensor allowing for the measurement of interaction forces [ZEM 04]; b) estimation of force during needle insertion from the deformation observed by vision [DIM 03]*

1.3.5. *Control*

As in the macroworld, control may be achieved according to three modes: autonomous, teleoperation and comanipulation modes. However, the latter is much less operable at milliscale and not at all for totally intracorporeal robots. Therefore, the choice of a mode depends on the robot but also on the level of assistance to the surgical gesture that it is intended to provide. This level is specified by the surgeon who is faced, among others, with the problem of sharing authority with a machine, and by the engineer who is faced with conflicting requirements of performance, safety and technological limitations.

1.3.5.1. *Autonomous mode*

What is rather obvious in surgical robotics is that most of the time the surgeon stays in the loop. Except probably for bone machining in orthopedics, most of the tasks are characterized by compliant or semirigid contacts with tissues and cannot be fully automated. However, in many applications autonomous behaviors are required. For the sake of simplicity, we can consider two levels:

– a low level sensory-based control: *force control* [POI 12], for instance, to maintain an instrument against an organ with a desired constant force, such as forceps against a beating heart [ORT 02, DOM 08]; or to virtually increase the stiffness of the robot when it approaches predefined boundaries (also

known as virtual fixtures or dynamic/active constraints) as implemented on the Acrobot system [JAK 03]; *visual control* [GAN 12], for instance, to track and maintain an instrument in the field of view of a laparoscope [VOR 07]; or to track 3D motion of organs to compensate for physiological motions [RIC 10];

– a higher decisional level where the robot is supposed to generate a motion and to move autonomously along a path computed from multisensory information, for instance, to reach a target with a steerable needle as in [BER 12] (Figure 1.20(c)).

1.3.5.2. *Teleoperation*

In teleoperation mode, the surgeon acts on a device (the master manipulator or master console) that, in turn, acts through a communication channel on a distant slave manipulator holding the instrument (Figure 1.26). It has been shown that the distance between the master and slave manipulators could be large, which paved the way to tele-echography [VIE 06] and telesurgery [MAR 01] applications where the patient is in a remote or non-accessible location such as a space shuttle or on a battlefield. However, issues such as communication flows and delays, cost of communication networks and safety of connection limit their possible development, mainly for surgery. In most surgical applications, both the master and slave manipulators are much closer, generally in the OR.

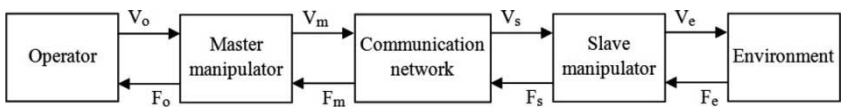

Figure 1.26. *General architecture of a teleoperation system (the symbols V and F denote velocities and forces)*

Many books and articles have been published on teleoperation since the first master–slave system was built by Goertz in the mid-1940s [GOE 54]. A good introduction to the control of these systems can be found in the reference paper of Lawrence [LAW 93] who introduced a generic bilateral teleoperation architecture, which may include up to four channels of data transmission (force and velocity in both directions). The performance of a teleoperation system is assessed by its transparence (ideally meaning that the impedance of the system should be close to zero such that the surgeon does not "feel" its weight, friction or inertia) and its stability (any bounded displacement or force input to the system will result in a bounded

displacement or force output). Practically, the control laws of the systems are intended to provide the best trade-off between transparency and stability that are conflicting design goals as shown by Lawrence.

As already mentioned in section 1.2.1, several master–slave architectures have been designed for MIS over the last two decades, among which the first commercial systems ZEUS (Computer Motion) and Da Vinci (Intuitive Surgical), and more recently for research purpose, the platforms Raven II from University of Washington [HAN 13] and MiroSurge from DLR [HAG 10]. We will go into more details about teleoperation architecture in section 1.4.1 with the example of the SPRINT robot of the EU FP7 Araknes project (Figure 1.5). More on teleoperation in surgical robotics may be found in [BAY 12].

1.3.5.3. *Comanipulation*

In comanipulation (also known as hands-on robotics or cooperative robotics), the surgeon holds and manually moves the instrument while the robot follows the resulting motion. Morel *et al.* [MOR 12b] have defined two main categories of systems: the serial comanipulator that adds mobilities in series to the arm of the surgeon (for instance a handheld laparoscopic instrument as JAiMY shown in Figure 1.2), and the parallel comanipulator that can exert forces on the instrument in addition to those produced by the surgeon or maintain it in position when the surgeon no longer holds it. Thus, with a serial comanipulator, the velocities of the surgeon and the active instrument are summed, while with the latter, forces are summed.

As already pointed out, regarding intracorporeal millirobotics, comanipulation may be used only to control partially intracorporeal devices. A significant benefit of such a control is the active filtering of high frequencies to limit the natural tremor of the surgeon. The handheld instrument MICRON from CMU [RIV 03, ANG 04] (Figure 1.27(a)) for vitroretineal applications in eye microsurgery is a good example of serial comanipulator providing active tremor compensation in 3D. It consists of two functional subassemblies: a sensing system (made up of three dual-axis accelerometers plus a triaxial magnetometer, and a data processing unit) that separates the tremor signal of the intentional movement and a three-DoF parallel manipulator with piezoelectric actuators controlled with the tremor signal that stabilizes the position of the tip of the needle. A more detailed description of the MICRON is given in section 1.4.3.

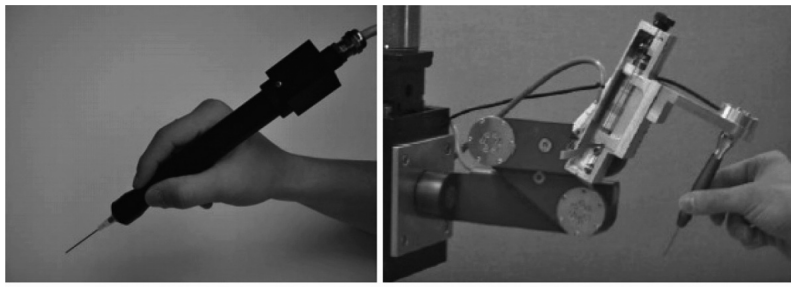

a) b)

Figure 1.27. *Examples of serial and parallel comanipulators: a) the MICRON [ANG 04] and b) the Steady-Hand robot [TAY 99]*

A representative example of parallel comanipulator is the Steady-Hand robot from John Hopkins University designed to perform submillimeter manipulation tasks [TAY 99] (Figure 1.27(b)). As outlined by the designers, the goal of the system was to provide manipulative transparency and immediacy of handheld tools, typically for ENT and eye surgery. The basic idea of the controller is a low-bandwidth force loop. The measured force exerted by the surgeon serves as set point of an inner velocity loop: the low-frequency forces, corresponding to the intended movement, generate a displacement while the high-frequency forces, corresponding to the surgeon's tremor, are blocked.

More on comanipulation in surgical robotics may be found in [MOR 12b]. Table 1.4 summarizes the comparative advantages and limitations of these three modes. An interesting comparison of microsurgery manipulation aids may be found in [MAC 12].

1.4. Examples of devices

We present hereafter a more detailed description of three examples of devices, illustrating different approaches and technologies for intracorporeal surgery at millimetric scale. In the first example – the robotic platform of the Araknes project for SPA surgery – microfabrication techniques such as micro-EDM (electrical discharge machining) were used to design the arms. However, the control techniques are the same as those commonly used for conventional robots in the macroworld. In the second example – a snake-like robot made up of concentric super-elastic tubes – the material and technology used raise new challenges of design and modeling. The last example – the

MICRON handheld instrument – highlights the interest of an integrative approach combining perception, data processing and robotics to develop smart instruments for microsurgery.

Mode	Advantages	Limitations
Autonomous	– Well fitted for complex machining of rigid materials such as bone cutting or milling; or to reach or return to memorized poses – Compensation of physiological motions (beating heart and respiratory movements)	– Description/learning of the surgeon's gesture to the robot – Modeling of the interactions with soft tissues – Safety issues more stringent that with the two other modes (the surgeon is not in the loop)
Teleoperation	– Intuitive manipulation of the instrument through the master interface, discarding the programming/learning phase – Compensation of physiological motions – Filtering of surgeon's tremor – The surgeon may be kept away from possible radiations	– Loss of physical contact between the surgeon and the patient – Cost (master + slave)
Comanipulation	– Best intuitiveness with direct overview of the operating field and direct manipulation of the instrument – Maintaining physical contact between the surgeon and the patient as in MIS – Filtering of surgeon's tremor	– More difficult to compensate for physiological motions – Sharing the workspace between the surgeon and the robot may introduce additional safety and design constraints – The surgeon is exposed to possible radiations – Restricted use for intracorporeal robotics

Table 1.4. *Comparative advantages and limitations of the control modes*

1.4.1. *The robotic platform of the Araknes project* [23]

The objective of the robotic platform of the EU FP7 Araknes project[24] was to transfer the technology of bimanual laparoscopic surgery to scarless single port endoluminal surgery (i.e. moving the required DoFs inside the peritoneal cavity, in which the robots are inserted through an umbilical or esophageal trocar). To assess the interest of such a platform, and to better define both hardware and software specifications, bariatric surgery procedures, aiming at reducing the size of the stomach, were chosen. From the hardware point of view, the robotic platform consists of:

– a dual-arm, SPRINT [PIC 10], already shown in Figure 1.5;

– an HMI based on two modified Omega.7 haptic devices (Force Dimension[25]). The handles were customized and ergonomically designed to reduce fatigue. They are equipped with contact sensors, which allow detecting whether the surgeon is using the HMI, and brakes to freeze the absolute pose of the devices when released by the surgeon;

– an external positioning platform: SPRINT is attached to an umbilical access port that is held and positioned using a double-delta parallel manipulator known as DIONIS (Figure 1.28) [BEI 11]. This dedicated kinematics provides a stiff support and generates a so-called remote center of motion (RCM) at the umbilicus level. It is manually controlled through a joystick to pre-position SPRINT in the area of interest and, at the moment, the motion of this external manipulator is not synchronized with the motion of the dual arm;

– a panoramic camera and an HD 3D camera developed and currently commercialized by Karl Storz GmbH[26];

– various macro- and nanobiological sensors (i.e. Raman spectroscopy, 2D Optical Coherence Tomography (OCT) and tissue ischemia) for diagnosis

23 Most materials of this section are from the PhD dissertation of A. Sanchez [SAN 13].

24 http://www.araknes.org/home.html.

25 http://www.forcedimension.com/.

26 https://www.karlstorz.com/cps/rde/xchg/SID-11573738-1ECEC66A/karlstorz-en/hs.xsl/14340.htm.

purposes, such as additional diagnosing tools that complement the information collected by the surgeon when palpating tissue during open surgery[27];

– a surgeon console with a commercial 3D monitor and dedicated chair and desk.

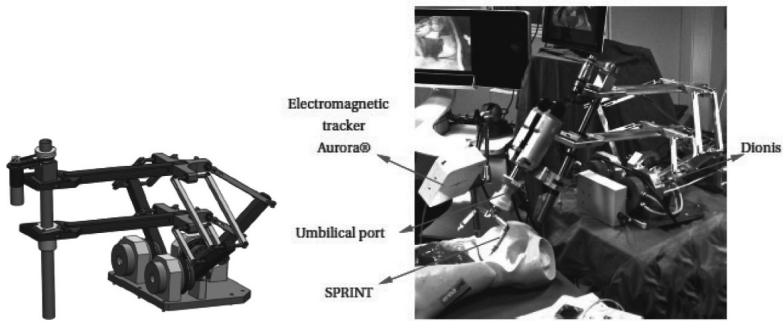

Figure 1.28. *CAD view of the umbilical port holder DIONIS (left) and its integration in the Araknes platform (courtesy of the BioRobotics Institute, SSSA, Pisa, Italy)*

Table 1.5 presents mechanical specifications of the dual-arm SPRINT, which can be compared with the ones of Endowrist from Da Vinci, IREP and DRIMIS. It is worth giving more information and discussing some design choices that have been made for SPRINT:

– The system has a total of 18 DoFs completely located inside the patient's body, i.e. each arm providing six DoFs (plus one DoF for grasping) and DIONIS providing four additional DoFs.

– A serial kinematics was preferred to a parallel one for its large workspace, high dexterity and obstacle avoidance capabilities.

– The actuators are miniature electrical motors (EC series, Maxon Motor AG, Ø 6 mm) that can be sterilized if needed. Custom low-level actuator control electronics that could also be sterilized and embedded in the arm were developed by ST Microelectronics, a partner of the Araknes project.

– Because of the power limitation of the actuators, the maximum force that can exert the tip of an arm is 5 N. This is not enough with respect to the

27 As discussed in section 1.3.4, many R&D efforts have yet to be done to develop force sensors suitable for the OR.

liver retraction task (that may require up to 30 N), which will continue to be achieved by employing a conventional retractor, but is enough to perform the other conventional tasks such as suturing. Furthermore, the gripper is tendon driven allowing gripping forces up to 15 N.

– Given the small size of the arms (Ø 6 mm), the only available sensors are the relative encoders of the miniature motors. Moreover, the impossibility of obtaining measurements at the joint level aggravates the effects of mechanical backlash (up to ±8 mm in the horizontal and vertical planes). Hence, a calibration procedure to compensate for these nonlinearities has had to be set up. To this end, an electromagnetic tracker (Aurora® by NDI Inc.,) was used to register the positions of markers stuck on the base and on the end effector of the SPRINT.

– Given the low dynamic requirements of the tasks and the software-limited operational speeds (for safety reasons), no significant joint (nor link) flexibility issues were observed.

– The platform complies with surgical constraints such as sterilizability, electrical isolation and biocompatibility for temporary contact with body organs lasting 1 h on average.

– The size, principally the diameter, should be reduced in the next version of the prototype.

Parameter	***SPRINT***	***da Vinci*** (EndoWrist)	***IREP*** [a]	***DRIMIS*** [b]
Maximum arm diameter	18 mm	5 mm	6.4 mm	10 mm
Umbilical port diameter	34 mm	N/A[c]	15 mm	N/A[d]
Maximum force	5 N	> 16 N	2 N	< 5 N
Cartesian speed	1 m/s 360^o/s	–	0.03 m/s 60^o/s	–
Arm length	120 mm	N/A	75 mm	100 mm
Number of internal DoFs	7	4	7	10
Repeatability	±1 mm –	±1.05 mm [e] –	±0.25 mm $\pm 1^o$	–
Wrist roll range	$\pm\infty$	$\pm 90^o$	–	$\pm 130^o$
Wrist pitch range	$[+130^o, -90^o]$	$\pm 90^o$	–	$\pm 90^o$
Gripper opening	150^o	150^o	–	–

a[BAJ 12].
b[SAL 04].
[c]Not applicable, robotic arm outside the peritoneal cavity.
dNot conceived for single-port access surgery.
e[HAI 09].

Table 1.5. *Mechanical specifications of SPRINT compared with EndoWrist, IREP and DRIMIS instruments [SAN 13a]*

Regarding the real-time control architecture [SAN 11], Table 1.6 summarizes the general hardware and software specifications. It is important to take into account that during the control of a surgical robot, if control tasks miss a deadline, a threat to the life of the patient could exist. Thus, a hard real-time operating system (RTOS) is mandatory in order to ensure that the system operates in a deterministic manner. In general, the developed software of the control architecture is based on open source components. Nowadays, these solutions are highly portable and customizable, which are desirable features in order to reuse such a system in future medical robotics projects.

Parameter	Description
RTOS	Hard real-time with Linux RTAI
High-level control frequency	1 kHz
Low-level control frequency	10 kHz
Communications with low-level controller	Ethernet MTAP protocol
Communications with surgeon's console	Ethernet UDP protocol
Programming language	mainly C, some C++
Documenting tools	with Doxygen v.1.8.2
Version control	Subversion v.1.7.7
IDE	Eclipse
No. of processors	3 @ 2.8 GHz (Dell Precision 650)

Table 1.6. *Control architecture specifications summary of the Araknes platform [SAN 13a]*

In addition, real-time communications between the high- and low-level actuator controllers are guaranteed by using a proprietary protocol developed by ST Microelectronics – Multimaster Tokened Access Protocol (MTAP) [CAL 08] – which allows to achieving a high-level control frequency of 1 kHz. At low level, the electronic boards developed by ST Microelectronics provide pulse width-modulated voltage regulation for the actuators. In the current implementation, this voltage regulation is performed using a closed-loop frequency of 10 kHz.

Regarding the haptic interface [SAN 12b], a frequency of 1 kHz is also used. This frequency is commonly employed in such devices due to the low human arm bandwidth, and also since such sampling frequency is sufficient to avoid perceiving undesired vibrations of the device. In general, it is very important that the mechanical design does not have resonance frequencies

situated within this range. Fortunately, commercially available haptic devices do meet such requirements.

A teleoperation control architecture has been developed. Two teleoperation schemes based on different robot control strategies, i.e. position–position and force–force, have been evaluated in terms of stability and transparency. An active observer was implemented in both cases in order to cope with modeling errors and disturbances. A realistic soft tissue model has also been used for obtaining better real-time approximations of the interaction forces. Figure 1.29 illustrates the master and slave position and force tracking profiles in free space as well as during contact motion for the Kelvin–Boltzmann model (section 1.3.1.2). It should be stated that the movements (Figure 1.29(a)) of the master during the first few seconds do not represent oscillations; rather, they are intentionally created by the operator to assess the system stability and performance in free space. From 40 s to 80 s and 100 s to 130 s, the slave robot is, respectively, in contact with a piece of meat and a so-called Phantom object (a more rigid environment). The results indicate good position matching at the master and the slave sides, showing high performance of the proposed control schemes. Between these two contact tests (from 80 s to 100 s), the operator stopped using the system in order to change the objects.

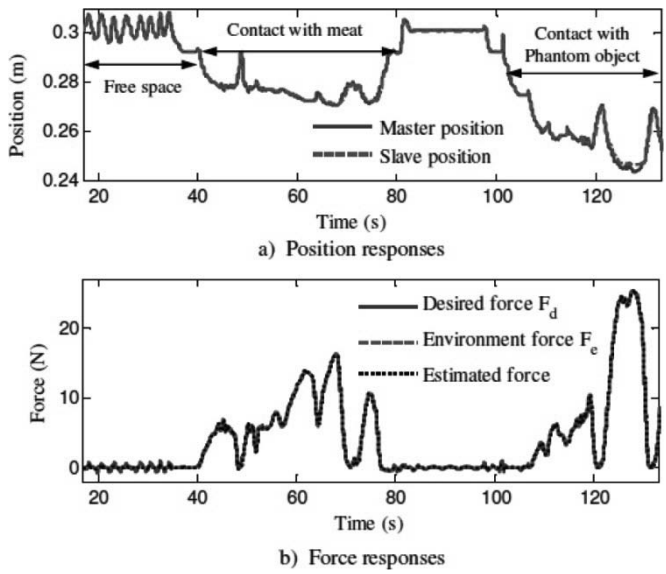

Figure 1.29. *Tracking performance of the teleoperation based on a K-B model of interaction [SAN 12a]*

Figure 1.29(b) shows the corresponding force including the desired force, the interaction force with the environment, and the estimated force in free space and under contact motion. Good force tracking performance is achieved during interaction. When the slave makes contact with a piece of flesh, the contact force magnitude is lower than in the case with the Phantom object. Indeed, during interaction with a more rigid object, the operator feels higher force feedback and as a result, he/she pushes against the environment through the master handle, leading to higher level of contact forces.

1.4.2. *A snake-like robot made of concentric super-elastic tubes*

Works on concentric super-elastic tubes for surgery were first presented in 2006 by Sears and Dupont at Boston University [SEA 06] and Webster III at Johns Hopkins University [WEB 06a] (Figure 1.8). They were motivated by the observation of several shortcomings when inserting flexible needles: as noted in [SEA 06], high-curvature steering requires a very flexible needle that leads to problems of buckling as well as excessive torsional flexibility, which can also lead to loss of steering control. Classified in the family of snake-like or continuum robots that can deform continuously, the concentric tubes robots (CTRs), also known as active cannulas, are an alternative to the cable/tendon-driven robots. Their basic features are the following:

– made up of NiTi hollow tubes, thus having super-elastic properties;

– the tubes are pre-bent and inserted inside each other;

– the outer diameter of a tube typically ranges from 0.5 to 2 mm: the smaller the outer diameter, the smaller the possible radius of curvature of the pre-bent tube, allowing it to negotiate tighter turns. However, pre-bending cannot exceed a limit, beyond which plastic deformation will appear;

– a pair of tubes provides two independent DoFs associated with relative translation and relative rotation of the tubes with respect to one another;

– depending on their bending stiffnesses, the behavior of a pair of tubes is different (Figure 1.30) [SEA 06]: when the stiffness of one tube is much larger than that of the other, the concentric tube pair conforms to the curvature of the stiffer tube but the more flexible tube relaxes to its original curvature when translated; when the stiffnesses are similar, the unstressed curvatures interact to determine their combined curvature, leading the curvature to vary when rotating the tubes. These behaviors are defined as a

domination-stiffness tube pair (with fixed curvature) and a *balanced-stiffness* tube pair (with variable curvature), respectively;

– CTR may combine various sequences of dominating-stiffness and balanced-stiffness tube pairs. Whatever the combination, the common axis of a CTR conforms to the mutual resultant curvature of the constituent pre-bent tubes;

– the lumen of the tubes can house wires for controlling articulated distal instruments, or be used to pass liquid or forms of energy;

– the tubes are individually actuated at their bases by dedicated actuation units that can apply differential rotations or translations. It should be noted that these units are generally bulky, the bulk of the whole controller increasing with the number of DoFs. As they must be close to the patient to limit the length of the tubes, hence the potentially undesired elastic deformations due to excessive length, the setting up of the robot within the operative area may be tricky.

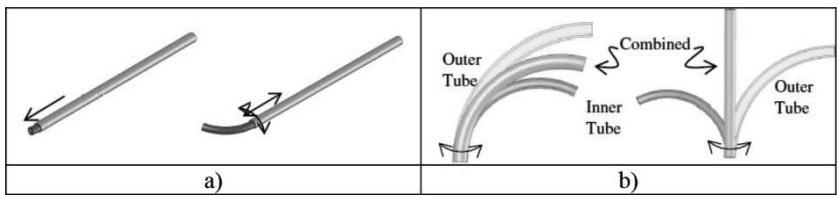

Figure 1.30. *a) Dominating-stiffness tube pair and b) balanced-stiffness pair [SEA 06]*

With such a design, instruments can generate their own steering forces rather than relying on tissue reaction forces [SEA 06]. There are several promising applications requiring high dexterity that rely on the possibility of miniaturization and customization, and on the intrinsically lightweight, modularity and low cost of the technology. Apart from needle insertion procedures, CTRs are well suited for accessing safely deep internal structures: for instance, in [BUT 12], a CTR is used to manipulate a flexible neuroendoscope in brain surgery; in [BED 11], a CTR is optimally designed for intracardiac beating-heart surgery under fluoroscopic and ultrasound imaging; in [SU 12], a feasibility study of a MRI-guided CTR is made for neurosurgery and percutaneous interventions; in [ANO 11], a systematic approach to optimizing the design of CTR for neurosurgical procedures is reported with simulation study results.

Dupont *et al.* [DUP 10] gave design guidelines for CTR. The curvature of individual tubes should be limited to avoid permanent deformation of the robot, and to prevent instabilities due to elastic interactions between torsion and bending of tubes. To manipulate distal links independently of proximal links, and to provide a good dexterity while minimizing lateral forces on tissue, they suggest designing a CTR as shown in Figure 1.31. In this example, the architecture consists of a sequence of five tubes within three telescoping sections of variable, fixed and variable curvature, respectively. The stiffnesses of the tubes are such that each telescoping section dominates all those sections extending from it, hence providing decoupling between links. Furthermore, choosing larger curvatures for the distal sections makes it possible to some extent to decouple tip displacement and tip orientation, as in conventional anthropomorphic robots whose wrists have intersecting axes. In [BED 11], further work has been done to include in the design rules the constraints imposed by a specific task and anatomical environment.

The shape and length of a CTR can be varied by controlling relative translations and rotations of the tubes. This requires deriving a kinematic model, whose complexity should not affect the real-time performance and precision of the position control. Several modeling approaches have been developed. In [WEB 09], the authors made use of minimum energy principles and Lie group theory as a framework for modeling. The starting hypothesis was that the overall CTR shape locally minimizes stored elastic energy. They validated the importance of modeling torsional effects to accurately predict the CTR shape (Figure 1.32). In [DUP 10], a framework for modeling was proposed. It is based on 3D beam-bending mechanics and includes torsion along the entire lengths of the tubes. It is also able to predict the above-mentioned torsion-bending instabilities. However, several effects were neglected such as shear of the cross-section, axial elongation, nonlinear constitutive behavior, friction between the tubes, etc. In [LYO 10], the control of the shape of the CTR was formulated as a planning problem: given the target location, the current CTR configuration, a geometric representation of obstacles and a simplified model that neglects beam mechanics, an optimization algorithm computes the length and orientation of each tube.

As for traditional serial robots, the inverse kinematics of CTR is not straightforward. The challenge is due to the nonlinear mapping between relative tube displacements and tip configuration as well as due to the multiplicity of solutions. A closed-form geometric approach is given for single and multiple sections in [NEP 09] by applying an analytical process to solve inverse kinematics based on modeling of each section with a spherical joint and

a straight rigid link. Jacobian-based methods represent another approach to robot-independent inverse kinematics. It finds a single solution to the problem by servoing a virtual copy of the robot from any initial guess (including the robot's current configuration) to the desired configuration (e.g. [SEA 07, WEB 08] for active cannula results). In the Jacobian-based inverse kinematics strategy, it is possible to build actuator limits into the control law so that the robot trajectory is always physically realizable [WEB 10].

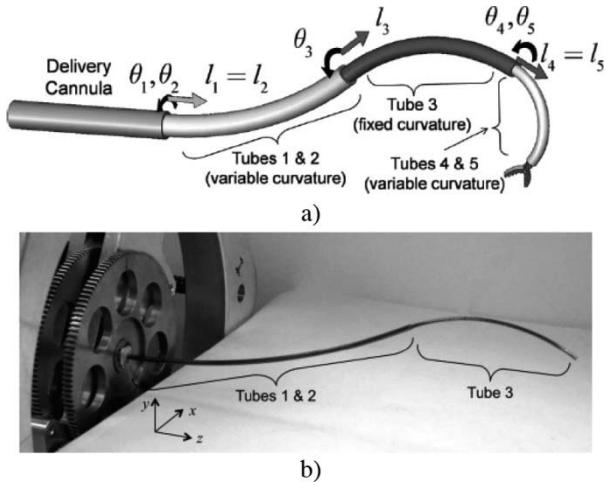

Figure 1.31. *a) Principle of a five-DoF CTR consisting of a sequence of balanced and dominating tube pairs; b) prototype of a three-DoF CTR based on this principle [DUP 10]*

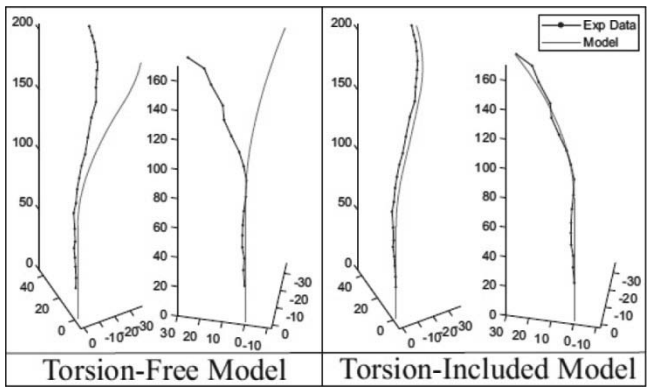

Figure 1.32. *Effect of including torsion in the kinematic model on the shape accuracy [WEB 08]*

Deformation caused by external contact force is another important issue for CTR. It is shown in [LOC 10] that tip loading could increase the mean tip error by almost 50% compared with the unloaded model. In [RUC 10], Cosserat-rod theory is applied to model forward kinematics to describe large deflections as a result of external point or distributed wrench loads.

It can be observed that the identification of robot-dependant kinematics and dynamics properties is essential in developing accurate and realistic CTR control algorithms. Systematic identification and calibration procedures have rarely been reported in the literature and it is expected that further research efforts toward this end would remarkably improve the CTR control performance and benefit newcomers in this area. Also, the use of exteroceptive sensing (namely medical imaging) in the feedback loop could compensate for the CTR model errors and disturbances.

1.4.3. *MICRON: a handheld robotized instrument for ophthalmic surgery*

In ophtalmic surgery, a high degree of precision and dexterity is demanded of the surgeon who has to manipulate very small structures (typically a few tens of micrometers, e.g. for membrane peeling during a vitreoretinal procedure, not exceeding contact forces of a few millinewtons). A further difficulty is the involuntary hand motion of the surgeon that may be one order of magnitude higher (>100 μm RMS in each principal axis) due to the so-called physiological tremor, a quasi-periodic motion (bandwidth between 8 and 12 Hz, >50 μm RMS in each principal axis), to which low-frequency drift and aperiodic sudden jerk components may be superimposed (Figure 1.33, top left). Therefore, it makes sense to investigate the potentialities offered by robots to compensate for these involuntary motions. A few prototypes have been developed since the very beginning of medical robotics, taking advantage of two specificities of the surgical field: (1) the surgeon can directly view the interior of the eye using a microscope; (2) the intraocular targets are close to the outer part of the eyeball, making them rather readily accessible by an instrument. Among the prototypes, let us mention (refer to [MAC 12] for a more comprehensive survey):

– a six-DoF slave parallel micromanipulator from Northwestern University for the treatment of retinal venous occlusion providing microscale spherical movement [GRA 93];

– the ophthalmic microsurgical robot from MIT [HUN 95] and robot-assisted microsurgery (RAMS) from JPL-NASA for vitreoretinal surgery [DAS 99], which are the first master–slave architectures with force feedback

designed and used to scale down the hand motion and filter the surgeon's tremor;

– the already mentioned Steady-Hand robot from JHU, USA, for microsurgery, namely ophthalmic surgery (Figure 1.27(b)) [TAY 99]. Unlike the earlier prototypes that are teleoperated, the Steady-Hand is comanipulated;

– more recently, the microsurgical manipulator from Columbia University providing intraocular dexterity [WEI 07b]: it consists of two identical arms attached to a head ring. Each arm is composed of a two-DoF intraocular dexterity robot (IODR) and a six-DoF parallel robot for precise positioning of the eye and the IODR. The IODR is made up of a mobile preshaped NiTi tube inserted in a straight tube that provides a combined translation and rotation motion of the surgical tool as presented in section 1.4.2.

Another approach to ophthalmic surgery is the handheld robotized instrument whose advantages are manifold: intuitiveness, safety, limited intrusion into the surgeon's workspace and low cost. Pioneering work in this area was done by Riviere at CMU , USA, [RIV 03] in the late 1990s with the MICRON (Figure 1.27(a)). The instrument detects its own motion, as does a handheld camera to stabilize the optical image, but it can also distinguish between desired and involuntary undesired motion. Then, the tip is moved in an equal but opposite direction to the undesired motion, the goal being to achieve a positioning accuracy of 10 μm. To meet these requirements, the instrument must perform three functions: motion sensing, estimation of involuntary hand motion and tip deflection control for compensation [RIV 03].

Motion sensing system: this is made up of three dual-axis miniature microelectromechanical systems (MEMS) accelerometers and a triaxial magnetometer housed in two locations as shown in Figure 1.33 (right). The choice of internally as opposed to externally referenced sensors was motivated by the better RMS sensing accuracy (~ 1 μm for an inertial sensor versus ~ 0.1 mm at about 2 m for an optical tracking system), and by the fact that it does not require maintaining a line of sight with an external reference source. Furthermore, an all-accelerometer solution compared with a conventional inertial navigation system with miniature gyros, offering the same quality in linear and angular inertial sensing, is justified by the poor resolution of the latter. The signals delivered by the sensors are then processed to compensate for deterministic errors and properly fused to derive the position and orientation of the instrument.

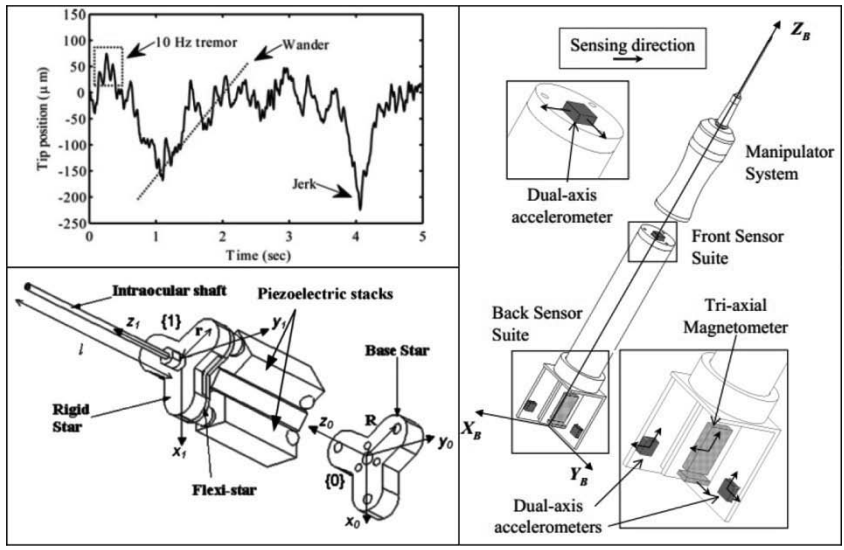

Figure 1.33. *Tremor signal and non-tremulous errors (top left) [MAC 12]; kinematics of the parallel manipulator (bottom left) [ANG 04]; sensing system design (right) [ANG 04]*

Estimation of involuntary hand motion: as mentioned above, tremor has an 8–12 Hz bandwidth, which is higher than the one of a voluntary motion (<1 Hz). However, a simple low-pass filter would cause a phase change between the input and output signals, hence a time delay lessening the positioning accuracy. In the approach proposed by Riviere *et al*. [RIV 03] and Ang [ANG 04], tremor is modeled as a quasi-periodic signal of unknown frequency within this frequency band. A weighted-frequency Fourier linear combiner (WFLC) is applied to the input signal after a band-pass filtering process to eliminate voluntary motion (below 7 Hz) and noise (>13 Hz). The resulting estimation of the tremor frequency is fed to a Fourier linear combiner (FLC) algorithm that adapts online the reconstructed tremor signal to its time-varying reference frequency online.

Tip deflection control: Figure 1.33 (bottom left) illustrates the principle of the three-DoF parallel singularity-free manipulator that has been designed to actively control the instrument tip. Referring to [RIV 03], the plastic "flexi-star" constrains the manipulator against rotation about the longitudinal axis and translation in directions transverse to this axis. Its center is clamped to

the stationary center column of the instrument, and the tip of each leg is pinned to the corresponding leg of the rigid star that holds the intraocular tool shaft. Each actuator consists of seven piezoelectric stacks, with the last stack resting against the base star. The choice of piezoelectric actuators is justified by their compactness in size (each stack measures 5 mm × 5 mm × 18 mm), high actuation force (840 N), large operating bandwidth and rapid response time (<50 μs). In return, the presence of hysteresis can attain 15% of maximum displacement. The maximum transverse and axial tip displacements with such a design are, respectively, 650 μm and 100 μm. From the control point of view, as the position of the tip is not measured, an open-loop strategy was implemented: given the estimated tremor signal as input, an inverse kinematics algorithm computes the joint variables of the parallel manipulator; then, an open-loop feed-forward controller with an inverse hysteresis model generates the reference signal to drive the piezoelectric actuators.

Figure 1.34 illustrates the performance of a MICRON of the first generation. Several subsequent versions have been developed since then [MAC 12] to improve performance (namely by active compensation of low-frequency and aperiodic motion; by reducing errors due to hysteresis by an appropriate control of the total charge stored in the actuator rather than the applied voltage; and by reducing backlashes due to the use of flexure joints) and to circumvent shortcomings (reduce size, provide greater range of motion and higher bandwidth).

Figure 1.35 shows a more recent version of the MICRON: it has a 400 μm range of motion at the tip of a typical 40 mm tool, 1 N force capability and a bandwidth more than 100 Hz; the inertial sensors that do not accurately detect the lower frequency components of hand motion (well below 10 Hz) were replaced by a system of two dc-optical sensors (position-sensitive detectors (PSDs)) that track three infrared LEDs mounted on the tool-holder and one LED on the handle allowing closed-loop control (with a resolution of 4 μm at a rate of 2 kHz). Figure 1.35(a) shows a “descendant” of the MICRON, the ITrem from Nanyang Technological University (NTU), Singapore [LAT 09] featuring an all-accelerometer inertial measurement unit comprising three optimally placed dual-axis miniature MEMS accelerometers. It also makes use of flexure joints. To compare with the performance of the first generation of handheld instruments, the performance of ITrem is also shown in Figure 1.34.

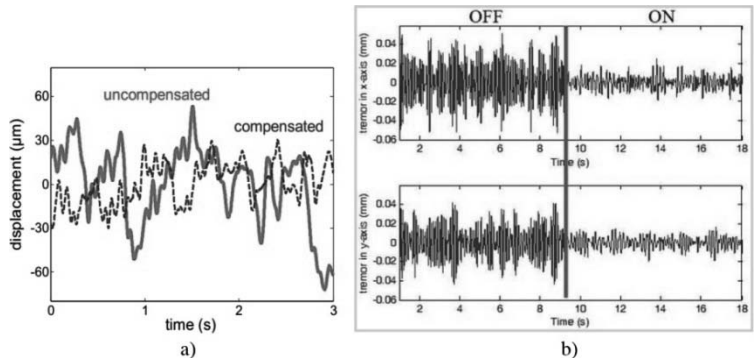

Figure 1.34. *a) Performance of the MICRON[28]: total range 52% reduction, RMS amplitude 47% reduction (compensated displacement in dashed line, uncompensated displacement in solid line); b) performance of the ITrem[29]*

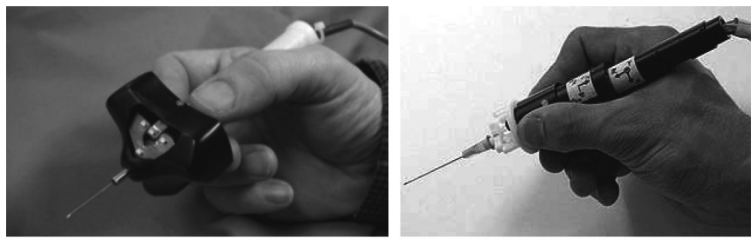

Figure 1.35. *a) Last version of the Micron showing tool and position sensor LEDs (max Ø of the LEDs housing=50 mm) [MAC 12]; b) the ITrem from NTU [LAT 09]*

1.5. Conclusion

We have presented in this chapter many prototypes that clearly contributed in some way to the progress of surgical robotics toward the use of miniature and smart robots and robotized instruments in the OR. The variety of applications for which these prototypes have been designed demonstrates the importance of most of the surgical specialties in such progress. For the sake of clarity, we have distinguished three classes of devices providing partially intracorporeal mobilities, then fully intracorporeal manipulation

28 http://www.lirmm.fr/uee05/presentations/lecturers/Ang.pdf.

29 http://www.mae.ntu.edu.sg/AboutMAE/Divisions/RRC_BioRobotics/Pages/IntelligentHandheld.aspx.

capabilities and finally intracorporeal mobility capabilities. The analysis of both functional and technical qualities and limitations of these examples has allowed us to review the scientific issues that are specific to robotics at milliscale, namely in the fields of modeling, design, actuation, sensing and control. Finally, we have described three robotic systems illustrating different scientific and technical approaches for intracorporeal surgery at millimetric scale.

Even if many advances have been made in the last decade, several challenges remain open to expand these systems with functions providing more dexterity in manipulation, more autonomy in movement control and more perception capabilities. Moreover, compared with conventional robots in the macroworld, and aside from miniaturization issues, new difficulties are raised to integrate robotic components and functions at this scale in a compact, robust and safe manner. This justifies in a sense the recent efforts made to radically explore different surgical and technical methods as will be explained in the following chapters.

Chapter 2

Intracorporeal Microrobotics

2.1. Introduction

We have seen a large number of intracorporeal robots working at milliscale. Throughout this book, so far, one may have felt that some of them are on the border between milliscale and microscale, pushed to downscaling by the medical trend to ever-decreasing invasive surgical interventions. In this chapter, we will follow this thread and deliver an overview of the ongoing research on intracorporeal robotics at microscale.

Let us start this chapter by recalling the three domains of interest we defined in the introduction:

– macroworld: volumic forces and torques (such as weight) dominate;

– microworld: surface and volumic forces and torques are balanced;

– nanoworld: surface forces and torques dominate;

with limits between these worlds, respectively, approximately 100 and 10 μm in accuracy and approximately 1 cm and 100 μm for the overall robot size.

In the context of intracorporeal interventions, this fits with the standard size of cells (10–100 μm) or with small anatomical structures, such as the inferior temporal retinal artery in the eye (in the range of 60–180 μm diameter for a healthy person down to a range of 40–100 μm for advanced glaucoma stage [JON 89]). Of course, the robots acting at that scale are not necessarily

of this size but the constraints of access to the inner space of the body make it unavoidable to try to minimize the tools. For instance, the digestive tract has a minimum diameter in the order of 10 mm.

To cope with these dimensional constraints, we have to move from conventional robotic tools toward micromechanical engineering (also known as microelecromechanical systems (MEMS) technology or microtechnology) and toward deeper insight into the physics. Following the same structure as Chapter 1, this chapter will first present the main concepts ruling the microworld, then will discuss the methodology required for robotics to enter the human body at microscale and will finally present a set of representative devices or prototypes.

2.2. Novel paradigms for intracorporeal robotics

2.2.1. *Classification of intracorporeal robots*

In the microworld, the classification of intracorporeal robots given in Chapter 1 (partially intracorporeal devices with active distal mobilities, intracorporeal manipulators and intracorporeal mobile robots) is further elaborated as:

Active catheters: these are partially intracorporeal devices with a distal mobility essentially used for steering assistance. Aside from the remote actuation at macroscale outside the body transmitted to the distal mobilities through wires, the microrobotic approach is to find other physical effects that would allow higher mobility, deeper access and better accuracy. One class of approaches includes the embedding of microactuators at the distal tip. Another class relates to steering through magnetic fields.

Distal micromechanisms: at the tip of endoscopes or catheters, one may wish to place localized active mobilities. Since the space available is limited, non-conventional fabrication techniques must be used. Indeed, for millirobots, the conventional robotics technology can still be used: rigid bodies separated by joints. At microscale, this approach can no longer be used mainly because of surface effects creating too much friction in the joints. Therefore, one must develop micromechanisms using flexure elements in place of joints [LIA 08, CHE 06].

Swimming microrobots: in the case of microrobots evolving in the body fluids such as blood or liquids in the stomach, one must take into account the physics of the microworld. Indeed, when the scale reduces, the apparent

viscosity of the fluids increases. Or more adequately, the viscous friction (surface effect) outweighs weight and inertia (volume effects). The so-called Reynolds number [PUR 77, PUR 97] characterizes the latter balance. The Reynolds number roughly follows the inverse of the apparent viscosity: at low scales, microrobots are said to be "swimming at low Reynolds number" [ALO 09].

Legged capsules: mobile microrobots inside the body may not always swim in fluids but stay in contact with tissues. Thus, one approach is to give them locomotion abilities. Since the wheel is of poor use in the wet, viscous and slippery environment inside the body, legged locomotion is preferred, where legs can be used either for propelling or slowing down the microrobots.

Magnetically guided capsules: mobile microrobots suffer even more than mobile macrorobots because of the energy issues. Of course, we cannot tether them with an electric thread. Therefore, attempts are made or foreseen to transfer the energy through the body via various means, such as radio frequency waves, ultrasounds, glucose motors [KIM 08, KIM 10] or chemicals. However, rather than transferring energy and converting it to mechanical energy, it is probably more efficient to directly act wirelessly on the mobile microrobots. This becomes true for magnetic field guidance of capsules of various sizes.

2.2.2. *Physical principles in use at microscale*

Two main principles, aside from the ones described in Chapter 1, are under the focus of investigation in intracorporeal microrobotics: the use of magnetic actuation and swimming in fluids at lower scales.

2.2.2.1. *Electromagnetics basics*

One convenient way of steering untethered intracorporeal robots is to use magnetic fields. Indeed, the latter allows us to apply forces and torques to any object having magnetic properties without any mechanical link between the object and the extracorporeal magnetic sources.

Since not all roboticists are very comfortable with electromagnetism, let us recall its basics, and take the opportunity to start writing them in the robotics notation.

The fundamental equations for electromagnetism for microrobotics are the *macroscopic* Maxwell equations [JAC 62]:

$$\begin{aligned} \nabla \cdot \vec{\boldsymbol{B}} &= 0 & \nabla \times \vec{\boldsymbol{E}} + \frac{\partial \vec{\boldsymbol{B}}}{\partial t} &= \vec{\mathbf{0}} \\ \nabla \cdot \vec{\boldsymbol{D}} &= \rho & \nabla \times \vec{\boldsymbol{H}} - \frac{\partial \vec{\boldsymbol{D}}}{\partial t} &= \boldsymbol{j} \\ \vec{\boldsymbol{D}} &= \epsilon_0 \vec{\boldsymbol{E}} + \boldsymbol{p_{ol}} & \vec{\boldsymbol{H}} &= \frac{1}{\mu_0} \vec{\boldsymbol{B}} - \boldsymbol{m_{ag}} \end{aligned} \quad [2.1]$$

where

– $\vec{\boldsymbol{E}}$ and $\vec{\boldsymbol{H}}$ are the electric and magnetic fields;

– ρ and $\boldsymbol{j}$ are the charge and current densities in the material medium;

– $\boldsymbol{p_{ol}}$ and $\boldsymbol{m_{ag}}$ are the polarization and magnetization of the material medium;

– $\vec{\boldsymbol{D}}$ and $\vec{\boldsymbol{B}}$ are the electric displacement and magnetic induction fields, derived from $\vec{\boldsymbol{E}}$ and $\vec{\boldsymbol{H}}$ through the medium;

– ϵ_0 and μ_0 are the vacuum electric permittivity and magnetic permeability;

– $\times$ is the vector cross-product;

– $\vec{}$ refers to a vector field, whereas a vector is denoted with lowercase boldface characters;

– ∇ is the 3×1 vector of partial derivative operators:

$$\nabla = \begin{pmatrix} \frac{\partial}{\partial e_1} \\ \frac{\partial}{\partial e_2} \\ \frac{\partial}{\partial e_3} \end{pmatrix} \quad [2.2]$$

where (e_1, e_2, e_3) are the three coordinates of space in the coordinate system used: Cartesian $(e_1 = x, e_2 = y, e_3 = z)$, spherical $(e_1 = \rho, e_2 = \theta, e_3 = \phi)$ or cylindrical $(e_1 = r, e_2 = \theta, e_3 = z)$.

Note that these equations are, in most cases, linear in $\vec{\boldsymbol{E}}$ and $\vec{\boldsymbol{B}}$ (the so-called fundamental electromagnetic fields), which allows for considering superposed fields by simple addition. Also note that, when these equations are considered in the air, we can assume, under regular conditions, that $\boldsymbol{p_{ol}} = \boldsymbol{m_{ag}} = \mathbf{0}$. Finally, note that $\vec{\boldsymbol{E}}$, $\vec{\boldsymbol{D}}$, $\vec{\boldsymbol{B}}$ and $\vec{\boldsymbol{H}}$ are vector fields: in each point $\boldsymbol{P}$ in space, they have a vector for value, e.g. $\boldsymbol{b}(\boldsymbol{P})$ is the (vector) value of $\vec{\boldsymbol{B}}$ in $\boldsymbol{P}$.

Associated with these laws is the force applied to a particle with charge q, located in $\boldsymbol{P}$ with velocity $\boldsymbol{v}$ (known as the Lorentz force):

$$\boldsymbol{\mathcal{F}} = q(\boldsymbol{e}(\boldsymbol{P}) + \boldsymbol{v} \times \boldsymbol{b}(\boldsymbol{P})) \quad [2.3]$$

From the latter equation, the force applied on a localized current distribution $\boldsymbol{j}$ can be derived. Such a localized current distribution has a magnetic moment density (or *magnetization*) in each of its points:

$$\boldsymbol{m_{ag}}(\boldsymbol{P'}) = \frac{1}{2}\boldsymbol{P'} \times \boldsymbol{j}(\boldsymbol{P'}) \quad [2.4]$$

and the associated integral *magnetic moment* $\boldsymbol{m}$:

$$\boldsymbol{m} \stackrel{def}{=} \iiint \boldsymbol{m_{ag}}(\boldsymbol{P'})d\boldsymbol{P'} = \frac{1}{2}\iiint \boldsymbol{P'} \times \boldsymbol{j}(\boldsymbol{P'})d\boldsymbol{P'} \quad [2.5]$$

and experiences the following magnetic torque:

$$\boldsymbol{\mathcal{T}} = \boldsymbol{m} \times \boldsymbol{b}(\boldsymbol{P}) \quad [2.6]$$

and magnetic force:

$$\boldsymbol{\mathcal{F}} = \nabla(\boldsymbol{m} \cdot \boldsymbol{b}(\boldsymbol{P})) = \nabla(\boldsymbol{m}^{\mathsf{T}}\boldsymbol{b}(\boldsymbol{P})) \quad [2.7]$$

2.2.2.1.1. Magnetic materials

By these force and torque, magnetic fields operate on every piece of matter [GRI 99]. Materials can be classified according to their magnetic properties.

Amagnetic materials: are the most frequent materials and are characterized by the fact that, on Earth and at human scale, the magnetic effects they encounter are negligible.

Diamagnetic materials: are magnetized in the opposite direction to the applied field. Their magnetization is thus of the form:

$$\boldsymbol{m_{ag}} = \chi_m \vec{\boldsymbol{H}}, \chi_m < 0 \quad [2.8]$$

where χ_m is called the magnetic susceptibility and is typically in the order of $10^{-4} - 10^{-9}$. Following equation [2.7], diamagnetic materials are (weakly) repelled by the magnetic field source.

Paramagnetic materials: are magnetized parallel to the applied field:

$$\boldsymbol{m_{ag}} = \chi_m \vec{\boldsymbol{H}}, \quad \chi_m > 0 \qquad [2.9]$$

where χ_m is typically in the order of 10^{-1}–10^{-6} (paramagnetism is thus stronger than diamagnetism). Paramagnetic materials are attracted by the magnetic source.

Ferromagnetic materials: are paramagnetic materials presenting a larger hysteresis loop. Until saturation, ferromagnetic materials behave (almost) linearly, as paramagnetic materials. Yet, the forces obtained using ferromagnetic material are typically in the order of 10^4 stronger than those obtained using paramagnetic material.

Once saturation is reached, the magnetization cannot increase anymore, despite the increase of the magnetic field. When the magnetic field decreases, the magnetization decreases along the "way back" of the hysteresis loop and reaches a non-zero *remanent* value in the absence of field.

This allows for "recording" the magnetization into the matter and making *permanent magnets*.

Iron, nickel and cobalt are the most well known ferromagnetic materials. However, some alloys made up of rare earth elements, such as neodymium-iron-bore (NdFeB) or samarium-cobalt (Sm-Co), can be used to make so-called *supermagnets* with extremely high remanent magnetization.

Assuming a uniform magnetization $\boldsymbol{m_{ag}}$ inside the volume V of an object, equation [2.5] provides us with the magnetic moment $\boldsymbol{m}$ of the object:

$$\boldsymbol{m} = \iiint \boldsymbol{m_{ag}} d\boldsymbol{P'} = V \boldsymbol{m_{ag}} \qquad [2.10]$$

Vectors $\boldsymbol{m}$ and $\boldsymbol{m_{ag}}$ are aligned along the same direction (denoted by the unit vector $\underline{\boldsymbol{m}}$) and thus their norms ($\bar{m}$ and M) are also linked by V:

$$\bar{m} = VM \qquad [2.11]$$

This relation is very important since it means that the magnetic moment of an object decreases linearly with its volume: a ferromagnetic object of 1 mm^3 will be 1,000 times less magnetizable than a similar object of 1 cm^3.

2.2.2.1.2. Magnetic field sources

To generate a magnetic field, we can use one or several magnetic sources. Recall that, under the linear assumption, the magnetic field obtained by several sources is the sum of the individual fields. Magnetic sources are of two kinds: permanent magnets and electromagnets. Permanent magnets are pieces of saturated ferromagnetic materials. Electromagnets are electric circuits (most often coils) that are designed for generating magnetic fields of specific shape and intensity.

The magnetic induction $\vec{\boldsymbol{B}}$ can be produced by various means that we discuss below:

Magnetic induction produced by a pure dipole: the magnetic induction produced by a pure dipole (i.e. non-physical), with magnetic moment $\boldsymbol{m}$ and placed at the origin of the reference frame, can be shown to be:

$$\boldsymbol{b}(\boldsymbol{P}) = \frac{\mu_0}{4\pi}\frac{1}{r^3}\left(3\boldsymbol{m}\cdot\underline{\boldsymbol{r}}\,\underline{\boldsymbol{r}} - \boldsymbol{m}\right) \qquad [2.12]$$

where $\boldsymbol{P} = r\underline{\boldsymbol{r}}$ (spherical coordinates) decomposes into its norm (r) and direction, represented by the unit vector $\underline{\boldsymbol{r}}$. Note that this classical equation can be rewritten in matrix form as:

$$\boldsymbol{b}(\boldsymbol{P}) = -\frac{\mu_0}{4\pi}\frac{1}{r^3}\left(\mathbf{I}_3 - 3\underline{\boldsymbol{r}}\,\underline{\boldsymbol{r}}^{\mathsf{T}}\right)\boldsymbol{m} \qquad [2.13]$$

which shows a linear dependence in $\boldsymbol{m}$ and nonlinearities both in the distance r and direction $\underline{\boldsymbol{r}}$ to the origin.

In the above equations, we observe a cubic term ($\frac{1}{r^3}$), which implies that an object located 10 times further away (for instance, 10 cm inside the body instead of 1 cm below the skin) will experience a magnetic field 1,000 times weaker.

Magnetic induction far away from any current distribution: far away from any current distribution, the magnetic induction generated can be approximated by the magnetic induction generated by a pure dipole. This property is very convenient and it is often assumed that the microrobot is

located far away from the magnetic sources. This assumption will be called the "far away" assumption in the following.

As a result, defining the magnetic induction is just a matter of defining $\boldsymbol{m}$. In the case of a single circular current loop, $\boldsymbol{m}$ is defined by its direction $\underline{\boldsymbol{m}}$ and norm $\bar{m}$:

$$\underline{\boldsymbol{m}} = \underline{\boldsymbol{z}}_{loop} \quad [2.14]$$

$$\bar{m} = \pi a^2 I \quad [2.15]$$

where I is the current circulating in the loop, $\underline{\boldsymbol{z}}_{loop}$ is the unit vector orthogonal to the loop plane oriented by the current direction (symmetry axis) and a is the loop radius. Applying equation [2.13] gives the magnetic induction generated by the single loop at point $\boldsymbol{P}$ far away from the loop center (i.e. $r >> a$):

$$\boldsymbol{b}(\boldsymbol{P}) = -\frac{\mu_0}{4\pi}\frac{\pi a^2}{r^3}\left(\mathbf{I}_3 - 3\underline{\boldsymbol{r}}\underline{\boldsymbol{r}}^{\mathsf{T}}\right)\underline{\boldsymbol{z}}_{loop} I \quad [2.16]$$

By extension, the magnetic induction generated by a solenoid coil made up of N loops can be approximated by:

$$\boldsymbol{b}(\boldsymbol{P}) = -\frac{\mu_0}{4\pi}\frac{\pi N a^2}{r^3}\left(\mathbf{I}_3 - 3\underline{\boldsymbol{r}}\underline{\boldsymbol{r}}^{\mathsf{T}}\right)\underline{\boldsymbol{m}} I \quad [2.17]$$

The latter equation is linear in the current I and the number of loops N. To increase the strength of an electromagnet, we can thus increase I or N. However, this is limited by the Biot and Savart law, Helmholtz coil:

$$E = R(N)I^2 \quad [2.18]$$

where E is the energy converted into heat by the circuit and $R(N)$ is the resistance of the circuit (which is, as a matter of fact, an increasing function of the length of the circuit).

Equation [2.17] is quadratic in a, which can be used to increase the magnetic induction more rapidly than by increasing the number of loops or the current. Unfortunately, in the medical context, the radius of the coils does not have a large range of acceptable values. Moreover, as the radius grows, the validity of the "far away" assumption reduces, which in turn would require experimental identification or numerical computation of the complex geometry.

Alternately, we can insert a ferromagnetic core inside the coil but this modifies the magnetic field outside the coil in a way that depends on the shape and dimension of the core (and on whether the core gets saturated or not). Moreover, this may again invalidate the "far away" assumption. This remains nevertheless the preferred solution for the engineer.

Magnetic induction inside a Helmholtz coil: a Helmholtz coil is a specific configuration, to be found in any undergraduate physics textbook, using two coaxial parallel coils, of the same radius a and at a distance a from each other, that are circulated by the same current I (in norm and circulation direction).

It can be shown, from the Biot and Savart law, that the magnetic induction $\vec{\boldsymbol{B}}$ between the two coils is almost uniform and aligned with the direction $\underline{\boldsymbol{z}}$ of the coils common direction. The mathematical expression of the approximated uniform magnetic induction is:

$$\vec{\boldsymbol{B}} = \mu_0 N a^2 I \underline{\boldsymbol{z}} \qquad [2.19]$$

where N is the number of loops in each coil, I is the current circulating in each coil and μ_0 is the magnetic permeability of the air. Here again, we can define:

$$\underline{\boldsymbol{m}} = \underline{\boldsymbol{z}} \qquad [2.20]$$

$$\bar{m} = \mu_0 N a^2 I \qquad [2.21]$$

Using two (respectively three) orthogonal Helmholtz coils allows us to generate a uniform magnetic induction in any direction in a plane (respectively in space) by the linear combination of the two (respectively three) individual magnetic inductions:

$$\vec{\boldsymbol{B}} = \mu_0 N_x a_x^2 I_x \underline{\boldsymbol{x}} + \mu_0 N_y a_y^2 I_y \underline{\boldsymbol{y}} + \mu_0 N_z a_z^2 I_z \underline{\boldsymbol{z}} \qquad [2.22]$$

Magnetic induction inside a Maxwell coil: the term *Maxwell coil* refers to two coil configurations. The first one comprises three centered coils: two of them are coaxial as in the Helmholtz configuration, while the last coil is orthogonal to the first two coils, with specific dimensions [MAX 73]. It generates in practice a more uniform magnetic induction than the Helmholtz coil. The second configuration is composed of two coaxial parallel coils of radius a, as in the Helmholtz configuration, but separated by the distance $\sqrt{3}a$ and circulated with currents of the same intensity I but in reverse directions. This

second configuration generates a magnetic field with uniform gradient [JEO 10]:

$$\vec{\boldsymbol{B}} = \mu_0 \frac{16}{3} \left(\frac{3}{7}\right)^{5/2} \frac{I}{a^2} \left(-0.5\underline{\boldsymbol{x}} - 0.5\underline{\boldsymbol{y}} + \underline{\boldsymbol{z}}\right) \quad [2.23]$$

where $\underline{\boldsymbol{z}}$ is the coil common direction while $\underline{\boldsymbol{x}}$ and $\underline{\boldsymbol{y}}$ are the other two orthogonal directions.

Magnetic induction in the neighborhood of a source with complex geometry: because the magnetic induction far away from any magnetic source can always be approximated by a pure dipole of moment $\boldsymbol{m}$, a complex-shaped source will only induce a local fluctuation around the center of the pure dipole. Moreover, the magnetic induction can always be assumed linear in the pure dipole magnetic moment amplitude $\bar{m}$ whatever the geometry. Therefore, we can state the following proposition.

PROPOSITION 2.1.– Any complex-shaped magnetic source can be modeled as the product of a geometric field $\vec{\boldsymbol{\mathcal{L}}}(\underline{\boldsymbol{m}})$ aligned with the direction of a magnetic moment $\underline{\boldsymbol{m}}$ by the amplitude of such a magnetic moment $\bar{m}$:

$$\vec{\boldsymbol{B}} = \vec{\boldsymbol{\mathcal{L}}}(\underline{\boldsymbol{m}})\bar{m}(I) \quad [2.24]$$

The field $\vec{\boldsymbol{\mathcal{L}}}(\underline{\boldsymbol{m}})$ will be called the *magnetic lines field*. The value of $\vec{\boldsymbol{\mathcal{L}}}(\underline{\boldsymbol{m}})$ in a given point $\boldsymbol{P}$ is thus a vector that will be noted $\boldsymbol{\ell}(\underline{\boldsymbol{m}}, \boldsymbol{P})$. The dyedra $(\boldsymbol{P}, \boldsymbol{\ell}(\underline{\boldsymbol{m}}, \boldsymbol{P}))$ uniquely defines the tangent line to $\vec{\boldsymbol{\mathcal{L}}}(\underline{\boldsymbol{m}})$ (and thus $\vec{\boldsymbol{B}}$) in $\boldsymbol{P}$. Moreover, we can generically make $\bar{m}$ a function of the current I in the source (either actual current in a coil or a constant unitary current in a permanent magnet).

The value of the magnetic induction $\vec{\boldsymbol{B}}$ in $\boldsymbol{P}$ is thus given by:

$$\boldsymbol{b}(\boldsymbol{P}) = \boldsymbol{\ell}(\underline{\boldsymbol{m}}, \boldsymbol{P})\bar{m}(I) \quad [2.25]$$

2.2.2.2. *Swimming at low Reynolds number*

The Reynolds number is a dimensionless quantity, which is defined as the ratio of the inertial forces $\boldsymbol{\mathcal{F}}_{in}$ to the viscous forces $\boldsymbol{\mathcal{F}}_v$ [STO 51, REY 83]:

$$Re = \frac{\|\boldsymbol{\mathcal{F}}_{in}\|}{\|\boldsymbol{\mathcal{F}}_v\|} \quad [2.26]$$

So when the viscous forces dominate the inertial forces, the Reynolds number is far below 1. The Reynolds number can also be expressed as a function of the relative object velocity with respect to the fluid v, the characteristic linear dimension L, the fluid density ρ and the fluid dynamic viscosity μ:

$$Re = \frac{\rho \|\boldsymbol{v}\| L}{\mu} \qquad [2.27]$$

For instance, the Reynolds number of a large whale swimming at 10 m/s in water is 300,000,000 and it is only 0.3 for a 0.3 mm long invertebrate larva at 1 mm/s or 0.00001 for a bacterium swimming at 0.01 mm/s [VOG 94]. As for microrobots, one obtains a Reynolds number in the order of 100 for a centimetric gastric endoscopic pill in water at 1 cm/s. There, viscosity does not have much influence. However, the Reynolds number would be only approximately 0.07 for a 30 μm robot navigating in an arteriole where the blood flow is approximately 7 mm/s. Here, viscous forces dominate inertial forces. In between, there is the vast "gray" zone of intracorporeal microrobots, where we will have to deal, to a variable extent, with viscosity.

Indeed, viscosity affects the swimming performances of microscale swimmers, as recalled below from [ABB 09]. Let us consider an incompressible flow of Newtonian fluid. The assumption of incompressible flow implies constant viscosity. In this case, a simplification of the Navier–Stokes equations yields [ALO 09]:

$$-\nabla \boldsymbol{p} + \eta \nabla^2 \boldsymbol{v} = \rho \frac{\partial \boldsymbol{v}}{\partial t} + \rho(\boldsymbol{v} \cdot \nabla)\boldsymbol{v} \qquad [2.28]$$

$$\nabla \cdot \boldsymbol{v} = 0 \qquad [2.29]$$

where η is the constant dynamic viscosity and $\boldsymbol{p}$ is the pressure. As viscous forces dominate at low Reynolds number regimes, the inertia terms are negligible. The Navier–Stokes equation thus becomes:

$$\eta \nabla^2 \boldsymbol{v} = \nabla \boldsymbol{p} \qquad [2.30]$$

$$\nabla \cdot \boldsymbol{v} = 0 \qquad [2.31]$$

This equation is linear and independent of time [LAU 09]. The consequence for locomotion is that the flow is reversible at low Reynolds numbers and gives rise to the so-called Scallop theorem [PUR 77]. Indeed, a

scallop in water displaces itself by opening slowly and then closing sharply. During the opening phase, water flows slowly into the scallop without inducing any motion, whereas during the closing phase, the water is violently expelled and produces a displacement of the scallop by counter-reaction. By repeating this procedure, similar to the stick-slip effect in microrobotics [FLO 08, RAK 08], the scallop can displace. However, at a low Reynolds number and because the flow is reversible, this would not work and the scallop would move back and forth around its initial position.

As a result, only non-reciprocal motions, such as corkscrew-type rotating propulsion, are suitable for low Reynolds number regimes. Theoretical studies on optimal motions have been conducted, such as [NAJ 04, ALO 09 and KHA 09], as well as on experimental robotics, with one flagellum [HON 96, ZHA 09, ZHA 10, TOT 12, ABB 09, GHO 09, HWA 10, HWA 11] or several [YE 13].

It should be noted that the Reynolds number reduces, for a given robot size, as the viscosity of the fluid increases. This is used in [XU 13] to perform dimensionless characterization of helical swimmers.

2.3. Methods

This section discusses the standard robotics methodology – models, design, actuation, sensing and control – and its necessary adaptation to the intracorporeal microworld.

2.3.1. *Models*

2.3.1.1. *Kinematics*

The fundamentals of kinematics apply to microrobots as to conventional robots. Forward and inverse kinematic models and static and differential kinematic models and dynamic models are concepts that still exist. Such concepts are largely described in many robotic textbooks, such as [KHA 02] for manipulators or [MOR 08] for mobile robots.

Yet, a specificity of microrobotics is that rigid body kinematics is not alone in the field of micromanipulator modeling. Indeed, as the size of the robots shrinks, the conventional design based on the succession of rigid bodies and joints no longer work. Indeed, surface effects increase the friction in the joints together as clearances necessarily decrease with the robot size

and desired accuracy. Thus, in order to produce actuation, one must turn oneself toward physical effects, other than electromagnetic conversion of current into torque/force in a motor. As a result, conventional joint mobilities are replaced by flexibilities to create mobility in a monolithic structure. For instance, flexure hinges (or compliant joints) are made by creating grooves (Figure 2.1) in the matter so that only a small volume of matter remains, resulting in a local weakness of the structure.

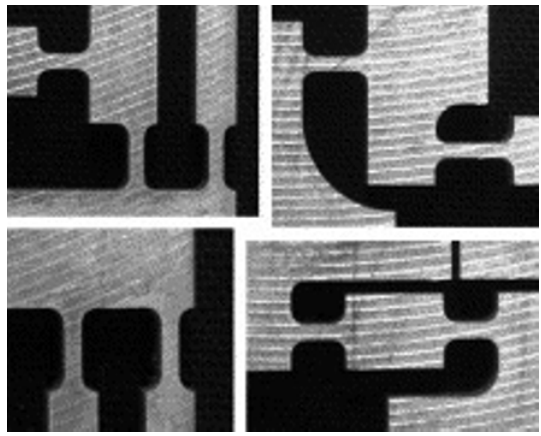

Figure 2.1. *Example of flexure joints [ZUB 09]: grooves appear in black and remaining matter in gray, forming, for instance, two horizontal flexure hinges in the lower right image*

To model such flexibilities, we can make use of several techniques, as in conventional robotics. One is the finite element method (FEM), which allows for taking into account the continuum mechanics of the flexible structure. It is valuable for understanding and characterizing the structure, but often too computationally heavy for being computed online for teleoperation or closed-loop control. Another consists of considering localized flexibilities: all the deformations of the structure are located in the (real or virtual) joints between virtually rigid bodies. This method is valuable for its low numerical complexity, but it is often a very rough approximation of the structure behavior. In between, one considers distributed flexibilities along each beam, in a sparsely discretized approximation of the continuum mechanics of the structure.

One current trend in the development of active catheters is to use telescopic catheters made up of concentric precurved tubes [WEB 06, SEA 06] (see section 1.4.3). This specificity allows us to

decompose their kinematics into a conventional rigid body kinematic model and the model of the deformations of the tubes [WEB 10].

2.3.1.2. *Dynamics*

Balance of forces is the basis of our world's physics. Yet, at the various scales, as stated in the introduction, some forces predominate others.

As far as intracorporeal microrobotics is concerned, dealing with objects in the order of 10–100 μm, the range of robots' size and weight is still rather large and covers several orders of magnitude: from some hundreds of micrometers in the larger dimension for the Octomag robots [KUM 10] to some tens of centimeters for a catheter. At the same scale, surface effects are no longer negligible as static or viscous friction, stiction and electrostatic forces. Moreover, in intracorporeal cavities, biological and chemical effects can also appear.

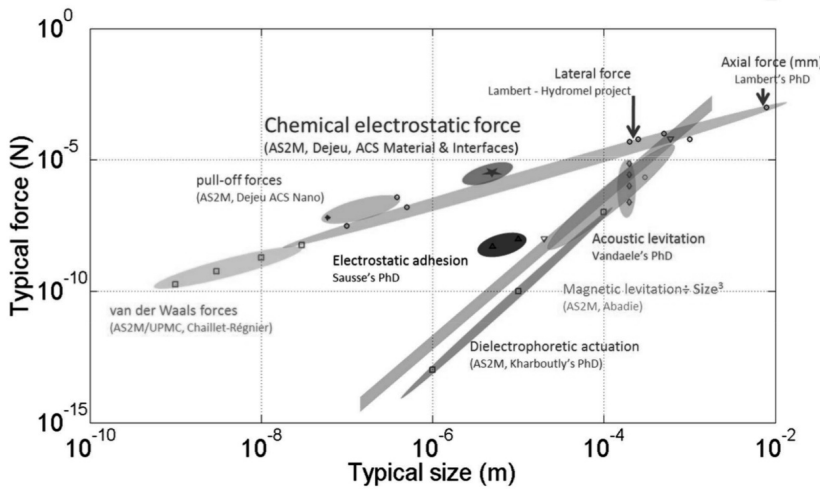

Figure 2.2. *Force amplitudes as a function of size [LAM 10]*

Intracorporeal microrobotics is thus the crossroad where "several physics meet", or more precisely stated, where none of the laws of physics dominate all the others (Figure 2.2). This is clearly a constraint for the roboticist, who must take all these effects into account for the modeling and control of microrobots. It is also a great opportunity for the researcher and the engineer because this opens wide the field of creativity and investigation, by mixing several effects rather than relying only on Euler mechanics. Combinations of various effects

belong to the so-called multiphysics approach, where two tools can be of great use: energy-based thinking and FEM simulation.

One of the most original concepts for novel intracorporeal intervention, and a fashionable research topic at the time of writing this book, is the use of magnetic fields to actuate microrobots without any contact through the skin, flesh and bones.

2.3.1.3. *Magnetic fields for robotics*

All the modeling in section 2.2.2.1 was derived in a unique reference frame that is defined by the pure dipole associated with the source. Moreover, in physics textbooks, one only deals with stationary (i.e. time invariant) sources or harmonic sources (i.e. sources with sinusoidal current). However, in microrobotics, the devices entail either several sources or mobile sources or sources with time-varying amplitude.

To present all these approaches in a common formalism, it is necessary to derive a generic model of electromagnetics for robotics. This section is the first attempt in that direction.

First, let us reformulate the magnetic induction in equation [2.25] with robotic notation:

$$\boldsymbol{b}(\tilde{\boldsymbol{P}}) = \boldsymbol{\ell}(\underline{\boldsymbol{m}}, {}^{w}\tilde{\boldsymbol{P}})\, \bar{m}(I) \qquad [2.32]$$

where we now use the homogeneous coordinates $\tilde{\boldsymbol{P}} = \begin{pmatrix} \boldsymbol{P} \\ 1 \end{pmatrix}$.

Second, let us express all the magnetic sources in the world frame. To do so, consider the rigid transformation of a magnetic induction field from a frame $\mathcal{R}_i$ to a frame $\mathcal{R}_j$:

$${}^{i}\mathbf{T}_{j} = \begin{pmatrix} {}^{i}\mathbf{R}_{j} & {}^{i}\boldsymbol{t}_{j} \\ \mathbf{0}_{1\times 3} & 1 \end{pmatrix} \qquad [2.33]$$

This rigid transformation allows changing the coordinates of the point where the field is calculated (${}^{i}\tilde{\boldsymbol{P}} = {}^{i}\mathbf{T}_{j}\, {}^{j}\tilde{\boldsymbol{P}}$) as well as of those of the magnetic line direction (${}^{j}\boldsymbol{\ell}(\bullet,\bullet) = {}^{j}\mathbf{R}_{i}\, {}^{i}\boldsymbol{\ell}(\bullet,\bullet)$). This results in the following proposition:

PROPOSITION 2.2.– CHANGE OF REFERENCE FRAME.– Given

– the position ${}^{j}\boldsymbol{P}$ of a magnetic object in frame $\mathcal{R}_j$;

– the field ${}^i\boldsymbol{b}({}^i\tilde{\boldsymbol{P}}) = {}^i\boldsymbol{\ell}({}^i\underline{\boldsymbol{m}}, {}^i\tilde{\boldsymbol{P}})\ \bar{m}(I)$ generated by a magnetic source expressed in frame $\mathcal{R}_i$;

– and the rigid transformation ${}^i\mathbf{T}_j$ from frame $\mathcal{R}_i$ to frame $\mathcal{R}_j$,

then the field can be expressed in frame $\mathcal{R}_j$ as:

$$ {}^j\boldsymbol{b}({}^j\tilde{\boldsymbol{P}}) = {}^j\mathbf{R}_i\, {}^i\boldsymbol{\ell}({}^i\underline{\boldsymbol{m}}, {}^i\mathbf{T}_j\, {}^j\tilde{\boldsymbol{P}})\ \bar{m}(I) \qquad [2.34] $$

Finally, let us apply the superposition theorem over all the sources expressed in a single frame $\mathcal{R}_w$:

PROPOSITION 2.3.– MICROROBOTIC TOTAL MAGNETIC INDUCTION.–

$$ {}^w\boldsymbol{b}({}^w\tilde{\boldsymbol{P}}) = \sum_{i=1}^{N} {}^w\mathbf{R}_i\, {}^i\boldsymbol{\ell}({}^i\underline{\boldsymbol{m}}, {}^i\mathbf{T}_w\, {}^w\tilde{\boldsymbol{P}})\ \bar{m}(I_i) \qquad [2.35] $$

In the frequent cases where the magnetic moment amplitude is a linear function of the current, then $\bar{m}(I_i) = s_i I_i$ and the above expression can be simplified into:

$$ {}^w\boldsymbol{b}({}^w\tilde{\boldsymbol{P}}) = \sum_{i=1}^{N} {}^w\mathbf{R}_i\, {}^i\boldsymbol{\sigma}({}^i\underline{\boldsymbol{m}}, {}^i\mathbf{T}_w\, {}^w\tilde{\boldsymbol{P}})\ I_i \qquad [2.36] $$

where ${}^i\boldsymbol{\sigma}({}^i\underline{\boldsymbol{m}}, {}^i\tilde{\boldsymbol{P}}) = s_i\, {}^i\boldsymbol{\ell}({}^i\underline{\boldsymbol{m}}, {}^i\tilde{\boldsymbol{P}})$ will be called the *shape* of the magnetic induction field generated by source i in the following. It is also called the unit-current field map in [KUM 10]. It is expressed here in the local frame associated with the source, but can be also expressed in the world frame, following proposition 2.2:

$$ {}^m\boldsymbol{\sigma}({}^m\underline{\boldsymbol{m}}, {}^w\tilde{\boldsymbol{P}}) = {}^w\mathbf{R}_i\, {}^i\boldsymbol{\sigma}({}^i\mathbf{R}_w\, {}^w\underline{\boldsymbol{m}}, {}^i\mathbf{T}_w\, {}^w\tilde{\boldsymbol{P}}) \qquad [2.37] $$

Note that, in equation [2.36], ${}^i\vec{\boldsymbol{\mathcal{L}}}({}^i\underline{\boldsymbol{m}})$ (see equation [2.24]) and s are the design parameters while ${}^w\mathbf{T}_i$ and I_i can serve either as design parameters or control input variables.

2.3.2. *Design*

Although it is not the purpose of this book to analyze the design aspects in detail it is however necessary to lend a few words to it.

Micromechatronic design: deals with the simultaneous design of the mechanical structure (using microfabrication techniques), the actuation, the perception means and the control architecture (electronics and software).

Biocompatibility: is a strong constraint, which must be taken into account as soon as possible, because biocompatibility of intracorporeal microrobots is certainly a more sensitive issue, at least in the general audience, than biocompatibility of larger medical robots. Indeed, the consequences of breakage or leakage of a microrobot are less tangible than those of a robot with components that are visible to the naked eye, and thereby more fearful and anxiogeneous. It is thus worth recalling here the outline of regulatory issues.

Following the ISO 10993 standard, medical devices are classified according to the duration and nature of their contact with the body, as well as to the chemical composition of the devices:

– *Class I* contains non-invasive medical devices or medical devices with temporary use.

– *Class IIa* concerns medical devices with short-term invasiveness and long-term invasive medical devices in the oropharyngeal sphere.

– *Class IIb* consists of long term invasive medical devices outside the oropharyngeal sphere.

– *Class III* is dedicated to long-term invasive medical devices in contact with the heart, vascular and nervous system.

Depending on the class they belong and local regulations (e.g. FDA in the United States and CE in Europe), each medical device must undergo various biocompatibility tests:

– Cytotoxicity: how toxic is it to cells?

– Sensitization: to what extent does it create an allergic response?

– Irritation.

– Systemic toxicity: how toxic is it to the whole body?

– Genotoxicity: to what extent does it affect the genetic material?

– Hemocompatibility: is it compatible with blood?

– Toxicokinetics: how does toxicity evolve with time?

– Carcinogenicity: to what extent does it generate cancer?

– Reproductive toxicity: how toxic is it to human reproduction?

– Local effects after implantation.

– Biodegradation of products and leachables[1].

At the time of writing this book, there does not exist any specific norm for intracorporeal microrobots. It is thus not clear whether we should consider them as medical devices (ISO 10993) or as robots (ISO 8373, 9283 and related), and thus which quality standards must be followed. Yet, a standardization process is ongoing for medical robots (ISO/TC184/SC2/JWG9: medical electrical equipment and systems using robotic technology) and will give guidelines in the coming years.

Intrinsic safety: means that whatever happens (failure or misuse) to a robot, no harmful consequence will result. This is required for intracorporeal robotics because the robot is in direct contact with(in) the patient [SAN 13].

One solution is to make redundant systems, as in avionics; another one is to take into account this feature all the way through the design. For instance, transcranial magnetic stimulation can be extrinsically safe if the robot workspace does not overlap with the human body [ZOR 12], or not if one uses a conventional anthropomorphic robotic arm.

In the case of intracorporeal microrobotics, intrinsic safety is even more necessary. Indeed, the surgeon usually neither has a direct perception of what is happening nor a direct way of emergency intervention. Moreover, the reduced size of the microrobots does not necessarily make them less harmful. Consider, for instance, a faulty controller during a magnetic manipulation in an MRI system. An error in the order of magnitude of a current could turn a capsule into a bullet. Alternately, the targeted delivery of an extremely active anticancer drug at the wrong location could have dramatic consequences.

---

1 Leachable: material that can leach out of the device.

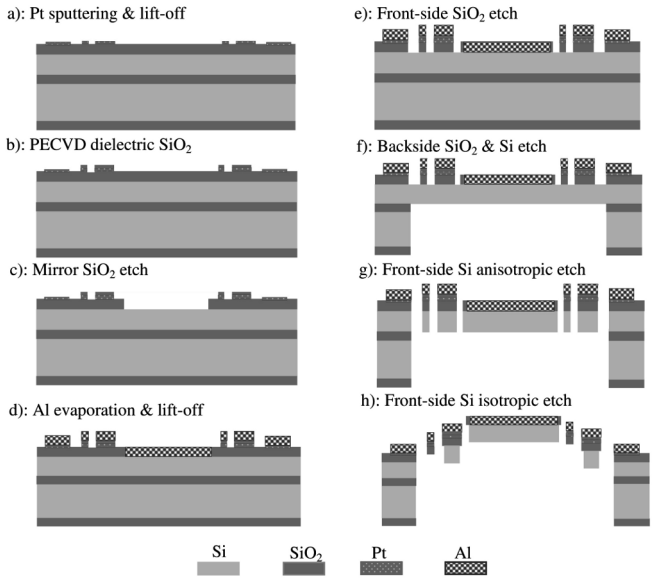

a)

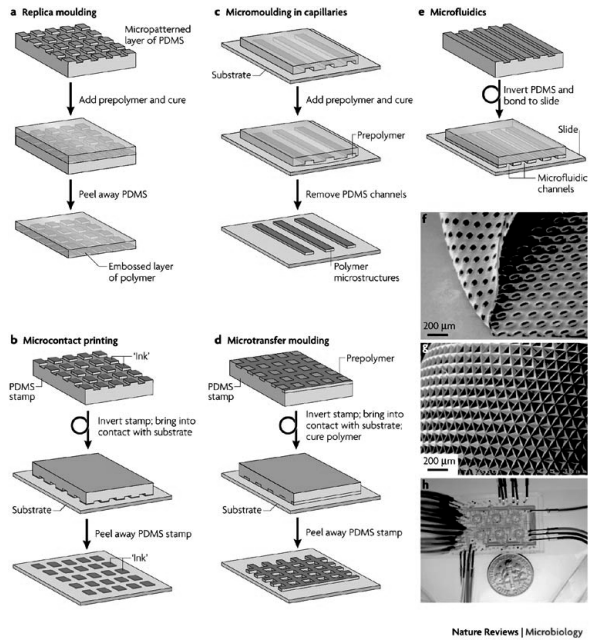

b)

Figure 2.3. *Examples of microfabrication process: a) for a MEMS mirror [SUN 10] or b) microbiology [WEI 07]*

Microfabrication techniques: when designing the intracorporeal microrobotic system, we necessarily need to take into account the available microfabrication techniques. Most often, one has to develop the fabrication process together with the system itself. Many processes make use of in-plane fabrication techniques, coming from the electronics industry, where successive layers are selectively deposited or removed from a silicon wafer (Figure 2.3). Detailed information on microfabrication techniques for microrobotics can be found in [BUC 10].

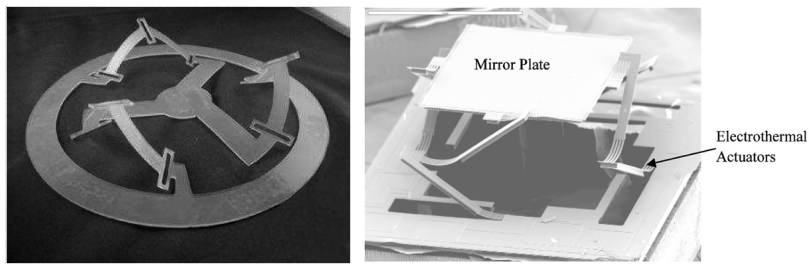

a) b)

Figure 2.4. *Out-of-plane mechanisms: a) a lamina emergent mechanism from [JAC 09] and b) a MEMS micromirror for OCT from [WEI 07a]*

Microassembly: Contrary to most MEMS devices, microrobots require complex structures that may not stay in the plane. A first class of approach relies on in-plane fabrication and out-of-plane spreading. Indeed, by imposing localized stress to a planar structure, some of its elements can bend and expand the structure into a 3D mechanism (Figure 2.4). Another class of approach is to rely on 3D assembly of several microparts, which requires the development of microassembly cells. Although of a relatively large size, such microassembly cells are designed to reach the appropriate accuracy [GAU 10b].

Two specific design methodologies for intracorporeal microrobots are worth being focused on.

The smart composite microstructures (SCM) developed by Wood [WOO 08] are based on in-plane fabrication and out-of-plane expansion of layered materials. However, they are not based on expensive silicon-wafer technologies but on a simple concept using cheap material. Rather than etching grooves in hard material to create flexure hinges, one can

glue precut rigid structures made up of carbon fibers on a flexible polymer layer (Figure 2.5). This concept has proven its efficiency for the realization of microflies and it will certainly become an indispensable technique in microrobotics.

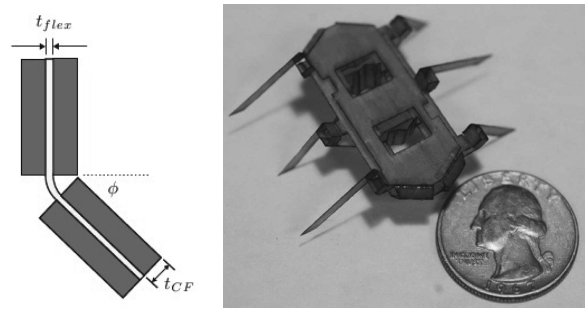

a) b)

Figure 2.5. *SCM: rigid carbon fiber patches attached on a flexible core a) allow for easy microfabrication of complex mechanisms b) [WOO 08]*

Another paradigm is emerging: soft robotics [TRI 08]. On the contrary to conventional robots that have rigid links and stiff motors, soft robots rely on soft and continuous deformation of their body; think of octopus arms or elephant trunks at macroscale. Recent events[2] have been focused on this paradigm, including some preliminary results related to biomedical microrobotics, such as self-assembling soft modular matter [YIM 13].

2.3.3. *Actuation*

2.3.3.1. *Smart materials*

This is a short summary of the main smart materials working principles, from the view of microrobotics. The readers interested in further details should refer to [CHA 10] and [GAU 10b].

2.3.3.1.1. Smart material physics

There exist as many smart materials as there are physical transduction effects, i.e. physical effects that convert one kind of energy (thermal,

2 http://www.birl.ethz.ch/sssr2012.

mechanical, electric and magnetic to name the main ones) into another (not necessarily different). We name here the main ones, for those readers who are unfamiliar with them.

– Electrostatic actuators convert electric energy (charges) into motion, due to attraction or repulsion between charged armatures of a capacitor with a variable shape:

$$\boldsymbol{\mathcal{F}}_{electrostatic} = -\frac{1}{2}\frac{\partial}{\partial x}\left(CV^2\right) \qquad [2.38]$$

where V is the potential between the two armatures, C is the capacity and x is a space variable describing the shape variation. In the case of two parallel plates, C is given by:

$$C = \epsilon\frac{S}{d} \qquad [2.39]$$

where ϵ is the dielectric constant of the material between the two plates, d is the distance between the two plates and S is the surface of the overlap between the two plates. So, one can generate forces either by allowing the plates to get closer ($x = d$) or to slide along each other ($x = S$).

Moreover, by changing the potential on each side of a capacitor, the armatures will be attracted to or repelled from each other. If we do not rigidly attach the armature, these forces will be transformed into motion. This allows us to make so-called comb-drive actuators that are widely used in the watch industry, for instance. They can be made in various shapes, to produce linear or rotary motion.

– Electrothermal materials convert electricity (namely current) into heat through the Joule effect, which in turn induces mechanical dilation. We can produce retraction due to the Peltier effect, which is the presence of cooling at an electrified junction of two different conductors. Together with additional mechanical constraints, one can produce various mechanical effects. For instance, if one builds a so-called bimorph by gluing together two layers made up of two different materials, with different thermal dilation coefficients, one can achieve bending because one material will dilate/retract less than the other one. Alternately, by heating a beam fixed at its two ends, one can convert thermal dilation into forces transverse to dilation. Such actuators are widely used in heat regulation for making electrovalves.

– Piezoelectric materials convert electricity (namely voltage) into mechanical deformation, by realignment of the crystalline structure of the material. We can find naturally piezoelectric mono-crystalline materials

(e.g. quartz and tourmaline) or we can synthesize artificial materials (e.g. PZT, $LiNbO_3$ and $BaTiO_3$) by polarization. The *direct* piezoelectric effect, discovered by Pierre and Jacques Curie, is the generation of charge under mechanical stress and forms the basis of many sensors (for instance microphones or ultrasound probe receivers). In contrast the *reverse* piezoelectric effect converts electric potential into material deformation and allows for piezoelectric actuators.

The piezoelectric equations relate variables of various origins: mechanical (strain S and stress T), electric (electric field E and electric displacement D) and thermal (absolute temperature θ and entropy σ). There exist several combinations of such variables, but the most intuitive one for actuation is:

$$S_i = \sum_{j=1}^{6} \sum_{m=1}^{3} s_{ij}^E T_j + d_{mi} E_m + \alpha_i^E \Delta\theta \quad i = 1..6, m = 1..3 \qquad [2.40]$$

where i, j, m, and n denote the geometric axes of space, α_i and s_{ij} are the standard thermal and mechanical expansion coefficients, respectively, and d_{mi} is the strain coefficient along axis i when a voltage is applied along axis m. These coefficients represent the anisotropic behavior of the material.

Since the coefficients d_{mi} are in the order of 0.1 nm/V, typical deformations of some tens of nanometers can be obtained under 100 V for elementary piezoelectric actuators with longitudinal effect (use of d_{33}). For elementary piezoelectric actuators with transverse effect (use of d_{31}), the deformations can reach some micrometers, due to the length/thickness ratio acting as an amplification factor.

Several kinds of actuators can be made of piezoelectric materials. The main two types are piezostacks and piezobeams. Piezostack actuators are obtained by stacking elementary piezoelectric actuators with longitudinal effects. The total deformation is thereby the sum of all elementary deformations. Piezobeams are made by at least two layers of material that deform differently under the electric field application, yielding a deflection of the beam orthogonally to the surfaces in contact. Unimorph piezobeams are thus made of one piezoelectric layer and one non-piezoelectric layer; bimorph and multimorph piezobeams are, respectively, made up of two or more piezoelectric layers.

– Shape memory alloys (SMA) also deform under external application of energy, such as temperature, electricity or magnetic field. The reason for this is the change of phase of the material, from austenite to martensite, and in reverse, using another kind of energy. For instance, one can deform

mechanically a branch of a pair of glasses to fit it to ones physiognomy and then have it recover its initial shape by heating it temporarily.

NiTi is the most common SMA for its properties: large strains (>5%), biocompatibility, mechanical resistance, little fatigue, little corrosion. The response time is rather large but proportionally decreases with the size of the actuator ($\sim$2 s for a 0.3 mm diameter NiTi thread vs. $\sim$0.5 s for a 0.05 mm diameter NiTi thread).

Other alloys have shape memory properties, such as NiMnGa, which is a magnetostrictive SMA with strains in the order of 5% under the application of a magnetic field in martensitic state, short response time ($\sim$1 ms) but little mechanical stress (<3 MPa).

– Electro-active polymers (EAPs) are artificial materials that can deform under electric stimulation. A detailed introduction to these materials, with focus on their biomedical applications, can be found in [CAR 09b]: polymer gels, ionic polymer-metal composites (IPMCs), conjugated polymers (polypyrrole), piezoelectric and electrostrictive polymers, dielectric elastomers. An example of EAP for microrobotics can be found in [JAG 00]. EAPs were recently shown to be MRI compatible [CAR 08] and should thus play a large role in the future of intracorporeal microrobotics. Some preliminary studies can be found, such as [KIM 03b], for a ciliary-based eight-legged walking microrobot using cast IPMC actuators.

– Even less conventional smart materials can be found, such as shape memory polymers [LEN 02, LIU 07], self-oscillating biomimetic polymer gels [MAE 10] or cellulose fibers [KIM 06] that may find their use in future intracorporeal microrobots.

2.3.3.1.2. Common features of smart materials

Smart materials are all different in their physics. However, they share many common features:

Temperature dependency: whatever the material, thermal dilation always exists. If not used for the actuation, it becomes a parasitic effect, which must either be physically counterbalanced in some way or taken into account by the control algorithms.

Hysteresis: most of the smart materials present hysteretic behaviors: the input–output relationship is different when the input increases and when it decreases. This is hardly physically counterbalanced and thus control must incorporate precompensators of the hysteresis.

Sensitivity to disturbances: at low scale, disturbances relatively increase. For instance, the simple fact of talking in a room makes a microbeam located in the room oscillate [BOU 11]. In industrial microrobotics, we can set up controlled environments to prevent most disturbances. In the healthy human body, the environment is somehow regulated (normally steady temperature and moisture, stable or monitorable blood pulsation and breathing rhythm). However, in the sick body, one can expect *unexpectable* disturbances.

Other nonlinearities: last but not least, these materials rarely exhibit a linear input–output transfer function of the energy. Therefore, many other sources of nonlinear behavior must be taken into account: nonlinear input–output transfer function, saturation, parasitic effects of any kind.

2.3.3.2. *Wireless actuation*

Actuation at microscale can be made using microactuators based on smart materials, with their respective characteristics in terms of range of motion and force, bandwidth, electric properties and biocompatibility, as discussed above and in section 1.3.3. Using microactuators is a valid solution for tethered partially intracorporeal robots, as a replacement for, or complement to, the traditional extracorporeal actuation acting on mechanical transmissions such as wires or tubes.

Of course, an alternative is the use of wireless actuation. Direct magnetic field actuation is, as shown in this chapter, the main source of research inspiration. However, some other research paths should be worth the investigation. One such path deals with remote ultrasonic actuators, because ultrasounds pass well through the body's structures and have frequencies close to the resonant frequencies of microstructures. Also using resonance, we could transfer energy wirelessly (electromagnetic waves at various wavelengths) not only to an embedded battery or capacitor, but also to a wireless microactuator. One could also think of making use of natural actuators such as the patient's muscles themselves (for instance to trigger localized peristalsis to propel videocapsules) or to grow muscle cells into a bio-microactuator embedded into a microrobot [PIL 11]. Further in actuality but not necessarily in relevance, one can fantasize over cybernetic small organisms (insects or larvas) that have extremely efficient microactuators or reversely, we can insert such biologic microactuators into man-made structures [AKI 11, AKI 12].

2.3.4. *Sensing*

Intracorporeal microrobotics requires sensing for at least two reasons. First, autonomous open-loop model-based control cannot be achieved. Indeed, this would require knowing in advance the variations of the anatomy and physiology, which modify the environment of the microrobotics. These variations are related to either one of the variability classes: intervariability from one person to another and intravariability within the same person, along time and sickness. Moreover, it is not possible to do any identification or calibration of the model to be used. Therefore, any intracorporeal microrobotic mission is unique and "one-shot", as in space. We would not like to perform such a mission blindly and without any real-time feedback[3].

Second, in the current state of the art, surgeons still want to keep "their hands on". Consequently, tele-micromanipulation and co-micromanipulation require some feedback also. As far as robotics is concerned, mainly position and, when possible, force must be sensed. Yet, additional physiological microsensing (e.g. temperature, pH other and ionic concentration) would need to be developed and embedded in or in the environment of the microrobot.

Consequently, sensing is an absolute prerequisite to intracorporeal microrobotics. Sensors can be classified into three main classes. The first class concerns microsensors that are embedded on the microrobot or distributed within the body to give feedback (temperature and pressure, for instance) on the microrobot environment. The second class contains medical imaging systems. The third class consists of other wireless localization systems, mainly in conjunction with magnetic manipulation.

2.3.4.1. *Microsensors*

Microsensors exist in an almost infinite amount of physical effects. We cannot go through all of them. Yet, a word should be lent piezoelectric microsensors. Indeed, piezoelectric materials offer direct and indirect effects, as presented in section 2.3.3. This opens the opportunity for self-sensing techniques [CLÉ 11], where physical effects due to the environment are not considered as simple disturbances but are converted into an online real-time estimation of the interaction between the microrobot and the environment. Thereby, one can embody the two functions, sensing and actuation, into a

3 Note that sending active pills without real-time feedback is called medication and is daily employed by medicine. However, doing the same with an intracorporeal microrobot (mobile or tethered) raises much more ethical, legal and societal concerns, despite the potential added-value.

single component, on the contrary to conventional robotics where these are usually obtained by the assembly of several components. This would partially solve the main problems of microsensors: miniaturization and embedding of the microsensors and their electronics in small volumes. However, the question of embedding both microsensors and microactuators is still open for robots of lower dimensions.

To overcome the limitations of microsensors, we can make use of medical imaging techniques.

2.3.4.2. *Medical imaging*

Medical imaging has revolutionized medicine in the last century, starting with the invention of X-ray imaging in the late 19th Century by Röntgen. Now, many imaging modalities are available to the surgeon, both at preoperative stage or along the execution of the operation. Some provide transparietal images (X-rays, echography, MRI), some provide intracorporeal images (endoscopy), some provide projective images (white light endoscopy, fluorescence, X-ray), some provide slices (CT scan, echography) and some provide volumes (MRI, 3D echography, OCT).

2.3.4.2.1. Intracorporeal vision

Intracorporeal vision takes several forms. It can conventionally use the visible light spectrum, as in capsular endoscopy or in laparoscopy. However, this has limitations. It does not "see" in all the places of the body (such as in the blood) and it only gives superficial information, whereas often the surgeon would like to know what is behind the surface (e.g. critical blood vessel or tumor border).

2.3.4.2.2. Narrow band imaging (NBI) and fluorescence

The full visible spectrum of light is not always needed or useful. In this way, to improve cancer diagnosis, some companies propose NBI devices. Indeed, the various tissues do not have the same optical properties. In particular, blood strongly absorbs green wavelength. Thus, if we use only the narrow band of the visible spectrum associated with green wavelength, then poorly vascularized tissues will reflect most of this illumination and appear in bright green color on an RGB sensor whereas dark regions of the image will correspond to heavily vascularized tissues. This enhanced contrast is of strong assistance to the surgeon to decide upon the location and extent of a cancerous tumor, since such tumors usually form a dense vascular network around them.

However, NBI is just "yet another cue" to detect cancer, based on the strong correlation between vascularization and tumors. It is nevertheless not

evidence. To go further, we can switch from light absorption properties to light emission properties of the tissues. Indeed, some proteins (e.g. porphyrins, elastine, and NADH) are *fluorescent* [PIE 09]. This means that, under illumination at a specific wavelength, they convert the incoming photon (light energy) into a step upward in their energy levels (electronic energy). These high energy levels are unstable. During the step downward to a stable lower energy level, the protein converts the electronic energy back into light by re-emitting a photon *at a different wavelength*. Knowing the autofluorescence spectrum of a given protein, one can hence design a dedicated optical setup with high specificity to observe the fluorescence of that protein only. Together with the knowledge of which protein(s) are a marker of a given cancer, one can in theory build a fluorescence imaging system with high specificity to that cancer. In practice, fluorescence imaging is regularly used in histological analysis of tissue slices. However, it is not yet embedded in intracorporeal microrobots, as far as we know.

Note that NBI and fluorescence imaging provide the surgeon with slightly subsurface information, since biological tissues are not completely opaque to light.

2.3.4.2.3. X-rays

X-rays are used in a wide variety of imagers to provide the surgeon with subsurface data. Radiography is the oldest one. It produces a single image, formerly on photographic films and now, because of flat panels, in numeric format. This image is the overlaid projection of all the layers of tissues that the X-rays went through, being absorbed differently by the various tissues. When used in real time, this technique is known as fluoroscopy. With contrast agent injection, these techniques are called coronarography or angiography, depending on the medical application field.

CT scanners also use X-rays. Instead of projecting them onto a flat panel, a CT scanner rotates around the body and projects one beam at a time that is collected by a receiver diametrically opposed to the X-ray source. The image of the slice of tissue (tomography) that was traversed is obtained by computing the inverse Radon transform of the signal at the receiver. Then, by moving the CT scanner along the body, we can reconstruct the whole body, slice by slice as illustrated by the Visible Human Project[4], with an accuracy below the millimeter.

---

4 http://www.nlm.nih.gov/research/visible/visible_human.html.

2.3.4.2.4. Magnetic resonance imaging

MRI is another technique for seeing through the body. It relies on intense magnetic fields in the order of several teslas. First, these fields are used to align the spin of the hydrogen atoms in the body in a specified direction. Then, the magnetic field constraints are turned off and the spins are relaxed to a non-coherent distribution in the tissues. Measuring the relaxation time, which differs from one tissue to another, allows for creating maps of the internal anatomy.

This technique provides a better separation of the tissues in the images, without any proven deleter effect on the patient. However, it has a smaller resolution than X-ray-based ones (around the millimeter), it is much more expensive and, as far as control is concerned, it is much slower. When fluoroscopy delivers videos at real-time frame rates (> 25 fps), conventional MRI takes approximately 100–200 ms (5–10 fps) to construct one image [GLA 13].

However, higher frame rates have been demonstrated [TAY 12, COO 12]. For instance, Cine MRI [COO 12] achieves *a posteriori* frame rate of 80 fps. More recently, a frame rate of 40 fps was even reported [BAU 13]. It should be noted that the frame rate increase is not due to advanced technology or faster signal processing, but due to novel advanced signal sampling, such as compressed sensing. Instead of regularly sampling a signal (following Shannon's theorem), one can use sparse sampling together with functional bases to identify the signal seen as a continuous function, not as a time series.

2.3.4.2.5. Echography

Echography is a good trade-off between real-time, accurate, poorly contrasted, nocive X-rays and slow, less accurate, highly contrasted, safe MRI. Indeed, it is based on the reflection of ultrasound waves on the tissues, and provides slices (or volumes in the case of 3D ultrasound probes) of the anatomy. The slices are obtained by tomography, based on the time of flight of the ultrasound sequences. It is used either from outside the body (as for prenatal diagnosis or even in medical robotics [MEB 10, SAU 08]) or from inside the body, with miniature probes (as in echoendoscopy).

It allows for real-time, cheap and safe imaging with a resolution in the order of the ultrasound wavelength, thus depending on the frequency of the acoustic wave, as opposed to the penetration depth, which depends on the wavelength. In standard clinics, the resolution is thus approximately 1 mm with a 10 cm penetration depth and for higher frequencies, it reaches some

tens of micrometers but to the cost of a penetration depth below 1 cm [FUJ 08].

2.3.4.2.6. Microscopy

The basis of confocal microscopy is the use of confocal planes, that is the two focal planes located on each side of a lens (Figure 2.6). By placing the light source (generally a laser) and the detector behind pinhole apertures that are in confocal configuration with a plane crossing the tissue sample, one can restrict the imaging of the point of focus on the tissue. Confocal images are thus obtained by XY scanning of the tissue surface. They thus form like conventional optical images but with a scene restricted to the focal plane. In addition, moving, the lens along the Z axis allows us to place the focal plane deeper in the tissue and thus to reconstruct a depth profile along the beam, and in association with the XY scanning a full volume. The resolution of confocal microscopy is in the order of 1 μm with a penetration depth approximately half a millimeter [FUJ 08], but the quality of the map that is reconstructed during the scanning depends on the stability of the relative location of the scanning beam and the anatomic piece. Recently, Morel *et al.* [ROS 11] implemented a visual servoing technique to compensate for physiological motions in fiber-based intracorporeal confocal microscopy, which allows us to build accurate mosaics of confocal images.

OCT works along the interferometry principle (Figure 2.7). A laser beam (i.e. a coherent light source) is sent to the tissues and partially reflected by the successive layers of tissues below the surface. Measuring the phase shift between the reflected light coming back from the tissues and from a reference path allows us to have an extremely accurate estimate of the distances between each layer along the beam path. By scanning the beam, one can reassemble the depth data into a volume, showing the geometric structure of the tissue sample. This volume needs be interpreted by the medical biologists for analysis and by the oncologist for diagnosis. OCT is foreseen as a potential contactless optical biopsy tool, because its resolution, in the order of 1–10 μm with a penetration depth up to 10 mm [FUJ 08], is very close to histological slices. The acquisition time depends on the size of the zone to be covered and the resolution of the sweeping motion, but is currently in the order of 1 or 2 s for an exploitable optical biopsy slice.

Yet, its limitation for intracorporeal use is related to the need of fibers to bring the laser down into the body and back out to the interferometer. Work is ongoing in the MEMS community to build micro-OCT systems that could be embedded at the tip of an endoscope [PAN 01].

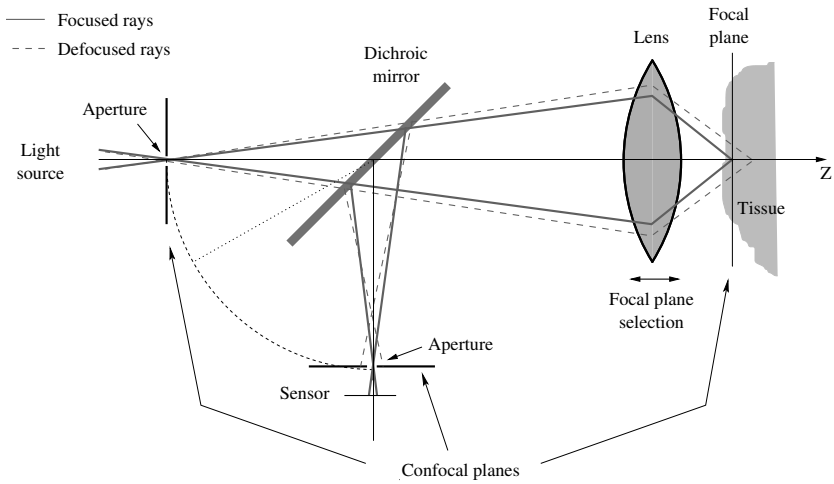

Figure 2.6. *Confocal microscopy images only the focal plane and thus generates very sharp images*

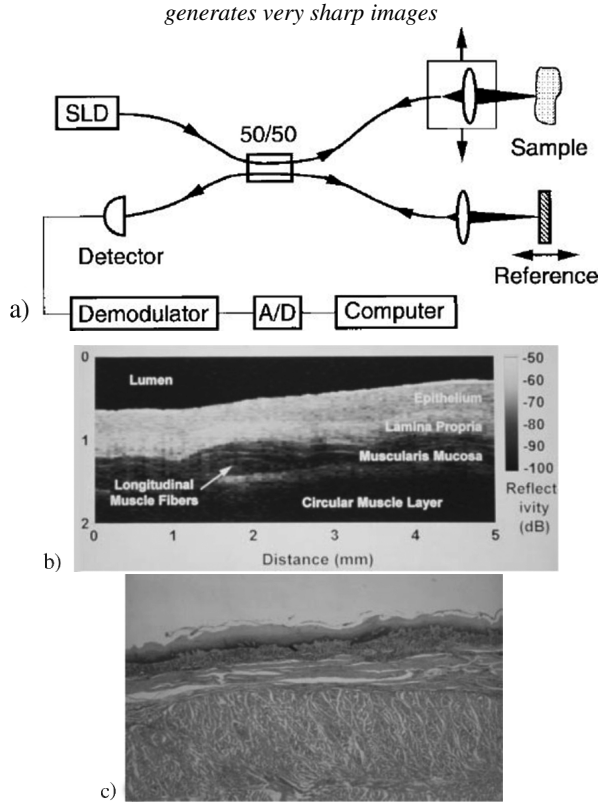

Figure 2.7. *Optical coherence tomography (OCT): a) schematic diagram; b) OCT image of porcine esophagus; c) histological section corresponding to the OCT image [IZA 96]*

2.3.4.3. *Wireless localization*

Manipulation of a wireless microrobot requires having real-time knowledge of its location in the body, to avoid the risk of losing control of it. Unmodeled disturbances or model discrepancies despite embedded microsensors of tethered microrobots may also require accurate localization of their tool tip. In both cases, external imaging techniques may solve the problem, but alternatives exist.

In particular, magnetic localization is extremely interesting, as part of the self-sensing paradigm (section 2.3.4.1), for magnetically actuated wireless microrobots. Indeed, the displacement of an object with magnetic properties in a magnetic field can be tracked. For instance, the Motilis centimetric capsule [GUI 06] replaces the usual camera by a set of coils that are used to transform the motion into induction currents. From the latter, one can accurately localize the capsule, track the motility of the intestine and estimate the 3D trajectory (successive positions as a function of time) of the capsule. At the same scale, three orthogonal Hall effect sensors are placed in a magnetically guided capsule to compute the magnetic induction field generated by the coupling of the on-board permanent magnet and the external guiding permanent magnet [SAL 12, DIN 13]. Similarly, in [MIL 12, POP 13], it is an array of six Hall sensors that are embedded in the capsule.

In fact, the presence of a magnetic object in a magnetic field modifies the latter. So, measuring the field with enough accuracy in sufficiently numerous points would allow us to fit a model dependent on the magnetic object location, as it is done in numerical dosimetry [SCO 05].

Another useful paradigm is simultaneous localization and mapping (SLAM). For instance, it is foreseen to reconstruct the geometry of the intestine walls with a centimetric videocapsule [CIU 12].

2.3.5. *Control*

2.3.5.1. *Control specificities at microscale*

The main specificities of control at microscale, as already partially discussed, are as follows:

– a relatively low quality of microfabrication and microassembly;

– a poor knowledge of physics at that scale, which prevents from using accurate models of the interaction with the environment;

– a poor signal-to-noise ratio of microsensors;

– a strong dependence on thermal variations and other sources of disturbances (such as human activity [BOU 11]);

– the prominence of imaging techniques, due to the strong use of teleoperation, which requires visual feedback to the operator;

– the large ratio between the user and the microrobot scales, yielding non-intuitive and non-transparent motion transduction;

As a result, a prerequisite to intracorporeal microrobotics is the development of efficient industrial microrobots and microfactories outside the operating room for the improvement of the intracorporeal microrobot manufacturing quality.

Independently from micromanufacturing, robust control is often needed to compensate for disturbances. Also, because of the presence of microscopes, visual servoing is often used for achieving high-precision assembly [TAM 10, JAS 10]. Imaging is also useful to tele-micromanipulation [NI 12].

In the medical domain, additional constraints make the control problem even more complex:

– the environment is far from being controlled, homogeneous and perfectly understood;

– biological intra- and inter- variability cast a doubt on model-based control approaches;

– patient safety and medical gesture repeatability cannot suffer approximate teleoperation by insufficiently trained surgeons.

As a result, image-based techniques are good candidates for local regulation of teleoperated tasks, as an alternative or complement to surgeon training, as demonstrated in ophthalmology [KUM 10] or digestive diagnosis [ROS 11]. More generally, sensor-based control [SAM 91], which has now reached maturity for autonomous robot navigation in unstructured environments (DARPA challenge, Mars rovers), should play a large role in the coming years. Indeed, surgeons tend to be more open to robotics as years pass by, probably due to the ubiquity of information technologies (smartphones and tablet PCs) and robotics (autonomous car parking, robot cleaners, robot toys) in the upper social classes.

2.3.5.2. *Control of magnetically actuated tools*

Several approaches have been taken to exploit the magnetic field according to what is made variable and controlled:

– position and orientation of the sources;

– currents in electromagnetic coils.

Moreover, we can make use either of the magnetic force or torque. All the combinations can be found in the literature, but there has not been any generic formulation of magnetic control so far. This section aims at filling this gap.

2.3.5.2.1. Trajectory tracking

Consider a proper definition of the Cartesian error:

$$\boldsymbol{e} = \begin{pmatrix} {}^{d}\boldsymbol{t}_c \\ \underline{\boldsymbol{u}}\theta \end{pmatrix} \quad [2.41]$$

with $({}^{d}\mathbf{R}_c, {}^{d}\boldsymbol{t}_c)$ being the residual rigid transformation between the desired (subscript d) and current (subscript c) reference frame of the microrobot, and $(\underline{\boldsymbol{u}}, \theta)$ is the axis and angle of ${}^{d}\mathbf{R}_c$.

Then, a second-order behavior of the Cartesian error:

$$\ddot{\boldsymbol{e}} + K_d\dot{\boldsymbol{e}} + K_p\boldsymbol{e} = 0 \quad [2.42]$$

can be obtained by a PD + feedforward controller:

$$\begin{pmatrix} {}^{d}\dot{\boldsymbol{v}}_c \\ {}^{d}\dot{\boldsymbol{\omega}}_c \end{pmatrix} = \begin{pmatrix} {}^{d}\dot{\boldsymbol{v}}_d \\ {}^{d}\dot{\boldsymbol{\omega}}_d \end{pmatrix} - K_d\dot{\boldsymbol{e}} - K_p\boldsymbol{e} \quad [2.43]$$

which thus defines the acceleration, in translation and rotation, to be applied to the microrobot.

2.3.5.2.2. Force and torque input

To achieve the above acceleration, we need to balance the magnetic, friction, external (such as gravity or buoyancy) and dynamic efforts:

$$\boldsymbol{\mathcal{F}}_{mag} = m\,{}^{d}\dot{\boldsymbol{v}}_c - \boldsymbol{\mathcal{F}}_f - \boldsymbol{\mathcal{F}}_e \quad [2.44]$$

$$\boldsymbol{\mathcal{T}}_{mag} = \mathbf{I}_{in}\,{}^{d}\dot{\boldsymbol{\omega}}_c - \boldsymbol{\mathcal{T}}_f - \boldsymbol{\mathcal{T}}_e \quad [2.45]$$

This brings us back to electromagnetics for these forces and torques must be generated using the available sources. Therefore, referring to equations [2.6] and [2.7], the following system needs be solved:

$$\nabla(\boldsymbol{m}_o^{\mathsf{T}}\boldsymbol{b}(\boldsymbol{P})) = \boldsymbol{\mathcal{F}}_{mag} \quad [2.46]$$

$$\boldsymbol{m}_o \times \boldsymbol{b}(\boldsymbol{P}) = \boldsymbol{\mathcal{T}}_{mag} \quad [2.47]$$

by shaping the magnetic field, given the desired magnetic force and torque, and the (measured) static state ($\boldsymbol{P}$ and $\boldsymbol{m}_o$) of the object to be moved.

The torque equation is easily understandable by a roboticist, but the force equation needs be translated into robotics notation:

$$\mathbf{J}_{\boldsymbol{b}}(\boldsymbol{P})^{\mathsf{T}}\boldsymbol{m}_o = \boldsymbol{\mathcal{F}}_{mag} \quad [2.48]$$

with:

$$\mathbf{J}_{\boldsymbol{b}}(\boldsymbol{P}) = \frac{\partial \boldsymbol{b}(\boldsymbol{P})}{\partial \boldsymbol{P}} = \begin{pmatrix} \frac{\partial \boldsymbol{b}(\boldsymbol{P})}{\partial x} & \frac{\partial \boldsymbol{b}(\boldsymbol{P})}{\partial y} & \frac{\partial \boldsymbol{b}(\boldsymbol{P})}{\partial z} \end{pmatrix} \quad [2.49]$$

the *magnetic Jacobian* matrix.

2.3.5.2.3. Magnetic field shaping

The actual control in rotation and translation of a magnetized object is computed by shaping the magnetic field, through constraints on *both* the value of the field and the value of its Jacobian in the object location.

Let us now derive a generic formulation of the problem, based on the generic model of magnetic induction of equation [2.36], assumed linear in the currents for the sake of clarity:

$${}^{w}\boldsymbol{b}({}^{w}\tilde{\boldsymbol{P}}) = \sum_{i=1}^{N} {}^{w}\mathbf{R}_i \, {}^{i}\boldsymbol{\sigma}({}^{i}\underline{\tilde{\boldsymbol{m}}}, {}^{i}\mathbf{T}_w \, {}^{w}\tilde{\boldsymbol{P}}) \, I_i \quad [2.50]$$

To do so, the magnetic Jacobian of the compound field must be derived. Because of linearity, it can easily be computed from the magnetic Jacobian matrices associated with each source, expressed in their local frame ${}^{i}\mathbf{J}_{\boldsymbol{b}}$. To do

so, just take the partial derivative of the previous equation with respect to $\boldsymbol{P}$, expressed in the world frame:

$$ {}^{w}\mathbf{J}_{\boldsymbol{b}}({}^{w}\tilde{\boldsymbol{P}}) = \sum_{i=1}^{N} {}^{w}\mathbf{R}_{i}\, {}^{i}\mathbf{J}_{\boldsymbol{\sigma}}({}^{i}\mathbf{T}_{w}\, {}^{w}\tilde{\boldsymbol{P}})\, {}^{i}\mathbf{R}_{w}\, I_{i} \qquad [2.51] $$

where:

$$ {}^{i}\mathbf{J}_{\boldsymbol{\sigma}}({}^{i}\tilde{\boldsymbol{P}}) = \frac{\partial\, {}^{i}\boldsymbol{\sigma}({}^{i}\underline{\tilde{\boldsymbol{m}}}, {}^{i}\tilde{\boldsymbol{P}})}{\partial\, {}^{i}\boldsymbol{P}} \qquad [2.52] $$

encodes the local variations of the magnetic shape and can thus be called the *magnetic shape variation matrix*.

As a result of the derivations above, we can now state the generic control problem:

PROPOSITION 2.4.– GENERIC MAGNETIC CONTROL PROBLEM.– Given

– a magnetized object with magnetic moment $\boldsymbol{m}_o$, located in $\boldsymbol{P}$;

– N magnetic sources;

– the shape ${}^{i}\boldsymbol{\sigma}({}^{i}\underline{\tilde{\boldsymbol{m}}}, {}^{i}\tilde{\boldsymbol{P}})$ of the field created by each source;

– the value of the individual magnetic shape variation matrices ${}^{i}\mathbf{J}_{\boldsymbol{\sigma}}({}^{i}\tilde{\boldsymbol{P}})$;

– the desired magnetic force $\boldsymbol{\mathcal{F}}_{mag}$ and torque $\boldsymbol{\mathcal{T}}_{mag}$ obtained from the trajectory tracking algorithm;

and given for generic control inputs

– the rigid transformation ${}^{w}\mathbf{T}_{i}$ from the world frame to the local frame associated with each source;

– the current I_i in each source;

then, the control of the displacement of the magnetic object must satisfy:

$$ \begin{aligned} {}^{w}\boldsymbol{m}_{o} \times \sum_{i=1}^{N} {}^{w}\mathbf{R}_{i}\, {}^{i}\boldsymbol{\sigma}({}^{i}\underline{\tilde{\boldsymbol{m}}}, {}^{i}\mathbf{T}_{w}\, {}^{w}\tilde{\boldsymbol{P}})\, I_{i} &= {}^{w}\boldsymbol{\mathcal{T}}_{mag} \\ \sum_{i=1}^{N} {}^{w}\mathbf{R}_{i}\, {}^{i}\mathbf{J}_{\boldsymbol{\sigma}}({}^{i}\mathbf{T}_{w}\, {}^{w}\tilde{\boldsymbol{P}})^{\mathsf{T}}\, {}^{i}\mathbf{R}_{w}\, {}^{w}\boldsymbol{m}_{o}\, I_{i} &= {}^{w}\boldsymbol{\mathcal{F}}_{mag} \end{aligned} \qquad [2.53] $$

REMARK.– No torque can be applied around the magnetic moment of the object because of the cross-product above. In other words, we must always check that the desired torque $\boldsymbol{\mathcal{T}}_{mag}$ is orthogonal to the object magnetic moment $\boldsymbol{m}_0$.

From this proposition, the control strategies found in the literature become clear. The first strategy consists of considering all sources fixed with respect to each other (constant global geometry) and of using only the currents as control inputs: control with static coils. The second strategy consists of considering only permanent magnets (constant current) and of moving one or several sources with respect to the world frame: control with permanent magnets. The last strategy is to use all the available DoFs: control with multiple mobile magnetic sources.

2.3.5.2.4. Control with static coils

When we use only static sources, the generic control problem simplifies into:

$$\underbrace{\begin{pmatrix}\mathbf{A}_T(\boldsymbol{m}_o,\boldsymbol{P})\\ \mathbf{A}_F(\boldsymbol{m}_o,\boldsymbol{P})\end{pmatrix}}_{\mathbf{A}(\boldsymbol{m}_o,\boldsymbol{P})}\begin{pmatrix}I_1\\ \vdots\\ I_N\end{pmatrix}=\begin{pmatrix}\boldsymbol{\mathcal{T}}_{mag}\\ \boldsymbol{\mathcal{F}}_{mag}\end{pmatrix} \qquad [2.54]$$

with:

$$\begin{aligned}\mathbf{A}_T(\boldsymbol{m}_o,\boldsymbol{P}) &= \begin{pmatrix}\boldsymbol{\tau}_1(\boldsymbol{m}_o,\boldsymbol{P}) & \dots & \boldsymbol{\tau}_N(\boldsymbol{m}_o,\boldsymbol{P})\end{pmatrix}\\ \mathbf{A}_F(\boldsymbol{m}_o,\boldsymbol{P}) &= \begin{pmatrix}\boldsymbol{f}_1(\boldsymbol{m}_o,\boldsymbol{P}) & \dots & \boldsymbol{f}_N(\boldsymbol{m}_o,\boldsymbol{P})\end{pmatrix}\\ \forall i=1..N,\quad \boldsymbol{\tau}_i(\boldsymbol{m}_o,\boldsymbol{P}) &= {}^w\boldsymbol{m}_o\times{}^w\mathbf{R}_i{}^i\boldsymbol{\sigma}({}^i\underline{\tilde{\boldsymbol{m}}},{}^i\mathbf{T}_w{}^w\tilde{\boldsymbol{P}})\\ \forall i=1..N,\quad \boldsymbol{f}_i(\boldsymbol{m}_o,\boldsymbol{P}) &= {}^w\mathbf{R}_i{}^i\mathbf{J}_{\boldsymbol{\sigma}}({}^i\mathbf{T}_w{}^w\tilde{\boldsymbol{P}})^{\mathsf{T}}{}^i\mathbf{R}_w{}^w\boldsymbol{m}_o\end{aligned}$$

Of course, $\mathbf{A}(\boldsymbol{m}_o,\boldsymbol{P})$ must be of rank 5 for this system to have a unique solution (remember "no torque around $\boldsymbol{m}_o$").

As usual, rotation and translation are partially decoupled: rotation can be controlled separately, while translation control is not independent from rotation control. Indeed, if one uses uniform fields, then no force is exerted, unless the object itself is able to transduce the magnetic energy into translation motion. On the contrary, as soon as one applies current to create forces, a magnetic induction field is created, which affects the orientation of the object.

The approaches in the literature can be classified into approaches where uniform fields are rotating, approaches with oscillating uniform fields and approaches solving the full problem.

Rotating uniform field approach: when using uniform fields, we cannot directly apply forces. However, one can create a self-rotation of a helix in order to create a corkscrew translation (Figure 2.8). This was proposed by Sendoh *et al.* [SEN 03] to have an endoscopic camera creep into the intestine. This approach was also used to swim helical flagella at a low Reynolds number [HON 96, ZHA 09, ZHA 10, MAH 11b, TOT 12, ABB 09, GHO 09]. In these applications, translation is thus induced by uniform fields due to a mechanical rotation-translation transduction.

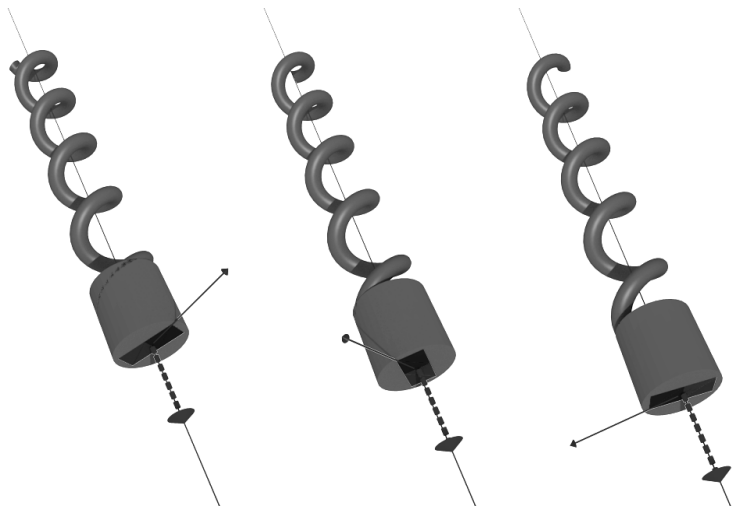

Figure 2.8. *Rotating uniform field approach: applying a uniform field (thin solid arrow), rotating around the corkscrew axis, onto a magnet orthogonal to the corkscrew axis creates a torque (thick dashed arrow) along the corkscrew axis, which rotates the corkscrew and makes it progress in the direction of the torque*

Oscillating uniform fields: another way to exploit the uniform magnetic field to create translation is to make resonant microhammers [KRA 09]. Indeed, two magnetized objects, located close to each other, tend to attract or repel each other when placed in a uniform magnetic field. Connecting two such objects by a microspring creates a resonant structure, which can exhibit translational properties, when placed in an oscillating magnetic field (Figure 2.9).

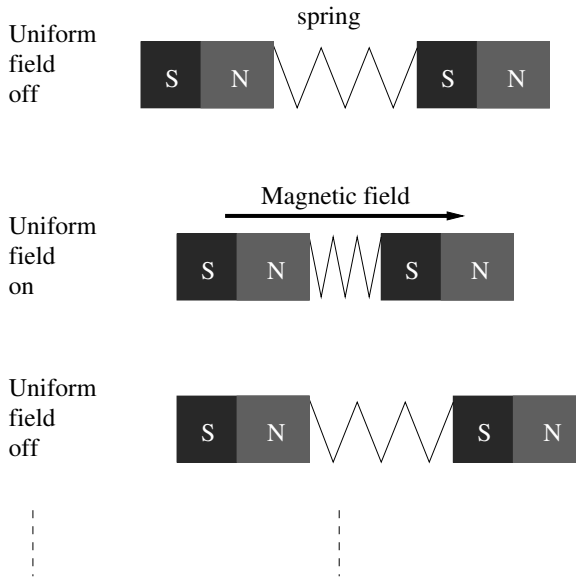

Figure 2.9. *Oscillating uniform fields can translate resonant microhammers*

In [BYU 11], the oscillation of a uniform field allows us to swing the 12 mm-long tail of a 1.44 mm $\times$ 3 mm $\times$ $(3.3 + 12)$ mm fish-like robot and have it swim in a fluid. This could have application in gastric endoscopy. Similarly, a microrobot with a 10 mm long tail was shown to swim under MRI conditions [KÓS 08].

In the same idea, for swimming at low Reynolds number (for instance in the stomach filled with agar-agar gel as in [REY 10]), asymmetry in shape can be obtained by switching on and off the uniform field around an artificial cilia made up of magnetic particles embedded in a polymer film, as investigated in the ARTIC European project [KHA 11].

Rotation-induced force approach: transduction from torque to force can be obtained by mechanical constraints, as for catheter guidance (Figure 2.10). Thereby, a catheter tip can be deflected laterally due to the mechanical constraint in the catheter and the change of orientation of magnets inserted along the tip [ROB 02, LAL 10, MUL 12].

Full-field approach: the most frequent use of the static coil approach is to solve simultaneously for the torque and the force. It is usually done in the plane with

two orthogonal coil pairs [IVA 13]. In 3D space, we most often uses three such orthogonal coil pairs [MAR 07, KEL 12, NGU 10, WAN 07] with a notable exception in ophthalmology where, because of the anatomic constraints, the out-of-plane motion is obtained with four coils located on the same side of the plane [KUM 10].

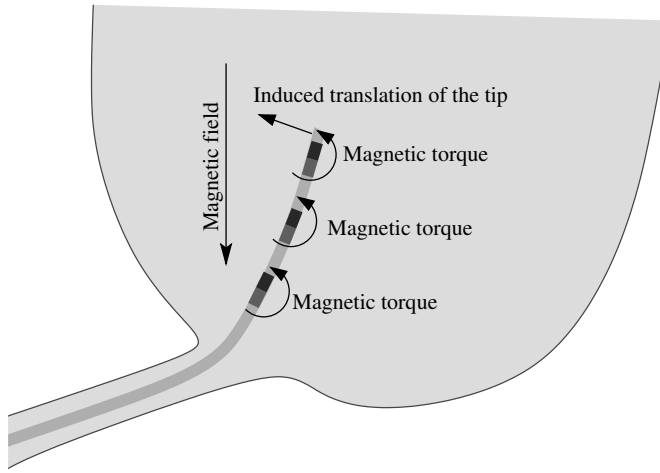

Figure 2.10. *Translation can be obtained with a uniform field due to mechanical constraints: each embedded magnet tends to align with the magnetic field and thus creates a circular translation of the next segments along the catheter*

In [JEO 11], a configuration with three Helmholtz coil pairs and one Maxwell coil pair, instead of the three conventional coil pairs as above, is used to drill into vascular clots.

2.3.5.2.5. Control with mobile permanent magnets

When using permanent magnets, the currents in equation [2.50] are considered as constant and unitary $I_i = 1$. This is a nonlinear problem in the components of ${}^{w}\mathbf{T}_i$. Therefore, it does not have a closed-form solution as the problem associated with static coils. This might explain why only the case with one magnetic source can be found in the literature, so far.

With only one source, the problem slightly simplifies into:

$$\begin{aligned} {}^{w}\boldsymbol{m}_o \times \left({}^{w}\mathbf{R}_m \, {}^{m}\boldsymbol{\sigma}({}^{m}\underline{\tilde{\boldsymbol{m}}}, {}^{m}\mathbf{T}_w \, {}^{w}\tilde{\boldsymbol{P}}) \right) &= {}^{w}\boldsymbol{\mathcal{T}}_{mag} \\ {}^{w}\mathbf{R}_m \, {}^{m}\mathbf{J}_{\boldsymbol{\sigma}}({}^{m}\mathbf{T}_w \, {}^{w}\tilde{\boldsymbol{P}})^{\mathsf{T}} \, {}^{m}\mathbf{R}_w \, {}^{w}\boldsymbol{m}_o &= {}^{w}\boldsymbol{\mathcal{F}}_{mag} \end{aligned} \quad [2.55]$$

Again, several approaches can be taken to solve it.

Full field approach: in [CIU 10b], magnetic manipulation of a wireless videocapsule was demonstrated, where the magnetic force generated by an external permanent magnet displaced by a robot arm is approximated by a finite-element mesh, fitted onto real measurement.

Rotation-induced force approach: a very pleasing result can be found in [MAH 11a], where the force applied to a slave permanent magnet is obtained by rotating a master permanent magnet. To do so, a specific rotational velocity profile is given to the master magnet such that the relative orientation between the master and slave magnets is stabilized to 90°. In this configuration, a magnetic force is necessarily applied along the direction orthogonal both to the master rotation axis and the direction of the vector from the master to the slave (Figure 2.11).

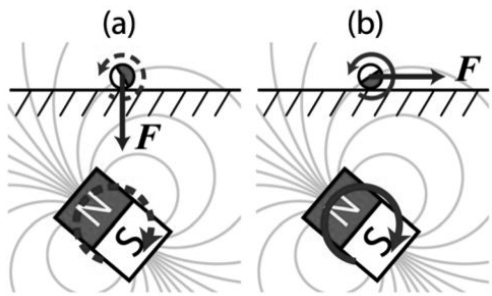

Figure 2.11. *a) Quasistatic rotation of a permanent magnet generates attraction. b) Appropriate dynamic control of the rotation generates lateral displacement [MAH 11a]*

Transduction from torque to force for catheter guidance can also be done using mobile permanent magnets, as in the Niobe II system (which will be shown further), or for the insertion of cochlear implant [CLA 12].

Torque approach: helical microrobots can also be steered using mobile permanent magnets [FOU 10, MAH 12, XU 13].

The capacity of applying torques to a wireless capsule was also used in [YIM 12] to enable rolling locomotion of a videocapsule on the walls of the stomach.

The last two approaches will be illustrated in section 2.4.

2.3.5.2.6. Control with multiple mobile sources

In a preliminary set-up for the Octomag, such an approach was used in [YES 06], where a microrobot is driven through a micromaze. In this set-up, a Maxwell coil and a Helmholtz coil are aligned and centered on a beam, to generate both uniform gradient and uniform field at the center. Thus, the microrobot will align on the common coil axis and will be translated along this axis. The second feature of the setup is to mechanically rotate the beam, to align the common coil axis with the channel of the micromaze where the microrobot is located. Thus, the microrobot is controlled by both moving the coils and changing their currents.

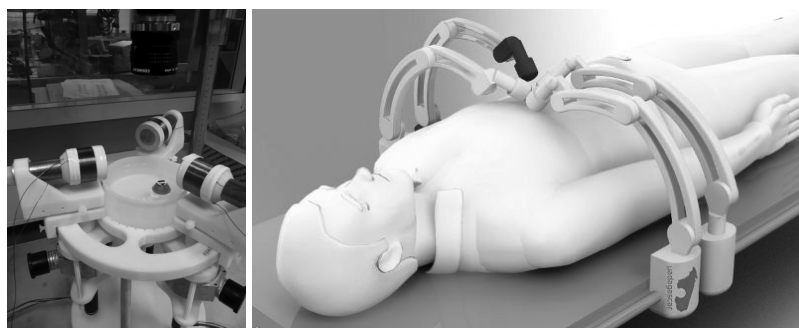

a) b)

Figure 2.12. *Control with multiple mobile sources: a) prototype for manipulation in the plane and b) conceptual view of its use in digestive endoscopy*

In a theoretical work [VÉR 12, VÉR 13], magnetic manipulation in a plane is done using three coils located at the vertices of an equilateral triangle and rotating around the axis orthogonal to the plane (Figure 2.12). Hence, the

system becomes redundant (three current inputs and three controlled source axes for only three DoFs), which opens the path for minimizing a secondary task (such as the manipulability index [MER 07]).

Also recently, a device incorporating an XY manipulator holding an electromagnet was reported to optimally steer a capsule prototype in a horizontal intestine mock-up [LIO 12].

2.4. Devices

2.4.1. *Magnetically guided catheters*

To steer catheters in the vascular system, there exist two robotic classes of solutions. The first one is to use wires to actuate the distal tip as in the Sensei X or Magellan robots from Hansen Medical (see section 1.2.1) or the CorPath robot from Corindus/Philips. The other solution is to actuate the distal tip using magnetic fields, as in the Niobe II system from Stereotaxis[5] or the CGCI system from Magnetecs [NGU 10], both shown in Figure 2.13. These two systems are exemplary of the use of unconventional robotics concepts: wireless actuation rather than mechanical transmission of motion.

They both work on the same principle of magnetic steering. However, Niobe II uses the combination of mobile permanent magnets with torque actuation, while CGCI uses the combination of fixed electromagnets with full five-DoF force and torque actuation. In that sense, catheter guidance control and imaging (CGCI) resembles the Octomag system described below.

On the other hand, Niobe II is rather self-standing because it *does* apply translations of the catheter tip despite the use of a uniform field. This is not due to the application of forces on the tip, as demonstrated by the reported impossibility to steer a capsule with this system [CAR 09a]. In fact, the translations are obtained by mechanical conversion of the magnetic torques. Indeed, three small magnets are placed along the flexible end of the catheter. Therefore, they all tend to align with the uniform magnetic field, which creates bending of the catheter's final few centimeters, and thus translations of the distal tip.

---

5 http://www.stereotaxis.com/physicians/the-lab/virtual-tour-us/.

2.4.2. *Distal tip mobility for endoluminal microphonosurgery*

The vocal folds are located in the periphery of the human body: they are inside the body but yet rather easy to reach. Indeed, by outstretching the patient's neck to its maximum, the surgeon has a direct line of sight to the larynx cavity and the vocal folds it contains. This allowed the development of the so-called laser microphonosurgery [JAK 72]. In this surgery, a microscope and a laser are aligned between the surgeon's eye and the vocal folds through a rigid and straight laryngoscope attached onto the patient's chest, in a set-up called *suspension (micro-)laryngoscopy* (Figure 2.14). Several commercial systems exist for such a clinical protocol that steers a CO_2 laser beam with a two-axis galvanometric actuated mirror. One of them, the Acublade by Lumenis, even possesses some automated procedures such as resection (cutting) along a segment and ablation (vaporizing) within a circle. This allows us to call it a robotized microsurgery tool.

The main drawbacks of such systems are as follows:

Suspension: insertion of the laryngoscope is reported to provoke cervical pain and various injuries (teeth, lingual nerve, oropharyngeal walls).

Safety: the laser beam travels in free space between the steering mirror and the vocal folds, resulting in burns due to misalignment.

Accuracy: the laser beam is shot at approximately 40 cm from the vocal folds, thus requiring an accuracy of approximately 0.015° (0.25 mrad) on the galvanometric axes if we want an accuracy of 100 μm on the laser spot center.

Focusing: the laser beam diverges, thus limiting the energy density on the vocal folds and, thereby, the resection/ablation capabilities.

To overcome these drawbacks, several paths are to be followed. The first path is to develop hollow core fibers [REM 12], which can bring a CO_2 laser down into the throat. However, such fibers are delicate to handle and the laser beam diverges rapidly. The second path relies on the DaVinci telemanipulator to perform transoral robotic surgery (TORS) [HOC 05], but in practice the size of the tools is still not fully adapted (Figure 2.15), which might give rise to collisions between tools and endoscope during the operation. Of course, we can follow both [SOL 07] but at what cost?

a)

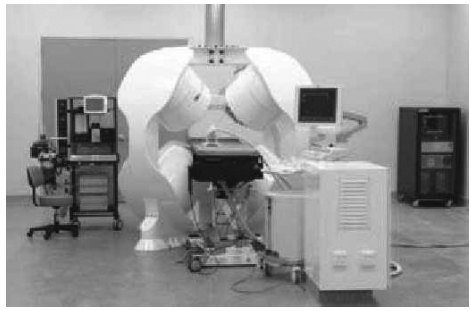

b)

Figure 2.13. *a) The Niobe system [CAR 07] and b) the CGCI system [NGU 10]*

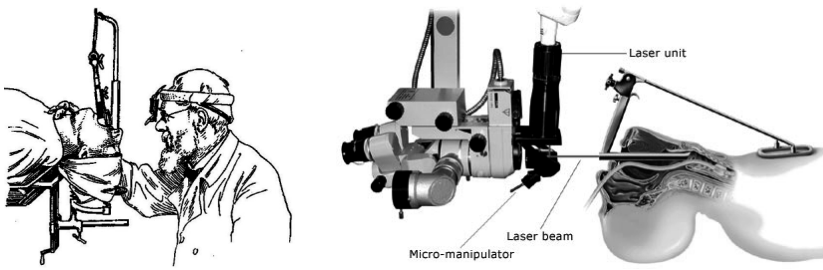

a) b)

Figure 2.14. *History of endoluminal microphonosurgery systems: a) in the 1910s, invention of the suspension laryngology [ALO 13]; b) in the 1970s, suspension laryngoscopic laser microsurgery [DEL 09]*

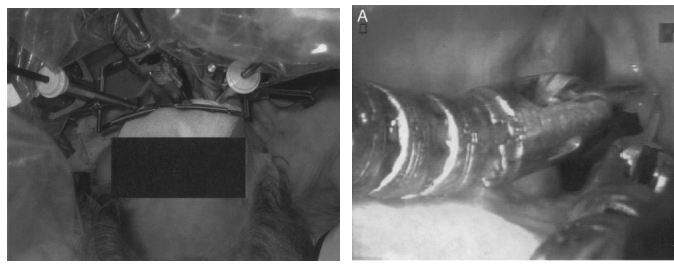

a) b)

Figure 2.15. *a) Trans-oral robotic surgery of the vocal folds: set-up and b) endoscopic view (right) from [HOC 05]*

The third path consists of using HARP, a flexible robotic tool that can bend along the natural curvature of the mouth and throat in order to avoid stretching the neck uncomfortably [RIV 12]. Made of a highly flexible body with 50 bodies (Figures 1.7 and 2.16(a)) and equipped at the distal tip with a camera and two arms holding forceps and a scalpel, it was clinically tested on a vocal fold injection. Yet, the overall width of the distal tip is approximately the same as the space available in the larynx (about 20 mm in diameter), which prevents using the two arms efficiently.

The last path is to bring the laser source closer to the vocal folds in an endoluminal operation, as in the EU-funded μRALP project (Figure 2.16(c)) [MAT 13]. Thereby, the safety risks are reduced (no free-space journey) and the optical accuracy is increased (reduced divergence of the laser due to a shorter distance). The patient's comfort can be improved if we use fiber-guided laser and the surgeon's ergonomy can also be enhanced because of the smart use of tactile screens for designing teleoperation devices [BAR 13]. Moreover, the angular resolution is less critical. Indeed, working with a laser steering device located at approximately 20 mm from the vocal folds releases the constraints on its angular resolution. For instance, an angular resolution of approximately 0.3° is needed from the actuation system to cope with a 100 μm laser spot resolution. Reversely, an angular resolution of 0.015° could allow some 5 μm laser spot resolution.

One device was presented recently in [PAT 12], where the use of an actuated miniature dual-wedge Risley device allows us to deflect a CO_2 laser beam (Figure 2.16(b)). Using piezo-acoustic linear actuators (custom motors from New Scale Technologies), an angular resolution of 5° was demonstrated, essentially due to a controller based on a look-up table together with open-loop control.

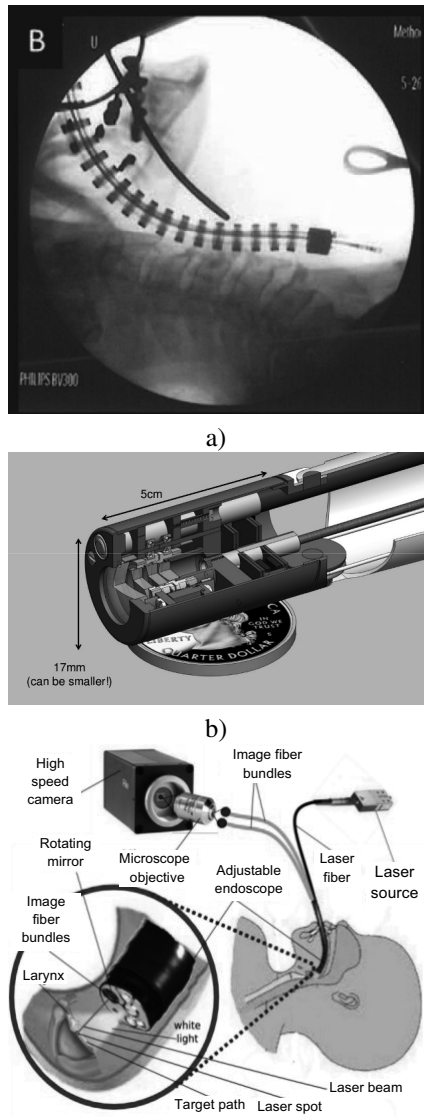

Figure 2.16. *Examples of endoluminal microphonosurgery systems: a) transoral highly flexible robot [RIV 12]; b) endoscopic laser scalpel [PAT 12]; c) the μRALP concept [MAT 13]*

However, bringing the laser steering device closer to the vocal folds increases the range of motion. With a standard length of 17–21 mm for the vocal folds, the angle to be swept by the laser at 20 mm distance is approximately 45°. Using reflective optics, we can convert this angular range for the laser into a 22.5° range for a planar mirror deflecting the laser beam. This is above the usual range of motion that can be reached by many MEMS mirrors (namely used for "micro" overhead projectors or micromirrors for OCT scanning). Moreover, most of the proposed MEMS mirrors do not cope with the biocompatibility constraints.

An additional constraint in laser surgery is to avoid heating the tissue. Otherwise, one burns the tissue rather than resecting or ablating it. Resection and ablation occur when the energy density is enough, and burns occur when the total energy is too high. Thus, we need either to pulse the laser with very short pulses (ultimately with femto second lasers) or sweep laser with longer pulses back and forth over the tissue. Since short pulses will tend to distort when traveling through optic fibers, the solution proposed in the μRALP project is to design a high-range ($\sim$20°), high-frequency ($\sim$20 Hz sweep, $\sim$200 Hz control) laser steering mechanism. This mechanism has parallel kinematics, is piezo-actuated through a motion amplification structure and is restricted to a 1 cm^3 available volume. At this scale (piezo-beams are 10 mm long and 1 mm wide), micro-fabrication and assembly is a challenge. To cope with the associated mechanical errors, a high-frequency visual servoing system is being implemented [AND 13a, AND 13b].

2.4.3. *Autonomous active capsules*

Two kinds of autonomous active capsules can be found in the literature: capsules that "swim" in liquids with their own propellers and capsules that "walk" in lumens with their own legs.

2.4.3.1. *Microswimmers*

In the framework of the VECTOR European project, an attempt was made to create a capsule for gastric inspection [CAR 09c]. To do so, advantage was taken of the fact that the stomach can be filled with water (or other liquids). Thereby, a centimetric capsule equipped with micropropellers (Figure 2.17) would be able to dive and navigate in this fluid environment [CAR 09c, CIU 11]. An alternative to propellers is to mimic a jellyfish by actuating polymer flaps [VAL 11].

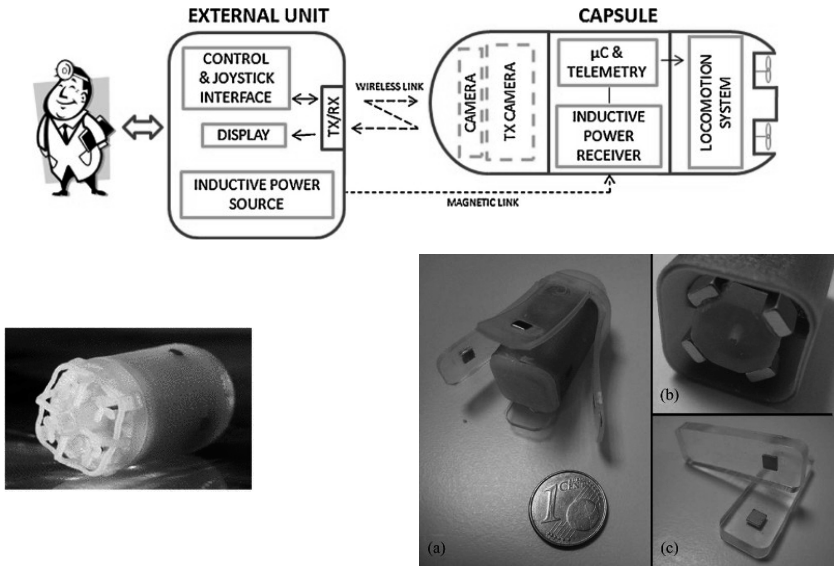

Figure 2.17. *A microsubmarine-like capsule from SSSA, Pisa: concept [CAR 09c] (above) and prototype [CIU 11] (below, left). An artificial jellyfish from SSSA [VAL 11] (below, right)*

2.4.3.2. *Legged capsules*

Several legged microrobots were proposed for intracorporeal interventions. Initially thought of for the vascular system, the VIROB robot (Figure 2.18) is a legged-microrobot, with a length of 4 mm and a diameter of 1 mm, equipped with fins that oscillate with an external magnetic field[6].

Another legged-capsule was designed during the EU-funded VECTOR project aiming at the exploration of the digestive tract [MOG 07]. This centimetric legged-capsule possesses two sets of four legs (Figure 2.18) that are alternately flapped open to progress in a lumen by walking on its walls. Yet, this solution, although very attractive, suffers from its power consumption: a "tender-capsule" was thus needed to carry the necessary battery.

Also for digestive tract exploration, the centimetric legged-capsule shown in Figure 2.18(c) has lower energy requirements. Indeed, it has flaps that can be opened to slow down its peristaltic progression in the intestine [GLA 08],

6 http://www.youtube.com/watch?v=_cs2cRI3lek.

due to the strong adhesive power of micro-structured pads on the flaps, inspired by the gecko legs. Similarly, micro structured Polydimethylsiloxane (PDMS) films are used to equip a 15 mm diameter capsule with micro threads [REN 12].

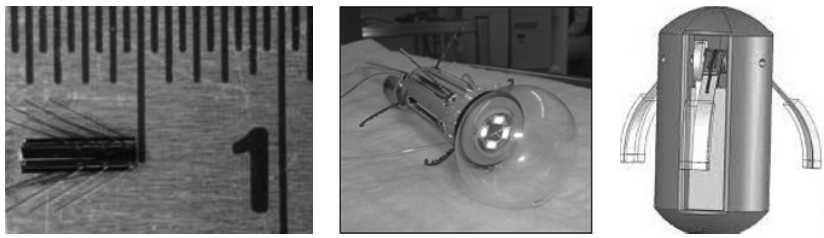

a) b) c)

Figure 2.18. *Examples of legged microrobots: a) the VIROB from Technion, Haïfa [VIR 08]; b) the EMILOC robotic capsule from SSSA, Pisa [MOG 07]; c) the capsule from CMU, Pittsburgh [GLA 08]*

2.4.4. *Magnetically guided capsules*

If we want to reduce the size of the autonomous intracorporeal robots, then one faces two challenges: limitation of the space available for electronics and actuators, and the decrease in the Reynolds number. To overcome the first challenge, one can use magnetic fields for wireless guidance.

2.4.4.1. *MagPieR*

The MagPieR microrobot [IVA 13] successively won three "NIST IEEE Mobile Microrobotic Challenge" at the 2010, 2011 and 2012 editions of the International Conference on Robotics and Automation. In 2010, it performed the "2-mm dash" at the velocity of 71.4 mm/s, which is 178.5 times its body length per second. In 2011 and 2012, it slalomed between four gates (Figure 2.19) in, respectively, $\sim$2 s and $\sim$1 s, because of the high-speed vision feedback control.

MagPieR is composed of a magnetic actuation system, a high-speed camera and a 388 μ m $\times$ 300 μ m $\times$ 224 μ m microfabricated magnetic microrobot immersed in a 3.5 mm $\times$ 2 mm arena. The magnetic actuation is made up of two orthogonal pairs of optimized Maxwell coils, with ferromagnetic cores, which allows for magnetic induction between 10 and 25 mT depending on the microrobot-to-coil distance.

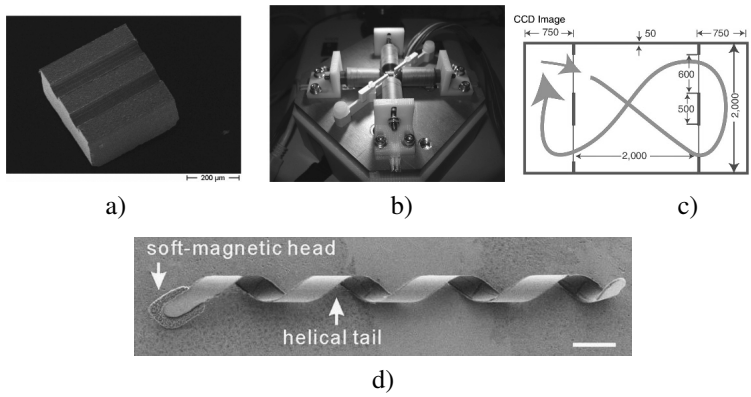

a) b) c)

d)

Figure 2.19. *Examples of a magnetically guided microrobot: a) the MagPieR from FEMTO-ST, Besançon and ISIR/UPMC, Paris [IVA 13]; b) its magnetic steering system; c) the arena; d) the artificial bacterial flagella from IRIS/ETH Zürich [ZHA 09]*

This microrobot is envisioned for biologic solutions to oncologic treatment rather than for direct intracorporeal surgical interventions.

2.4.4.2. *Helical microrobots*

In the last two decades, several research groups have been studying helical microrobots [HON 96, ZHA 09, ZHA 10, TOT 12, ABB 09, GHO 09, XU 13]. Among these, the artificial bacterial flagella (ABF) is probably the most consistently studied so far. It is approximately 50 μm long (Figure 2.19(d)) and is steered by three orthogonal Helmholtz coil pairs [ZHA 09] delivering a 2 mT field. It has demonstrated high manipulability properties (steering and forward/backward motion) in a 3D volume and is the source of many theoretical contributions. Probably the most distinctive, with respect to standard robotics, is the propulsion characteristics curve: the ABF rotates synchronously with the rotating magnetic induction field, with a linear increase of the rotation speed, up to a so-called *step-out frequency*. The latter is the upper limit of the rotation frequency of the rotating magnetic induction field above which the ABF looses synchronization and thereby does not rotate anymore.

2.4.4.3. *Octomag*

The structure of the Octomag (Figure 2.20) is a set of eight electromagnets, with ferromagnetic cores, used to displace a 400 μm long magnetic drug-carrying capsule or a 2.7 mm long magnetic puncturing

microrobot. It is developed in the ophthalmic domain for the injection of medication in the retinal vein. It was tested *in vitro* for injection in the vasculature of a chicken embryo (as a good model of the human retinal vessel) [KUM 10] and *in vivo* in rabbit eye [ULL 13].

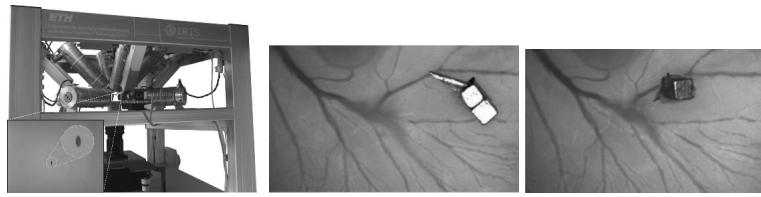

a) b) c)

Figure 2.20. *Example of a magnetically guided microrobot: a) the Octomag system from ETH, Zürich [KUM 10], b) the in vitro ∼2.7 mm long microrobot at rest and c) puncturing*

Four of the coils are arranged in a plane, as for the MagPieR microrobot, to control the displacement and orientation in the horizontal plane. The other four are placed on the four upward diagonals and allow us to control the height (by compensating the gravity) and inclination. This configuration generates a nonlinear magnetic induction field. However, the authors modeled it through the superposition theorem and the pure dipole model for each coil, fitted on data recorded in the workspace. This turned out to be enough in the 20 mm $\times$ 20 mm workspace.

2.4.4.4. *Endoscopic capsule manipulation*

To wirelessly manipulate endoscopic capsules, without the limitations associated with legged-locomotion, we can use a large external permanent magnet mounted on a robot arm (Figure 2.21) to interact with a small permanent magnet inserted in the capsule [CIU 10a]. The use of a robot is shown to definitely improve the manipulability of the capsule with respect to manual displacement of the external magnet.

However, even with a robot, this manipulation using permanent magnets is rather unstable, due to the nonlinearities of the magnetic induction field, and thereby it is very difficult to accurately achieve a stable orientation during the displacement. An improvement was thus proposed in [VAL 10], where a micromotor is placed within the capsule, which takes in charge the orientation, while the external permanent magnet is responsible for the displacement.

2.5. Conclusion

In this chapter, we have gone through the vast spectrum of concepts, more or less known in conventional robotics, that are necessary to apprehend what intracorporeal microrobotics is or can be. Thereby, we have seen that smart materials together with in-plane microfabrication were needed to design and implement actuated mechanical structures, as an extension of what is already practiced in intracorporeal millirobotics. As for sensing, we have preferred to spend more time on medical imaging than on other microsensors, because due to the size constraints, it is difficult to integrate microsensors onto intracorporeal microrobots. Also, medical practice tends towards even more image-based procedures (neurosurgery, NOTES, among others) because imaging is often the only sensing modality available at that scale.

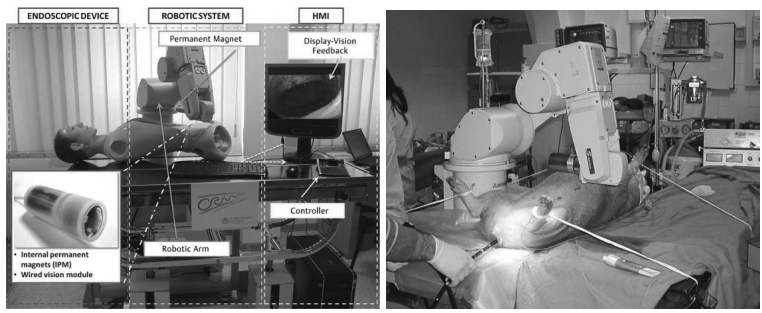

Figure 2.21. *Example of a magnetically guided microrobot: concept and clinical trial set-up of the endoscopic capsule magnetic manipulator from SSSA, Pisa [CIU 10a]*

We have focused on two concepts that are specific to the microscale: magnetic actuation and swimming at low Reynolds numbers. In particular, we have made a big effort to synthetize the various magnetic actuation approaches (mobile permanent magnets or static electromagnets, force- or torque-based control) in a single robotic formal framework, both for modeling and control.

We finally presented examples of the four classes of either partially or fully intracorporeal microrobots: magnetically steered catheters, micromechanisms at the distal tip of an endoscope, autonomous locomotion and magnetically steered capsules. We covered only a small subset of the few existing systems and many proofs of concept that were presented in the last decade, and it would probably need yet another book to cover exhaustively the tremendous (and still exponentially rising) activity in intracorporeal microrobotics.

In addition to the investigation of additional novel concepts for sensing, actuation or design, there still remains a huge amount of work to be done to enhance the autonomy, accuracy and reliability of robots evolving in the human body at microscale. Intracorporeal microrobotics is thus probably the next battlefield of medical robotics research, with a high potential of innovation toward the OR, together with ethical, legal and societal issues that will have to be solved before effective use in everyday medical practice.

The next chapter will bring the reader even further down in scale and will introduce him/her to the conceptual wonders of the unconventional use of physical principles for sub-micrometric robotics.

Chapter 3

In vitro Non-Contact Mesorobotics

3.1. Introduction

This chapter deals with the robotic tools developed to perform operation on biological cells whose size is mostly less than 100 µm and is usually around 5–10 µm. This scale, placed between nanoscale (1–100 nm) and microscale (10 µm to 1 mm), is usually named mesoscale[1]. At this scale, the object behavior looks amazing and highly original robot principles have been developed. Some examples of cell size are described in Table 3.1.

The positioning and sorting of cells follow two objectives: the cell sorting and the single-cell positioning. The first case consists of sorting a sample containing a huge number of cells or of analyzing the concentration of a specific type of cells in a sample. The typical example is to sort the platelet and the other blood cells. The processes used are based on statistical analysis and currently have a success rate of less than 5%.

In the second case, the issue is significantly different and the cell is considered as a single object that can be positioned. The objective is to handle, position, rotate, release and/or act on a single cell. It deals with the classical robotic manipulation operations and is usually called "robotic

1 The term "mesoscale" is also used to describe the intermediate scale between microscale and macroscale. In this chapter, the prefix "meso" will be used to define the intermediate scale between nanoscale and microscale.

cell micromanipulation[2]". The typical example is the intracytoplasmic sperm injection (ICSI) used in *in vitro* fertilizations (IVF) in which oocyte and spermatozoon are both manipulated using tools. Robotic cell micromanipulation is also increasingly used to better understand the functioning of the cell, to exploit single cells as biosensors or to study and develop stem-cell-based therapies.

This chapter presents original solutions enabling the robotic manipulation of single cells for *in vitro* applications.

Cell type	**Diameter**
Microbes	2–3 µm
Lymphocytes	7–15 µm
Hepatocytes	~ 10 µm
Macrophages	20–35 µm
Oocytes	100–200 µm

Table 3.1. *Example of cell sizes*

Two major methods are proposed in the literature to perform robotic cell micromanipulation. The simplest method is the use of micropipettes to grasp the cell by vacuum (e.g. oocyte handling in ICSI). It works on large cells (e.g. oocytes) whose size is larger than 10 µm. In the case of smaller cells, the contact with the micropipette could destroy them and non-contact manipulation principles are proposed based on magnetic, electrostatic, optical or acoustic principles.

2 The term "micromanipulation" has two different meanings in biology and robotics. In biology, it means a modification of the intrinsic properties of the cell (e.g. DNA manipulation). In robotics, it means the action of handling, positioning and releasing a micro-object. In this chapter, we make use of the robotic definition of the term "micromanipulation".

Section 3.2 deals with the physical principles used in non-contact manipulation of cells. Section 3.3 describes the original scientific challenges induced when using non-contact forces to perform robotic manipulation. Finally, section 3.4 proposes several examples in which these principles have been experimented.

3.2. Principles

3.2.1. *Introduction*

The four principles used to perform non-contact manipulation at mesoscale are, respectively, based on optical effects, electrostatics, magnetic principles and acoustic effects [GAU 10a, GAU 10b]. The first two principles will be presented in detail later in this chapter. As magnetic effects have been widely presented in Chapter 2, only specific methods dedicated to *in vitro* manipulation are mentioned in this introduction. Concerning the fourth principle, acoustic effects have been used to manipulate single cells only recently and this promising approach is also presented only in this introduction.

As presented in Chapter 2, magnetic forces can be used to manipulate microrobots inside bodies and in *in vitro* devices. Another method exploiting magnetic non-contact manipulation is based on magnetotactic bacteria (MTB). These bacteria (MTB) are a diverse group of microorganisms with the ability to orient and migrate along geomagnetic field lines. This unique feature is based on specific intracellular organelles, the so-called magnetosomes, which comprise nanometer-sized particles of magnetic iron organized into chains (Figure 3.1).

The modification of the magnetic field orientation induces an immediate rotation of the MTB. Consequently, the control of the magnetic field enables control of the trajectory of MTBs in an *in vitro* device [MAR 09b, MAR 13a]. An example of the open-loop control of a population of bacteria is shown in Figure 3.1. Recent works also report experiments on the trajectory control of a single MTB using closed-loop control based on vision feedback (Figure 3.2) [KHA 13a].

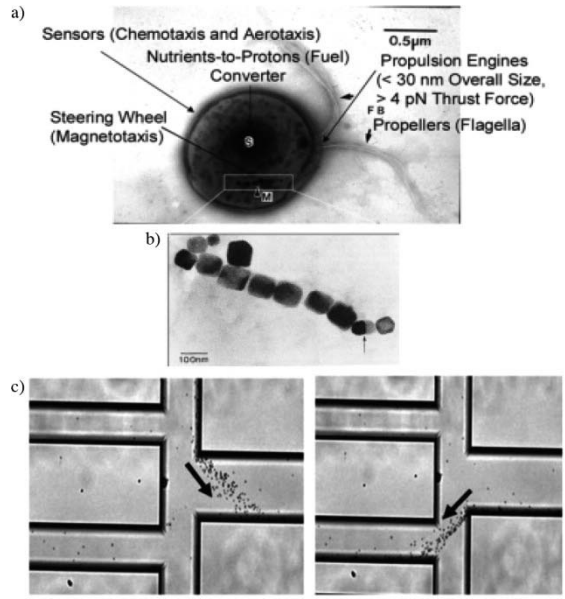

Figure 3.1. *a) Magnetotactic bacteria (MTB) and its chain of magnetosomes b) and c); Trajectory control of a population of MTB in microchannel by an external magnetic field [MAR 09b, MAR 13a]*

The fourth original principle is to use acoustic effects to propel cells. To date, many acoustic-based particle manipulation functions (e.g. focusing, separating, sorting, mixing and patterning) have been realized [DIN 12]. A large majority of these approaches are not able to precisely manipulate single microparticles or cells along a reference path. Recently, the standing surface acoustic wave (SAW) presented by Ding *et al.* [DIN 12] was the first acoustic manipulation method to precisely control a single microparticle along a reference trajectory within a single-layer microfluidic channel in two dimensions (Figure 3.3). Cell viability tests were conducted to verify the system compatibility with biological objects. With its advantages in biocompatibility, miniaturization and versatility, the acoustic tweezers will probably become a powerful tool for single-cell manipulation in the future.

The two principles widely used in non-contact manipulation at mesoscale, which are the laser trapping principle and electrostatic principle, are presented in the following sections.

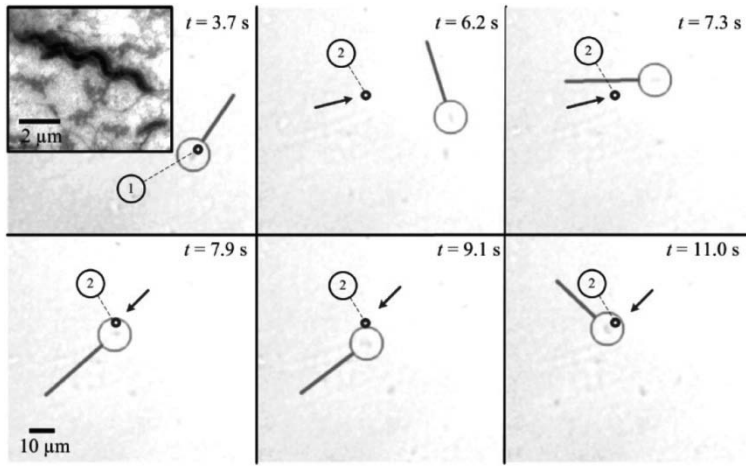

Figure 3.2. *Closed-loop motion control of an MTB with an external magnetic field. The MTB should move from the initial point 1 to the reference position 2 with a maximal final error of 30 µm. The gray circle emphasizes the location of the MTB and the grey line represents the velocity of the MTB. The inset shows a scanning electron microscopy image of the spiral membrane of the MTB. The MTB goes from location 1 to reference position 2 in 7.9 s. When the reference position is reached, the bacteria still moves and cannot be stopped with the magnetic field. Consequently, the controller induces rotation of the MTB around the reference position 2 in order to guarantee an error up to 30 µm (from t = 7.9–11 s) [KHA 13a]*

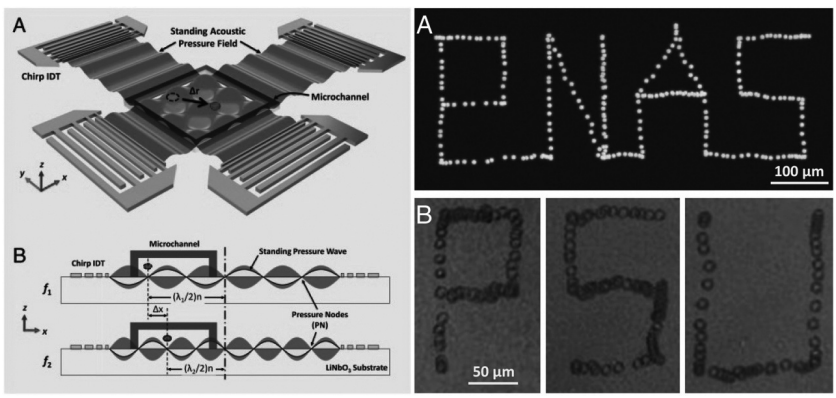

Figure 3.3. *Acoustic tweezers for single-cell manipulation: device structure and working mechanism of the acoustic tweezers (left); stacked images of independent 2D single particle and cell manipulation (right) [DIN 12]*

3.2.2. *Laser trapping*

3.2.2.1. *General principle*

Optical tweezers exploit radiation pressure usually induced by a laser beam to manipulate micro-objects. They act on transparent objects with refractive indices higher than the refractive index of the medium. In this case, the particles are attracted to the region of highest light intensity [ASH 86]. Consequently, a particle placed at the center of a laser beam follows the trajectory of the beam. This method enables the manipulation of objects whose sizes range from a few tens of nanometers to a few tens of micrometers [VEI 12, DHO 02, PLE 02, LAN 03].

The general principle of optical tweezers is shown in Figure 3.4. When light rays are refracted by the surface of the object, their path is altered, and this results in a radiation pressure on the object. If the object is offset from the center of the beam, the radiation pressure on its surface produces a force whose radial component (along $\vec{r}$) tends to move the object back to the center of the beam. When the object lies on the central axis of the laser beam, the vertical component of the radial pressure tends to place the center of the spherical object toward the focal point. Experimentally, reflected rays produce an additional vertical force component, and the stable position is slightly offset along the $\vec{z}$ axis relative to the focal point of the beam and depends on the size of the micro-object. Several applications of optical tweezers are described below in section 3.4.1.

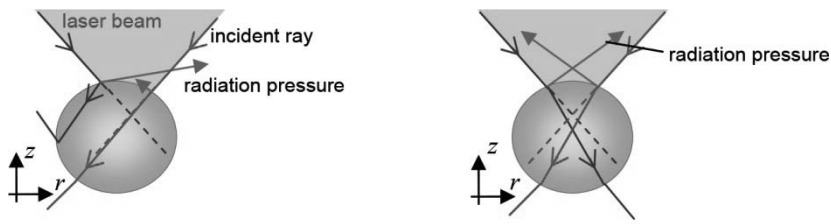

a) *Radiation pressure applied to an object offset from the beam axis*

b) *Radiation pressure applied to an object on the beam axis*

Figure 3.4. *Laser trapping principle*

3.2.2.2. *Radiation force calculation*

Let us consider that the beam is tightly focused by a high numerical aperture objective lens, converging to a near-diffraction-limited size with a

focal waist ω_0, and then re-expanding. The most important force is the radiation force acting on a dielectric spherical nanoparticle due to interactions between the light electric field and induced dipole moment of the polarizable dielectric sphere. For a uniform dielectric sphere, the susceptibility is isotropic and the polarization $\overrightarrow{P_o}$ is parallel to $\vec{E}$. Thus, the gradient force, related to spatial Lorentz force, exerted on the nanoparticles can be expressed as [USM 12, HAR 96]:

$$\overrightarrow{F_{rad}} = (\overrightarrow{P_o}.\vec{\nabla})\vec{E} = \frac{1}{2}\alpha\vec{\nabla}|E|^2 \quad [3.1]$$

where $\alpha = 4\pi n_3^2 \varepsilon_0 r_1^3[(n_1^2 - n_3^2)/(n_1^2 + 2.n_3^2)]$, ε_0 is the vacuum permittivity, r_1 is the radius of the nanoparticle, n_1 is the refractive index of the particle and n_3 is the index of the medium. The radiation force can also be expressed as [USM 12]:

$$\overrightarrow{F_{rad}} = -\alpha E_r^2 \left[\frac{r}{\omega_0^2} - \frac{1}{2}\frac{K^2 r}{\omega_0^2} - \frac{K^2 r^3}{\omega_0^4}\right] \quad [3.2]$$

where $K = \frac{\lambda\omega_0}{\pi}$, λ is the wavelength of the laser and ω_0 is the beam waist. E_r can be approximated by [USM 12]:

$$E_r^2 = \frac{4P}{\pi\omega_0 n_3 \varepsilon_0 c} \quad [3.3]$$

where P is the average laser power. Examples of parameter values in the above equations based on typical laser power and polystyrene particles are reported in Table 3.2.

Parameter	Value
α/r_1^3	$2.5\ 10^{-11}\ NV^{-2}$
K	$1.6/\pi$
P	$350\ mW$
ω_0	$460\ nm$
E_r	$24.4\ 10^6\ V{\cdot}m^{-1}$

Table 3.2. *Example of numeric values in case of polystyrene nanospheres and typical laser power [USM 12]*

Figure 3.5 shows the radiation force as a function of the radial position of the nanosphere. It clearly shows that the center of the beam is a stable equilibrium. However, it also shows that the level of force is very low (in the region of piconewtons), which is one of the major drawbacks of this method compared to dielectrophoresis (DEP) and magnetophoresis (see section 3.2.3).

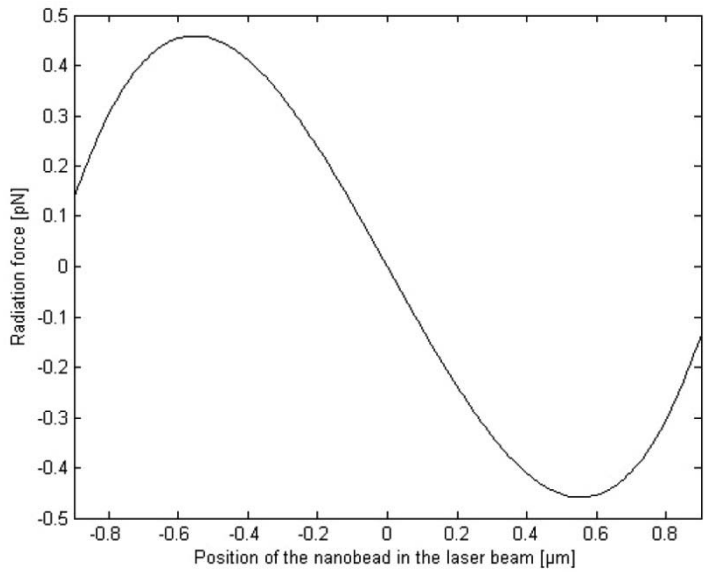

Figure 3.5. *Example of radiation force as a function of the radial position of a polystyrene nanosphere whose diameter is 50 nm*

Other forces such as the scattering force due to the momentum transfer of light and the temporal force function of the pulse duration can be considered [USM 12]. Moreover, more complex models based on numeric calculation are available in the literature, especially for biological cell manipulation [LI 13b]. As shown in Figure 3.6, laser trapping is also able to apply torque on non-symmetric objects making it possible to control the angular position of cylindrical particles [YOG 12, WOE 10].

3.2.2.3. *Radiation force measurement*

Modeling of the laser trapping force requires the identification of many parameters. The simplified example proposed in equation [3.2] has six parameters and this number is increasing rapidly for more detailed models

[LI 13a]. The second method to determine the force applied by a laser on an object is to estimate it experimentally. As the level of force is very low (in the region of piconewtons), force sensors used at macroscale *cannot* be used. The estimation is based on the measure of the velocity of the object induced by the force.

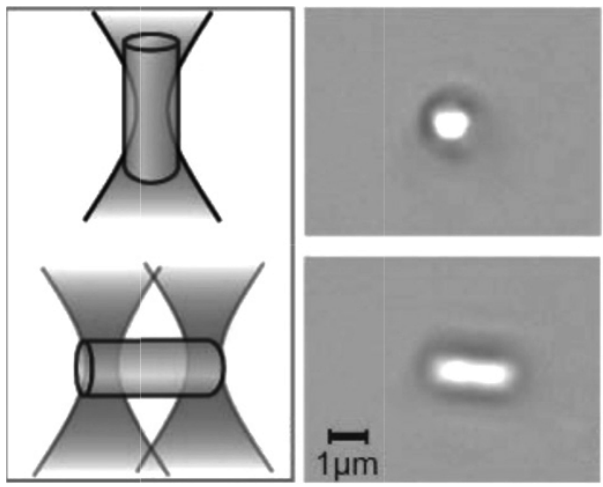

Figure 3.6 *Rotation of a non-symmetric micro-object using laser trapping. Two laser beams are required to place the cylinder horizontally [WOE 10]*

Considering that the inertia of the object can be neglected compared to the viscous effect, the trajectory of an object manipulated by optical tweezers satisfies the equilibrium between the laser force $\vec{F}_{rad}$ and the drag force $\vec{F}_{visc}$ (see section 3.3.1):

$$\vec{F}_{rad} + \vec{F}_{visc} = 0 \qquad [3.4]$$

where $\vec{F}_{visc} = -3\pi d_1 \mu_3 \vec{V}$, μ_3 is the dynamic viscosity of the medium and d_1 is the cell diameter. Knowing the dynamic viscosity of the medium and the cell size, equation [3.4] enables us to determine the laser trapping force based on the measure of the object velocity. Figure 3.7 shows a typical force measurement result.

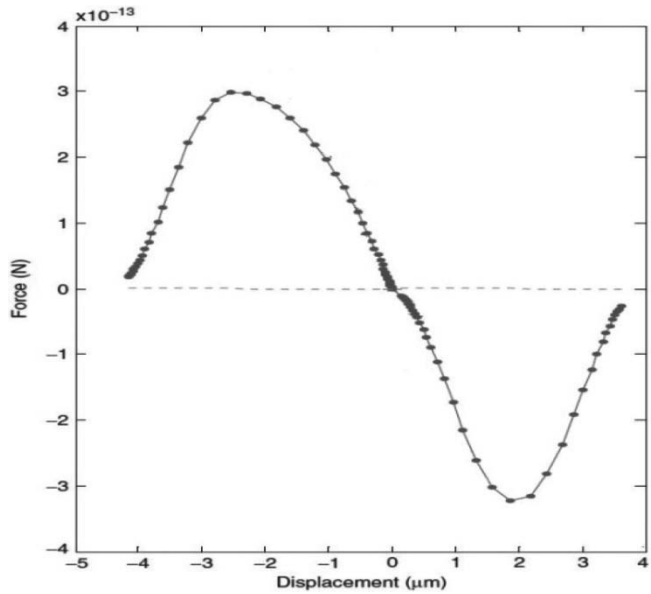

Figure 3.7. *Example of laser trapping force identification based on the measure of the object velocity. Object is a yeast cell with a diameter of approximately 5 µm [HU 07]*

3.2.3. *Electrostatic principles*

3.2.3.1. *General principle*

One of the most promising principles to manipulate single cells is the use of the electrostatic principle. The general expression of the electrostatic force acting on an object having a charge q and an electric dipole with a moment $\overrightarrow{m(t)}$ is:

$$\overrightarrow{F_{elec}} = q\vec{E} + \left(\overrightarrow{m(t)}.\vec{\nabla}\right).\vec{E} \qquad [3.5]$$

where $\vec{E}$ is the electric field.

The first term $q\vec{E}$ is linear and is a function of the electrostatic charge q. The electrical charge of a micro-object or a biological cell is mainly due to surface charges and is function of the chemical interaction with the medium. Usually, electrostatic charges on micro-objects are modified by the pH or the ionic force of the medium.

In the second term $\left(\overrightarrow{m(t)}.\overrightarrow{\nabla}\right).\vec{E}$, the electrostatic moment is a function of the gradient of the electric field $\vec{E}$, and of the electric permittivity of the medium and the object. We are going to show that the nonlinearity of this second term (proportional to the square of the electric field $\overrightarrow{E}$) may be exploited for micromanipulation.

As the permittivity of the material is constant, the force induced by the second term is more repeatable than the first term, which is highly dependent on the surrounding medium interaction. The use of a periodic electric field $\overrightarrow{E(t)}$ (typically sinusoidal or square shape signals) with a zero center amplitude induces a variable force $\overrightarrow{F_{elec}(t)}$ characterized by:

− a first linear term whose average value is zero;

− a second nonlinear term having a non-zero average value.

Using a frequency of $\overrightarrow{E(t)}$ sufficiently high to consider only the average force, the latter is only function of the moment of electric permittivities of the object and the medium and is not disturbed by a variation of the charge q. This average force is called the "dielectrophoretic force"[3] and is widely used in micromanipulation of artificial and biological particles at mesoscale. The second advantage of using periodic electric field is to avoid electrolysis on the electrodes generating the electric field.

3.2.3.2. *Force calculation*

The equivalent moment of a spherical particle of radius r with complex dielectric constant[4] κ_1 in a medium of complex dielectric constant κ_3 is:

$$\overrightarrow{m(t)} = 4\pi r^3 \varepsilon_3 \frac{\kappa_1 - \kappa_3}{\kappa_1 + 2\kappa_3} \vec{E}(\mathrm{t}) \qquad [3.6]$$

The complex part of this equation, which depends on the excitation pulsation, is known as the Clausius Mossotti function $K(w)$:

3 Dielectrophoresis is different from electrophoresis, which is a sorting and characterization principle of micro-object and cells using the first term $q\vec{E}$ of equation [3.5] by applying a constant electric field.

4 The complex dielectric constant κ_i is a function of the excitation pulsation w of the electric field and is defined by $\kappa_i = \varepsilon_i + jw\sigma_i$, where ε_i and σ_i represent the dielectric constant and electrical conductivity, respectively.

$$K(w) = \frac{\kappa_1 - \kappa_3}{\kappa_1 + 2\kappa_3} \quad [3.7]$$

To establish a simplified expression of the force, let us consider the case of a stationary alternating field $\overrightarrow{E(t)}$ [POH 78]:

$$\vec{E} = \overrightarrow{E_0}\cos(wt) \quad [3.8]$$

The dipole moment modeling the electrical behavior of the particle is consequently:

$$\overrightarrow{m(t)} = 4\pi r^3 \varepsilon_3 \left[\mathrm{Re}\big(K(w)\big)\cos(wt) + \mathrm{Im}\big(K(w)\big)\sin(wt)\right]\vec{E} \quad [3.9]$$

Hence:

$$\overrightarrow{F(t)} = 4\pi r^3 \varepsilon_3 \left[\mathrm{Re}\big(K(w)\big)\cos(wt) + \mathrm{Im}\big(K(w)\big)\sin(wt)\right] cos(wt)\left(\overrightarrow{E_0}.\overrightarrow{\nabla}\right).\overrightarrow{E_0} \quad [3.10]$$

The dielectrophoretic force $\overrightarrow{F_{DEP}}$, which is the mean force of $F(t)$, is then:

$$\overrightarrow{F_{DEP}} = \pi r^3 \varepsilon_3 \mathrm{Re}\big(K(w)\big).\overrightarrow{\nabla}\left(\overrightarrow{E_0}\right)^2 \quad [3.11]$$

This equation represents the mean force applied to a dielectric object subjected to an alternating electric field of pulsation w. In the case of dielectric media, this force can be written in the well-known form:

$$\overrightarrow{F_{DEP}} = \pi r^3 \varepsilon_3 \frac{\varepsilon_1 - \varepsilon_3}{\varepsilon_1 + 2\varepsilon_3}\overrightarrow{\nabla}\left(\overrightarrow{E_0}\right)^2 \quad [3.12]$$

3.2.3.3. *Torque calculation*

DEP is also able to induce torque on micro-objects. Indeed, the electric field applies a torque $\overrightarrow{\Gamma_{\mathrm{elec}}(\mathrm{t})}$ on a dielectric object having a dielectric moment:

$$\overrightarrow{\Gamma_{\mathrm{elec}}(\mathrm{t})} = \overrightarrow{\mathrm{m}(\mathrm{t})} \times \overrightarrow{\mathrm{E}(\mathrm{t})} \quad [3.13]$$

To obtain a simplified expression of the torque, we will consider the case of a planar rotating field $\overrightarrow{E(t)}$ with a constant magnitude satisfying:

$$\overrightarrow{E(t)} = E_0[\cos(wt)\,\vec{x} + \sin(wt)\,\vec{y}] \quad [3.14]$$

Thus, the dipole moment is:

$$\overrightarrow{m(t)} = 4\pi r^3 \varepsilon_3 E_0 \begin{bmatrix} \big(Re\big(K(w)\big)\cos(wt) + Im\big(K(w)\big)\sin(wt)\big)\vec{x} \\ +\big(Re\big(K(w)\big)\sin(wt) - Im\big(K(w)\big)\cos(wt)\big)\vec{y} \end{bmatrix} \quad [3.15]$$

The torque, also known as the dielectrophoresis torque, represents the mechanical torque acting on a dielectric object in a rotating electric field:

$$\overrightarrow{\Gamma_{DEP}} = 4\pi r^3 \varepsilon_3 Im\big(K(w)\big) {E_0}^2 \quad [3.16]$$

3.2.3.4. *Typical behaviors*

Depending on the sign of the Clausius Mossotti factor $K(w)$, objects can undergo two possible motions:

− $\mathrm{Re}(K(w)) > 0$: objects are attracted to regions of high electric field produced by the electrodes. This case is known as positive dielectrophoresis (pDEP);

− $\mathrm{Re}(K(w)) < 0$: objects are repelled from the electrodes to regions of weak electric field. This case is known as negative dielectrophoresis (nDEP).

In some cases, the sign of the Clausius Mossotti factor $K(w)$ is different for high frequency and low frequency. When it happens, the control of the frequency w enables to switch from pDEP to nDEP.

3.2.3.5. *Particle–particle interaction*

The model proposed above deals with the interaction between a unique micro-object and an electric field. In most of the application cases (cell sorting, microassembly), several micro-objects are moving simultaneously in the field, and particle–particle interactions have to be considered. Recently, some models of such interaction have been proposed (Figure 3.8) [HOS 13, HOU 12]. Numerical results show that in a fluid media, similar particles form a chain parallel to the applied electric field, whereas dissimilar particles form a chain perpendicular to the applied electric field. Irrespective of initial position and orientation, particles are first aligned parallel or perpendicular to the electric field depending on their similarity or dissimilarity. The acceleration and deceleration of particles were observed and analyzed at different phases of the trajectories [HOS 13].

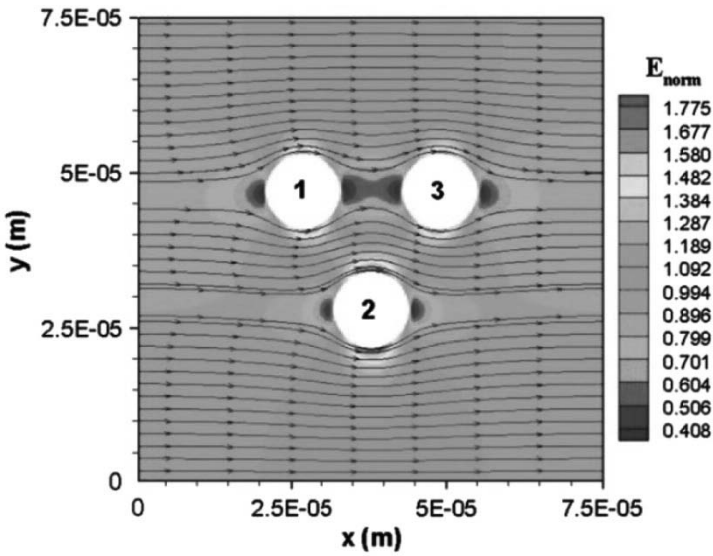

Figure 3.8. *Example of numerical simulation of particle–particle interaction in DEP. The electric fields generated by objects 1 and 3 have an overlap, inducing significant forces between both objects. Object 2 has no significant interaction with the two others. The interaction between objects could be attractive or repulsive [HOS 13]*

3.3. Scientific challenges

This section deals with the typical scientific challenges in non-contact mesomanipulation, covering modeling, system design, perception and control issues.

3.3.1. *Modeling*

Modeling the trajectory of a micro-object (e.g. a biological cell) in a non-contact micromanipulation system is the a first step enabling us to improve the design and define the control strategy. In the case of laser trapping, the behavior is simple to model as the object can be considered to be linked to the center of the beam via a virtual mechanical spring. In the case of magnetophoresis and DEP, the modeling is more complex because of the strong nonlinearities of the magnetic and electric fields around the object. This section presents current solutions to improve modeling of DEP,

especially to build models that enable the design of control laws. The principles can be extended easily to magnetophoresis.

3.3.1.1. *Driving force modeling*

To compute the DEP force applied on a microparticle, two main approaches can be used: (1) simulation based on finite element modeling (FEM), which is characterized by its capacity to simulate the DEP force whatever the shape of electrodes, and (2) analytic formulation that requires less computation time compared to that of the former method, but is limited to very simple geometries. Because of the large variety of electrodes and their geometric complexity, it can be very difficult to directly integrate analytic equations. The most interesting way is then to combine both numerical and analytic methods in a hybrid method taking advantage of both.

First, the computation of the DEP force requires the calculation of the electric field $\vec{E}$ and its gradient in equation [3.12]. To compute the electric field $\vec{E}$ with respect to the applied voltages, a general method was presented in [KHA 09b] and [KHA 10a], which consists of computing the electric charge density on the electrodes. Indeed, the electric charge density Q is linearly dependent on the applied voltages U on the electrodes. More precisely, the general expression of the electric voltage applied on the *i*th electrode with respect to time t is:

$$U_i sin(\omega t) \qquad [3.17]$$

Considering *n* electrodes, the electric charge density Q is:

$$\mathrm{Q} = \sum_{\mathrm{i}=1}^{\mathrm{n}-1} \mathrm{C_i}\, \mathrm{U_i} \qquad [3.18]$$

where $\mathrm{U_i}$ is the magnitude of the applied voltage on the *i*th electrode and $\mathrm{C_i}$ is the elementary intercapacitance between the electrodes influenced by the *i*th electrode. In other words, $\mathrm{C_i}$ is the charge density on all electrodes created by applying the elementary voltage:

$$\mathrm{U} = [\mathrm{U_1}, \ldots, \mathrm{U_{n-1}}] = [0, \ldots, \mathrm{U_i} = 1, \ldots 0] \qquad [3.19]$$

The intercapacitance C_i depends only on the geometric shape of the electrodes and the permittivity of the medium. Therefore, to reduce the computation time, the capacitance C_i can be precomputed and stored in a database. As the geometric shape of the electrodes is usually complex, an FEM-based simulation is used to compute the capacitance $\mathrm{C_i}$. After

computing C_i using $n-1$ FEM-based simulations (n is the number of electrodes), the electric charge density Q on electrodes is then computed analytically with respect to the applied voltages.

This method may be illustrated on a typical example of geometry (Figure 3.9), namely a configuration having four electrodes ($n = 4$).

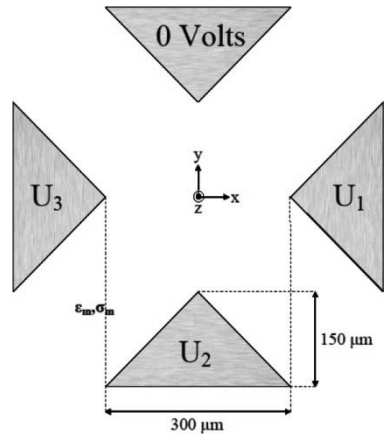

Figure 3.9. *Example of a four-electrode geometry*

To compute the electric charge density Q with respect to the applied voltages U = [U_1, U_2, U_3], $n - 1 = 3$ FEM-based simulations are required. Figure 3.10 shows the elementary intercapacitances C_1 and C_3 representing the elementary charge density Q on the electrodes when applying, respectively, U = [1,0,0] and U = [0,0,1]. Figure 3.11 shows the electric charge density Q when applying U = [75V, 0 75V] established as a linear combination of elementary intercapacitances C_1 and C_3.

Once the matrix of the electric charge density Q is computed, the electric field can be calculated analytically in each point of the medium. The electric field $\vec{E}(x,y,z)$ at point $M(x,y,z)$ is the sum of the contribution of each point P on the electrodes having a surface dS and a charge density Q(P):

$$\vec{E}(x,y,z) = \iint \frac{Q}{4\pi\epsilon_3 \|r\|^3} \vec{r} dS \qquad [3.20]$$

where $\vec{r} = \overrightarrow{MP}$. The DEP force can be computed analytically with respect to equation [3.12]. Figure 3.12 illustrates the functions of the DEP modeling

simulator (DMS). It computes the geometric shape of the electrodes, the applied voltages and a position to define the DEP force in the specified position *M*. The major interest of this hybrid method is to generate a model in which the control parameter U can be easily changed during simulation. Consequently, it enables to simulate closed-loop control of DEP devices.

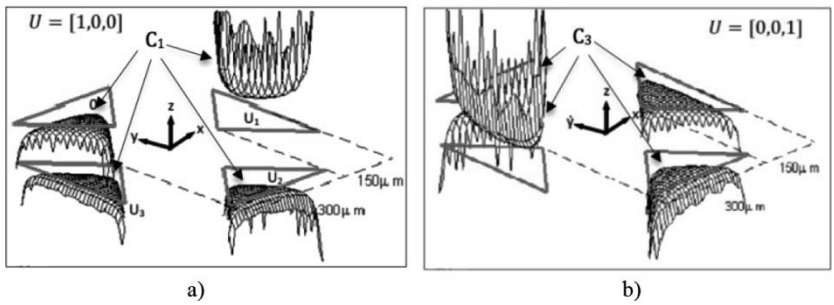

Figure 3.10. *a) Elementary intercapacitance C_1: charges Q on the electrodes when $U = [1,0,0]$; b) elementary intercapacitance C_3: charges Q on the electrodes when $U = [0,0,1]$*

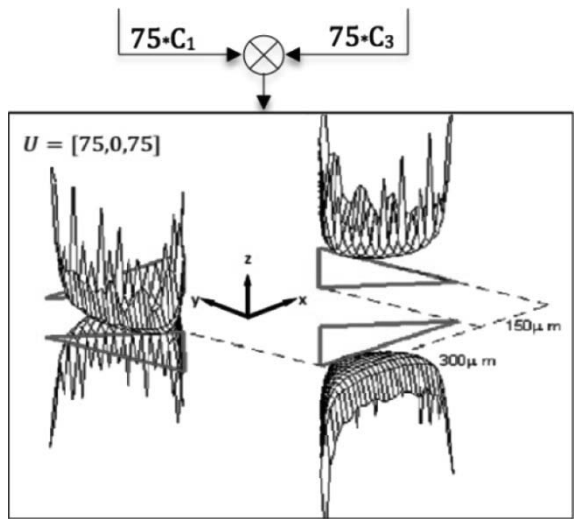

Figure 3.11. *The electric charge density Q when $U = [75\,V, 0, 75\,V]$ computed as a linear combination of intercapacitances C_1 and C_3*

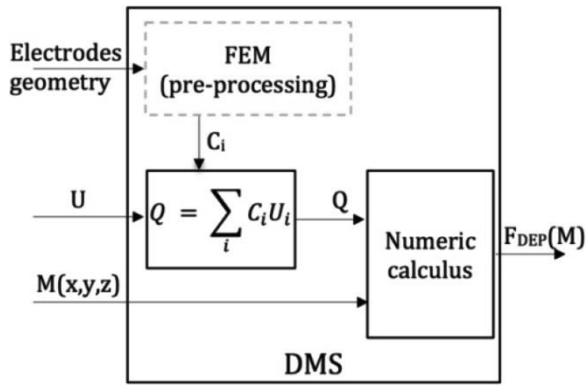

Figure 3.12. *The general architecture of the hybrid DEP modeling simulator*

3.3.1.2. *Dynamic behavior*

The determination of the dynamic behavior of the micro-object requires evaluating the impact of inertia and calculating the viscous force. In microfluidics, the drag force applied to an object having a velocity V is determined by the Stokes' law [GAU 10a]:

$$\vec{F}_{visc} = -k\mu_3\vec{V} \quad [3.21]$$

where μ_3 is the dynamic viscosity of the medium and k is a function of the object geometry. As an example for a sphere of diameter d_1:

$$k = 3\pi d_1 \quad [3.22]$$

Stokes' law is valid in the microfluidic regime (Reynolds number $R_e < 1$) and can be extended to the case of a flow with a Reynolds number lower than 10. The concept of a drag force coefficient C_x as used for drag force calculation at macroscale is not valid in the case of microfluidics[5].

Using Newton's second law, the particle motion is defined by:

$$\overrightarrow{F_{DEP}} + \vec{P} - k\mu_3\vec{V} = m\vec{a} \quad [3.23]$$

5 A drag force coefficient C_x is sometimes used in microfluidics, but with the C_x being a function of the Reynolds number R_e. The expression obtained is equivalent to the Stokes law, but does not clearly express the linear relation between drag force and velocity.

where m is the mass of the particle and $\vec{a}$ is the acceleration. Usually at microscale, the dynamic expression $m\vec{a}$ can be neglected compared to the forces. However, this hypothesis should be carefully analyzed for each case. Indeed, for high-speed micromanipulation (e.g. DEP and magnetophoresis), the inertia could still have some impact on the trajectory of very small objects (e.g. 50 µm spheres). The analysis of the impact of the inertia can be based on the analysis of a linearized model of equation [3.23] around an operating point x_0. To illustrate the method, we consider only one direction (along $\vec{x}$) but it can be used in the three directions. The following method illustrated on DEP force can also be extended to magnetophoresis.

The linearized model of equation [3.23] is classically:

$$\frac{\boldsymbol{x(p)}}{\boldsymbol{x_0(p)}} = \frac{-\frac{\boldsymbol{\partial F_{DEP}}}{\boldsymbol{\partial x}}[\boldsymbol{x_0}]}{\boldsymbol{mp^2 + k\mu_3 p - \frac{\partial F_{DEP}}{\partial x}[x_0]}} \qquad [3.24]$$

The damping factor of this second-order equation is:

$$\xi = \frac{k\mu_3}{2\sqrt{m}}\left(\frac{\partial F_{DEP}}{\partial x}[x_0]\right)^{-1/2} \qquad [3.25]$$

If the damping factor is significantly greater than 1, the inertia of the micro-object can be neglected. As the behavior in DEP (and magnetophoresis) is nonlinear, the damping factor of the linearized model is a function of the operating point x_0. Hence, the identification of the damping factor should be made along the whole trajectory in order to determine the impact of inertia. If the inertia is negligible, equation [3.23] becomes:

$$\overrightarrow{F_{DEP}} + \vec{P} - k\mu_3\vec{V} = 0 \qquad [3.26]$$

In this case, the velocity of the micro-object is only limited by the viscosity. Equation [3.26] is a nonlinear first-order equation, the solution of which induces usually a non-continuous velocity. Indeed, as the inertia is small, the acceleration of the object is high and we can consider that the new velocity is reached instantaneously. This is a typical characteristic at mesoscale in which velocity could be considered as a non-continuous parameter.

To illustrate the scale effect of the impact of inertia on a micro-object trajectory, we show in Figure 3.13 a simple example of two punctual electrodes for which the calculation of the electric field can be done

analytically as a function of the electric voltage. We consider an electric sinusoidal signal with a magnitude $U_0 = 100\,V$ and a frequency ω, a polystyrene object ($\varepsilon_1 = 2.4$) with a radius $r = 10\,\mu m$, immersed in water ($\varepsilon_3 = 80$), and a distance d = 100 μm. In this example, the damping factor is 14, value significantly greater than 1 and the inertia can be neglected. However, with a radius $r = 20\,\mu m$, the damping factor is 2 and the inertia cannot be neglected anymore. This example shows that in non-contact manipulation, the inertia of very small objects (e.g. $r = 20\,\mu m$) should still be considered. Even at microscale and mesoscale, the impact of inertia of a micro-object on its trajectory should be carefully analyzed for each of the application cases.

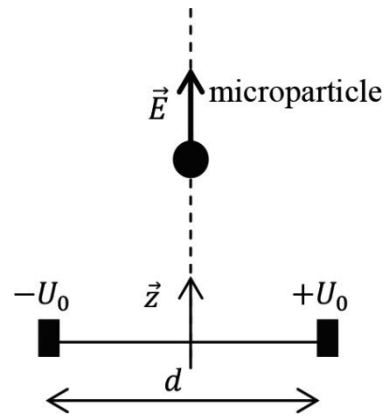

Figure 3.13. *Elementary electrodes used to calculate analytically the electric field with respect to the electric potential*

Moreover, taking the weight into account or not in the trajectory modeling should also be analyzed very carefully. In most cases, weight has to be considered because it defines the final equilibrium position. Indeed, in equation [3.26], the steady-state position is defined by the equilibrium between the weight and the DEP force.

This example shows that all the assumptions made in microscale modeling should be carefully checked. The scale effect analysis enables us to determine the impact of miniaturization on the volume effect (inertia, weight)

compared to surface effect (van der Waals force) or linear effect (viscous force). It is widely assumed that volume effects are negligible at micro-, meso- and nanoscales and that only surface and linear effects have to be considered. The modeling and design of real systems (especially for high-speed non-contact manipulation) is slightly more complicated and volume effects should also be carefully analyzed[6].

3.3.2. *Design*

The design of a non-contact micromanipulation system is based on several trade-offs and is particularly complex in the case of magnetophoresis and DEP. We will present the major design rules in these two cases.

The design of a micromanipulation system consists of the definition of the shape and the size of field sources (e.g. electrodes or coils), and could include the shape and the size of manipulated parts in case of indirect manipulation with a microtool. The design is based on a mechatronic approach in which the electrical and mechanical behaviors have to be taken into account. Figure 3.14 shows the typical block diagram of a non-contact micromanipulation system including the field generation (magnetic or electric field) and the system dynamics.

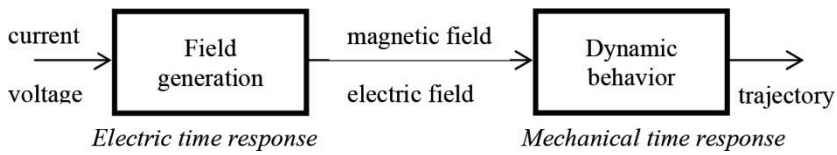

Figure 3.14. *Block diagram of a non-contact micromanipulation system*

As the system is characterized by a high dynamics (typically time response lower than 10 ms), the electric time response cannot always be neglected compared to the mechanical one. Consequently, both time responses should be optimized during design. As an example, in the case of

6 It is especially true for high speed non-contact manipulation in which the acceleration $\ddot{x}$ is very high and the inertial term $m\ddot{x}$ could be significant despite a small mass m. The usual assumption that inertia is negligible is usually only true at low acceleration.

magnetophoresis, enlarging the coils used to generate the magnetic field enables us to generate a larger magnetic force, thus reducing the mechanical time response. However, it also induces a larger inductance that increases the electric time response. The optimization of the size of the coil then has to be checked carefully.

The second trade-off deals with the characteristic of the dynamic behavior. The dielectrophoretic and magnetophoretic forces are, respectively, proportional to the electrical and magnetic field gradients. It means that a regular and constant field does not induce forces. The source has to be designed to generate non-contact fields inducing large field gradients. However, the larger the gradient on the electrodes (e.g. electric point effect), the smaller the electric field will be at the center of the workspace. In other words, maximizing the force near the electrodes minimizes the force in the center of the workspace. The behavior of the system is consequently highly nonlinear, and the larger the maximal force, the lower the linearity. The design of the system requires finding a good trade-off between the level of force and the linearity of the behavior.

A third trade-off has to be made on the size of the manipulated object that has also a strong impact on the dynamics. Indeed, large micro-objects (e.g. 100 μm) are limited by inertia while small objects (e.g. 1 μm) are limited by viscosity. For optimization purposes, two criteria can be considered: the average velocity V of the object and the time T taken by an object to move along a length equal to its characteristic size (e.g. the diameter of the object).

Two asymptotic behaviors can be reached: the behavior in which the inertia is negligible (viscous-force-driven behavior), and the behavior in which inertia is predominant (inertia-driven behavior). When the inertia is negligible, the smaller the object and the average velocity, the larger the time T. When the inertia is not negligible, the average velocity is almost constant, then the larger the object, the larger the time T. The maximum velocity is reached when the inertia is not negligible. The time T is maximal at the frontier between the two asymptotic behaviors.

Based on the requirements of the application at hand, and taking into account the three optimizations described above, the optimal design of a DEP or a magnetophoresis system can be achieved.

3.3.3. *Perception*

At microscale, the number of sensors for measuring the position of a micro-object is very limited. Vision is widely used and appears as the most interesting perception means.

As far as trajectory control is concerned, the current challenge is to reach high velocity controlled in closed loop. Vision systems allow us to manipulate objects along a high-velocity trajectory [KHA 13b]. However, because of the large magnification required to observe microscale objects, vision is limited to planar sensor as 3D vision requires complex methods such as confocal microscopes.

New ways enabling 3D measurement could be explored in the near future. For example, the measure of the position of the object via the measure of impedance variation in DEP is possible [GAW 12]. These measurements are still limited to object characterization. However, the principle could be reused in a sensor-based closed-loop control for non-contact manipulation.

3.3.4. *Control*

This section describes the general issues of control for non-contact mesorobotics. The major issue comes from the particularity of the device and especially the nonlinearity of the behavior and the high dynamics compared to the sensors. The major criteria to evaluate the relevance and the performance of a control strategy are the selectivity, the velocity (or working throughput) and the robustness.

The selectivity, which is the ability to manipulate an object without perturbing the trajectory of the others, is a strong challenge both in DEP and magnetophoresis. Indeed in laser trapping, the laser can be easily focused on the targeted object. In DEP and magnetophoresis, the physical field (electrostatic or magnetic) induces a force on all the objects in the field. Two strategies have been developed to enable a selective manipulation. The first method consists of designing microrobots that move only if the field frequency is in accordance with their resonance frequency. It has been successfully tested in magnetophoresis in [VOL 08]. The second method consists of blocking the non-targeted objects in order to keep them immobile in the field. This principle has been tested experimentally in [PAW 09], where electrostatic anchoring is used to block magnetic microrobots.

Voltages on electrodes patterned on the substrate generate an electrostatic force on selected objects to immobilize them.

The velocity and robustness criteria deal with a common trade-off in control law synthesis. Currently, the experiments described in the literature focus more on the velocity of the trajectory than on robustness. Because of the nonlinearity of the behavior (in both DEP and magnetophoresis), the controllers are intrinsically nonlinear. They are based on the inverted geometric model [KHA 13a]. Because of the high velocity compared to the sampling rate of the vision sensor, blind phases must be considered. During these, the controller is not able to acquire a new image of the device coming from the camera. Predictive control has then been proposed to update the control vector during this phase [KHA 10b]. Some of the controllers are also using predictive control in order to compute the optimal reachable trajectory [BEL 10].

Concerning laser trapping, the system can be considered as linear and the control law is easier to synthetize. The first closed-loop control of non-contact manipulation was performed by Professor Arai using laser trapping and visual processing [ARA 04]. However, the lack of perception means requires specific strategies to be able to observe the system with a relevant frequency. Adaptative observers for optical tweezers were recently proposed in [LI 13a].

3.4. Experimental devices

This section deals with the experimental devices used in non-contact mesoscale manipulation based on laser trapping and DEP. The devices based on magnetophoresis were presented in Chapter 2.

3.4.1. *Laser trapping*

3.4.1.1. *General architecture*

The general architecture of the laser tweezers exploiting laser trapping (see section 3.2.2) is shown in Figure 3.15. Micromanipulations are usually made on an inverted microscope to which a laser beam has been added. Usually, the laser position is controlled with biaxial galvano mirrors. The control data are generated in a PC and transferred to the motor drivers via DA converters. The images of the manipulation are obtained from a CCD camera

mounted on a microscope via an image capture board. In case of multiobject manipulation, some other light generation principles can be used (see section 3.4.1.3).

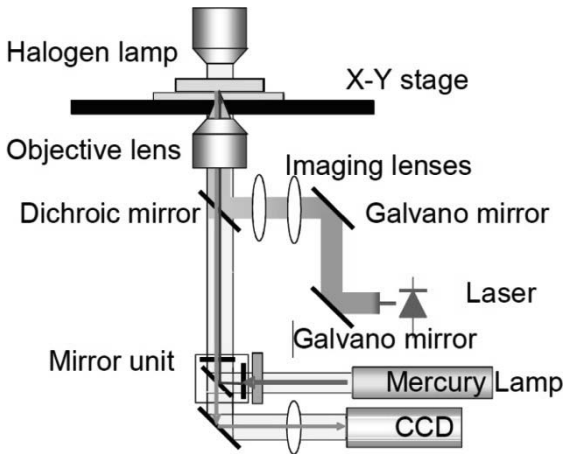

Figure 3.15. *Architecture of an optical tweezer [MAR 11]*

This principle enables us to manipulate several types of micro-objects such as manufactured spheres, biological cells, nanowires and nanotubes [AGA 05]. Because of the laser power, the direct manipulation of biological cells could affect the biological function of the cell. Consequently, this principle is also used for indirect manipulation of cells that are pushed by a microtool moved by laser trapping [ARA 04, OND 12].

Various commercial devices are available for manipulating objects such as the "LaserTweezer®" system available from the company Cell Robotics International, "Palm® Microlaser Systems" from the company PALM Microlaser Technologies as well as the "Optical Tweezer systems" from the company Elliot Scientific. The order of magnitude of forces is around few piconewtons for objects whose diameters are around few micrometers [EMI 04, NAM 04].

3.4.1.2. *Single-object manipulation*

Some applications require manipulating single objects using only one laser beam. As presented in section 3.2.2, laser trapping is also able to induce

torque and enables us to control the angular position of the micro-objects. Figure 3.16 shows a typical example in which each micro-object was positioned sequentially using a laser beam [VEI 12].

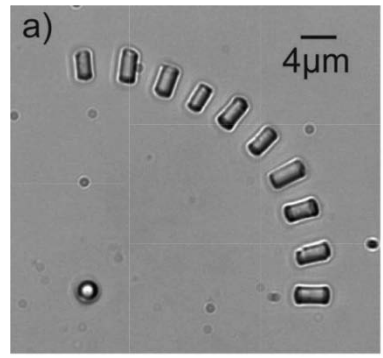

Figure 3.16. *Angular positioning of objects manipulated sequentially by laser trapping [VEI 12]*

In most of the application cases, and especially for biological applications, single-cell laser trapping is combined with another principle in order to induce long-range displacements. The typical application case is the microflow cytometer[7] in which cells should be sorted as a function of their morphology or fluorescence properties [ASH 12]. In Figure 3.17, two types of cells coming from a single microchannel should be sorted into two different microchannels. The laser trapping is used to modify the position of certain cells in the flow in order to "send" them in the right channel. In this case, liquid flow is used for long-range transfer, and single-cell manipulation by laser trapping is used for local positioning.

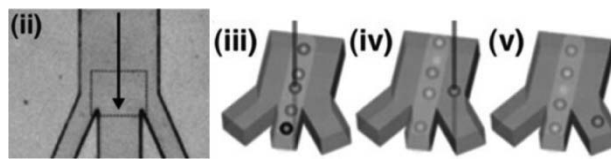

Figure 3.17. *Single-cell trapping for cell sorting in a microfluidic device [ASH 12]*

7 Microflow cytomer is also called microFACS in comparison with the fluorescence-activated cell sorting (FACS) usually used in cell sorting.

3.4.1.3. *Multiobject manipulation*

In most of the applications, the user would like to manipulate several objects at the same time. This requires creating several optical traps in the framework. Three methods enabling multiobject manipulation are available: time-shared scanning (TSS) [SAS 91, ARA 04, ARA 09], generalized phase contrast (GPC) [ERI 02a, ERI 02b, ARA 09] and holographic optical tweezers (HOT) [DUF 98, CHA 06, GRI 07, CON 11].

The first method involves the use of a single laser beam while the objects are sequentially moved one by one. The laser beam is switched from one object to another by moving the beam fast enough compared to the average velocity of the objects [SAS 91, ARA 04]. This method can be used to move objects in three dimensions as shown in Figure 3.18 [ARA 04]. The object being manipulated is moved in the camera plane as well as vertically.

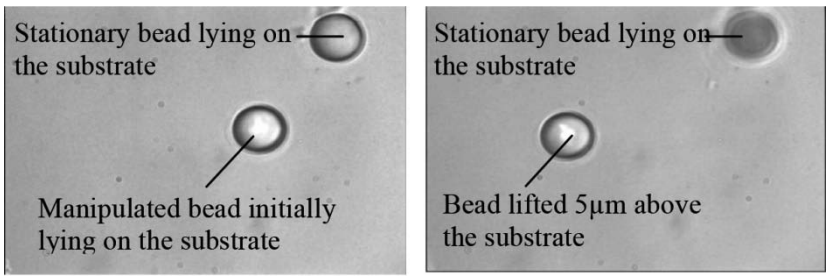
Stationary bead lying on the substrate
Manipulated bead initially lying on the substrate
Stationary bead lying on the substrate
Bead lifted 5µm above the substrate

Figure 3.18. *3D manipulation of seven microdiameter polystyrene beads using laser trapping [ARA 04]*

The movement of several objects can also be obtained by simultaneously moving several optical traps as is done with the above-mentioned HOT and GPC methods. The idea is to structure the light in such a way that several optical traps are created [DUF 98, CHA 06, GRI 07, CON 11]. Simultaneous movements of these traps can be driven by a computer. This process enables a large number of beads or cells to be manipulated in parallel.

A demonstration of the abilities of these methods is given in Figure 3.19 [OND 12]. The control of the micro-objects' positioning is done using an Apple iPad2 as a master device. Ten micro-objects can be manipulated simultaneously using this interface.

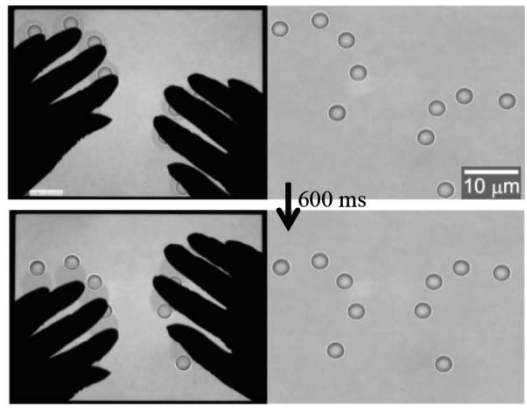

Figure 3.19. *Telemanipulation of 10 microspheres using HOT technique [OND 12]*

As the advantage of TSS trapping is high-speed manipulation and that of GPC is parallel trapping, hybrid methods combining both have been investigated. In the example of Figure 3.20 [ARA 09], the outer two beads were manipulated quickly with a maximum velocity of 54 µm/s while nine beads were trapped by GPC keeping a stable and fixed position.

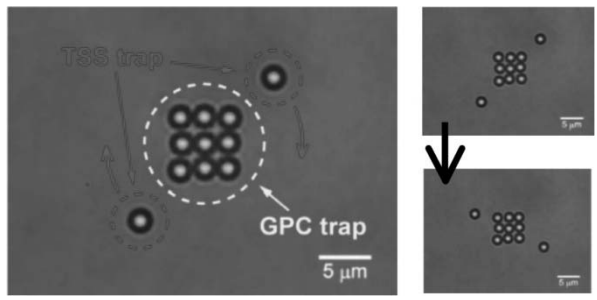

Figure 3.20. *Multitrapping using both GPC and TSS trapping [ARA 09]*

3D multiple trapping of micro-objects paves the way for controlling several microtools around a cell. This concept of "cell microsurgery" has been recently proposed by Maruyama *et al.* [MAR 10]. Figure 3.21 shows an illustration of this concept in which two microtools are manipulated using six laser trapping systems. The microtools could be used to perform cell mechanical operations or tests.

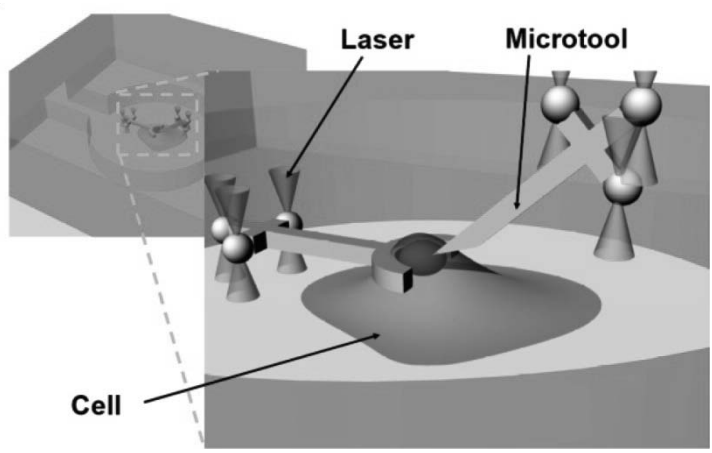

Figure 3.21. *Principle of cell surgery using microtools driven by laser trapping [MAR 10]*

3.4.1.4. *Biological cell characterization*

Mechanical forces acting on cells greatly affect their physical functions such as adhesion, phagocytosis and cell division, as well as movement behavior in aqueous solutions [WU 10, GRE 07, BUS 04, SUN 04]. The ability to accurately measure these forces is essential to understand physiological and pathological events at a single-cell level. However, due to complexity and fragility of the biological structures, it is a challenge to measure these piconewton forces. Laser trapping enables us to apply piconewton forces on micro-objects and, as shown in Figure 3.22, it is an interesting tool for characterizing and measuring properties of cells [GUI 13, WU 10, MEJ 09, TAN 10a, TAN 10b].

Recently, the combination of laser tweezer and Raman spectroscopy (LTRS) has been investigated to characterize the oxygenation response of cells to an applied mechanical force [CHA 13, LU 13, LAF 13b]. Individual cells were subjected to different forces by varying the laser power of a single-beam optical trap, and the intensities of several oxygenation-specific Raman spectral peaks were monitored to determine the oxygenation state of the cells. These studies demonstrated the potential use of LTRS as a single-cell, label-free analytical tool to characterize the functional (e.g. mechanical deformability and oxygen binding) properties of cells.

The measure of the applied force can also be used to give a haptic feedback to the human operator. Recent works have shown that the applied force can be measured using an event-based camera, with a 1 kHz bandwidth enabling haptic feedback [NI 12a, NI 12b, NI 13].

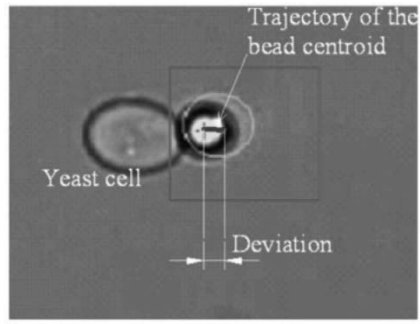

Figure 3.22. *Force applied by a laser-trapped bead on a yeast cell in order to characterize its mechanical properties. The force applied is a function of the deviation between the laser center and the bead center (see Figures 3.5 and 3.7) [WU 10]*

At a smaller scale, the generation of piconewton forces is used to characterize DNA. Figure 3.23 shows a typical experimental test where a DNA bundle is attached to two microspheres manipulated using HOT technique [FAR 10].

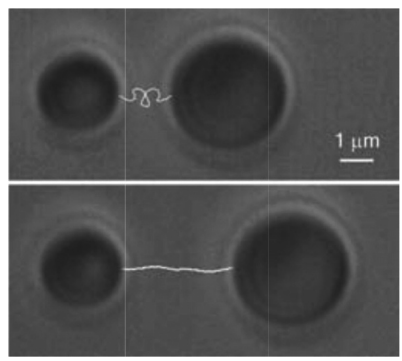

Figure 3.23. *DNA mechanical characterization using laser trapping. DNA bundles are attached to both microspheres manipulated by laser trapping. A vision system measures the distance between the laser center and the center of the beads enabling the measurement of the force (see Figures 3.5 and 3.7) [FAR 10]*

3.4.2. *DEP systems*

3.4.2.1. *Device architectures*

Several ways exist for generating the electric field required in DEP. Most of the DEP devices are based on microelectrodes sputtered on the substrate. Electrode depositions are done by standard microfabrication techniques that enable us to build planar electrodes. As DEP is done in liquid, most of the devices make use of microchannels that are also built using standard microfluidic techniques. Figure 3.24 shows a typical example of a DEP system combining microchannels and microelectrodes.

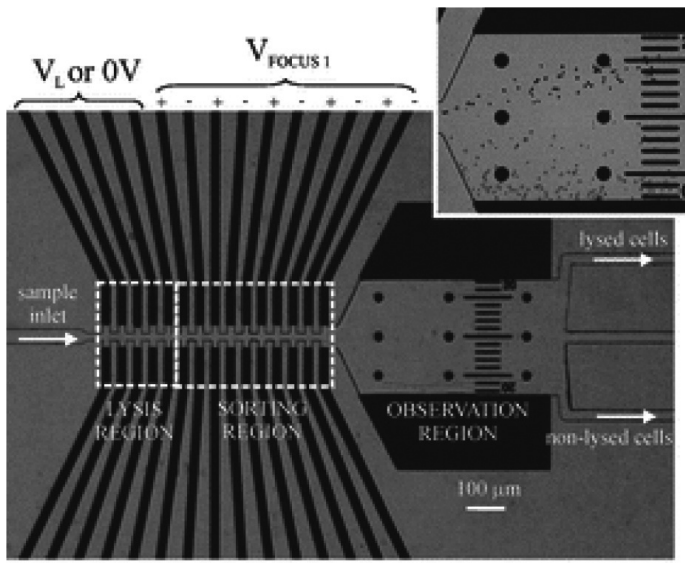

Figure 3.24. *Example of electrodes used in DEP devices. Cells penetrate into the device via the sample inlet (left). In the sorting region, cells are split into two populations according to their electrical properties moving to the upper side and lower side of the device. Because of the laminar flow, both cell populations are not mixed after the sorting region. In the observation region (see inset), the two cell populations go, respectively, to the upper and lower outlets [MER 10]*

Recently, innovative microfabrication principles using pyrolysis have been investigated to build 3D electrodes based on carbon (Figure 3.25). It paves the way for new architectures of electrodes out of the plane [MAR 13b].

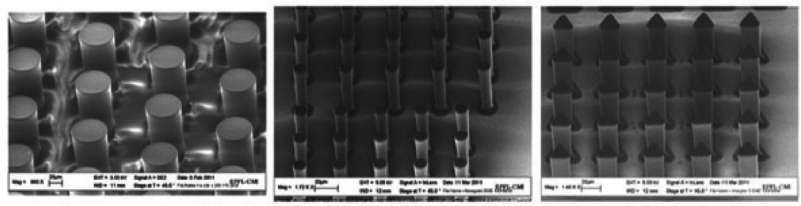

Figure 3.25. *3D carbon electrodes for DEP applications. The columns on the SEM images are carbon electrodes that are conductive. This technology enables us to build out-of-plane electrodes that have been tested in dielectrophoresis devices [MAR 13b]*

Using electrodes placed on the substrate does not enable us to change their position during the experiments. To tackle this drawback, some of the DEP devices make use of mobile electrodes. This approach is similar to the mobile magnetic sources presented in section 2.3.5.2). In this case, microelectrodes are built on fingers or tweezers and are moved during the experiments. Mobile electrodes are usually used for two typical application cases with micromanipulation (Figure 3.26): (1) exploiting pDEP, micro-objects can be trapped on the top of a finger [KOD 13]; (2) exploiting nDEP, micro-object can be removed from two-fingered tweezers [GAU 06].

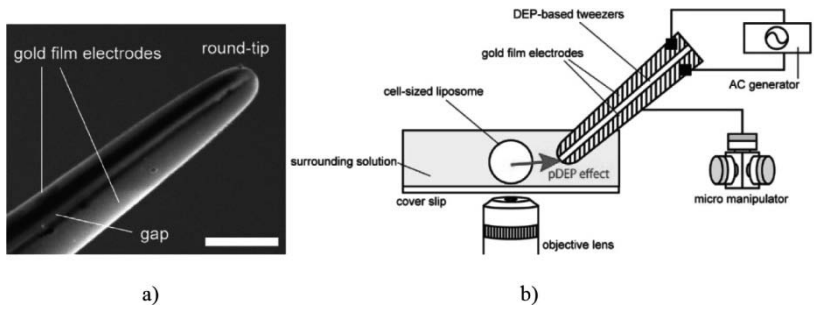

Figure 3.26. *Moving electrodes for DEP applications. a) Electrodes have been deposited on a tip; the grasping of the beads is performed by attractive force induced by positive DEP. b) The bead release is made by cutting off the voltage cancelling the attractive DEP force [KOD 13]*

Finally, one of the most promising ways to generate programmable electric fields for DEP are the optoelectronic tweezers (OET) also called optically induced DEP (ODEP) [CHI 05, LIA 13] that combine the advantages of optical tweezers and DEP. This technique offers the ability to

dynamically create real-time, reconfigurable, “virtual” electrodes, and the generated DEP force can span a large working area on the chip, while using approximately 100,000 times less optical power than laser-based optical tweezers. The ODEP chip has been employed to enable massively parallel manipulation of micro-, meso- and nanoparticles using virtual electrodes that are optically projected from a PC-based system with any desired geometric pattern (Figure 3.27).

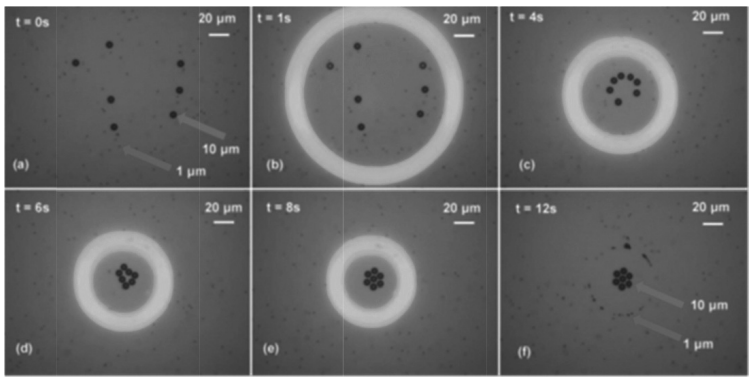

Figure 3.27. *Example of micro-object manipulation using a programmable ODEP device. The lighting (large circle) induces charges on the ITO substrate generating the ODEP force on the microbead. The geometry of the lighting surface is changed during the manipulation enabling more complex trajectories than electrode-based DEP devices [LIA 13]*

As shown in Figure 3.28, the ODEP device consists of a sandwich structure, including a top glass substrate coated with a transparent and conductive indium tin oxide (ITO) film that is used as an electrode, a liquid layer containing the objects to be manipulated and a bottom layer with a thin photoconductive film deposited onto another ITO glass substrate [LIA 13].

3.4.2.2. *Single-cell manipulation*

The typical structure used in single-object manipulation is based on four electrodes placed around the manipulated particle (see Figure 3.9). Using a stationary electric field, an equilibrium point is produced in the center of the four electrodes by nDEP. When using a rotating electric field, a torque can also be applied to the micro-object. This principle has, for example, been used to control the rotation of an oocyte, with rotation velocity of the order of 60°/s being achieved [TSU 01].

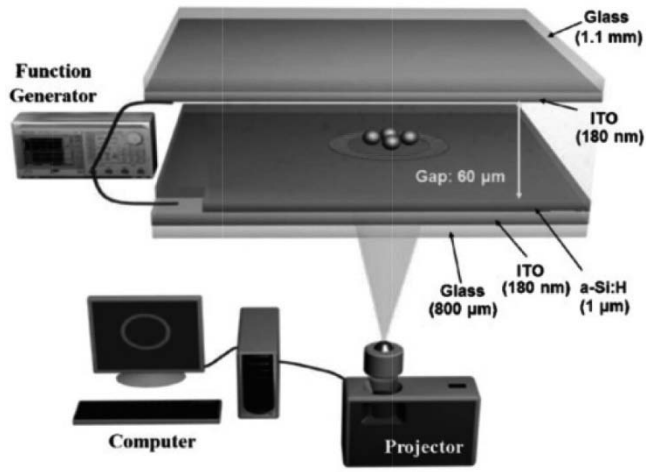

Figure 3.28. *Architecture of a programmable ODEP device [LIA 13]*

Despite the fact that electrode voltage is trivial to modify, most of the experiments done in DEP make use of a constant[8] electric field. Some recent works have shown that high-velocity closed-loop control of microparticles using DEP was possible. From an experimental point of view, the main challenge is to build a control loop able to guarantee a high-frequency sampling, which requires optimizing the position measurement, the controller and the voltage generator. At microscale, the most used position sensor is the optical camera. Thus, using vision as feedback, the camera must provide high-speed acquisition of images with a high-speed communication protocol. As for the voltage generator, the DA converter must have a very short latency also controlled via a fast communication protocol. A technological solution has been proposed in [KHA 13a] using the "Photonfocus" camera with Camera Link communication protocol, able to acquire more than 1,000 images/s in region of interest (ROI) mode. Figure 3.29 shows an experimental trajectory control where the object velocity reaches 2,000 µm/s. The velocity (2 mm/s) could appear quite low, but it is significantly high for beads with a radius of 40 µm. It means that a 40 µm bead requires only 20 ms to move along a distance equivalent to its size. As a comparison, considering a 4 m car, it should reach 720 km/h in order to be able to move along a comparable distance at this scale in 20 ms.

8 Indeed, most of the DEP devices make use of DC voltage with constant amplitude.

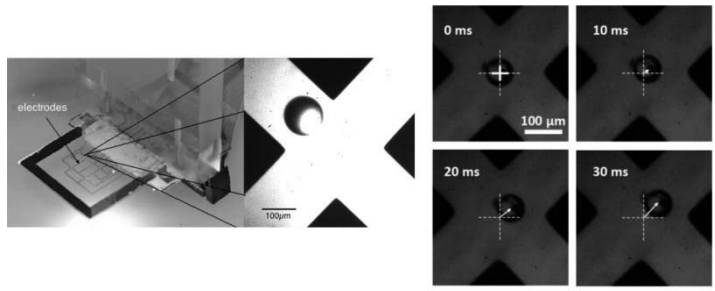

Figure 3.29. *Closed-loop control of a microbead trajectory by DEP. a) View of the system captured by the camera during the trajectory control. b) Examples of images the reference trajectory is an x = y trajectory [KHA 13a]*

The four-electrode structure can also be replicated on the substrate in order to generate numerous stable points on it. Figure 3.30 shows an example of such a device used for multiple-particle positioning. It can be shown that the particles (e.g. biological cells [FRE 03]) can be placed at any stable position.

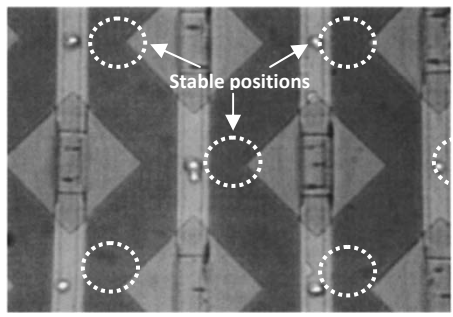

Figure 3.30. *Positioning of biological cells using DEP self-alignment [FRE 03]*

3.4.2.3. *Cell sorting*

Particle sorting, and in particular the sorting of biological cells, finds many applications in the field of medical research. The advantage of separating targeted types of cells from an undifferentiated population is that researchers can perform more precise and better targeted studies. For example, the separation of cancerous and non-cancerous cells can be used to improve the assessment of specific treatments.

Some of the sorting methods exploit the fact that each population of cells could have different dielectric constants, inducing different behaviors in a DEP device. Thus, an electrical signal with a specific frequency can be applied so that one population displays nDEP while the other population displays pDEP, enabling the two cell populations to be sorted [BEC 99, YAS 13]. The DEP force can then be used to separate cells into two populations.

The combination of dielectrophoretic force and fluidic effect appears to be one of the most promising solutions to sort large numbers of cell populations. A flow of particles (biological or artificial) in suspension in water travels along a microchannel etched onto one face with a network of electrodes that apply an electric field. The parabolic velocity established in the microchannel is used to sort the cells (Figure 3.31). The altitude of each particle in the microchannel is given by the equilibrium between the dielectrophoretic force (assumed vertical) and the gravitational force. In this way, the cells that feel a large nDEP force are strongly repelled from the boundary of the channel and then move into a region where the fluid velocity is large. Thus, the velocity in the flow of a population of particles depends directly on these electrical properties. This technique makes the sorting more selective and practical, because it takes place in a flow of particles rather than on particles in a stable medium [HAM 13]. As done in the laser trapping example of Figure 3.17, DEP has also been combined with microfluidics to build microflow cytometers [NAS 08].

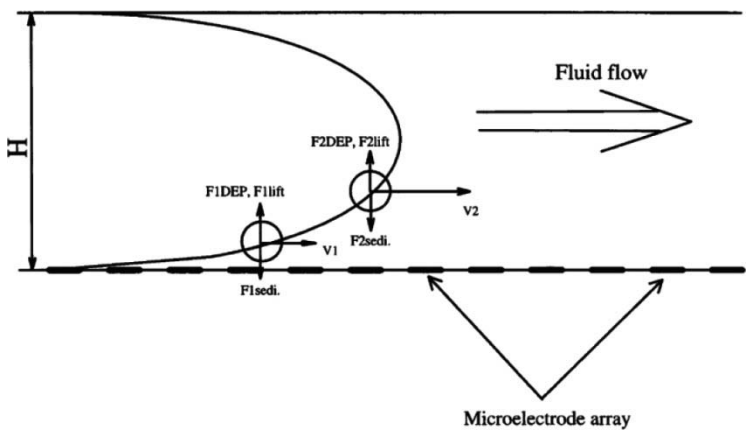

Figure 3.31. *DEP field-flow-fractioning (DEP-FFF) separation technique [HUA 97]*

3.4.2.4. *Other applications*

Microfluidic cell electrofusion consists of controlling the fusion of two cells using a DEP field. Indeed, high-strength electric field can produce minipores on cell membrane and induce cell fusion. It can be generated by a constricting electric field with microstructures or two microelectrodes (Figure 3.32). Cell electrofusion in microfluidic devices attracted great attention in recent years due to its widespread potential of applications in cell-based studies. In these microfluidic devices, many manipulation methods, such as chemical conjugation, DEP and microfluidics, are used to improve the cell pairing accuracy.

In comparison with the traditional electrofusion or other cell-fusion methods, microfluidic cell-electrofusion has many advantages such as precise manipulation, high efficiency in cell pairing and fusion, higher cell viability, lower sample contamination and a smaller Joule heating effect. A review of these techniques is available in [HU 13]. An example of experiment is shown in Figure 3.33.

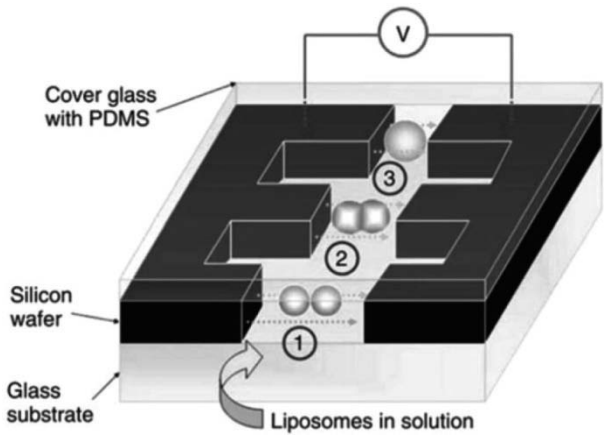

Figure 3.32. *Principle of cell electrofusion. Step 1: dielectrophoretic force creates a contact between two cells; step 2: electric field induces cell electroporation; step 3: fusion of the two cells [HU 13]*

DEP is also used to control cell hydrolysis parameters [MER 12]. This approach enables efficient electroporation of cells by exposing them over a long time to high electrical fields, and enables easy observation of the cell behavior without the need of physical traps.

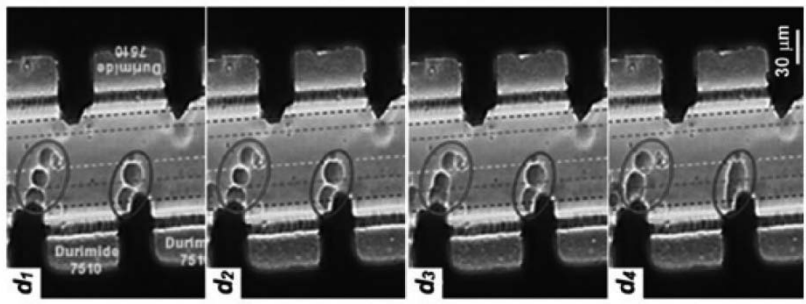

Figure 3.33. *Experimental cell electrofusion. The black parts are the electrodes used to generate DEP. Electrofusion of cells appears in gray circles [HU 11]*

At nanoscale, DEP is used for self-positioning of nanowires or carbon nanotubes on electrodes [PAT 12b, CAO 12]. The assembly obtained (Figure 3.34) consists of a chemical nanosensor. However, at nanoscale, DEP can only be used in an open-loop manner and the position of the nanowires cannot be controlled because of the lack of position sensors. Practically, a lot of nanowires are not in an adequate place and only some of the self-assembled devices can be used as sensors. Developing closed-loop control of DEP positioning at this scale is still a huge challenge for the deployment of powerful manufacturing methods to self-assemble such kinds of nanosensors.

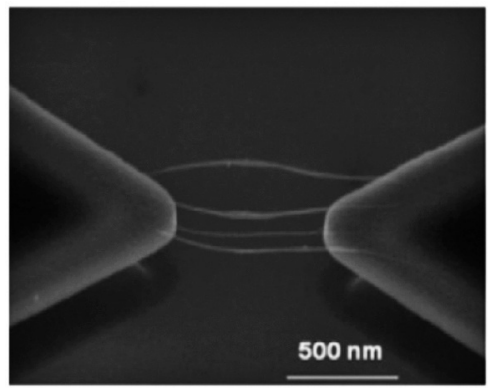

Figure 3.34. *Positioning of carbon nanotubes using DEP self-assembly [PAT 12b]*

3.5. Conclusion

This chapter was dedicated to non-contact micro-nano-robots for manipulation of biological meso-objects whose size is from 100 nm to several tens of micrometers. The most common driving forces at this scale are: (1) magnetic force, (2) dielectrophoretic force and (3) radiation pressure in the case of laser tweezers. As magnetic forces have been widely presented in Chapter 2, we have focused on a description of the physical principles, scientific challenges and applications of the two latter driving principles.

The models of DEP and radiation forces exploited in laser tweezers were presented. We have seen that such devices can induce forces on meso-objects whose order of magnitude is, respectively, a few nanonewtons and tens of piconewtons. These forces, greater than the weight of the meso-object, are exploited to manipulate them without mechanical contact. Unlike at upper scales, the dynamic behavior of meso-objects is mainly driven by viscous forces rather than inertia. Indeed, in most cases, inertia is negligible and velocity can be considered as a discontinuous parameter.

Performing robotic operations at this particular scale requires improving the modeling, design, perception and control methods. We have proposed a generic method to build models for DEP force based on a minimum of basic FEM simulations. We have identified several trade-offs characterizing the design of these particular robotic systems. Moreover, the measure of position or force applied on meso-objects is still a big challenge prior to achieving with reliable automatic manipulation at this scale. We have also highlighted that the nonlinear behavior induced by these physical principles requires nonlinear control laws.

The current major devices available in the world for non-contact manipulation at mesoscale were also presented. Laser tweezers enable us to manipulate a large number of meso-objects but at low velocity. DEP systems are mostly dedicated to single-cell manipulation but enable high-velocity positioning. We also have reported that both principles are increasingly combined with microfluidic channels in order to transfer objects over a large distance.

Chapter 4 presents the future challenges of biomedical robots at nanoscale up to 100 nm based on merged approaches between robotics and chemistry.

Chapter 4

Toward Biomedical Nanorobotics

4.1. Applicative challenges

So far, this book has presented the state of the art of biomedical robotics from millimetric scale to the frontier of nanoscale (100 nm). On the bottom scale, the manipulation and characterization of biological nano-objects and the assembly of nanocomponents for biological applications are still a challenge.

4.1.1. *In vitro applications*

In biology, nanoscale is the scale of the internal components of cells such as DNA. The development of nanorobots able to act on these components would first be a unique opportunity to better understand the internal functioning of the cell. Indeed, the test of elementary functioning of each cell component requires grasping it and testing chemical and/or mechanical response to various biological or chemical stimuli. For instance, the characterization of DNA mechanical behavior has been recently performed in [LAF 13a].

Knowing the internal functioning of cells, nanorobots could also be used to perform diagnosis by acting or testing internal materials or functionalities inside them. In the distant future, they could also be used as therapeutic tools for modifying or correcting functions inside cells (cell therapy).

4.1.2. *Nanoassembly for biomedical applications*

Nanorobots should also be able to build systems from nanotechnologies that could be used in the biomedical field, especially in embedded monitoring devices. Some proofs of concept of nanosensors based on the assembly of a nanowire between two electrodes have recently been proposed in the literature [CHE 13, EVO 04, LUP 12, ZHA 12]. However, these systems are still too expensive for the market. Indeed, two processes currently exist: (1) self-assembly whose reliability is extremely low and (2) nanolithography in scanning electronic microscope (SEM), which is reliable but expensive. Using micro- or nanorobots to assemble such kinds of chemical sensors should be a reliable and powerful method in the future, and should enable us to contribute to the advent of multiple chemical nanosensors.

4.1.3. *In vivo applications*

The first possible application of *in vivo* nanorobots deals with the injection of millions of nanorobots able to target diseased cells. Their mission would be to destroy or to cure targeted cells that would be evacuated out of the body afterwards. To be able to act on millions of cells at the same time, these nanorobots should be controlled with a local controller taking into account biochemical stimuli. In other words, the nanorobots would consist of chemical vectors in which a chemical-based controller would be implemented.

A second *in vivo* application of nanorobotics deals with cell therapy using a microrobotic carrier (either fully or partially intracorporeal) through the natural orifices of the body. In such an application, the microrobotic carrier would bring a nanotool in contact with a cell to be "repaired". Unlike the million-nanorobot swarm, this approach would thus consist of a single robot (or a number reasonably accessible to the human mind) scanning a surface on the lumen wall. The design and control of such a system would have to find a trade-off between velocity, accuracy and safety, which is the core of robotics research. Nevertheless, cell therapy will, here again, most probably rely on both robotics and biochemistry.

4.2. Scientific challenges

4.2.1. *New paradigm removing frontiers between sciences*

In a general way, the study and development of nanorobots will require highly multidisciplinary research involving chemistry, biochemistry, biology,

bioengineering and engineering such as robotics and automation. The next generation of scientists working in this field will establish a new scientific paradigm crossing the frontiers of different fields of science to build what might be called *biochemtronics*.

Indeed, all the functions of the future nanorobots will be based on chemistry or biochemistry, thus on biochemical-based sensors and actuators as well as on chemical-based controllers. At nanoscale, these *biochemtronics* components will replace the current mechatronics components of conventional robot structures. Programming languages will be replaced by chains of macromolecules comparable to the biological DNA coding cell functioning. Most of these *biochemtronics* components do not yet exist and should be discovered, studied and developed in future years.

One of the most important challenges when developing engineering at nanoscale is the reliability of components. Indeed, going from the physical proof of the concept of a phenomenon to its practical use requires us to identify and to control the predominant parameters to guarantee a high level of repeatability. Improving the repeatability of the physical principles demonstrated at nanoscale is currently a major challenge.

4.2.2. *Energy sources*

Developing nanoscale engineering also implies dealing with the management of energy required for any biological, chemical or robotic action. Making use of a mesoscaled robot (e.g. 10 μm long) with embedded energy and control is definitely impossible. However, at that scale, nature has developed cells such as bacteria, which have a reasonable autonomy in terms of power and control.

Two major ways should be studied in the future in order to provide autonomous meso- or nanoscaled robots. The issue could be compared with the history of machine design in the macroworld. In fact, the first solution that humans figured out to induce movement and mechanical work were animals. Indeed, an animal stores its own power, has its own local closed loops and can be easily controlled by human through a simple interface (e.g. a halter). Humans then switched slowly to machinery with the advent of the industrial revolution at the end of the 18th Century. They moved very recently to robotics with the progress in the fields of energy storage, computing and mechatronics. However, at meso- and nanoscale, energy remains a huge challenge and the first step could be to just “domesticate”

mobile cells (such as lymphocytes) and build interfaces to make it possible to control their movement. This way is typically followed by Martel in Canada (Figure 3.1, [MAR 09b, MAR 13a]).

4.2.3. *How far away is this future?*

It appears that all the challenges described above cannot be solved within a few years or a few tens of years. Nanoengineering, or *biochemtronics*, will require time to emerge as a new field of science. Indeed, merging the above-mentioned disciplines will probably take one or two generations of scientists. Until then, we can expect that incremental progress will be made where different types of systems will be developed and improved, adding more and more functionalities, reliability, and autonomy. The development of nanorobots also raises ethical, legal and societal issues that will require time to be solved, and will probably put constraints on the proposed technological solutions.

Therefore, much scientific effort has yet to be made for present and future generations to develop multiscale biomedical robots.

Bibliography

[ABB 07] ABBOTT D.J., BECKE C., ROTHSTEIN R.I., *et al*., "Design of an endoluminal NOTES robotic system", *Proceedings of the IEEE/RSJ International Conference on Intelligent Robots and Systems (IROS)*, San Diego, CA, pp. 410–416, 29 October–2 November 2007.

[ABB 09] ABBOTT J., COSENTINO LAGOMARSINO M., ZHANG L., DONG L., *et al*., "How should microrobots swim?", *The International Journal of Robotics Research*, vol. 28, nos. 11–12, pp. 1434–1447, 2009.

[AGA 05] AGARWAL R., LADAVC K., ROICHMAN Y., *et al*., "Manipulation and assembly of nanowires with holographic optical traps", *Optics Express*, vol. 13, no. 22, pp. 8906–8912, 2005.

[AKI 11] AKIYAMA Y., ODAIRA K., IWABUCHI K., *et al*., "Long-term and room temperature operable bio-microrobot powered by insect heart tissue", *Proceedings of the IEEE 24th International Conference on Micro Electro Mechanical Systems (MEMS)*, Cancun, Mexico, pp. 145–148, 2011.

[AKI 12] AKIYAMA Y., ODAIRA K., SAKIYAMA K., *et al*., "Rapidly-moving insect muscle-powered microrobot and its chemical acceleration", *Biomedical Microdevices*, vol. 14, no. 6, pp. 979–986, 2012.

[ALO 09] ALOUGES F., DESIMONE A., LEFEBVRE A., "Biological fluid dynamics: swimming at low Reynolds numbers", in *Encyclopedia of Complexity and System Science*, Springer Verlag, 2009. Available at: http://www.cmap.polytechnique.fr/~lefebvre/PUBLI/AlougesDeSimoneLefebvre_encyclopedia_swimmer.pdf

[ALO 13] ALOY A., GRASL M., "Endoscopy of larynx and trachea with rigid laryngo-tracheoscopes under superimposed high-frequency jet ventilation (SHFJV)", in *Endoscopy*, S. AMORNYOTIN, (ed.) Chapter 9, InTech, pp. 141–200, 2013.

[AND 13a] ANDREFF N., DEMBÉLÉ S., TAMADAZTE B., *et al*., "Epipolar geometry for vision-guided laser surgery", *10th International Conference on Informatics in Control, Automation and Robotics (ICINCO)*, Reykjavik, Iceland, 29–31 July 2013.

[AND 13b] ANDREFF N., TAMADAZTE B., DEMBÉLÉ S., *et al*., "Preliminary variation on multiview geometry for vision-guided laser surgery", *Workshop on Multiple View Geometry in Robotics*, Berlin, Germany, 24–28 June 2013.

[ANG 04] ANG W.T., Active tremor compensation in handheld instruments for microsurgery, PhD Thesis, Carnegie Mellon University, 2004.

[ANO 11] ANOR T., MADSEN J.R., DUPONT P.E., "Algorithms for design of continuum robots using the concentric tubes approach: a neurosurgical example", *Proceedings of the IEEE International Conference on Robotics and Automation (ICRA)*, Shanghai, China, pp. 667–673, 9–13 May 2011.

[ARA 04] ARAI F., YOSHIKAWA K., SAKAMI T., *et al*., "Synchronized laser micromanipulation of multiple targets along each trajectory by single laser", *Applied Physics Letters*, vol. 85, no. 19, pp. 4301–4303, 2004.

[ARA 09] ARAI F., ONDA K., IITSUKA R., *et al*., "Multi-beam laser micromanipulation of microtool by integrated optical tweezers", *Proceedings of the IEEE International Conference on Robotics and Automation (ICRA)*, Kobe, Japan, pp. 1832–1837, 12–17 May 2009.

[ARA 10] ARATA J., SAITO Y. FUJIMOTO H., "Outer shell type 2 DoF bending mainpulator using spring-link mechanism for medical applications", *Proceedings of the IEEE International Conference on Robotics and Automation (ICRA)*, Anchorage, AK, pp. 1041–1046, 3–8 May 2010.

[ASC 03] ASCARI L., STEFANINI C., MENCIASSI A., *et al*., "A new active microendoscope for exploring the sub-arachnoid space in the spinal cord", *Proceedings of the IEEE International Conference on Robotics and Automation (ICRA)*, Taipei, Taiwan, pp. 2657–2662, 14–19 September 2003.

[ASH 86] ASHKIN A., DZIEDZIC J.M., BJORKHOLM J.E., *et al*., "Observation of a single-beam gradient force optical trap for dielectric particles", *Optics Letters*, vol. 11, no. 5, pp. 288–90, 1986.

[ASH 12] ASHOK P.C., DHOLAKIA K., "Optical trapping for analytical biotechnology", *Current Opinion in Biotechnology*, vol. 23, pp. 16–21, 2012.

[BAJ 12] BAJO A., GOLDMAN R.E., WANG L., *et al*., "Integration and preliminary evaluation of an insertable robotic effectors platform for single port access surgery", *Proceedings of the IEEE International Conference on Robotics and Automation (ICRA)*, Saint Paul, MN, pp. 3381–3387, 14–18 May 2012.

[BAR 04] BAR-COHEN Y. (ed.), *Electroactive Polymer (EAP) Actuators as Artificial Muscles – Reality, Potential and Challenges*, vol. PM136, SPIE Press, 2004.

[BAR 12] BARDOU B., NAGEOTTE F., ZANNE P., *et al*., "Improvments in the control of flexible endoscopic system", *Proceedings of the IEEE International Conference on Robotics and Automation (ICRA)*, Saint Paul, MN, pp. 3725–3732, 14–18 May 2012.

[BAR 13] BARRESI G., DESHPANDE N., MATTOS L., *et al*., "Usability and performance: comparative evaluation of surgeon interfaces in laser phonomicrosurgery", *3rd Joint Workshop on New Technologies for Computer/Robot Assisted Surgery*, Verona, Italy, September 2013.

[BAU 13] BAUER R.W., RADTKE I., BLOCK K.T., *et al*., "True real-time cardiac MRI in free breathing without ECG synchronization using a novel sequence with radial k-space sampling and balanced SSFP contrast mode", *The International Journal of Cardiovascular Imaging*, vol. 29, no. 5, pp. 1059–1067, 2013.

[BAY 12] BAYLE B., BARBÉ L., "Tele-manipulation", in TROCCAZ J. (ed.), *Medical Robotics*, ISTE, London, John Wiley & Sons, New York, pp. 269–301, 2012.

[BEC 99] BECKER F., GASCOYNE P., HUANG Y., *et al*., Method and apparatus for manipulation using spiral electrodes, US Patent No. 5858192, 1999.

[BED 11] BEDELL C., LOCK J., GOSLINE A., *et al*., "Design optimization of concentric tube robots based on task and anatomical constraints", *Proceedings of the IEEE International Conference on Robotics and Automation (ICRA)*, Shangai, China, pp. 398–403, 9–13 May 2011.

[BEI 11] BEIRA R., SANTOS-CARRERAS L., ROGNINI G., *et al*., "Dionis: a novel remote-center-of-motion parallel manipulator for minimally invasive surgery", *Applied Bionics and Biomechanics, Special Issue in Surgical Robotics*, vol. 8, no. 2, pp. 191–208, 2011.

[BEL 10] BELHARET K., FOLIO D., FERREIRA A., "Endovascular navigation of a ferromagnetic microrobot using MRI-based predictive control", *Proceedings of the IEEE/RSJ International Conference on Intelligent Robots and Systems (IROS)*, pp. 2804–2809, Taipei, Taiwan, 18–22 October 2010.

[BER 12] BERNARDES M.C., ADORNO B.V., POIGNET P., *et al*., "Semi-automatic needle steering system with robotic manipulator", *Proceedings of the IEEE International Conference on Robotics and Automation (ICRA)*, Saint Paul, MN, pp. 1595–1600, 14–18 May 2012.

[BHA 12] BHATTACHARYA Y.S., ANANTHAMURTHY S., "Characterizing the rotation of non symmetric objects in an optical tweezer", *Optics Communications*, vol. 285, pp. 2530–2535, 2012.

[BOU 11] BOUDAOUD M., HADDAB Y., GORREC Y.L., *et al*., "Noise characterization in millimeter sized micromanipulation systems", *Mechatronics*, vol. 21, no. 6, pp. 1087–1097, 2011.

[BOW 10] BOWMAN R., GIBSON G., PADGETT M., "Particle tracking stereomicroscopy in optical tweezers: control of trap shape", *Optics Express*, vol. 18, no. 11, pp. 11785–11790, 2010.

[BUC 10] BUCHAILLOT L., "Microtechnology and micromanipulation", in RÉGNIER S., CHAILLET N. (eds), *Microrobotics for Micromanipulation*, Chapter 5, ISTE, London, John Wiley & Sons, New York, pp. 335–368, 2010.

[BUS 04] BUSTAMANTE C., CHEMLA Y.R., FORDE N.R., *et al*., "Mechanical processes in biochemistry", *Annual Review of Biochemistry*, vol. 73, pp. 705–748, 2004.

[BUT 12] BUTLER E.J., HAMMOND-OAKLEY R., CHAWARSKI S., *et al*., "Robotic neuro-endoscope with concentric tube augmentation", *Proceedings of the IEEE/RSJ International Conference on Intelligent Robots and Systems (IROS)*, Vilamoura, Algarve, Portugal, pp. 2941–2946, 7–12 October 2012.

[BYU 11] BYUN D., CHOI J., CHA K., *et al*., "Swimming microrobot actuated by two pairs of Helmholtz coils system", *Mechatronics*, vol. 21, no. 1, pp. 357–364, 2011.

[CAL 08] CALTABIANO D., BRUGALI D., SANNINO R., *et al*., "A real-time communication protocol for interconnecting robotic smart devices", *Proceedings of the IEEE/RSJ International Conference on Intelligent Robots and Systems (IROS)*, Nice, France, pp. 1896–1901, 22–26 September 2008.

[CAO 12] CAO J., NYFFELER C., LISTER K., *et al*., "Resist-assisted assembly of single-walled carbon nanotube devices with nanoscale precision", *Carbon*, vol. 50, pp. 1720–1726, 2012.

[CAR 07] CARPI F., GALBIATI S., CARPI A., "Controlled navigation of endoscopic capsules: concept and preliminary experimental investigations", *IEEE Transactions on Biomedical Engineering*, vol. 54, no. 11, pp. 2028–2036, 2007.

[CAR 08] CARPI F., KHANICHEH A., MAVROIDIS C., *et al*., "MRI compatibility of silicone-made contractile dielectric elastomer actuators", *IEEE/ASME Transactions on Mechatronics*, vol. 13, no. 3, pp. 370–374, 2008.

[CAR 09a] CARPI F., PAPPONE C., "Magnetic maneuvering of endoscopic capsules by means of a robotic navigation system", *IEEE Transactions on Biomedical Engineering*, vol. 56, no. 5, pp. 1482–1490, May 2009.

[CAR 09b] CARPI F., SMELA E. (eds), *Biomedical Applications of Electroactive Polymer Actuators*, Wiley, 2009.

[CAR 09c] CARTA R., TORTORA G., THONÉ J., *et al*., "Wireless powering for a self-propelled and steerable endoscopic capsule for stomach inspection", *Biosensors and Bioelectronics*, vol. 25, no. 4, pp. 845–851, 2009.

[CHA 00] CHANG J.K., CHUNG S., LEE Y., *et al*., "Endovascular micro tools", *Proceedings of the 1st Annual International IEEE-EMBS Special Topic Conference on Microtechnologies in Medicine & Biology*, Lyon, pp. 119–126, 12–14 October 2000.

[CHA 06] CHAPIN S.C., GERMAIN V., DUFRESNE E.R., "Automated trapping assembly and sorting with holographic optical tweezers", *Optics Express*, vol. 14, no. 26, pp. 13095–100, 2006.

[CHA 10] CHAILLET N., RÉGNIER S. (eds), *Microrobotics for Micromanipulation*, ISTE, London, John Wiley & Sons, New York, June 2010.

[CHA 13] CHAN J.W., "Recent advances in laser tweezers Raman spectroscopy (LTRS) for label-free analysis of single cells", *Journal of Biophotonics*, vol. 6, no. 1, pp. 36–48, 2013.

[CHE 05] CHEUNG E., KARAGOZLER M.E., PARK S., *et al*., "A new endoscopic microcapsule robot using beetle inspired microfibrillar adhesives", *Proceedings of the IEEE/ASME International Conference on Advanced Intelligent Mechatronics*, Monterey, CA, pp. 551–557, 24–28 July 2005.

[CHE 06] CHEN S.-C., CULPEPPER M.L., "Design of a six-axis micro-scale nanopositioner – μHexFlex", *Precision Engineering*, vol. 30, no. 3, pp. 314–324, 2006.

[CHE 13] CHEN X., WONG C.K.Y., YUAN, *et al.,* "Review on nanowire-based gas sensors", *Sensors and Actuators B: Chemical*, vol. 177, pp. 178–95, 2013.

[CHI 05] CHIOU P.Y., OHTA A.T., WU M.C., "Massively parallel manipulation of single cells and microparticles using optical images", *Nature*, vol. 436, pp. 370–372, 2005.

[CIU 10a] CIUTI G., DONLIN R., VALDASTRI P., *et al*., "Robotic versus manual control in magnetic steering of an endoscopic capsule", *Endoscopy*, vol. 42, no. 2, pp. 148–152, 2010.

[CIU 10b] CIUTI G., VALDASTRI P., MENCIASSI A., *et al*., "Robotic magnetic steering and locomotion of capsule endoscope for diagnostic and surgical endoluminal procedures", *Robotica*, vol. 28, no.2, pp. 199–207, 2010.

[CIU 11] CIUTI G., MENCIASSI A., DARIO P., "Capsule endoscopy: from current achievements to open challenges", *IEEE Reviews in Biomedical Engineering*, vol. 4, pp. 59–72, 2011.

[CIU 12] CIUTI G., VISENTINI-SCARZANELLA M., DORE A., MENCIASSI A., DARIO P., YANG G.Z., "Intra-operative monocular 3D reconstruction for image-guided navigation in active locomotion capsule endoscopy", *Proceedings of the IEEE/RAS-EMBS International Conference on Biomedical Robotics and Biomechatronics (BioRob)*, Rome, Italy, pp. 768–774, 24–27 June 2012.

[CLA 12] CLARK J., LEON L., WARREN F., ABBOTT J., "Magnetic guidance of cochlear implants: proof-of-concept and initial feasibility study", *Journal of Medical Devices*, vol. 6, pp. 035002, 10 August 2012.

[CLÉ 11] CLÉVY C., CHAILLET N., RAKOTONDRABE M., *Signal Measurement and Estimation Techniques for Micro and Nanotechnology*, Springer, 2011.

[CON 11] CONKEY D.B., TRIVEDI R.P., PAVANI S.R.P., *et al.*, "Three-dimensional parallel particle manipulation and tracking by integrating holographic optical tweezers and engineered point spread functions", *Optics Express*, vol. 19, no. 5, pp. 3835–3842, 2011.

[COO 12] COOLEN B.F., ABDURRACHIM D., MOTAAL A.G., *et al.,* "High frame rate retrospectively triggered cine MRI for assessment of murine diastolic function", *Magnetic Resonance in Medicine*, vol. 69, no. 3, pp. 648–656, 2012.

[DAL 02] D'ALESSIO A., PIRO E., TADINI B., *et al.,* "One-trocar transumbilical laparoscopic-assisted appendectomy in children: our experience", *European Journal of Pediatric Surgery*, vol. 12, no. 1, pp. 24–27, 2002.

[DAR 03] DARIO P., HANNAFORD B., MENCIASSI A., "Smart surgical tools and augmenting devices", *IEEE Transactions on Robotics and Automation, Special Issue on Medical Robotics*, vol. 19, no. 5, pp. 782–792, October 2003.

[DAS 99] DAS H., ZAK H., JOHNSON J., *et al.,* "Evaluation of a telerobotic system to assist surgeons in microsurgery", *Computer Aided Surgery*, vol. 4, no. 1, pp. 15–25, 1999.

[DEG 06] DEGANI A, CHOSET H., WOLF A., *et al.,* "Highly articulated robotic probe for minimally invasive surgery", *Proceedings of the IEEE International Conference on Robotics and Automation (ICRA)*, Orlando, FL, pp. 4167–4172, 15–19 May 2006.

[DEL 09] DELAERE P., Available at http://www.kuleuven.be/cltr/en/larynx/dir_laryn.htm.

[DHO 02] DHOLAKIA K., SPALDING G., MACDONALD M., "Optical tweezers: the next generation", *Physics World*, vol. 15, pp. 31–35, 2002.

[DI 13] DI NATALI C., BECCANI M., VALDASTRI P., "Real-time pose detection for magnetic medical devices", *IEEE Transactions on Magnetics*, vol. 49, no. 7, pp. 3524–3527, 2013.

[DIM 03] DIMAIO S.P., SALCUDEAN S.E., "Needle insertion modeling and simulation", *IEEE Transactions on Robotics and Automation*, vol. 19, no. 5, pp. 864–875, 2003.

[DIN 12] DING X., LIN S.-C.S., KIRALY B., *et al.,* "On-chip manipulation of single microparticles, cells, and organisms using surface acoustic waves", *Proceedings of the National Academy of Sciences of the United States of America*, vol. 109, no. 28, pp. 11105–11109, 2012.

[DOM 08] DOMINICI M., POIGNET P., DOMBRE E., "Compensation of physiological motion using linear predictive force control", *Proceedings of the IEEE/RSJ International Conference on Intelligent Robots and Systems (IROS)*, Nice, France, pp. 1173–1178, 22–26 September 2008.

[DOM 12a] DOMBRE E., POIGNET P., PIERROT F., "Design of medical robots", in TROCCAZ J. (ed.), *Medical Robotics*, ISTE, London, John Wiley & Sons, New York, 2012.

[DOM 12b] DOMBRE E., CHAILLET N., DE MATHELIN M., "Towards intracorporeal robotics", in TROCCAZ J. (ed.), *Medical Robotics*, ISTE, London, John Wiley & Sons, New York, 2012.

[DUF 98] DUFRESNE E. R., GRIER D.G., "Optical tweezer arrays and optical susbtrates created with diffractive optics", *Review of Scientific Instruments*, vol. 69, no. 5, pp. 1974–1977, 1998.

[DUP 10] DUPONT P.E., LOCK J., ITKOWITZ B., *et al.,* "Design and control of concentric-tube robots", *IEEE Transactions on Robotics*, vol. 26, no. 2, pp. 209–225, 2010.

[EMI 04] EMILIANI V., SANVITTO D., ZAHID M., *et al.,* "Multi force optical tweezers to generate gradients of forces", *Optics Express*, vol. 12, pp. 3906–3910, 2004.

[ERI 02a] ERIKSEN R.L., MOGENSEN P.C., GLÜCKSTAD J., "Multiple-beam optical tweezers generated by the generalized phase-contrast method", *Optics Letters*, vol. 27, no. 4, pp. 267–269, 2002.

[ERI 02b] ERIKSEN R.L., DARIA V.R., GLÜCKSTAD J., "Fully dynamic multiple-beam optical tweezers", *Optics Express*, vol. 10, no. 14, pp. 597–602, 2002.

[EVO 04] EVOY S., DI LELLO N., DESHPANDE V., *et al.,* "Dielectrophoretic assembly and integration of nanowire devices with functional CMOS operating circuitry", *Microelectronic Engineering*, vol. 75, pp. 31–42, 2004.

[FAR 10] FARRE A., VAN DER HORST A., BLAB G.A., *et al.,* "Stretching single DNA molecules to demonstrate high-force capabilities of holographic optical tweezers", *Journal Biophoton*, vol. 3, no. 4, pp. 224–233, 2010.

[FEN 06] FENG W., GUO S., CHI C., *et al.,* "Realization of a catheter driving mechanism with micro tactile sensor for intravascular neurosurgery", *Proceedings of the IEEE International Conference on Robotics and Biomimetics*, Kunming, China, pp. 1628–1633, 17–20 December 2006.

[FLO 08] FLOYD S., PAWASHE C., SITTI M., "Dynamic modeling of stick slip motion in an untethered magnetic micro-robot", *Robotics: Science and Systems IV*, Zurich, Switzerland, June 2008.

[FOU 10] FOUNTAIN T., KAILAT P., ABBOT J., "Wireless control of magnetic helical microrobots using a rotating-permanent-magnet manipulator", *Proceedings of the IEEE International Conference on Robotics and Automation (ICRA)*, Anchorage, AK, pp. 576–581, 3–8 May 2010.

[FRE 03] FRENEA M., FAURE S.P., LE PIOUFLE B., *et al.,* "Positioning living cells on a high-density electrode array by negative dielectrophoresis", *Materials Science and Engineering C*, vol. 23, pp. 597–603, 2003.

[FUJ 08] FUJIMOTO J., DREXLER W., *Optical Coherence Tomography*, Springer, 2008.

[GAN 12] GANGLOFF J., NAGEOTTE F., POIGNET P., "Vision-based control", in TROCCAZ J. (ed.), *Medical Robotics*, ISTE, London, John Wiley & Sons, New York, 2012.

[GAU 06] GAUTHIER M., GIBEAU E., HÉRIBAN D., "Submerged robotic micromanipulation and dielectrophoretic micro-object release", *Proceedings of the 9th International Conference on Control, Automation, Robotics and Vision (ICARCV)*, Singapore, 5–8, December 2006.

[GAU 10a] GAUTHIER M., LAMBERT P., REGNIER S., "The physics of the microworld", in REGNIER S., CHAILLET N. (eds), *Microrobotics for Micromanipulation*, Chapter 1, ISTE London, Wiley, 2010.

[GAU 10b] GAUTHIER M., RÉGNIER S. (eds), *Robotic Micro-Assembly*, Wiley, 2010.

[GAW 12] GAWAD S., VALERO A., BRASCHLER T., *et al.,* "On-chip flow cytometry", B. BHUSHAN (ed.), *SpringerScience + Business Media B.V.*, pp. 1913–1923, 2012.

[GHO 09] GHOSH A., FISCHER P., "Controlled propulsion of artificial magnetic nanostructured propellers", *Nano Letters*, vol. 9, no. 6, pp. 2243–2245, 2009.

[GLA 08] GLASS P., CHEUNG E., SITTI M., "A legged anchoring mechanism for capsule endoscopes using micropatterned adhesives", *IEEE Transactions on Biomedical Engineering*, vol. 55, no. 12, pp. 2759–2767, 2008.

[GLA 13] GLADDEN L.F., SEDERMAN A.J., "Recent advances in flow MRI", *Journal of Magnetic Resonance*, vol. 229, pp. 2–11, 2013.

[GLO 04] GLOZMAN D., SHOHAM M., "Flexible needle steering and optimal trajectory planning for percutaneous therapies", *Proceedings of the 7th International Conference on Medical Image Computing and Computer Assisted Intervention, MICCAI 2004*, Saint-Malo, pp. 137–144, 26–30, September 2004.

[GOE 54] GOERTZ R.C., "Electronically controlled manipulator", *Neucleonics*, vol. 12, no. 11, pp. 46–47, 1954.

[GRA 93] GRACE K.W., COLGATE J.E., GLUCKSBERG M.R., *et al.,* "A six degree of freedom micromanipulator for ophthalmic surgery", *Proceedings of the IEEE International Conference on Robotics and Automation (ICRA)*, Atlanta, GA, pp. 630–635, 2–6 May 1993.

[GRE 07] GREENLEAF W.J., WOODSIDE M.T., BLOCK S.M., "High-resolution, single-molecule measurements of biomolecular motion", *Annual Review of Biophysics and Biomolecular Structure*, vol. 36, pp. 171–190, 2007.

[GRI 99] GRIFFITHS D., *Introduction to Electrodynamics*, 3rd ed., Prentice Hall, 1999.

[GRI 07] GRIER A., LOPEZ W., Apparatus and method to generate and control optical traps to manipulate small particles, US Patent No. 7161140, 2007.

[GUI 06] GUIGNET R., BERGONZELLI G., SCHLAGETER V., *et al.,* "Magnet tracking: a new tool for in vivo studies of the rat gastrointestinal motility", *Neurogastroenterology and Motility*, vol. 18, pp. 472–478, 2006.

[GUI 13] GUILFORD W.H., BLOODGOOD R.A., "Laser trap measurements of flagellar membrane motility", *Methods in Enzymology*, vol. 525, pp. 85–107, 2013.

[GUO 02] GUO S., FUKUDA T., ASAKA K., "Fish-like underwater microrobot with 3 DoF", *Proceedings of the IEEE International Conference on Robotics and Automation (ICRA)*, Washington, DC, pp. 738–743, 11–15 May 2002.

[GUO 05] GUO S., SAWAMOTO J., PAN Q., "A novel type of microrobot for biomedical application", *Proceedings of the IEEE/RSJ International Conference on Intelligent Robots and Systems (IROS)*, Edmonton, Alberta, Canada, pp. 2265–2270, 2–6 August 2005.

[HAG 05] HAGA Y., MUYARI Y., MINETA T., *et al.,* "Small diameter hydraulic active bending catheter using laser processed super elastic alloy and silicone rubber tube", *Proceedings of the 3rd Annual International IEEE-EMBS Special Topic Conference on Microtechnologies in Medicine & Biology*, Kahuku, Oahu, Hawaii, pp. 245–248, 12–15 May 2005.

[HAG 10] HAGN U., KONIETSCHKE R., TOBERGTE A., *et al.,* "DLR MiroSurge: a versatile system for research in endoscopic telesurgery", *The International Journal of Computer Assisted Radiology and Surgery*, vol. 5, no. 2, pp. 183–193, 2010.

[HAI 10] HAIDEGGER T., KAZANZIDES P., RUDAS I., *et al.,* "The importance of accuracy measurement standards for computer-integrated interventional systems", *Proceedings of the EURON GEM Sig Workshop on the Role of Experiments in Robotics Research*, *IEEE International Conference on Robotics and Automation (ICRA)*, Anchorage, AK, pp. 1–6, 3–8 May 2010.

[HAM 13] HAMADA R., TAKAYAMA H., SHONISHI Y., *et al.,* "A rapid bacteria detection technique utilizing impedance measurement combined with positive and negative dielectrophoresis", *Sensors and Actuators B*, vol. 181, pp. 439–445, 2013.

[HAN 13] HANNAFORD B., ROSEN J., FRIEDMAN D.W., *et al.,* "Raven-II: an open platform for surgical robotics research", *IEEE Transactions on Biomedical Engineering*, vol. 60, no. 4, pp. 954–959, April 2013.

[HAR 96] HARADA Y., ASAKURA T., "Radiation forces on a dielectric sphere in the Rayleigh scattering regime", *Optics Communication*, vol. 124, pp. 529–541, 1996.

[HAR 05] HARADA K., TSUBOUCHI K., FUJIE M.G., *et al.,* "Micro manipulators for intrauterine fetal surgery in an open MRI", *Proceedings of the IEEE International Conference on Robotics and Automation (ICRA)*, Barcelona, Spain, pp. 504–509, 18–22 April 2005.

[HAR 09] HARADA K., SUSILO E., MENCIASSI A, *et al.,* "Wireless reconfigurable modules for robotic endoluminal surgery", *Proceedings of the IEEE International Conference on Robotics and Automation (ICRA)*, Kobe, Japan, pp. 2699–2704, 12–17 May 2009.

[HO 12] HO M., DESAI J.P., "Towards the development of a SMA-actuated MRI-compatible tendon-driven neurosurgical robot", *Proceedings of the IEEE International Conference on Robotics and Automation (ICRA)*, Saint Paul, MN, pp. 683–688, 14–18 May 2012.

[HOC 05] HOCKSTEIN N., NOLAN J., O'MALLEY B., *et al.,* "Robot-assisted pharyngeal and laryngeal microsurgery: results of robotic cadaver dissections", *The Laryngoscope*, vol. 115, pp. 1003–1008, June 2005.

[HON 96] HONDA T., ARAI K., ISHIYAMA K., "Micro swimming mechanisms propelled by external magnetic fields", *IEEE Transactions on Magnetics*, vol. 32, no. 5, pp. 5085–5087, September 1996.

[HOS 13] HOSSAN M.R., DILLON R., ROY A.K., *et al.,* "Modeling and simulation of dielectrophoretic particle-particle interactions and assembly", *Journal of Colloid and Interface Science*, vol. 394, pp. 619–629, 2013.

[HOU 12] HOUSE D.L., LUO H., CHANG S., "Numerical study on dielectrophoretic chaining of two ellipsoidal particles", *Journal of Colloid and Interface Science*, vol. 374, pp. 141–149, 2012.

[HU 07] HU Z., WANG J., LIANG J., "Experimental measurement and analysis of the optical trapping force acting on a yeast cell with a lensed optical fiber probe", *Optics & Laser Technology*, vol. 39, pp. 475–480, 2007.

[HU 11] HU N., YANG J., QIAN S., *et al.,* "A cell electrofusion microfluidic device integrated with 3D thin-film microelectrode arrays", *Biomicrofluidics*, vol. 5, no.3, pp. 034121–034121-12, 2011. Available at: http://www.ncbi.nlm.nih.gov/pmc/articles/PMC3364834/

[HU 13] HU N., YANG J., JOO S.W., *et al.,* "Cell electrofusion in microfluidic devices: a review", *Sensors and Actuators B*, vol. 178, pp. 63–85, 2013.

[HUA 97] HUANG Y., WANG X.B., BECKER F.F., *et al.,* "Introducing dielectrophoresis as a new force field for field-flow fractionation", *Biophysical Journal*, vol. 73, no. 2, pp. 1118–1129, August 1997.

[HUN 95] HUNTER J.W., JONES L.A., SAGAR M.A., *et al.,* "Ophtalmologic microsurgical robot and associated virtual environment", *Computers in Biology & Medicine*, vol. 25, no. 2, pp. 173–182, 1995.

[HWA 10] HWANG G., HALIYO S., RÉGNIER S., "Remotely powered propulsion of helical nanobelts", *Robotics: Science and Systems VI*, Zaragoza, Spain, June 2010.

[HWA 11] HWANG G., BRAIVE R., COURAUD L., *et al.,* "Electro-osmotic propulsion of helical nanobelt swimmers", *The International Journal of Robotics Research*, vol. 30, no. 7, pp. 806–819, 2011.

[IKU 03] IKUTA K., HASEGAWA T., DAIFU S., "Hyper redundant miniature manipulator 'Hyper Finger' for remote minimally invasive surgery in deep area", *Proceedings of the IEEE International Conference on Robotics and Automation (ICRA)*, Taipei, Taiwan, pp. 1098–1102, 14–19 September 2003.

[IKU 06] IKUTA K., ICHIKAWA H., SUZUKI K., *et al.,* "Multi-degree of freedom hydraulic presure driven safety active catheter", *Proceedings of the IEEE International Conference on Robotics and Automation (ICRA)*, Orlando, FL, pp. 4161–4166, 15–19 May 2006.

[IVA 13] IVAN A., HWANG G., AGNUS J., *et al.,* "NIST and IEEE challenge for MagPieR: the fastest mobile microrobots in the world", *IEEE Robotics Automation Magazine*, vol. 20, no. 2, pp. 63–70, 2013.

[IZA 96] IZATT J.A., KULKARNI M. D., WANG H.-W., *et al.,* "Optical coherence tomography and microscopy in gastrointestinal tissues", *IEEE Journal of Selected Topics in Quantum Electronics*, vol. 2, no. 4, pp. 1017–1028, 1996.

[JAC 62] JACKSON J., *Classical Electrodynamics*, Wiley, 1962.

[JAC 09] JACOBSEN J., CHEN G., HOWELL L., *et al.,* "Lamina emergent torsional (LET) joint", *Mechanism and Machine Theory*, vol. 44, no. 11, pp. 2098–2109, 2009.

[JAG 00] JAGER E., IMMERSTRAND C., MAGNUSSON K.-E., *et al.,* "Biomedical applications of polypyrrole microactuators: from single-cell clinic to microrobots", *1st Annual International IEEE-EMBS Special Topic Conference on Microtechnologies in Medicine and Biology*, Lyon, France, pp. 58–61, 12–14 October 2000.

[JAG 05] JAGANNATH S.B, KANTSEVOY S.V, VAUGHN C.A., *et al.,* "Peroral transgastric endoscopic ligation of fallopian tubes with long-term survival in a porcine model", *Gastrointestinal Endoscopy*, vol. 61, no. 3, pp. 449–453, 2005.

[JAK 72] JAKO G., "Laser surgery of the vocal cords. An experimental study with carbon dioxide lasers on dogs", *The Laryngoscope*, vol. 82, pp. 2204–2216, 1972.

[JAK 03] JAKOPEC M., RODRIGUEZ Y BAENA F., HARRIS S.J., *et al.,* "The hands-on orthopaedic robot 'Acrobot': early clinical trials of total knee replacement surger", *IEEE Transactions on Robotics and Automation*, vol. 19, no. 5, pp. 902–911, October 2003.

[JAS 10] JASPER D., FATIKOW S., "Line scan-based high-speed position tracking inside the SEM", *International Journal of Optomechatronics*, vol. 4, no. 2, pp. 115–135, 2010.

[JEO 10] JEON S., JANG G., CHOI H., *et al.,* "Magnetic navigation system with gradient and uniform saddle coils for the wireless manipulation of micro-robots in human blood vessels", *IEEE Transactions on Magnetics*, vol. 46, no. 6, pp. 1943–1946, June 2010.

[JEO 11] JEONG S., CHOI H., CHA K., *et al.,* "Enhanced locomotive and drilling microrobot using precessional and gradient magnetic field", *Sensors and Actuators A*, vol. 171, no. 2, pp. 429–435, 2011.

[JON 89] JONAS J., *et al*., "Parapapillary retinal vessel diameter in normal and glaucoma eyes", *Investigative Ophtalmology and Visual Science*, vol. 30, no. 7, pp. 1599–1603, 1989.

[KAR 06] KARAGOZLER M.E., CHEUNG E., KWON J., *et al.,* "Miniature endoscopic capsule robot using biomimetic micro-patterned adhesives", *Proceedings of the IEEE/RAS-EMBS International Conference on Biomedical Robotics and Biomechatronics (BioRob)*, Pisa, Italy, 20–22 February 2006.

[KEL 12] KELLER H., JULOSKI A., KAWANO H., *et al.,* "Method for navigation and control of a magnetically guided capsule endoscope in the human stomach", *Proceedings of the IEEE/RAS-EMBS International Conference on Biomedical Robotics and Biomechatronics (BioRob)*, Rome, Italy, pp. 859–865, 24–27 June 2012.

[KHA 02] KHALIL W., DOMBRE E., *Modeling, Identification and Control of Robots*, Hermes Penton Science, 2002.

[KHA 09a] KHADERI S., BALTUSSEN M., ANDERSON P., *et al.,* "Nature-inspired microfluidic propulsion using magnetic actuation", *Physical Review E*, vol. 79, no. 4, pp. 046304, 2009. Available at: http://pre.aps.org/abstract/PRE/v79/i4/e046304

[KHA 09b] KHARBOUTLY M., GAUTHIER M., CHAILLET N., "Modeling the trajectory of a micro-particle in a dielectrophoresis device", *Journal of Applied Physics*, vol. 106, no. 11, pp. 114312–114312-7, December 2009. Available at: http://ieeexplore.ieee.org/xpl/login.jsp?tp=&arnumber=5353527&url=http%3A%2F%2Fieeexplore.ieee.org%2Fstamp%2Fstamp.jsp%3Ftp%3D%26arnumber%3D5353527

[KHA 10a] KHARBOUTLY M., GAUTHIER M., CHAILLET N., "Modeling the trajectory of a microparticle in a dielectrophoresis device", *Proceedings of the IEEE International Conference on Robotics and Automation (ICRA)*, Anchorage, AK, pp. 4125–4130, 3–8 May 2010.

[KHA 10b] KHARBOUTLY M., GAUTHIER M., CHAILLET N., "Predictive control of a micro bead's trajectory in a dielectrophoresis-based device", *Proceedings* of the *IEEE/RSJ International Conference on Intelligent Robots and Systems (IROS)*, Taipei, Taiwan, pp. 5616–5621, 18–22 October 2010.

[KHA 11] KHADERI S., CRAUS C., HUSSONG J., *et al.,* "Magnetically-actuated artificial cilia for microfluidic propulsion", *Lab on a Chip*, vol. 11, no. 12, pp. 2002–2010, 2011.

[KHA 13a] KHALIL I.S.M., MAGDANZ V., *et al.,* "Magnetic control of potential microrobotic drug delivery systems: nanoparticles, magnetotactic bacteria and self-propelled microjets", *Proceedings of the 35th Annual International Conference of the IEEE on Engineering in Medicine and Biology Society (EMBS)*, Osaka, Japan, pp. 5299–5302, 3–7 July 2013.

[KHA 13b] KHARBOUTLY M., GAUTHIER M., "High speed closed loop control of a dielectrophoresis based system", *Proceedings of the IEEE International Conference on Robotics and Automation (ICRA)*, Karlsruhe, Germany, pp. 1438–1443, 6–10 May 2013.

[KIM 03a] KIM B., JEONG Y., LIM H.Y., *et al.,* "Functional colonoscope robot system", *Proceedings of the IEEE International Conference on Robotics and Automation (ICRA)*, Taipei, Taiwan, pp. 1092–1097, 14–19 September 2003.

[KIM 03b] KIM B., RYU J., JEONG Y., *et al.,* "A ciliary based 8-legged walking micro robot using cast IPMC actuators", *Proceedings of the IEEE International Conference on Robotics and Automation (ICRA)*, Taipei, Taiwan, pp. 2940–2945, 14–19 September 2003.

[KIM 05] KIM B., PARK S., JEE C.Y., *et al.,* "An earthworm-like locomotive mechanism for capsule endoscopes", *Proceedings of the IEEE/RSJ International Conference on Intelligent Robots and Systems (IROS)*, Edmonton, Alberta, Canada, pp. 2997–3002, 2–6 August 2005.

[KIM 06] KIM J., YUN S., OUNAIES Z., "Discovery of cellulose as a smart material", *Macromolecules*, vol. 39, no. 12, pp. 4202–4206, 2006.

[KIM 08] KIM J., PARK J., LEE J., *et al.,* "Biohybrid microsystems actuated by cardiomyocytes: microcantilever, microrobot, and micropump", *Proceedings of the IEEE International Conference on Robotics and Automation (ICRA)*, Pasadena, CA, pp. 880–885, 19–23 May 2008.

[KIM 10] KIM J., YOON E., PARK S., "Biohybrid walking microrobot with welf-assembled cardiomyocytes", *Climbing and Walking Robots*, Chapter 21, MIRIPOUR B., (ed.), pp. 351–369, 2010.

[KOD 13] KODAMA T., OSASAKI T., KAWANO R., *et al.,* "Round-tip dielectrophoresis-based tweezers for single micro-object manipulation", *Biosensors and Bioelectronics*, vol. 47, pp. 206–212, 2013

[KÓS 05] KÓSA G., SHOHAM M., ZAAROOR M., "Propulsion of a swimming micro medical robot", *Proceedings of the IEEE International Conference on Robotics and Automation (ICRA)*, Barcelona, Spain, pp. 1327–1331, 18–22 April 2005.

[KÓS 08] KÓSA G., JAKAB P., JOLÉSZ F., *et al.,* "Swimming capsule endoscope using static and RF magnetic field of MRI for propulsion", *Proceedings of the IEEE International Conference on Robotics and Automation (ICRA)*, Pasadena, CA, 19–23 May 2008.

[KRA 09] KRATOCHVIL B., FRUTIGER D., VOLLMERS K., *et al.,* "Visual servoing and characterization of resonant magnetic actuators for decoupled locomotion of multiple untethered mobile microrobots", *Proceedings of the IEEE International Conference on Robotics and Automation (ICRA)*, Kobe, Japan, pp. 1010–1015, 12–17 May 2009.

[KUM 10] KUMMER M., ABBOTT J., KRATOCHVIL B., *et al.,* "OctoMag: an electromagnetic system for 5-DOF wireless micromanipulation", *IEEE Transactions on Robotics*, vol. 26, no. 6, pp. 1006–1017, September 2010.

[LAF 13a] LAFITTE N., HADDAB Y., LE GORREC Y., *et al.,* "Active control of silicon nanotweezers detects enzymatic reaction at the molecular level", *Proceedings of the IEEE 17th International Conference on Transducers & Eurosensors*, Barcelona, Spain, pp. 2357–2360, 16–20 June 2013.

[LAF 13b] LAFRATTA C.N., "Optical tweezers for medical diagnostics", *Analytical and Bioanalytical Chemistry*, vol. 405, no. 17, pp. 5671–5677, 2013.

[LAL 10] LALANDE V., GOSSELIN F., MARTEL S., "Catheter steering using a magnetic resonance imaging system", *Proceedings of the Annual International Conference of the IEEE on Engineering in Medicine and Biology Society (EMBC)*, pp. 1874–1877, 2010.

[LAM 10] LAMBERT P., Surface Tension Effects in Microrobotics, Habilitation work toward the supervision of doctoral candidates, University of Franche-Comté, 2010.

[LAN 03] LANG M.J., BLOCK S.M., "Resource letter: LBOT-1: laser-based optical tweezers", *American Journal of Physics*, vol. 71, pp. 201–215, 2003.

[LAT 09] LATT W.T., TAN U.X., SHEE C.Y., *et al.,* "Compact sensing design of a handheld active tremor compensation instrument", *IEEE Sensors Journal*, vol. 9, no. 12, pp. 1864–1871, 2009.

[LAU 09] LAUGA E., POWERS T., "The hydrodynamics of swimming microorganisms", *Reports on Progress in Physics*, vol. 72, pp. 096601, 2009. Available at: http://iopscience.iop.org/0034-4885/72/9/096601/pdf/0034-4885_72_9_096601.pdf

[LAW 93] LAWRENCE D.A., "Stability and transparency in bilateral teleoperation", *IEEE Transactions on Robotics and Automation*, vol. 9, no. 5, pp. 624–637, 1993.

[LEE 04] LEE Y.P., KIM B., LEE B.G., *et al.,* "Locomotive mechanism design and fabrication of biomimetic micro robot using shape memory alloy", *Proceedings of the IEEE International Conference on Robotics and Automation (ICRA)*, New Orleans, LA, pp. 5007–5012, 26 April–1 May 2004.

[LEH 08] LEHMAN A.C., WOOD N.A., DUMPERT J., *et al.,* "Robotic natural orifice translumenal endoscopic surgery", *Proceedings of the IEEE International Conference on Robotics and Automation (ICRA),* Pasadena, CA, pp. 2969–2974, 19–23 May 2008.

[LEN 02] LENDLEIN A., KELCH S., "Shape-memory polymers", *Angewandte Chemie International Edition*, vol. 41, no. 12, pp. 2034–2057, 2002.

[LI 06] LI W.D., GUO W., LI M.T., *et al.,* "Design and test of a capsule type endoscope robot with novel locomation principle", *Proceedings of the 9th International Conference on Control, Automation, Robotics and Vision (ICARCV)*, Singapore, pp. 373–378, 5–8 December 2006.

[LI 13a] LI R., REN K.F., HAN X., *et al.,* "Analysis of radiation pressure force exerted on a biological cell induced by high-order Bessel beams using Debye series", *Journal of Quantitative Spectroscopy & Radiative Transfer*, vol. 126, pp. 69–77, 2013.

[LI 13b] LI X., CHEAH C.C., HU S., *et al.,* "Dynamic trapping and manipulation of biological cells with optical tweezers", *Automatica*, vol. 49, pp. 1614–1625, 2013.

[LIA 08] LIAW H.C., SHIRINZADEH B., "Enhanced adaptive motion tracking control of piezo-actuated flexure-based four-bar mechanisms for micro/nano manipulation", *Sensors and Actuators A*, vol. 147, no. 1, pp. 254–262, 2008.

[LIA 13] LIANG W., LIU N., DONG Z., *et al.,* "Simultaneous separation and concentration of micro-and nano-particles by optically induced electrokinetics", *Sensors and Actuators A*, vol. 193, pp. 103–111, 2013.

[LIO 12] LIONÁIRD C.Ó., WALSH S.P., BARRY L., *et al.,* "An optimized electromagnetic system for endoscopic capsule propulsion: report on a benchtop feasibility study", *24th International Conference of the Society for Medical Innovation and Technology (SMIT)*, Barcelona, Spain, 20–22 September 2012.

[LIU 07] LIU C., QIN H., MATHER P.T., "Review of progress in shape-memory polymers", *Journal of Materials Chemistry*, vol. 17, pp. 1543–1558, 2007.

[LIU 13] LIU R., MAO Z., MATTHEWS D. L., *et al.,* "Novel single-cell functional analysis of red blood cells using laser tweezers: Raman spectroscopy: application for sickle cell disease", *Experimental Hematology*, vol. 41, no. 7, pp. 656–661, 2013.

[LOC 10] LOCK J., LAING G., MAHVASH M., *et al.,* "Quasistatic modeling of concentric tube robots with external loads", *Proceedings of the IEEE/RSJ International Conference on Intelligent Robots and Systems (IROS)*, Taipei, Taiwan, pp. 2325–2332, 18–22 October 2010.

[LOW 06] LOW S.C., TANG S.W., THANT Z.M., *et al.,* "Master-slave robotic system for therapeutic gastrointestial endoscopic procedure", *Proceedings of the Annual International Conference of the IEEE on Engineering in Medicine and Biology Society (EMBS)*, New York, pp. 3850–3853, 30 August–3 September 2006.

[LUP 12] LUPAN O., CHOW L., PAUPORTE T., *et al.,* "Highly sensitive and selective hydrogen single-nanowire nanosensor", *Sensors and Actuators B*, vol. 173, pp. 772–780, 2012.

[LYO 10] LYONS L., WEBSTER III R.J., ALTEROVITZ R., "Planning active cannula configurations through tubular anatomy", *Proceedings of the IEEE International Conference on Robotics and Automation (ICRA)*, Anchorage, AK, pp. 2082–2086, 3–8 May 2010.

[MAC 12] MACLACHLAN R.A., BECKER B.C., TABARÉS J.C., *et al.,* "Micron: an actively stabilized handheld tool for microsurgery", *IEEE Transactions on Robotics*, vol. 28, no. 1, pp. 195–212, 2012.

[MAE 10] MAEDA S., HARA Y., YOSHIDA R., *et al.,* "Active polymer gel actuators", *International Journal of Molecular Sciences*, vol. 11, no. 1, pp. 52–66, 2010.

[MAH 11a] MAHONEY A., ABBOTT J., "Managing magnetic force applied to a magnetic device by a rotating dipole field", *Applied Physics Letters*, vol. 99, no. 13, pp. 134103-1–134103-3, 2011. Available at: http://www.telerobotics.utah.edu/uploads/Main/Mahoney_APL11.pdf

[MAH 11b] MAHONEY A., SARRAZIN J., BAMBERG E., *et al.,* "Velocity control with gravity compensation for magnetic helical microswimmers", *Advanced Robotics*, vol. 25, pp. 1007–1028, 2011.

[MAH 12] MAHONEY A., COWAN D., MILLER K., *et al.,* "Control of untethered magnetically actuated tools using a rotating permanent magnet in any position", *Proceedings of the IEEE International Conference on Robotics and Automation (ICRA)*, Saint Paul, MN, pp. 3375–3380, 14–18 May 2012.

[MAN 95] MANKINS J.C., Technology readiness levels, a white paper, NASA, 6 April 1995. Available at http://orion.asu.edu/Additional Reading/Mankins_trl.pdf.

[MAR 01] MARESCAUX J., LEROY J., GAGNER M., *et al.,* "Tansatlantic robot assisted-telesurgery", *Nature*, vol. 413, pp. 379–380, 2001.

[MAR 06] MARTEL S., TREMBLAY C.C., NGAKENG S., *et al.,* "Controlled manipulation and actuation of micro-objects with magnetotactic bacteria", *Applied Physics Letters*, vol. 89, no. 23, pp. 233904–1-233904-3, 2006. Available at: http://scitation.aip.org/docserver/fulltext/aip/journal/apl/89/23/1.2402221.pdf?expires=1387535133&id=id&accname=freeContent&checksum=C5B9EA09465D1AE40A1DA1C01E77B114

[MAR 07a] MARESCAUX J., DALLEMAGNE B., PERRETTA S., *et al.,* "Surgery without scars: report of transluminal cholecystectomy in a human being", *Archives of Surgery*, vol. 142, no. 9, pp. 823–826, 2007.

[MAR 07b] MARTEL S., MATHIEU J.-B., FELFOUL O., *et al.,* "Automatic navigation of an untethered device in the artery of a living animal using a conventional clinical magnetic resonance imaging system", *Applied Physics Letters*, vol. 90, no. 11, pp. 114105–1-114104-3, 2007. Available at: http://scitation.aip.org/docserver/fulltext/aip/journal/apl/90/11/1.2713229.pdf?expires=1387535335&id=id&accname=freeContent&checksum=C6BFF4A5A7CFDBE0CF82A75F92CBB9B7

[MAR 09a] MARTEL S., FELFOUL O., MATHIEU J.-B., *et al.,* "MRI-based medical nanorobotic platform for the control of magnetic nanoparticles and flagellated bacteria for target interventions in human capillaries", *The International Journal of Robotics Research*, vol. 28, no. 9, pp. 1169–1182, 2009.

[MAR 09b] MARTEL S., MOHAMMADI M., FELFOUL O., *et al.,* "Flagellated magnetotactic bacteria as controlled MRI-trackable propulsion and steering systems for medical nanorobots operating in the human microvasculature", *The International Journal of Robotics Research*, vol. 28, no. 4, pp. 571–582, 2009.

[MAR 10] MARUYAMA H., IITSUKA R., ONDA K., *et al.,* "Massive parallel assembly of microbeads for fabrication of bicrotools having spherical structure and powerful laser manipulation", *Proceedings of the IEEE International Conference on Robotics and Automation (ICRA)*, Anchorage, AK, pp. 482–487, 3–8 May 2010.

[MAR 11] MARUYAMA H., INOUE N., MASUDA T., *et al.,* "Selective injection and laser manipulation of nanotool inside a specific cell using optical pH regulation and optical tweezers", *Proceedings of the IEEE International Conference on Robotics and Automation (ICRA)*, Shanghai, China, pp. 2674–2679, 9–13 May 2011.

[MAR 13a] MARTEL S., "Microrobotics in the vascular network: present status and next challenges", *Journal of Micro-Bio Robotics*, vol. 8, no. 1, pp. 41–52, 2013.

[MAR 13b] MARTINEZ-DUARTE R., CAMACHO-ALANIS F., RENAUD P., *et al.,* "Dielectrophoresis of lambda-DNA using 3D carbon electrodes", *Electrophoresis*, vol. 34, no. 7, pp. 1113–1122, 2013.

[MAT 13] MATTOS L., ANDREFF N., "The µRALP project: new technologies and systems for robot -assisted laser phonomicrosurgery", *3rd Joint Workshop on New Technologies for Computer/Robot Assisted Surgery*, Verona, Italy, 11–13 September 2013.

[MAX 73] MAXWELL J.C., *A Treatise on Electricity and Magnetism*, Clarendon Press, Oxford, 1873.

[MEB 10] MEBARKI R., KRUPA A., CHAUMETTE F., "2D ultrasound probe complete guidance by visual servoing using image moments", *IEEE Transactions on Robotics*, vol. 26, no. 2, pp. 296–306, 2010.

[MEJ 09] MEJEAN C.O., SCHAEFER A.W., MILLMAN E.A., *et al.,* "Multiplexed force measurements on live cells with holographic optical tweezers", *Optics Express*, vol. 17, pp. 6209–6217, 2009.

[MEN 01] MENCIASSI A., ARENA A., PHEE L., *et al.,* "Locomotion issues and mechanisms for microrobots in the gastrointestinal tract", *Proceedings of the 32nd International Symposium on Robotics (ISR)*, Seoul, Korea, pp. 428–432, April 2001.

[MEN 03] MENCIASSI A., EISINBERG A., CARROZZA M.C., *et al.,* "Force sensing microinstrument for measuring tissue properties and pulse in microsurgery", *IEEE/ASME Transactions on Mechatronics*, vol. 8, no. 1, pp. 10–17, March 2003.

[MEN 04] MENCIASSI A., STEFANINI C., GORINI S., *et al.,* "Legged locomotion in the gastrointestinal tract", *Proceedings of the IEEE/RSJ International Conference on Intelligent Robots and Systems (IROS)*, Sendai, Japan, pp. 937–942, 28 September–2 October 2004.

[MER 07] MERLET J.-P., "Jacobian, manipulability, condition number and accuracy of parallel robots", in THRUN S., BROOKS R., DURRANT-WHYTE H. (eds), *Robotics Research*, *Springer Tracts in Advanced Robotics*, vol. 28, Springer, Berlin/Heidelberg, Germany pp. 175–184, 2007.

[MER 10] MERNIER G., PIACENTINI N., BRASCHLER T., *et al.,* "Continuous-flow electrical lysis device with integrated control by dielectrophoretic cell sorting", *Lab on Chip*, vol. 10, pp. 2077–2082, 2010.

[MER 12] MERNIER G., MAJOCCHI S., MERMOD N., *et al.,* "In situ evaluation of single-cell lysis by cytosol extraction observation through fluorescence decay and dielectrophoretic trapping time", *Sensors and Actuators B*, vol. 166–167, pp. 907–912, 2012.

[MIL 12] MILLER K.M., MAHONEY A.W., SCHMID T., *et al.,* "Proprioceptive magnetic-field sensing for closed-loop control of magnetic capsule endoscopes", *Proceedings* of the *IEEE/RSJ International Conference on Intelligent Robots and Systems (IROS)*, Vilamoura, Algarve, Portugal, pp. 1994–1999, 7–12 October 2012.

[MIN 07] MINHAS D., ENGH J., FENSKE M., *et al.,* "Modeling of needle steering via duty-cycled spinning", *Proceedings of the Annual International Conference of the IEEE on Engineering in Medicine and Biology Society (EMBS)*, Lyon, France, pp. 2756–2759, 23–26 August 2007.

[MOG 07] MOGLIA A., MENCIASSI A., SCHURR M.O., *et al.,* "Wireless capsule endoscopy: from diagnostic devices to multipurpose robotic systems", *Biomedical Microdevices*, vol. 9, no. 2, pp. 235–243, 2007.

[MOR 08] MORIN P., SAMSON C., "Motion control of wheeled mobile robots", in SICILIANO B., KHATIB O., (eds.), Springer Verlag, pp. 799–826, 2008.

[MOR 12a] MOREIRA P., LIU C., ZEMITI N., *et al.,* "Soft tissue force control using active observers and viscoelastic interaction model", *Proceedings of the IEEE International Conference on Robotics and Automation (ICRA)*, Saint Paul, MN, pp. 4660–4666, 14–18 May 2012.

[MOR 12b] MOREL G., SZEWCZYK J., VITRANI M.-A., "Comanipulation", in TROCCAZ J. (ed.), *Medical Robotics*, ISTE, London, John Wiley & Sons, New York, 2012.

[MUL 12] MULLER L., SAEED M., WILSON M., HETTS S., "Remote control catheter navigation: options for guidance under MRI", *Journal of Cardiovascular Magnetic Resonance*, vol. 14, no. 1, 2012. Available at: http://www.ncbi.nlm.nih.gov/pmc/articles/PMC3461467/

[NAG 07] NAGY Z., ABBOTT J.J., NELSON B., "The magnetic self-aligning hermaphroditic connector: a scalable approach for modular microrobots", *Proceedings of the IEEE/ASME International Conference on Advanced Intelligent Mechatronics (AIM)*, 2007.

[NAG 08] NAGY Z., OUNG R., ABBOTT J.J., *et al.,* "Experimental investigation of magnetic self-assembly for swallowable modular robots", *Proceedings of the IEEE/RSJ International Conference on Intelligent Robots and Systems (IROS)*, Nice, France, pp. 1915–1920, 22–26 September 2008.

[NAJ 04] NAJAFI A., GOLESTANIAN R., "Simple swimmer at low Reynolds numbers: three linked spheres", *Physical Review E*, vol. 69, pp. 062901–1-062901-4, 2004. Available at: http://pre.aps.org/abstract/PRE/v69/i6/e062901

[NAM 04] NAMBIAR R., GAJRAJ A., MEINERS J.-C., "All-optical constant-force laser tweezers", *Biophysical Journal*, vol. 87, pp. 1972–1980, 2004.

[NAS 08] NASCIMENTO E. M., NOGUEIRA N., SILVA T., *et al.,* "Dielectrophoretic sorting on a microfabricated flow cytometer: label free separation of Babesia bovis infected erythrocytes", *Bioelectrochemistry*, vol. 73, pp.123–128, 2008.

[NEP 09] NEPPALLI S., CSENCSITS M.A., JONES B.A., *et al.,* "Closed-form inverse kinematics for continuum manipulators", *Advanced Robotics*, vol. 23, pp. 2077–2091, 2009.

[NET 09] NETO M.G., RAMOS A., CAMPOS J., "Single port laparoscopic access surgery", *Techniques in Gastrointestinal Endoscopy*, vol. 11, pp. 84–93, 2009.

[NG 00] NG W.S., PHEE S.J., SEOW C., *et al.,* "Development of a robotic colonoscope", *Digestive Endoscopy*, vol. 12, pp. 131–135, 2000.

[NGU 10] NGUYEN B., MERINO J., GANG E., "Remote navigation for ablation procedures", *European Cardiology*, vol. 6, no. 3, pp. 50–56, 2010.

[NI 12a] NI Z., BOLOPION A., AGNUS J., BENOSMAN R., *et al.,* "Stable haptic feedback based on a dynamic vision sensor for microrobotics", *Proceedings of the IEEE/RSJ International Conference on Intelligent Robots and Systems (IROS)*, Vilamoura, Algarve, Portugal, pp. 3203–3208, 7–12 October 2012.

[NI 12b] NI Z., BOLOPION A., AGNUS J., BENOSMAN R., *et al.,* "Asynchronous event-based visual shape tracking for stable haptic feedback in microrobotics", *IEEE Transactions on Robotics*, vol. 28, no. 5, pp. 1081–1089, 2012.

[NI 13] NI Z., PACORET C., BENOSMAN R., RÉGNIER S., "2D high speed force feedback teleoperation of optical tweezers", *Proceedings of the IEEE International Conference on Robotics and Automation (ICRA)*, Karlsruhe, Germany, pp. 1692–1697, 6–10 May 2013.

[OHS 08] OHSHIMA R., TAKAYAMA T., OMATA T., *et al.,* "Assemblable three fingered five-DoF hand for laparoscopic surgery", *Proceedings of the IEEE International Conference on Robotics and Automation (ICRA)*, Pasadena, CA, pp. 3896–3901, 19–23 May 2008.

[OLE 05] OLEYNIKOV D., RENTSCHLER M., HADZIALIC A., *et al.,* "Miniature robots can assist in laparoscopic cholecystectomy", *Surgical Endoscopy*, vol. 19, pp. 473–476, 2005.

[OND 12] ONDA K., ARAI F., "Parallel teleoperation of holographic optical tweezers using multi-touch user interface", *Proceedings of the IEEE International Conference on Robotics and Automation (ICRA)*, Saint Paul, MN, pp. 1069–1074, 14–18 May 2012.

[ORT 02] ORTMAIER T.J., Motion compensation in minimally invasive robotic surgery, PhD Thesis, University of Munich, 2002.

[OTA 06] OTA T., PATRONIK N.A., ZENATI M.A., *et al.,* "Percutaneous subxiphoid access to epicardium using a miniature crawling robotic device", *Innovations*, vol. 1, no. 5, pp. 227–231, 2006.

[OTA 08] OTA T., DEGANI A., SCHWARTZMAN D., *et al.,* "A novel highly articulated robotic surgical system for epicardial ablation", *Proceedings of the Annual International Conference of the IEEE on Engineering in Medicine and Biology Society (EMBS)*, Vancouver, Canada, pp. 250–253, 20–24 August 2008.

[PAN 01] PAN Y., XIE H., FEDDER G.K., "Endoscopic optical coherence tomography based on a microelectromechanical mirror", *Optics Letters*, vol. 26, no. 24, pp. 1966–1968, 2001.

[PAR 05] PARK P.O., BERGSTRÖM M., IKEDA K., *et al.,* "Experimental studies of transgastric gallbladder surgery: cholecystectomy and cholecystogastric anastomosis", *Gastrointestinal Endoscopy*, vol. 61, no. 4, pp. 601–606, 2005.

[PAR 06] PARK S., PARK H., PARK S., *et al.,* "Capsular locomotive microrobot for gastrointestinal tract", *Proceedings of the Annual International Conference of the IEEE on Engineering in Medicine and Biology Society (EMBS)*, New York, pp. 2211–2214, 30 August–3 September 2006.

[PAT 05] PATRONIK N.A., ZENATI M.A., RIVIERE C.N., "Preliminary evaluation of a mobile robotic device for navigation and intervention on the beating heart", *Computer Aided Surgery*, vol. 10, no. 4, pp. 225–232, July 2005.

[PAT 12a] PATEL S., RAJADHYAKSHA M., KIROV S., *et al.,* "Endoscopic laser scalpel for head and neck cancer surgery", *Proceedings SPIE*, *Photonic Therapeutics and Diagnostics VIII*, 82071S, 3 February 2012. Available at: http://proceedings.spiedigitallibrary.org/proceeding.aspx?articleid=1310590

[PAT 12b] PATHANGI H., GROESENEKEN G., WITVROUW A., "Dielectrophoretic assembly of suspended single-walled carbon nanotubes", *Microelectronic Engineering*, vol. 98, pp. 218–221, 2012.

[PAW 09] PAWASHE C., FLOYD S., SITTI M., "Multiple magnetic microrobot control using electrostatic anchoring", *Applied Physics Letters*, vol. 94, no. 16, pp. 164108–1-164108-3, 2009. Available at: http://scitation.aip.org/docserver/fulltext/aip/journal/apl/94/16/1.3123231.pdf?expires=1387538192&id=id&accname=freeContent&checksum=3985B3A8C87AD1782110F44B1E93F1E1

[PEI 01] PEIRS J., REYNAERTS D., VAN BRUSSEL H., "A miniature manipulator for integration in a self-propelling endoscope", *Sensors and Actuators A*, vol. 92, pp. 343–349, 2001.

[PEI 03] PEIRS J., REYNAERTS D., VAN BRUSSEL H., *et al.,* "Design of an advanced tool guiding system for robotic surgery", *Proceedings of the IEEE International Conference on Robotics and Automation (ICRA)*, Taipei, Taiwan, pp. 2651–2656, 14–19 September 2003.

[PEI 04] PEIRS J., CLIJNEN J., REYNAERT D., *et al.,* "A micro optical force sensor for force feedback during minimally invasive robotic surgery", *Sensors and Actuators A*, vol. 115, pp. 447–455, 2004.

[PIC 10] PICCIGALLO M., SCARFOGLIERO U., QUAGLIA C., *et al.,* "Design of a novel bimanual robotic system for single-port laparoscopy", *IEEE/ASME Transactions on Mechatronics*, vol. 15, no. 6, pp. 871–878, 2010.

[PIE 09] PIERALLI C., ATTOUI C., BOIREAU W., *et al.,* "Low cost optical detection of DNA hybridization on biochips", *Laser Physics*, vol. 19, no. 2, pp. 259–264, 2009.

[PIL 11] PILAREK M., NEUBAUER P., MARX U., "Biological cardio-micro-pumps for microbioreactors and analytical micro-systems", *Sensors and Actuators B*, vol. 156, no. 2, pp. 517–526, 2011.

[PIS 99] PISKUN G, RAJPAL S., "Transumbilical laparoscopic cholecystectomy utilizes no incisions outside the umbilicus", *Journal of Laparoendoscopic & Advanced Surgical Techniques*, vol. 9, no. 4, pp. 361–364, 1999.

[PLA 08] PLATT S.R., HAWKS J.A., RENTSCHLER M.E., *et al.,* "Modular wireless wheeled *in vivo* surgical robot", *Proceedings of the ASME International Design Engineering Technical Conference & Computers and Information in Engineering Conference, IDETC/CIE*, New York, 3–6 August 2008.

[PLE 02] PLEWA J., DELSOL T., LANCELOT R., *et al.,* "Prospects for holographic optical tweezers", *Proceedings of the NATO Science Program on Toxicogenomics and Proteomics*, pp. 181–201, 2002.

[POH 78] POHL H.A., *Dielectrophoresis*, Cambridge University Press, 1978.

[POI 12] POIGNET P., BAYLE B., "Interaction modeling and force control", in TROCCAZ J. (ed.), *Medical Robotics*, ISTE, London, John Wiley & Sons, New York, 2012.

[PON 05] PONS J.L., *Emerging Actuator Technologies – A Micromechatronic Approach*, Wiley, 2005.

[POP 13] POPECK K., MAHONEY A., ABBOTT J., "Localization method for a magnetic capsule endoscope propelled by a rotating magnetic dipole field", *Proceedings of the IEEE International Conference on Robotics and Automation (ICRA)*, Karlsruhe, Germany, pp. 3559–3564, 6–10 May 2013.

[PRA 13] PRAKASH R., KALER K., "Liquid dielectrophoresis dispensing of vesicles for on-chip nucleic acid isolation and detection", *Colloids and Surfaces A: Physicochemical and Engineering Aspects*, vol. 432, pp. 42–49, 2013.

[PUR 77] PURCELL E., "Life at low Reynolds number", *American Journal of Physics*, vol. 45, no. 1, pp. 3–11, 1977.

[PUR 97] PURCELL E., "The efficiency of propulsion by a rotating flagellum", *Proceedings of the National Academy of Sciences of the United States of America*, vol. 94, no. 21, pp. 11307–11311, 1997.

[QUI 07] QUIRINI M., WEBSTER III R.J., MENCIASSI A., *et al.,* "Design of a pill-sized 12-legged endoscopic capsule robot", *Proceedings of the IEEE International Conference on Robotics and Automation (ICRA)*, Rome, Italy, pp. 1856–1862, 10–14 April 2007.

[RAK 08] RAKOTONDRABE M., HADDAB Y., LUTZ P., "Voltage/frequency proportional control of stick-slip Microsystems", *IEEE Transactions on Control Systems Technology*, vol. 16, no. 6, pp. 1316–1322, 2008.

[REM 12] REMACLE M., RICCI-MACCARINI A., MATAR N., *et al.,* "Reliability and efficacy of a new CO_2 laser hollow fiber: a prospective study of 39 patients", *European Archives of Otorhinolaryngology*, vol. 269 no. 3, pp. 917–21, March 2012.

[REN 06] RENTSCHLER M.E., DUMPERT J., PLATT S.R., *et al.,* "Mobile in vivo biopsy robot", *Proceedings of the IEEE International Conference on Robotics and Automation (ICRA)*, Orlando, FL, pp. 4155–4160, 15–19 May 2006.

[REN 12] RENTSCHLER M.E., SLIKER L.J., TERRY B.S., *et al.,* Robotic capsule endoscope for minimally invasive surgical procedures, micro-patterned treads for friction enhancement of a robotic capsule endoscope in a biological environment, and process for fabrication of micro-treads, US Patent App. 13/692,743, 2012.

[REY 83] REYNOLDS O., "An experimental investigation of the circumstances which determine whether the motion of water shall be direct or sinuous, and of the law of resistance in parallel channels", *Philosophical Transactions of the Royal Society*, vol. 174, pp. 935–982, 1883.

[REY 10] REY J.F., OGATA H., HOSOE N., *et al.,* "Feasibility of stomach exploration with a guided capsule endoscope", *Endoscopy*, vol. 42, pp. 541–545, 2010.

[RIC 10] RICHA R., POIGNET P., LIU C., "3D motion tracking for beating heart surgery", *International Journal Robotics Research*, vol. 29, nos. 2–3, pp. 218–230, 2010.

[RIV 03] RIVIERE C.N., ANG W.T., KHOSLA P.K., "Toward active tremor canceling in handheld microsurgical instruments", *IEEE Transactions on Robotics and Automation*, vol. 19, no. 5, pp. 793–800, 2003.

[RIV 12] RIVERA-SERRANO C., JOHNSON P., ZUBIATE B., *et al.,* "A transoral highly flexible robot: novel technology and application", *The Laryngoscope*, vol. 122, pp. 1067–1071, 2012.

[ROB 02] ROBERTS T., HASSENZAHL W., HETTS S., *et al.,* "Remote control of catheter tip deflection: an opportunity for interventional MRI", *Magnetic Resonance in Medicine*, vol. 48, no. 6, pp. 1091–1095, 2002.

[RÖS 09] RÖSE A., WOHLLEBER C., KASSNER S., *et al.,* "A novel piezoelectric driven laparoscopic instrument with multiple degree of freedom parallel kinematic structure", *Proceedings of the IEEE/RSJ International Conference on Intelligent Robots and Systems (IROS)*, St. Louis, MO, pp. 2162–2167, 11–15 October 2009.

[ROS 11] ROSA B., HERMAN B., SZEWCZYK J., *et al.,* "Laparoscopic optical biopsies: in vivo robotized mosaicing with probe-based confocal endomicroscopy", *Proceedings of the IEEE/RSJ International Conference on Intelligent Robots and Systems (IROS)*, San Francisco, CA, pp. 1339–1345, 25–30 September 2011.

[RUB 12] RUBBERT L., Conception de mécanismes compliants pour la robotique chirurgicale, PhD Thesis, Strasbourg University, France, 2012.

[RUC 10] RUCKER D.C., JONES B.A., WEBSTER III R.J., "A geometrically exact model for externally loaded concentric-tube continuum robots", *IEEE Transactions on Robotics*, vol. 26, no. 5, pp. 769–780, 2010

[SAL 04] SALLE D., Conception optimale d'instruments robotisés à haute mobilité pour la chirurgie mini-invasive, PhD Thesis, Pierre and Marie Curie University, Paris, France, 2004.

[SAL 12] SALERNO M., CIUTI G., LUCARINI G., *et al.,* "A discrete-time localization method for capsule endoscopy based on on-board magnetic sensing", *Measurement Science and Technology*, vol. 23, no. 1, pp. 015701, 2012. Available at: http://iopscience.iop.org/0957-0233/23/1/015701/article

[SAM 91] SAMSON C., LE BORGNE M., ESPIAU B., *Robot Control: the Task Function Approach*, Clarendron Press, Oxford University Press, Oxford, UK, 1991.

[SAN 11] SANCHEZ L.A., PETRONI G., PICCIGALLO M., *et al.,* "Real-time control and evaluation of a teleoperated miniature arm for single port laparoscopy", *Proceedings of the Annual International Conference of the IEEE on Engineering in Medicine and Biology Society (EMBS)*, Boston, MA, pp. 7049–7053, 30 August–3 September 2011.

[SAN 12a] SANCHEZ L., LE M.Q., LIU C., *et al.,* "The impact of interaction model on stability and transparency in bilateral teleoperation for medical applications", *Proceedings of the IEEE International Conference on Robotics and Automation (ICRA)*, Saint Paul, MN, pp. 1607–1613, 14–18 May 2012.

[SAN 12b] SANTOS-CARRERAS L., Increasing haptic fidelity and ergonomics in teleoperated surgery, PhD Thesis, Ecole Polytechnique Fédérale de Lausanne (EPFL), Switzerland, 2012.

[SAN 13a] SANCHEZ L., Control of meso-robots for endoluminal surgery, PhD Thesis, University of Montpellier 2, France, August 2013.

[SAN 13b] SANCHEZ L., LE M., RABENOROSOA K., *et al.,* "A case study of safety in the design of surgical robots: the ARAKNES platform", in LEE S., CHO H., YOON K.-J., LEE J. (eds), *Intelligent Autonomous Systems 12*, vol. 194 of *Advances in Intelligent Systems and Computing*, Springer, pp. 121–130, 2013.

[SAS 91] SASAKI K., KOSHIO M., MISAWA H., *et al.,* "Pattern formation and flow control pattern formation and flow control of fine particles by laser-scanning micromanipulation", *Optics Letters*, vol. 16, pp. 1463–65, 1991.

[SAU 08] SAUVÉE M., POIGNET P., DOMBRE E., "Ultrasound image-based visual servoing of a surgical instrument through nonlinear model predictive control", *The International Journal of Robotics Research*, vol. 27, no. 1, pp. 25–40, 2008.

[SCO 05] SCORRETTI R., BURAIS N., NICOLAS L., *et al.,* "Modeling of induced current into the human body by low-frequency magnetic field from experimental data", *IEEE Transactions on Magnetics*, vol. 41, no. 5, pp. 1992–1995, 2005.

[SEA 06] SEARS P., DUPONT P., "A steerable needle technology using curved concentric tubes", *Proceedings of the IEEE/RSJ International Conference on Intelligent Robots and Systems (IROS)*, Beijing, China, pp. 2850–2856, 9–15 October 2006.

[SEA 07] SEARS P., DUPONT, P.E., "Inverse kinematics of concentric tube steerable needles", *Proceedings of the IEEE International Conference on Robotics and Automation (ICRA)*, Rome, Italy, pp. 1887–1892, 10–14 April 2007.

[SEI 05] SEIBOLD U., KÜBLER B., HIRZINGER G., "Prototype of instrument for minimally iInvasive surgery with 6-axis force sensing capability", *Proceedings of the IEEE International Conference on Robotics and Automation (ICRA)*, Barcelona, Spain, pp. 498–503, 18–22 April 2005.

[SEN 03] SENDOH M., ISHIYAMA K., ARAI K., "Fabrication of magnetic actuator for use in a capsule endoscope", *IEEE Transactions on Magnetics*, vol. 39, no. 5, pp. 3232–3234, 2003.

[SIM 05] SIMAAN N., "Snake-like units using flexible backbones and actuation redundancy for enhanced miniaturization", *Proceedings of the IEEE International Conference on Robotics and Automation (ICRA)*, Barcelona, Spain, pp. 3023–3028, 18–22 April 2005.

[SOL 07] SOLARES C., STROME M., "Transoral robot-assisted CO2 laser supraglottic laryngectomy: experimental and clinical data", *The Laryngoscope*, vol. 117, no. 5, pp. 817–20, 2007.

[STO 51] STOKES G., "On the effect of the internal friction of fluids on the motion of pendulums", *Transactions of the Cambridge Philosophical Society*, vol. 9, pp. 8–106, 1851.

[SU 12] SU H., CARDONA C., SHANG W., CAMILO A., *et al.,* "A MRI-guided concentric tube continuum robot with piezoelectric actuation: a feasibility study", *Proceedings of the IEEE International Conference on Robotics and Automation (ICRA)*, Saint Paul, MN, pp. 1939–1945, 14–18 May 2012.

[SUN 04] SUN Y.L., LUO Z.P., FERTALA A., *et al.,* "Stretching type II collagen with optical tweezers", *Journal of Biomechanics*, vol. 37, pp. 1665–1669, 2004.

[SUN 10] SUN J., GUO S., WU L., *et al.,* "3D in vivo optical coherence tomography based on a low-voltage, large-scan-range 2D MEMS mirror", *Optics Express*, vol. 18, no. 12, pp. 12065–12075, June 2010.

[SWA 07] SWAIN P.A., "Justification for NOTES – Natural Orifice Transluminal Endosurgery", *Gastrointestinal Endoscopy*, vol. 65, no. 3, pp. 514–516, 2007.

[SZE 11] SZEWCZYK J., MARCHANDISE E., FLAUD P., *et al.,* "Active catheters for neuroradiology", *Journal of Robotics and Mechatronics*, vol. 23, no. 1, pp. 105–115, 2011.

[TAK 01] TAKEMURA K., HARAD D., MANEO T., "Development of a master slave system for active endoscope using a multi-DoF ultrasonic motor", *Proceedings of the 32nd International Symposium on Robotics (ISR)*, Seoul, Korea, pp. 499–504, April 2001.

[TAK 07] TAKAYAMA T., OMATA T., FUTAMI T., *et al.,* "Detachable-fingered hands for manipulation of large internal organs in laparoscopic surgery", *Proceedings of the IEEE International Conference on Robotics and Automation (ICRA)*, Rome, Italy, pp. 244–249, 10–14 April 2007.

[TAK 10] TAKAKI, T., OMASA, Y., ISHII, I., *et al.,* "Force visualization mechanism using a Moiré fringe applied to endoscopic surgical instruments", *Proceedings of the IEEE International Conference on Robotics and Automation (ICRA)*, Anchorage, AK, pp. 3648–3653, 3–8 May 2010.

[TAM 10] TAMADAZTE B., MARCHAND E., DEMBÉLÉ S., *et al.,* "CAD model-based tracking and 3D visual-based control for MEMS microassembly", *The International Journal of Robotics Research*, vol. 29, no. 11, pp. 1416–1434, 2010.

[TAN 10a] TAN Y.H., SUN D., HUANG W.H., "Mechanical modeling of red blood cells during optical stretching", *ASME Journal of Biomechanical Engineering*, vol. 132, no. 4, pp. 044504, 2010. Available at: http://biomechanical.asmedigitalcollection.asme.org/article.aspx?articleid=1421605

[TAN 10b] TAN Y.H., SUN D., WANG J.Z., *et al.,* "Mechanical characterization of human red blood cells under different osmotic conditions by robotic manipulation with optical tweezers", *IEEE Transactions on Biomedical Engineering*, vol. 57, pp. 1816–1825, 2010.

[TAY 99] TAYLOR R.H., JENSEN P., WHITCOMB L.L., *et al.,* "Steady-hand robotic system for microsurgical augmentation", *The International Journal of Robotics Research*, vol. 18, no. 12, pp. 1201–1210, 1999.

[TAY 12] TAYLER A.B., HOLLAND D.J., SEDERMAN A.J., *et al.,* "Exploring the origins of turbulence in multiphase flow using compressed sensing MRI", *Physical Review Letters*, vol. 108, pp. 264505, 2012.

[TIW 10] TIWARI M.M., REYNOSO J.F., LEHMAN A.C., *et al.,* "In vivo miniature robots for natural orifice surgery: state of the art and future perspectives", *World Journal of Gastrointestinal Surgery*, vol. 2, no. 6, pp. 217–223, 27 June 2010.

[TOT 12] TOTTORI S., ZHANG L., QIU F., *et al.,* "Magnetic helical micromachines: fabrication, controlled swimming, and cargo transport", *Advanced Materials*, vol. 24, no. 6, pp. 811–816, February 2012.

[TRI 08] TRIVEDI D., RAHN C.D., KIER W.M., *et al.,* "Soft robotics: biological inspiration, state of the art, and future research", *Applied Bionics and Biomechanics*, vol. 5, no. 3, pp. 99–117, 2008.

[TSU 01] TSUKADA N., KUDOH K., YAMAMOTO A., *et al.,* "Development of oocyte rotation system for biological cell manipulation", *Proceedings of the 32nd International Symposium on Robotics (ISR)*, Seoul, Korea, April 2001.

[ULL 13] ULLRICH F., BERGELES C., POKKI J., *et al.,* "Mobility experiments with microrobots for minimally invasive intraocular surgery", *Investigative Ophthalmology & Visual Science*, vol. 54, no. 4, pp. 2853–2863, April 2013.

[USM 12] USMAN A., CHIANG W.-Y., MASUHARA H., "Optical trapping and polarization-controlled scattering of dielectric spherical nanoparticles by femtosecond laser pulses", *Journal of Photochemistry and Photobiology A: Chemistry*, vol. 234, pp. 83–90, 2012.

[VAL 10] VALDASTRI P., QUAGLIA C., BUSELLI E., *et al.,* DARIO P., *et al.*, "A magnetic internal mechanism for precise orientation of the camera in wireless endoluminal applications", *Endoscopy*, vol. 42, no. 6, pp. 481–486, 2010.

[VAL 11] VALDASTRI P., SINIBALDI E., CACCAVARO S., *et al.,* "A novel magnetic actuation system for miniature swimming robots", *IEEE Transactions on Robotics*, vol. 27, no. 4, pp. 769–779, 2011.

[VAN 04] VAN MEER F., ESTÈVE D., GIRAUD A., *et al.,* "2D silicon macro-force sensor for tele-operated surgical instrument", *Proceedings of the International Conference on MEMS, NANO and Smart Systems (ICMENS)*, Banff, Canada, pp. 468–472, 25–27 August 2004.

[VAN 05] VAN MEER F., GIRAUD A., ESTÈVE D., *et al.,* "A disposable plastic compact wrist for smart minimally invasive surgical tool", *Proceedings of the IEEE/RSJ International Conference on Intelligent Robots and Systems (IROS)*, Edmonton, Canada, pp. 3501–3507, August 2005.

[VAN 11] VANCAMBERG L., SAHBANI A., MULLER S., *et al.,* "Needle path planning for digital breast tomosynthesis biopsy using a heterogeneous model", *Proceedings of the IEEE International Conference on Robotics and Automation (ICRA)*, Shanghai, China, pp. 5749–5755, 9–13 May 2011.

[VAN 13] VAN DER SCHAAR P.J., DIJKSMAN J.F., DE GAST H.B., *et al.,* "A novel ingestible electronic drug delivery and monitoring device", *Gastrointestinal Endoscopy*, vol. 78, no. 3, pp. 520–528, 2013.

[VEI 12] VEIGA-GUTIÉRREZ M., WOERDEMANN M., PRASETYANTO E., *et al.,* "Optical-tweezers assembly-line for the construction of complex functional zeolite L structures", *Advanced Materials*, vol. 24, pp. 5199–5204, 2012.

[VÉR 12] VÉRON B., ABADIE J., HUBERT A., *et al.,* "Magnetic manipulation with several mobile coils towards gastrointestinal capsular endoscopy", *Proceedings of the European Conference on Mechanism Science*, Santander, Spain, pp. 681–690, September 2012.

[VÉR 13] VÉRON B., HUBERT A., ABADIE J., *et al.,* "Geometric analysis of the singularities of a magnetic manipulation system with several mobile coils", *Proceedings of the IEEE/RSJ International Conference on Intelligent Robots and Systems (IROS)*, Tokyo, Japan, pp. 4996–5001, 3–8 November 2013.

[VIE 06] VIEYRES P., POISSON G., COURRÈGES F., *et al.,* "A tele-operated robotic system for mobile tele-echography: the OTELO project", in ISTEPANIAN R., LAXMINARAYAN S., PATTICHIS C.S., (eds.), *M-health, Emerging Mobile Health Systems*, Chapter 23, Springer, pp. 461–474, 2006.

[VOG 94] VOGEL S., *Life in Moving Fluids: The physical Biology of Flow*, Princeton Press, 1994.

[VOL 08] VOLLMERS K., FRUTIGER D.R., KRATOCHVIL B. E., *et al.,* "Wireless resonant magnetic microactuator for untethered mobile microrobots", *Applied Physics Letters*, vol. 92, no. 14, pp. 144103–1-144103-3, 2008.

[VOR 07] VOROS S., ORVAIN E., LONG J.-A., *et al.,* "Automatic detection of instruments in laparoscopic images: a first step towards high level command of robotized endoscopic holders", *The International Journal of Robotics Research*, vol. 26, nos. 11–12, pp. 1173–1119, 2007.

[WAN 06] WANG X., MENG Q.H., "An inchworm-like locomotion mechanism based on magnetic actuator for active capsule endoscope", *Proceedings of the IEEE/RSJ International Conference on Intelligent Robots and Systems (IROS)*, Beijing, China, pp. 1267–1272, 9–15 October 2006.

[WAN 07] WANG X., MENG M.-H., "A magnetic stereo-actuation mechanism for active capsule endoscope", *Proceedings of the Annual International Conference of the IEEE on Engineering in Medicine and Biology Society (EMBS)*, Lyon, France, pp. 2811–2814, 23–26 August 2007.

[WEB 06a] WEBSTER III R.J., OKAMURA A.M., COWAN N.J., "Toward active cannulas: miniature snake-like surgical robots", *Proceedings of the IEEE/RSJ International Conference on Intelligent Robots and Systems (IROS)*, Beijing, China, pp. 2857–2863, 9–15 October 2006.

[WEB 06b] WEBSTER III R.J., KIM J., COWAN N., *et al.,* "Nonholonomic modeling of needle steering", *The International Journal of Robotics Research*, vol. 25, nos. 5–6, pp. 509–525, 2006.

[WEB 08] WEBSTER III R.J., ROMANO J.R., COWAN N., "Kinematics and calibration of active cannulas", *Proceedings of the IEEE International Conference on Robotics and Automation (ICRA)*, Pasadena, CA, pp. 3888–3895, 19–23 May 2008.

[WEB 09] WEBSTER III R.J., SWENSON J.P., ROMANO J.M., *et al.,* "Closed-form differential kinematics for concentric tube continuum robots with application to visual servoing", *11th International Symposium on Experimental Robotics 2008, Springer Tracts in Advanced Robotics*, vol. 54, Springer, Berlin, pp. 485–494, 2009.

[WEB 10] WEBSTER III R.J., JONES B.A., "Design and kinematic modeling of constant curvature continuum robots: a review", *The International Journal of Robotics Research*, vol. 29, no. 13, pp. 1661–1683, 2010.

[WEI 07a] WEIBEL D., DILUZIO W., WHITESIDES G., "Microfabrication meets microbiology", *Nature Reviews Microbiology*, vol. 5, pp. 209–218, March 2007.

[WEI 07b] WEI W., GOLDMAN R., SIMAAN N., *et al.,* "Manipulators for orbital manipulation and intraocular dexterity", *Proceedings of the IEEE International Conference on Robotics and Automation (ICRA)*, Rome, Italy, pp. 3389–3395, 10–14 April 2007.

[WOE 10] WOERDEMANN M., GLÄSENER S., HÖRNER F., *et al.,* "Dynamic and reversible organization of zeolite L crystals induced by holographic optical tweezers", *Advanced Matererials*, vol. 22, pp. 4176–4179, 2010.

[WOO 08] WOOD R., AVADHANULA S., SAHAI R., *et al.,* "Microrobot design using fiber reinforced composites", *Journal of Mechanical Design*, vol. 130, no. 5, 2008.

[WU 10] WU Y., SUN D., HUANG W., "Mechanical force characterization in manipulating live cells with optical tweezers", *Journal of Biomechanics*, vol. 44, pp. 741–746, 2010.

[XU 08] XU K., SIMAAN N., "An investigation of the intrinsic force sensing capabilities of continuum robots", *IEEE Transactions on Robotics*, vol. 24, no. 3, pp. 576–587, 2008.

[XU 09] XU K., GOLDMAN R.E., DING J., *et al.,* "System design of an insertable robotic effector platform for single port access (SPA) surgery", *Proceedings of the IEEE/RSJ International Conference on Intelligent Robots and Systems (IROS)*, St. Louis, MO, pp. 5546–5552, 11–15 October 2009.

[XU 12] XU K., ZHENG X., "Configuration comparison for surgical robotic systems using a single access port and continuum mechanisms", *Proceedings of the IEEE International Conference on Robotics and Automation (ICRA)*, Saint Paul, MN, pp. 3367–3374, 14–18 May 2012.

[XU 13] XU T., HWANG G., ANDREFF N., *et al.,* "Modeling and swimming property characterizations of scaled-up helical microswimmers", *IEEE/ASME Transactions on Mechatronics*, 2013. Available at: http://ieeexplore.ieee.org/xpl/articleDetails.jsp?arnumber=6553581

[YAM 03] YAMASHITA H., KIM D., HATA N., *et al.,* "Multi-slider mechanism for endoscopic forceps manipulators", *Proceedings of the IEEE/RSJ International Conference on Intelligent Robots and Systems (IROS)*, Las Vegas, NV, pp. 2577–2582, 27–31 October 2003.

[YAN 12] YANAGIDA T., ADACHI K., YOKOJIMA M., *et al.,* "Development of a peristaltic crawling robot attached to a large intestine endoscope using bellows – type artificial rubber muscles", *Proceedings of the IEEE/RSJ International Conference on Intelligent Robots and Systems (IROS)*, Vilamoura, Algarve, Portugal, pp. 2935–2940, 7–12 October 2012.

[YAS 13] YASUKAWA T., YAMADA J., SHIKU H., *et al.,* "Positioning of cells flowing in a fluidic channel by negative dielectrophoresis", *Sensors and Actuators B*, vol. 186, pp. 9–16, 2013.

[YE 13] YE Z., RÉGNIER S., SITTI M., "Rotating magnetic miniature swimming robots with multiple flexible flagella", *IEEE Transactions on Robotics*, 2013. Available at: http://ieeexplore.ieee.org/xpl/articleDetails.jsp?reload=true&arnumber=6600934

[YES 06] YESIN K., VOLLMERS K., NELSON B., "Modeling and control of untethered biomicrorobots in a fluidic environment using electromagnetic fields", *The International Journal of Robotics Research*, vol. 25, nos. 5–6, pp. 527–536, 2006.

[YIM 12] YIM S., SITTI M., "Design and rolling locomotion of a magnetically actuated soft capsule endoscope", *IEEE Transactions on Robotics*, vol. 28, no. 1, pp. 183–194, 2012.

[YIM 13] YIM S., SITTI M., "SoftCubes: towards a soft modular matter", *Proceedings of the IEEE International Conference on Robotics and Automation (ICRA)*, Karlsruhe, Germany, pp. 530–536, 6–10 May 2013.

[ZAH 10] ZAHRAEE A., PAIK J., SZEWCYZK J., *et al.,* "Towards the development of a hand-held surgical robot for laparoscopy", *IEEE Transactions on Mechatronics*, vol. 15, no. 6, pp. 853–861, 2010.

[ZEM 04] ZEMITI N., ORTMAIER T., MOREL G., "A new robot for force control in minimally invasive surgery", *Proceedings of the IEEE/RSJ International Conference on Intelligent Robots and Systems (IROS)*, Sendai, Japan, pp. 3643–3648, 28 September–2 October 2004.

[ZHA 09a] ZHANG B., KOBAYASHI Y., CHIBA T., *et al.,* "Robotic patch-stabilizer using wire driven mechanism for minimally invasive fetal surgery", *Proceedings of the Annual International Conference of the IEEE on Engineering in Medicine and Biology Society (EMBS)*, Minneapolis, MN, pp. 5076–5079, 2–6 September 2009.

[ZHA 09b] ZHANG L., ABBOTT J., DONG L., *et al.,* "Artificial bacterial flagella: fabrication and magnetic control", *Applied Physics Letters*, vol. 94, no. 6, pp. 064107–1-064107-3, 2009. Available at: http://scitation.aip.org/docserver/fulltext/aip/journal/apl/94/6/1.3079655.pdf?expires=1387544378&id=id&accname=freeContent&checksum=63A0C29B8D73D7FFADEAEBD1B418728A

[ZHA 10] ZHANG L., PEYER K., NELSON B., "Artificial bacterial flagella for micromanipulation", *Lab Chip*, vol. 10, pp. 2203–2215, 2010.

[ZHA 11] ZHANG B., KOBAYASHI Y., MAEDA Y., *et al.,* "Development of a 6-DoF wire-driven robotic manipulator for minimally invasive fetal surgery", *Proceedings of the IEEE International Conference on Robotics and Automation (ICRA)*, Shanghai, China, pp. 2892–2897, 9–13 May 2011.

[ZHA 12] ZHANG G.J., NING Y., "Silicon nanowire biosensor and its applications in disease diagnostics: a review", *Analytica Chimica Acta*, vol. 749, pp. 1–15, 2012.

[ZOR 12] ZORN L., RENAUD P., BAYLE B., *et al.,* "Design and evaluation of a robotic system for transcranial magnetic stimulation", *IEEE Transactions on Biomedical Engineering*, vol. 59, no. 3, pp. 805–815, 2012.

[ZUB 09] ZUBIR M., SHIRINZADEH B., TIAN Y., "Development of a novel flexure-based microgripper for high precision micro-object manipulation", *Sensors and Actuators A*, vol. 150, no. 2, pp. 257–266, 2009.

Index

A, B, C

active catheter, 3, 5, 8, 28, 56, 67
actuation, 75–79
biocompatible, 27, 30, 71
camera, 6, 13, 19, 20, 39, 49, 86, 92, 100, 104, 132, 135, 138, 142, 143
colonoscope, 5, 11, 16–18, 28
comanipulation, 36–37, 38
computer tomography (CT), 24
concentric tube, 2, 8, 9, 21, 28, 44
continuum robot, 8, 28–30, 44

D, E

dielectrophoretic force, 119, 120, 144, 145, 147
distal mobilities/mobility, 2–5, 17, 56
echography/ultrasound, 83–84
electro-active polymer (LAP), 78
electromagnet/coil, 62, 97
electrostatic actuator, 76
electrothermal materials, 76
endoluminal laser surgery/laser surgery, 39

F, H

flexible endoscope, 10, 11
flexure hinge, 67, 74
fluorescence, 81, 82, 134
force control, 21, 34
force sensor, 24, 30, 31, 33, 34, 40, 117
handheld, instrument, 2, 4, 28, 36–38, 48–52
helical microrobot, 105

I, L

interface, 16, 24, 42, 135, 151, 152
ipmc, 78
laser trapping, 114–122, 132–138
laser tweezers, 132, 147
locomotion, 1, 16, 17, 19, 25, 26, 57, 65, 96, 106, 107

M

magnetic
  actuation, 57, 104, 107
  force, 59, 88–90, 95, 111, 130, 147

induction, 19, 58, 61–64, 69, 70, 86, 89, 91, 104–106
moment, 59–61, 64, 70, 90, 91
torque, 59, 97
magnetic resonance imaging (MRI), 24, 83
magnetophoresis, 116, 122, 123, 127, 129, 130, 131, 132
magnetophoretic force, 130
magnetotactic bacteria (MTB), 111, 112
manipulator, 8, 11, 30, 35, 36, 39, 49, 50, 51, 97, 107
MEMS, 49, 56
microassembly, 74–75, 86, 121
microfabrication, 21, 37, 71–75, 86, 107, 139
micromechatronics, 71
microscopy, 84–85
microsurgery, 36, 37, 38, 49, 98, 99, 136
microswimmer, 102–103
minimally invasive surgery (MIS), 3
mobile robot, 19–20, 25, 56, 66
modular robot, 13–16, 25, 28

N

non-contact
force, 111
manipulation, 110–112, 128, 129, 131, 147
micromanipulation, 129
NOTES, 6, 10–13, 28, 107

O, P, R

out-of-plane mechanism, 74
permanent magnet, 64, 86, 91, 95, 106
piezoelectric actuator, 26, 27, 36, 51, 77
PZT, 77
reynolds number, 57, 64–62, 92, 93, 104, 107, 126
robotized instrument, 2, 13, 18, 48–52

S, T, V, X

sensing, 30–34, 80–86
single cell manipulation, 112, 113, 134, 141–143, 147
SMA, 26–28, 77, 78
smart material, 75
SPA, 7, 10–13, 28, 37
teleoperation, 35–36, 38
visual control, 35
X-ray, 81, 82